# Rapidly Converging Boundary Integral Equation Solvers in Computational Electromagnetics

Technische Universität München
Lehrstuhl für Hochfrequenztechnik

École nationale supérieure Mines-Télécom Atlantique Bretagne-Pays de la Loire
École doctorale MathSTIC

# Rapidly Converging Boundary Integral Equation Solvers in Computational Electromagnetics

Simon B. Adrian

Vollständiger Abdruck der von der Fakultät für Elektrotechnik und Informationstechnik der Technischen Universität München zur Erlangung des akademischen Grades eines

*Doktor-Ingenieurs*

genehmigten Dissertation.

| | |
|---|---|
| Vorsitzender: | Prof. Dr.-Ing. Ulf Schlichtmann |
| Prüfer der Dissertation: | 1. Prof. Dr.-Ing. Thomas F. Eibert<br>2. Prof. Dr. Francesco P. Andriulli<br>IMT Atlantique<br>3. Prof. Dr. Romanus Dyczij-Edlinger<br>Universität des Saarlandes<br>4. Prof. Dr. Ralf Hiptmair<br>Eidgenössische Technische Hochschule Zürich |

Die Dissertation wurde am 27.09.2017 bei der Technischen Universität München eingereicht und durch die Fakultät für Elektrotechnik und Informationstechnik am 22.01.2018 angenommen.

Simon Adrian received the Bachelor of Science (B.Sc.) degree in Electrical Engineering and Information Technology from the Technical University of Munich (TUM), Germany, in 2009, the Master of Science (M.S.) degree in Electrical and Computer Engineering from the Georgia Institute of Technology, Atlanta, USA, in 2010, and the Diplom-Ingenieur (Dipl.-Ing.) degree in Electrical Engineering and Information Technology from the TUM in 2012.

His diploma thesis was conducted under the supervision of professor Andriulli at the École nationale supérieure Mines-Télécom Atlantique Bretagne Pays de la Loire (IMT Atlantique), Brest, France. In May 2012, he joint the research staff at the Chair of High-Frequency Engineering at TUM and the Computational Electromagnetics Research Laboratory at IMT Atlantique. He pursued his Doktor-Ingenieur (Dr.-Ing.) degree under the joint supervision of professor Andriulli (IMT Atlantique) and professor Eibert (TUM).

Simon Adrian is laureate of an IEEE Antennas and Propagation Society Pre-Doctoral Research Award and an IEEE Antennas and Propagation Society Doctoral Research Award. He was awarded with the Kurt-Fischer-Preis 2012 for his diploma thesis. He was one of the finalists in the student paper competition at IEEE APS/URSI Symposium in 2012. His contribution to the student paper competition at IEEE APS/URSI Symposium in 2013 was selected as an honorable mention paper. He received the Second Prize in the Third International URSI Student Prize Paper Competition of the URSI General Assembly and Scientific Symposium 2014, the Best Young-Scientist-Paper Award of the Kleinheubacher Tagung 2014, the Third Prize Student Paper Award of the IEEE APS/URSI Symposium, and the First Prize EMTS 2016 Young Scientist Best Paper Award of the URSI International Symposium on Electromagnetic Theory 2016.

*My parents, brother, and all those I hold dear*

**Präkonditionen** [pʀɛːkɔndiːt͡sɪoːˈnɛn]: restlose Abklärung von Vorbedingungen; eine absurdum geführte Transparenz; das Röntgen von Mietern durch Immobilienmakler oder von Menschen durch die Krankenkassen*

*Der große Polt: Ein Konversationslexikon*

Gerhard Polt

* G. Polt. *Der große Polt: Ein Konversationslexikon.* 6th ed. Zürich: Kein & Aber, 2017, p. 117. For those who dwell in Munich, the word "Präkonditionen" has a negative touch as indicated by Gerhard Polt, who defines it as the "total clarification of preconditions; a transparency to the point of absurdity," for example, as it is observed in the "x-raying of tenants by real estate agents." This treatise is devoted to the development of so-called "preconditioners" in the context of boundary integral equation methods for that it vindicates at least partially the term "preconditions."

# Abstract

The electric field integral equation (EFIE) and the combined field integral equation (CFIE), which are commonly used to solve scattering and radiation problems, suffer from the dense-discretization and the low-frequency breakdown: if the average edge length of the mesh is reduced, or if the frequency is decreased, then the condition number of the system matrix grows. This leads to slowly or non-converging iterative solvers.

This dissertation presents new paradigms for rapidly converging integral equation solvers: to overcome the ill-conditioning, we advance and extend the state of the art both in hierarchical basis and in Calderón preconditioning techniques. For the EFIE, we introduce a hierarchical basis for structured and unstructured meshes based on generalized primal and dual Haar prewavelets. Furthermore, a framework is introduced which renders the hierarchical basis able to efficiently precondition the EFIE in the case that the scatterer is multiply connected. The applicability of hierarchical basis preconditioners to the CFIE is analyzed and an efficient preconditioning scheme is derived.

In addition, we present a refinement-free Calderón multiplicative preconditioner (RF-CMP) that yields a system matrix which is Hermitian, positive definite (HPD), and well-conditioned. Different from existing Calderón preconditioners, no dual basis functions and thus no refinement of the mesh is required. Since the matrix is HPD—in contrast to standard discretizations of the EFIE—we can apply the conjugate gradient (CG) method as iterative solver, which guarantees convergence. Eventually, the RF-CMP is extended to the CFIE. Particular attention is paid to obtain a preconditioner that is stable on multiply connected objects, both for the EFIE and the CFIE.

# Zusammenfassung

Diese Dissertation stellt neue Paradigmen zur Vorkonditionierung von Integralgleichungen zur Lösung elektromagnetischer Streu- und Ausstrahlungsprobleme vor. Integralgleichungsverfahren werden häufig für Probleme dieser Art eingesetzt, da—neben einer Reihe weiterer Vorteile—offene Randbedingungen nicht aufwendig modelliert werden müssen und keine numerische Dispersion auftritt. Für die Problembeschreibung werden typischerweise die elektrische Feldintegralgleichung und die kombinierte Feldintegralgleichung verwendet. Leider sind diese schlecht konditioniert: Wird die Anzahl der Unbekannten erhöht oder die Frequenz verringert, dann wächst die Konditionszahl der Systemmatrix, die durch die Diskretisierung der jeweiligen Integralgleichung entsteht.

Um diese schlechte Konditionierung zu verhindern, werden in dieser Dissertation die Hierarchische-Basen- und die Calderón-Vorkonditionierung weiterentwickelt. Zuerst wird eine auf Haar-Prewavelets basierende hierarchische Basis vorgestellt, die auf strukturierten wie auch unstrukturierten Diskretisierungsgittern verwendet werden kann. Mit dieser Basis wächst die Konditionszahl nur noch logarithmisch mit der Anzahl der Unbekannten. Dazu wird die Haar-Basis sowohl für das primäre als auch für das duale Gitter verallgemeinert. Um den Skalarpotentialoperator der elektrischen Feldintegralgleichung vorzukonditionieren, werden die Divergenzterme, die in der Variationsformulierung auftreten, mittels inverser Laplace-Matrizen indirekt entfernt: Die Entfernung geschieht durch Anwendung iterativer Verfahren, die mittels algebraischer Mehrgittervorkonditionierer stabilisiert werden. Für den Vektorpotentialoperator der elektrischen Feldintegralgleichung wird gezeigt, dass eine angepasste inverse Transformationsmatrix der dualen Haar-Basis als Vorkonditionierer eingesetzt werden kann. Dieses Ergebnis wird unter Verwendung einer diskreten Calderón-Identität erreicht, welche den hypersingulären Randintegraloperator und den Einfachschicht-Randintegraloperator in Bezug setzt. Nebenbei ergibt sich dadurch ein Haar-Basis-Vorkonditionierer für den hypersingulären Operator, der unter anderem in der numerischen Modellierung elektrostatischer und akustischer Probleme relevant ist.

Wenn eine Geometrie mehrfach zusammenhängend ist, müssen sogenannte globale Schleifenfunktionen zu quasi-Helmholtz-Zerlegungen hinzugefügt werden. Diese Funktionen sind numerisch aufwendig zu konstruieren bzw. anzuwenden. Um dennoch hierarchische Basen als Vorkonditionierer einsetzen zu können, ohne dabei die quasilineare Gesamtkomplexität des Lösungsalgorithmus zu gefährden, wird ein neues Verfahren vorgestellt, welches erlaubt, diese Basen mit quasi-Helmholtz-Projektoren zu kombinieren, wodurch die explizite Konstruktion der globalen Schleifenfunktionen umgangen wird.

Anschließend wird die Anwendbarkeit von hierarchischen Basen als Vorkonditionierer auf die kombinierte Feldintegralgleichung untersucht. Es wird gezeigt, dass die hierarchischen Schleifenfunktionen, welche den Vektorpotentialoperator nicht vorkonditionieren können, sehr wohl bei der kombinierten Feldintegralgleichung angewendet werden können. Darüber hinaus wird ein Verfahren mit quasi-Helmholtz-Projektoren vorgestellt, das es erlaubt Hierarchische-Basen-Vorkonditionierer im Rahmen der kombinierten Feldintegralgleichung auf unstrukturierten Diskretisierungsgittern zu nutzen.

Für die meisten Anwendungen sind diese hierarchischen Vorkonditionierer ausreichend. Im asymptotischen Grenzfall, wenn also die Anzahl der Unbekannten gegen Unendlich strebt, würde die Konditionszahl dennoch schrankenlos wachsen. Werden hingegen Calderón-Vorkonditionierer verwendet, so konvergiert die Konditionszahl gegen eine Konstante. In dieser Dissertation wird die Calderón-Vorkonditierung derart weiterentwickelt, dass keine dualen Basisfunktionen und daher auch kein baryzentrisch verfeinertes Diskretisierungsgitter benötigt wird. Es basiert auf spektralen Äquivalenzen von Laplace-Matrizen und diskretisierten Integraloperatoren (vornehmlich des Einfachschichtpotentialoperators und des hypersingulären Operators). Insbesondere gelingt es dabei auch, den Vorkonditionierer so auszulegen, dass mehrfach zusammenhängende Geometrien ohne Stabilitätsprobleme behandelt werden können. Im Gegensatz zu existierenden Verfahren ist die entstehende Systemmatrix hermetisch und positiv definit. Dadurch ist es möglich, dass iterative Verfahren der konjugierten Gradienten anzuwenden, das Konvergenz garantiert und im Vergleich zu anderen Krylov-Unterraumverfahren geringe numerische Zusatzkosten aufweist.

Schließlich wird der neue Calderón-Vorkonditionierer auf die kombinierte Feldintegralgleichung erweitert. Diese Erweiterung ist notwendig, da die elektrische Feldintegralgleichung bei geschlossenen Geometrien für deren Resonanzfrequenzen nicht mehr eindeutig lösbar ist. Dabei gibt es verschiedene Herausforderun-

gen: Zunächst ist eine direkte Anwendung des neuen Verfahrens nicht möglich, weil der Teil des Vorkonditionierers für den Vektorpotentialoperator zu einer schlecht-konditionierten Systemmatrix der ebenso enthaltenen magnetischen Feldintegralgleichung führen würde. Daneben würde die vorkonditionierte Matrix nicht mehr hermitesch und positiv definit sein. Besondere Aufmerksamkeit erfordern schließlich mehrfach zusammenhängende Geometrien, da der toroidale Teil des quasi-harmonischen Helmholtz-Unterraums so mit der Frequenz skaliert, dass sich für den statischen Grenzfall ein Nullraum ergibt. Das neue Verfahren führt, wie schon im Fall der elektrischen Feldintegralgleichung, zu einer Systemmatrix, die hermitesch, positiv definit und wohlkonditioniert ist—sowohl für einfach als auch mehrfach zusammenhängende Geometrien.

# Résumé

Cette dissertation présente de nouveaux paradigmes de préconditionnement d'équations intégrales pour la résolution de problèmes de diffusion et de radiation électromagnétique. Les équations intégrales sont communément utilisées pour résoudre ces problèmes elles incorporent naturellement les conditions aux limites ouvertes et elles ne ne souffrent pas de problèmes de dispersion numérique. Malheureusement, certaines de ces équations intégrales, en particulier l'équation intégrale du champ électrique et l'équation intégrale du champ combiné sont mal conditionnées. C'est à dire que, si le nombre d'inconnues augmente ou que la fréquence diminue, le conditionnement du problème se dégrade, ce qui a pour conséquence le ralentissement ou la non-convergence de solveurs itératifs.

Pour remédier à ce mauvais conditionnement, nous nous basons sur et étendons l'état de l'art dans le domaine des bases hiérarchiques et des techniques de préconditionnement de type Calderón. Dans un premier temps, la thèse est dédiée à l'amélioration des préconditionneurs à bases hiérarchiques. Nous présentons une base pour des maillages structurés et non structurés, dans laquelle le conditionnement croît logarithmiquement en fonction du nombre d'inconnues. Cela représente un nette amélioration par rapport à l'état de l'art, qui atteint au mieux une croissance proportionnelle à la racine carrée du nombre d'inconnues. Nous obtenons ce résultat en généralisant dans un premier temps la base de Haar aux maillages triangulaires et leur dual. Pour préconditionner l'opérateur potentiel scalaire de l'équation intégrale du champ électrique nous supprimons les termes de divergence apparaissant dans sa forme variationnelle grâce à l'utilisation de l'inverse des laplaciens de graphes. Pour stabiliser cette inversion nous utilisons des préconditionneurs à grilles multiples déjà existant. Pour de l'opérateur du potentiel vecteur de l'équation intégrale du champ électrique, nous montrons que la matrice de transformation inverse de la base de Haar doit être utilisée. Ce résultat est obtenu grâce à une identité de Caldérón scalaire discrétisée qui lie l'opérateur hypersingulier à l'opérateur potentiel simple couche bien connu en électrostatique. Cette démarche a aussi permis l'obtention d'un préconditionneur

à base de Haar pour l'opérateur hypersingulier, opérateur qui apparaît dans la modélisation de problèmes électrostatiques et en acoustiques.

Dans le cas de géométries à connexions multiples, les boucles globales doivent être prises en compte et ajoutées aux décompositions quasi-Helmholtz. La construction et l'application de ces fonctions sont coûteuses en termes de calcul. Afin d'utiliser les préconditionneurs à base hiérarchique sans nuire à la complexité dominante engendrée par une méthode rapide, nous montrons que la base hiérarchique peut être utilisée sans la construction explicite des boucle globales. Ce résultat est obtenu grâce au développement d'un système permettant de combiner les projecteurs quasi-Helmholtz à la base hiérarchique. Le principe en lui même est agnostique de la base concrète, et par conséquent peut être combiné à n'importe quelle base hiérarchique disponible.

Ensuite nous nous intéressons à l'application du préconditionneur à base hiérarchique à l'équation intégrale du champ combiné. Nous démontrons que les boucles hiérarchiques, qui ne peuvent pas résoudre la détérioration de la solution due à la discrétisation dense pour la partie du potentiel vecteur de l'équation intégrale du champ électrique, peuvent être effectivement utilisées pour l'équation intégrale du champ combiné. De plus, nous proposons une nouvelle méthode permettant l'utilisation de préconditionneurs à bases hiérarchiques à la fois sur des maillages structurés et non-structurés dans le contexte de l'équation intégrale du champ combiné. Nous utilisons le fait que l'équation du champ combiné est bien conditionnée pour le sous-espace de Helmholtz solénoïdal et ainsi nous utilisons les projecteurs quasi-Helmholtz : ces projecteurs sont mettent en évidence une base hiérarchique non-solénoïdale permettant de préconditionner la partie de l'opérateur du potentiel scalaire dans l'équation intégrale du champ combiné.

Les nouveaux préconditionneurs à base hiérarchique suffisent pour la majorité des applications. Cependant le conditionnement des problèmes devrait tendre asymptotiquement vers l'infini. C'est pourquoi dans un second temps, nous surmontons cette limitation en introduisant le préconditionneur multiplicatif de Caldéron sans raffinement (RF-CMP) qui, contrairement aux autres méthodes, ne nécessite pas une seconde discrétisation de l'équation intégrale du champ électrique avec les fonctions de base duales. Tout d'abord, nous dérivons cette technique pour l'équation intégrale du champ électrique en nous basant sur l'équivalence spectrale entre les laplaciens (de graphe) et les opérateurs intégraux discrétisés (les opérateurs simple couche et hypersingulier). Une attention particulière a été portée à l'obtention d'une formulation stable dans le cas des

géométries à connexion multiple. Contrairement à d'autres préconditionneurs, le système matriciel résultant est Hermitien, défini positif ce qui permet l'utilisation de la méthode des gradients conjugués. A la différence des autres méthodes des sous-espaces de Krylov, la méthode des gradients conjugués a une convergence garantie et a un surcoût calculatoire minimal.

Enfin, le RF-CMP est étendu à l'équation intégrale du champ combiné. Nous obtenons ainsi une formulation sans résonances artificielles. Il y a là plusieurs défis : premièrement l'application directe du RF-CMP est impossible puisque la partie du préconditionneur pour l'opérateur du potentiel vecteur rendrait l'équation intégrale du champ magnétique mal conditionnée. Deuxièmement, nous n'aurions pas un système matriciel hermitien défini positif. Et enfin nous n'obtiendrions pas une formulation stable pour des géométries à connexions multiples. Cela est du au fait que l'équation intégrale du champ magnétique n'est pas entièrement bien conditionnée puisqu'elle possède un noyau statique associé à la partie toroïdale du sous-espace de Helmholtz quasi-harmonique. La nouvelle formulation est construite de façon à ce que le système préconditionné soit, comme pour l'équation intégrale du champ électrique, hermitien défini positif et reste stable pour des géométries à connexions multiples.

# Contents

# Preface and Acknowledgment

> I am so used to plunging into the unknown that any other surroundings and form of existence strike me as exotic and unsuitable for human beings.†
>
> *Conquest of the Useless*
> Werner Herzog

When I plunged into my dissertation research, I did not know what challenges and issues I would encounter, and what the outcome of all my efforts would be. While I would never dare to compare these efforts with, let's say, the effort it takes to move a ship across a mountain ridge from one river system into another, I found the existence as doctoral student quite suitable for me.‡ This is not only due to the fun I had whilst exploring the unknown, but also due to the people who I have met in that quest.

The research of this thesis was carried out at the Chair of High-Frequency Engineering at the Technical University of Munich and the Computational Electromagnetics Research Laboratory at the École nationale supérieure Mines-Télécom of Atlantique Bretagne-Pays de la Loire. During my *Lehrjahre*, I have met many wonderful people both in my academic and my private life and I would like to express my sincere gratitude to all of them.

First, I would like to thank my advisors professor Thomas Eibert and professor Francesco Andriulli. This work would not have been possible without their guidance, counsel, encouragement, and the many fruitful discussions we

† W. Herzog. *Conquest of the Useless: Reflections from the Making of Fitzcarraldo.* 1st ed. Ecco: New York, 2009, p. 248.

‡ As a side note for (future) doctoral students, I found that the film "Burden of Dreams" is a great source of motivation helping to master the (occasional) periods of frustration.

had—a guidance which was, in fact, not limited to this work alone. Their (not only scientifically) inspiring nature will always remain an example for me. *Von ganzem Herzen danke ich* professor Eibert for introducing me to the world of high-frequency engineering and for giving me a large measure of freedom in my teaching. *Io ringrazio di cuore* Francesco for introducing me to Calderón and hierarchical basis preconditioning, letting me use his boundary element code, the myriad Skype sessions, and all the adventures we had together.

Moreover, I am grateful to professor Romanus Dyczij-Edlinger and professor Ralf Hiptmair for serving on my thesis committee and for their invaluable feedback, and to professor Ulf Schlichtmann for chairing the committee.

My advisors enabled me to visit many conferences, which allowed me to get feedback on my research early on by meeting researchers from all over the world. The many interesting discussions, not necessarily limited to my own research, made the conference visits so priceless. To name but a few, I would like to thank professors Hakan Bağci, Shanker Balasubramaniam, Amir Boag, Kristof Cools, Leslie Greengard, Ludger Klinkenbusch, Eric Michielssen, Andrew Peterson, Sebastian Schöps, Felipe Vico, Karl Warnick, Thomas Weiland, Daniel Weile, and Dr. Yves Beghein for the many inspiring conversations.

A special thanks goes to professor Yaniv Brick, who honored me with his friendship since we meet at IEEE International Symposium on Antennas and Propagation in Orlando. I am deeply grateful not only for our discussions on common research interests, but also for introducing me to the IEEE Education Committee and to the Japanese cuisine!

That my stays at the end of the earth[§] have been so enjoyable, I owe very much to my friends and co-workers professor Rajendra Mitharwal, Dr. Abdelrahman Ijjeh, Dr. Maxim Abalenkov, Dr. Maxim Dr. Lyes Rahmouni, Dr. Axelle Pillain, Dr. John Erick Ortiz Guzman, Adrien Merlin, and Alexandre Dely not only for many fruitful discussions, but also for showing me around in Brittany and only thanks to them I did not get "lost in translation" when I had to deal with French red-tape. A special thanks goes to Alexandre and Adrien, who "helped" me in writing the French abstract. *Merci beaucoup !*

I would also like to thank all my friends and colleagues from Munich, who made the Chair of High-Frequency Engineering an ideal working place. First, I would

§ The école nationale supérieure Mines-Télécom Atlantique Bretagne-Pays de la Loire is located in the *Département Finistère*, where the name *Finistère* derives from Latin *Finis Terræ*.

like to thank all the students I could advise, and in particular, I would like to thank Han Na for testing METIS and Daniela Geisinger for exploring the capabilities of the Julia programming language for me. Moreover, I wish to express my gratitude to Thomas Mittereder for his rapid IT support, to my undergraduate advisor Dr. Uwe Siart, who so often helped me out with his profound knowledge of LaTeX and the art of typography, to Dr. Georg Schnattinger, Dr. Oliver Wiedenmann, and Ole Neitz for making some of my conference visits a unique experience, to Jonas Kornprobst, who showed me some particular cool TikZ hacks, to Josef Knapp and Christian Koenen, with whom I had the pleasure to teach the "Hauptseminar Hochfrequenztechnik", to Dr. Robert Brem, Dr. Mark Eberspächer, Christoph Eisner, Fabian Faul, Gerhard Hamberger, Dr. Susanne Hipp, Bernd Hofmann, Safiullah Khan, Raimund Mauermayer, Björn Möhring, Dr. Arndt Ott, Alexander Paulus, Dr. Dennis Schobert, and Mehmet Taygur for great lunch time and coffee break discussions on science, philosophical matters, and many other topics. I also like to thank Jonas and Josef for proofreading parts of my thesis.

Whom I would like to pay a special tribute is my dear friend Dr. Michael Gruber for proofreading many of my papers, for numerous discussions on integral equations and electromagnetics, science, and other philosophical questions, for the fun we had in developing and teaching together the "Hauptseminar Hochfrequenztechnik"—and for dragging me over the Watzmann safely.

Last but not least, I would like to thank all my friends for being part of my life and my parents, who taught me some of the most important life lessons, and my dear brother, for their constant love and support.

Munich, Germany
April 3, 2018

Simon B. Adrian

# Part I.

# Prelude

Chapter 1

# Introduction

Kinder, schafft Neues!
Richard Wagner

Seven score and twelve years ago, James C. Maxwell published twenty equations which describe the behavior of electromagnetic fields [Max65] and which we refer today as "Maxwell's equation" (though the equations as they are taught in university nowadays are fewer in number thanks to the introduction of vector calculus and the omission of Lorentz force law [SS03; Art13]).[1] Despite the many decades which have passed since their publication, finding a solution to Maxwell's equations for an arbitrary problem remains a challenge. Analytic solutions are known only for a few canonical geometries such as a sphere [Mie08], but even for a geometry as simple as a torus no analytic solution is known [Lau67; BCP13; Ven06].

Yet, there is a need for obtaining these solutions: if we were not be able to solve Maxwell's equations, the design process of any device with electromagnetic properties would be limited to extensive prototyping and experimentation, a process which is both expensive and time consuming. Given the number of quotidian electromagnetic devices and systems such as television, radio, microwave ovens, satellite communication systems, radar systems, electrical motors and generators, medical imaging systems, it is evident that we need methods that allow us to predict the (electromagnetic) behavior of these devices and systems at an early stage in the design process.

1 Important contributions to the formalism we are using today stem from Oliver Heaviside [Hea; Hea93] and Heinrich Hertz [Her84; Her90]. The first textbook on Maxwell's equations, which according to [Art13] presented the theory in a clear and instructive manner, was published by August Föppl [FA07]. For a detailed discussion on the evolution of Maxwell's equations, see [Art13].

## a) Fragmentary[2] Review of Numerical Techniques

If there is no analytic solution, one must resort to a numerical technique, which yields an approximate solution. A plethora of techniques have been developed, and the choice of the method depends on the problem to be solved. For example, if a scatterer spans several millions of wave lengths, then asymptotic techniques based on geometrical or physical optics are required [Kel62; KP74; Ufi07]. These methods, however, cannot always guarantee convergence to the physical solution. In particular for electrically small or midsize problems with non-smooth surfaces, this problem becomes critical.

In order to guarantee convergence, numerically exact methods must be used. They are typically divided into local and global methods. A local method discretizes in most cases a (partial) differential operator commonly resulting in a sparse linear system. Typical examples are the finite difference time domain (FDTD) method [Yee66], the finite integration technique (FIT) [Wei77], the transmission line matrix method (TLM) [JB71; Hoe85], or the finite element method (FEM) [Jin14]. While these methods are well-suited for many applications, scattering or radiation problems are not their strength: local methods require the discretization of the entire domain, which is impossible to achieve for open problems (i.e., where the domain is unbounded). In order to minimize the computational resources, the domain must be truncated artificially. This can be achieved by using, for example, absorbing boundary conditions [BT80] or the perfectly matched layer technique [Ber94]. While good results can be obtained, there is still a trade-off between accuracy and computational effort.

Another issue, which plagues local methods is numerical dispersion, that is, if the frequency is increased while keeping the ratio of the average edge length of the mesh and the wavelength constant, then the phase becomes polluted and is eventually lost [BS97]. Remedies for this problem usually comprise the use of higher order basis functions, which leads to a densely populated linear system in the asymptotic limit (and thus to the loss of one of the most charming properties of local methods).

2 A cornucopia of numerical methods has been presented in the past decades for the solution of Maxwell's equations. Hence, the methods discussed in this section are mere samples to illuminate the context in which integral equation methods are situated. For a more complete discussion of the different techniques, the reader may consider standard textbooks such as [Jin15].

Integral equation based methods, which belong to the class of global methods, only demand the discretization of the scatterer or the antenna, respectively: open boundary conditions are modeled within the analytical formulation so that no additional effort is required. If the obstacle is homogeneous (or consists of a several homogeneous subdomains), a further reduction in the computational effort is possible since it suffices to discretize the surface resulting in a surface integral equation that has to be solved. In addition, integral equation based methods do not suffer from numerical dispersion, though of course, the linear system emerging from a standard discretization of an integral equation is densely populated.

The dense system matrix has been one of the main reasons why integral equations were not in the focus of the scientific community for a long time: since the matrix is fully populated, the computational complexity to obtain a solution becomes at least quadratic both in memory and in time consumption. Given the computational resources available in the last century, research was mostly limited to, for example, thin-wire approximations or 2-D problems [Har01; Sar83]. The issue has been overcome with the advent of fast methods that allowed to reduce the cost of a single matrix-vector product as well as the memory consumption to quasilinear complexity, that is, if $N$ is the number of unknowns, the complexity is $\mathcal{O}(N \log^{\alpha} N)$, where $\alpha \in \mathbb{R}^{+}$ is a constant depending on the respective method. Among the most popular methods are the multilevel fast multipole method (MLFMM), multilevel matrix decomposition algorithm (MLMDA), hierarchical matrices, or adaptive cross approximation (ACA) [GR87; HN89; SLC97; Dar00; MB96; ZVL05; Beb00; BR03].

The physical scenario considered in this thesis is the scattering of electromagnetic waves by perfectly electrically conducting (PEC) objects, that is, a known electromagnetic wave impinges on an obstacle and the scattered wave shall be computed. As a variant of this scenario, we also take radiation problems into account, where we solve for the wave radiated by an antenna which is fed by a voltage-gap source.

Given these scenarios, the focus is on surface integral equation methods, where we do not solve directly for the electric or magnetic field, but instead electric and magnetic currents are obtained on the surface of the scatterer by applying the surface equivalence principle [SC39; Pet+98]. Depending on the formulation, these currents can have a physical meaning or can be purely artificial.

For solving a PEC problem, there are in essence two integral operators available, the electric field integral equation (EFIE) and the magnetic field integral equation (MFIE) operator, which lead to the EFIE [Rum54] and the MFIE [Mau49]. While both of them yield the physical electric surface current density, their properties differ in many regards: most prominently, the EFIE works for both closed and open surfaces (e.g., an infinitely thin metal sheet would be an example of an open surface), while the MFIE is only applicable to closed surfaces. They do share, however, a common problem: if we have an electrically large object with a closed surface (i.e., the size of the scatterer spans several wavelengths), then both the EFIE and the MFIE suffer from spurious modes; at resonance frequencies, the operators have a null space and the electric current is not uniquely determined anymore. This issue usually results in a loss of accuracy and slow convergence if an iterative solver is used. The classic remedy is to combine the EFIE and the MFIE to the combined field integral equation (CFIE) [MH78], where we still solve for the physical current. Alternatively, a combined source integral equation (CSIE), as for example proposed in [MH79] or analogously to [BW65], can be used. In this case, however, the solution is not the physical current anymore. Whatever strategy is chosen, the resulting combined integral equation operator will inherit properties of the EFIE and the MFIE operator. Hence, both operators must be studied and dealt with.

## b) Computational Complexity and Ill-Conditioned Integral Equations

It was mentioned that fast methods can compress the system matrix so that the memory consumption and the cost of a single matrix-vector product scale only quasilinearly in the number of unknowns. The overall numerical costs for obtaining the solution of the scattering problem, however, have not been discussed so far. To obtain the solution, two approaches are possible: a direct inversion of the system matrix or the usage of an iterative solver, typically one belonging to the class of Krylov subspace methods. The advantage of a direct inversion is its robustness: we are guaranteed to obtain the inverse matrix, whereas iterative solvers can converge slowly or, in the worst case, do not converge at all.

In general, the direct inversion of the system matrix is of limited practicality since the numerical costs scale cubically in $N$. Even if the inverse matrix is obtained, for multiple right-hand sides it is still impractical since the cost of single matrix-vector product scales quadratically in $N$. Recently, advances have been made in the field of fast direct methods in the static [Mar09] and in the dynamic regime [GHM13; BLB14; GJM14; Guo+16], where in the latter case [Guo+16] it is observed that the memory requirement scales as $\mathcal{O}(N \log^2 N)$ and the computational costs for obtaining the inverse as $\mathcal{O}\big(N^{1.5} \log N\big)$. Since the inverse is compressed, a single matrix-vector product has quasilinear complexity, which makes these methods particularly for multiple right-hand side problems interesting. For large problems, however, any growth exceeding quasilinear complexity can be prohibitive.

For iterative methods, the computational costs scale as $\mathcal{O}\big(N_{\text{iter}} N \log^\alpha N\big)$, where $N_{\text{iter}}$ is the number of iterations that the iterative solver needs to converge. The decisive question is whether there is an upper bound for $N_{\text{iter}}$ independent of $N$. In the case of an integral equation of the second kind—the MFIE is a typical example [Yla+13]—there is such an upper bound (apart from the resonance frequencies, where the MFIE operator has a null space). Thus if a mesh is refined, that is, $N \longrightarrow \infty$, then $N_{\text{iter}} \longrightarrow C$, where $C \in \mathbb{N}$ is some constant.

For an integral equation of the first kind, the EFIE is a typical example [Yla+13], the situation is more complicated. For most Krylov subspace methods no sharp bounds on $N_{\text{iter}}$ can be given. For illustration purposes and for the sake of simplicity, we assume that the conjugate gradient (CG) method is used (which is actually not applicable since it requires a Hermitian, positive definite (HPD) matrix [HS52], which neither the EFIE nor the MFIE are), then the number of iterations $N_{\text{iter}}$ used by the CG method can be bounded by the square root of the condition number of the system matrix [She94; AK01]. The condition number is the ratio of the largest over the smallest singular value and in the case of the EFIE the condition number scales linearly in $N$ and so the computational costs are $\mathcal{O}\big(N^{1.5} \log^\alpha N\big)$ for the EFIE and $\mathcal{O}\big(N^{1.25} \log^\alpha N\big)$ for the CFIE or the CSIEs.

Clearly, if $N_{\text{iter}}$ grows with increasing $N$, then the quasilinear complexity set by the respective fast method is lost. Given the considerations on the CG method, if the leading complexity set by the fast method shall be maintained, the system matrices of the EFIE or CFIE must be transformed such that the condition number of the resulting system matrix has an upper bound independent of $N$.

Whenever the growth of the condition number is unbounded in $N$, the problem is ill-conditioned in $N$ and this growth is referred to as the dense-discretization breakdown. This terminology is necessary since other forms of ill-conditioning can exist, in particular, the EFIE suffers from the so-called low-frequency breakdown: the condition number grows when the frequency is decreased.

Historically, in fact, when no fast method was available and the computational resources were more limited than today, the low-frequency breakdown was, with respect to ill-conditioning, the pressing problem (and not that much the dense-discretization breakdown). The low-frequency breakdown originates from the fact that the EFIE operator is composed of two operators, the vector and the scalar potential operator, which scale with $k$ and $1/k$, respectively, where $k$ is the wavenumber. Since the scalar potential has a null space associated with solenoidal functions, the system matrix possess two branches of singular values and these branches are driven apart when the frequency is decreased.

To resolve these issues or their practical impact at least partially, there are essentially three means: (i) developing a new formulation which does not suffer from these defects, (ii) domain decomposition approaches, and (iii) construct a suitable preconditioner. A preconditioner can be understood as one or two matrices which are multiplied left and right to the system matrix, respectively, and which should yield a lower condition number of the overall matrix. Examples for new formulations are the augmented EFIE [QC08] or the decoupled potential integral equation [Vic+16]. These approaches resolve the problems, however, only partially [QC08] or are limited to smooth objects [Vic+16].

Domain decomposition methods are well-suited if the object is electrically large or discretized with many unknowns. They divide the domain into smaller subdomains, where in each subdomain the problem is solved independently from the other subdomains. Transmission conditions are required to prevent unphysical reflections from the boundary of the subdomains. While these approaches work well for FEMs, which are local in nature, one needs more elaborate transmission conditions in the case of integral equations: some methods perform decently for simple problems [Bra+00] or specific problems such as the scattering from antenna arrays [SM00; PM03; MLV07], they fail, however, when confronted with intricate problems. A possible remedy comprises the use of second order transmission conditions [RL10; PWL11], though at the price of the introduction of auxiliary unknowns. More recent methods avoid the introduction of auxiliary unknowns by introducing a penality term [Pen+16].

## c) Review of Preconditioning Techniques

Preconditioners, to be effective, must be carefully designed. For example, to cure the low-frequency breakdown a simple Jacobi preconditioner is not sufficient. Instead, the low-frequency breakdown has been cured by using quasi-Helmholtz decompositions such as the loop-star and the loop-tree decomposition [WG81; WGK95; BK95; Vec99; ZC00; Eib04]. Here, the loop functions are a solenoidal basis and the star or tree functions complementing the loop functions are non-solenoidal. By scaling these functions in frequency, the low-frequency breakdown is resolved. These preconditioners, however, cannot cure the dense-discretization breakdown. In fact, the loop-star preconditioner is even more sensible to the dense-discretization breakdown [And12a]. Another approach to overcome the low-frequency breakdown is the augmented EFIE [QC08], which does not require an explicit quasi-Helmholtz decomposition and which has the advantage that for multiply connected geometries the global loops are not needed (which are otherwise costly to obtain). Recently, quasi-Helmholtz projectors have been presented, which can cure the low-frequency breakdown and do not require a search for the global loops [And12a; And+13].

One cure for the dense-discretization breakdown are near-zone preconditioners. Typically, fast methods such as the MLFMM or the ACA distinguish between near- and far-interactions. The near-interactions can be extracted from the system matrix as sparse matrix with $\mathcal{O}(N)$ elements. Since the near matrix is the dominant part of the system matrix, its inverse is a good candidate as preconditioner. This inverse, however, must be obtained. A classic approach is the incomplete LU factorization [Ben02; Saa03], which was invented by Varga [Var59]. The LU factorization decomposes a matrix into the product of two triangular matrices, which, however, do not maintain the sparsity of the original matrix rendering it a costly preconditioner. The incomplete LU factorization discards some of the elements of the LU decomposition, whereby the computational costs are small at the price of a less effective preconditioner [Mv77]. While various strategies have been proposed in the past for obtaining an incomplete LU decomposition, it remains a challenge to get an incomplete LU decomposition which works sufficiently for any given problem without the need to optimize its parameters [SV00; CDG00; LLB03; MG07; Car09].

Another near-zone preconditioner approach is based on using a sparse approximate inverse (SAI): it is assumed that the inverse can be approximated by

a sparse matrix up to a certain error (an error measured typically with respect to the Frobenius norm) [Che+01; LZL04; Car+05; CB12; PS14]. The construction of the SAI preconditioner is an optimization problem and because of the use of the Frobenius norm, SAI preconditioners are usually easier to parallelize than incomplete LU decompositions [MG07].

A third near-zone preconditioner approach is based on an iterative inversion of the near-zone matrix in an inner-outer solver scheme. Compared with the incomplete LU or SAI approaches, no additional setup time is required; this advantage comes at the price of increased computational costs per iteration step [Eib03; WE13].

What all these near-zone preconditioning schemes have in common is that it is difficult to assess how the condition number depends on the number of unknowns. Nonetheless, it can be said that, while they usually improve the conditioning, they cannot cure the dense-discretization breakdown in the asymptotic limit $N \longrightarrow \infty$, different from schemes which take into account the underlying mathematical nature of these operators.

The two most popular strategies in this regard are Calderón preconditioning techniques and hierarchical basis preconditioners. Calderón preconditioning leverages the fact that the EFIE operator applied to itself equals the identity operator plus a compact operator. In other words, it becomes an integral equation of the second kind. Thus there is an upper bound for $N_{\text{iter}}$ independent from $N$. The discretization of the Calderón identity is by no means trivial: a simple multiplication of the system matrix with itself would just square the condition number. Instead an inverse Gram matrix is needed to link the two EFIE operators [SW98]. The EFIE is commonly discretized with Rao-Wilton-Glisson (RWG) functions; if the second EFIE operator is discretized with RWG basis functions as well, then the Gram matrix is singular [CN02].

To bypass this problem, different strategies were proposed. In [CN02] the authors resorted to a saddlepoint formulation. The contributions of [Ada04; AC04] split the product of the EFIE operator with itself by considering that the operator is composed of the vector and the scalar potential operator and by discretizing each of the products of the scalar and the vector potential operator separately. In particular, the vanishing of the term, where the scalar potential operator is applied to itself, is enforced. The contribution [Con+02] follows a similar approach compared with [AC04] in the sense that here as well the different products of the vector and the scalar potential operator are treated separately,

where they are simplified by using Stokes' theorem. [BLA05] focuses on the CSIE and uses a localized admittance operator for combining the EFIE with the MFIE. In order to link this operator to the domain of the EFIE operator, projections using the Gram-Schmidt orthogonalization are used, which increases the computational costs. In [Bru+09], the CFIE and CSIE are preconditioned by regularizing the EFIE operator with the vector potential in the context of a Nyström discretization. Similarly to [Vic+16], a smooth surface is required.

What the approaches for the EFIE, mentioned in the previous paragraph, have in common is that open surfaces need a special treatment—if they can be treated at all. Also, significant changes of an existing code are required. With the introduction of Buffa-Christiansen (BC) functions a direct discretization of the Calderón identity became possible [BC07] so that this technique could be easily integrated into an existing code [And+08].[3] The price for the increased comfort is, however, that the number of unknowns is increased by a factor of six since the EFIE is discretized on the barycentrically refined mesh. In addition, (minor) modifications of the existing solver code are still necessary since half-RWGs have to be added on the boundary of open surfaces in order to represent the BC functions. Further issues related to multiply connected geometries are discussed in Chapter 8.

Hierarchical basis preconditioners are usually explicit quasi-Helmholtz decompositions similar to a loop-star or loop-tree basis, yet with the difference that the basis itself is ill-conditioned in such a way that the ill-conditioning of the EFIE is counteracted. The roots of hierarchical basis preconditioners come from wavelet analysis. Since the first wavelets have been one-dimensional functions (the Haar wavelets as one of the most famous examples [Haa10]), these methods were first applied to thin-wire approximations or two-dimensional problems [Alp+93; SL93; GCC95; WC95; Sar97; SS02; Ala+03; Ger+06]. The focus was less on preconditioning, but on compressing the system matrix and accelerating the matrix-vector product [And+05]. In the finite element community, various hierarchical bases were presented for preconditioning differential operators [Yse86; Dah97; Sv97].

One of the key properties of wavelets is that they form a set of orthogonal functions (if only functions of different levels are orthogonal to each other, they are called prewavelets). For preconditioning purposes it turns out that such an or-

3 In fact, a discretization of the Calderón identity could have been obtained before the introduction of the BC functions since the Chen-Wilton (CW) functions would haven been applicable as well [CW90].

thogonality is desirable if the goal is to cure the dense-discretization breakdown. Early hierarchical bases for the EFIE did not necessarily have this property or only had this property for the non-solenoidal basis [VPV05; BSJ05; VVP07; ATV07]. They did improve the conditioning compared with a conventional loop-star or loop-tree preconditioner, but when the non-solenoidal basis is complemented with loop or hierarchical loop functions (the latter based on Yserentant's hierarchical nodal basis [Yse86]), the overall system remained ill-conditioned. In [ATV10], a hierarchical basis preconditioner for the EFIE was presented that yielded a logarithmic growth of the condition number (see also the analysis in [HM12]).

What all of these approaches for three-dimensional problems have in common is that they are limited to structured meshes. Such a mesh is obtained by starting from a coarse mesh that captures (sufficiently) the geometrical details of the scatterer. Assuming that a triangulation is used, a refined mesh is generated by connecting the midpoints of the edges of the triangles; this so-called dyadical refinement is repeated until the desired resolution is reached [ATV07]. For these meshes, existing hierarchical preconditioners can yield a condition number that grows only logarithmically in $N$. When a scatterer is smooth, these approaches would result, in order to be practical, in a loss of geometrical details and thus a possibly large geometrical error can occur. This problem was partially alleviated by a hierarchical basis preconditioner generalized to unstructured meshes [AVV08]—partially, because only the non-solenoidal basis was generalized and so the condition number still grows with $\mathcal{O}(N^{1/2})$. Compared with Calderón preconditioning, the implementation is easier (no dual functions are required) and the computational costs are smaller. In the asymptotic limit $N \longrightarrow \infty$, in particular for unstructured meshes, the hierarchical basis preconditioner can, however, not prevent the dense-discretization breakdown.

## d) Scope and Outline of the Thesis

This dissertation presents new paradigms for the preconditioning of the EFIE and the CFIE for solving electromagnetic scattering and radiation problems, that is, we advance and extend the state of the art both in hierarchical basis and in Calderón preconditioning techniques. To this end, Part I presents

the background material and equations, which will be used throughout the thesis: Chapter 2 introduces fundamental concepts from differential geometry and Sobolev space theory. Chapter 3 covers the electromagnetic theory and equations required to model scattering problems and Chapter 4 discusses the discretization of these equations.

Part II is dedicated to the advancement of hierarchical basis preconditioners. *Chapter 5* presents a basis which is defined on structured and on unstructured meshes. Thereby, a condition number is obtained for the EFIE that grows only logarithmically in $N$; this improves the state of the art [AVV08], where the growth is $\mathcal{O}\left(N^{1/2}\right)$.[4] This result is obtained by first generalizing the Haar basis, both for the primal triangular and for its dual mesh. To precondition the scalar potential part of the EFIE, the divergence terms appearing in its variational formulation are removed by using inverse graph Laplacians. This inversion is performed implicitly by solving the associated linear system iteratively, where for the stabilization algebraic multigrid preconditioners are employed. For the vector potential part of the EFIE, it is shown that an inverse Haar basis transformation matrix must be used. This result is derived by leveraging a discretized scalar Calderón identity that relates the hypersingular to the single layer operator known from electrostatics. As an interesting auxiliary result, we thus get a Haar basis preconditioner for the hypersingular operator, an operator not only used in electrostatics but also, for example, in acoustics.

When a geometry is multiply connected, so called global loops have to be added to the quasi-Helmholtz decompositions. These functions are numerically expensive to construct and/or to apply.[5] In order to use hierarchical basis preconditioners without destroying the leading complexity set by a fast method, *Chapter 6* shows how the hierarchical basis can be applied without the need to explicitly find the global loops. Thereby, the complexity of a fast method can be maintained. This result is obtained by developing a framework that allows to combine quasi-Helmholtz projectors, which were first introduced in [And12a], with the hierarchical basis. The scheme itself is agnostic to the concrete basis and thus can be combined with any hierarchical basis available.

4 Also [ATV10] yields a logarithmic growth of the condition number, but it is limited to structured meshes.

5 They can be applied efficiently if more computational complexity is spend on their construction.

*Chapter 7* analyzes the applicability of hierarchical basis preconditioners to the CFIE. It shows that the hierarchial loops, which cannot cure the dense-discretization breakdown of the vector potential part of the EFIE, can effectively be applied to the CFIE. In addition, we propose a scheme that allows to use the hierarchical basis preconditioners on both structured and unstructured meshes in the context of the combined field integral equation: by employing quasi-Helmholtz projectors, the fact that the CFIE is well-conditioned on the solenoidal Helmholtz subspace is used. These projectors are accompanied by a hierarchical non-solenoidal basis for preconditioning the scalar potential part of the CFIE.

The new hierarchical basis preconditioners are sufficient for most applications. Still, in the asymptotic limit $N \longrightarrow \infty$, the condition number would grow to infinity. Part III overcomes this limitation by introducing the refinement-free Calderón multiplicative preconditioner (RF-CMP) that different from existing Calderón preconditioners does not require a second discretization of the EFIE operator with dual basis functions. *Chapter 8* derives this technique for the EFIE. It is based on spectral equivalences between (graph) Laplacians and discretized integral operators (namely the single layer and the hypersingular operator). Particular care was devoted to multiply connected geometries to obtain a formulation that remains stable on these. In contrast to other preconditioners, the resulting system matrix is HPD which allows the application of the CG method. Different from other Krylov subspace methods, the CG method guarantees convergence and has the least computational overhead among the Krylov methods.

*Chapter 9* extends this method to the CFIE resulting in a formulation that is well-conditioned and free from spurious resonances. There are several challenges: first of all, a direct application of the preconditioner from Chapter 8 is not possible since the part of the preconditioner for the vector potential operator would render the MFIE ill-conditioned. Secondly, it would not yield an HPD system matrix, and thirdly, the formulation would not be stable on multiply connected geometries. The reason is that the MFIE is not entirely well-conditioned since it possesses a static null space associated with the toroidal part of the quasi-harmonic Helmholtz subspace [Bog+11]. The new formulation is constructed such that the preconditioned system is—as in the case of the EFIE—HPD and remains well-conditioned on multiply connected geometries.

Finally, Chapter 10 concludes this thesis and outlines possible future research directions.

Chapter 2

# Mathematical Preliminaries

Advanced mathematical concepts concerning function spaces will be frequently used in the subsequent chapters. The most important results are reviewed here. The reader may find definitions of commonly used terms such as "open" or "closed" in [Rud91]. Similarly, we presume that the reader is familiar with concepts such as normed vector spaces.

## a) Notation

"Physical vectors", that is, vectors that are situated in $\mathbb{R}^2$ or $\mathbb{R}^3$ such as the electric field $\boldsymbol{E}$, the position vector $\boldsymbol{r}$, or the surface current density $\boldsymbol{j}$, are written in a bold, italic, and serif font. We use for non-physical vectors or matrices a bold, italic, and sans-serif font (e.g., $\boldsymbol{A} \in \mathbb{R}^{n\times n}$ is a matrix), and we distinguish matrices from vectors by using capital letters for matrices and minuscules for vectors (this rule does not apply to "physical vectors", where we follow standard conventions). Scalar integral operators are denoted with a calligraphic font such as the single layer operator $\mathcal{V}$, and vector integral operators with a bold calligraphic font such as the EFIE operator $\boldsymbol{\mathcal{T}}$. There is an exception to every rule: this thesis follows the convention used in most textbooks that the space of test functions $\mathcal{D}(\Omega)$ and the Schwartz space $\mathcal{S}(\Omega)$ are denoted with a calligraphic letter.

## b) Surfaces and Mathematical Operators

This thesis deals with the solution of electromagnetic scattering problems by three-dimensional obstacles. Mathematically, such an obstacle can be considered as a subset $\Omega \subset \mathbb{R}^3$. In order to obtain results on the existence and regularity of a

solution, this subset cannot be arbitrary. The less regular such a set is, the more difficult it becomes to obtain rigorous mathematical statements. First of all, we require that $\Omega$ is a domain.

**Definition 2.1** (Domain)**.** A domain is a connected, open subset $\Omega$ of a finite dimensional vector space.

Since the focus is on the modeling of realistic scattering problems, it is presupposed in the following that $\Omega$ is a bounded domain. In order to define function spaces, in which we can seek for a solution of the scattering problem, we need to make statements on the regularity of the surface.[6]

To impose more constraints on $\Omega$, we need to introduce the classical $C^k$-function spaces. As a concise way of denoting derivatives, we define a derivative operator and use the multi-index notation: a vector $\boldsymbol{\alpha} = (\alpha_1, \alpha_2, \dots, \alpha_d)$ for $d \in \mathbb{N}$ with $\alpha_i \in \mathbb{N}_0$ is called a multi-index. Its absolute value is $|\boldsymbol{\alpha}| = \alpha_1 + \dots + \alpha_d$. Then we define the derivative operator

$$\mathrm{D}^{\boldsymbol{\alpha}} u := \begin{cases} \left(\frac{\partial}{\partial x}\right)^{\alpha_1} \left(\frac{\partial}{\partial y}\right)^{\alpha_2} u(\boldsymbol{r}), & \text{for } d = 2, \\ \left(\frac{\partial}{\partial x}\right)^{\alpha_1} \left(\frac{\partial}{\partial y}\right)^{\alpha_2} \left(\frac{\partial}{\partial z}\right)^{\alpha_3} u(\boldsymbol{r}), & \text{for } d = 3, \end{cases} \tag{2.1}$$

where, in a slight abuse of notation,

$$\boldsymbol{r} = \begin{cases} (x, y)^{\mathrm{T}} \in \mathbb{R}^2, & \text{for } d = 2, \\ (x, y, z)^{\mathrm{T}} \in \mathbb{R}^3, & \text{for } d = 3, \end{cases} \tag{2.2}$$

is the position vector. In addition, we define[7]

$$\boldsymbol{r}^{\boldsymbol{\alpha}} := \begin{cases} x^{\alpha_1} y^{\alpha_2}, & \text{for } d = 2, \\ x^{\alpha_1} y^{\alpha_2} z^{\alpha_3}, & \text{for } d = 3. \end{cases} \tag{2.3}$$

6 For the sake of simplicity, we only consider single-body problems. An extension to multibody problems is possible.

7 Clearly, these definitions can be generalized to the $n$-dimensional case. For the sake of simplicity, we constrain ourselves here to the cases which are relevant for the modeling of realistic scattering scenarios.

The set $C^k$ denotes the space of all continuous functions $u$ where $u$ is $k$-times continuously differentiable. We equip this space with the norm

$$\|u\|_{C^k(\Omega)} := \sum_{|\boldsymbol{\alpha}|\leq k} \sup_{\boldsymbol{r}\in\Omega} \left|\mathrm{D}^{\boldsymbol{\alpha}} u(\boldsymbol{r})\right| . \tag{2.4}$$

The space $C^\infty$ denotes the space of functions which have infinitely many continuous derivatives and we refer to these as smooth functions.

For a scattering problem, more relevant than the properties of $\Omega$ are the properties of it's boundary: the surface $\Gamma$. To describe it, we follow closely the treatment in [Néd01].

**Definition 2.2** (Surface)**.** Let $\Omega \subset \mathbb{R}^3$ be a domain. We call the boundary of $\Omega$,

$$\Gamma = \partial\Omega := \overline{\Omega} \setminus \Omega \tag{2.5}$$

a (two-dimensional) surface.

**Definition 2.3** (Ball $\mathbb{B}_r^d(\boldsymbol{r})$)**.** We define the $d$-dimensional ball $\mathbb{B}_r^d(\boldsymbol{r}) \subset \mathbb{R}^d$ with center $\boldsymbol{r}$ and radius $r$ as

$$\mathbb{B}_r^d(\boldsymbol{r}) := \left\{ \boldsymbol{r}' \,:\, \left|\boldsymbol{r} - \boldsymbol{r}'\right| < r \right\} . \tag{2.6}$$

**Definition 2.4** (Regular $C^k$-Surface)**.** Let $\Omega \subset \mathbb{R}^3$ be a simply connected domain and $\Gamma$ its surface. Moreover, we assume that we have a covering of $\Omega$, that is, a finite union of open sets $U_i$ with $i \in [0, p]$ and

$$\Gamma \in \bigcup_{i=0}^{p} U_i . \tag{2.7}$$

In addition, we require that

$$\Gamma \cap U_0 = \emptyset , \tag{2.8}$$

which means that $U_0$ is completely contained inside $\Gamma$. A surface is called regular when there exists a diffeomorphism[8] $\phi_i$ for each $U_i$ that maps the set $U_i$ into the unit ball $\mathbb{B}_1^3(\mathbf{0})$ such that the $\Gamma \cap U_i$ is mapped into the equatorial plane $z = 0$

8 A diffeomorphism is a bijective, continuously differentiable function whose inverse function is continuously differentiable as well.

of the unit ball, $\Omega \cap U_i$ is mapped into the region $z < 0$ of the unit ball, and $(\mathbb{R}^3 \setminus \overline{\Omega}) \cap U_i$ is mapped into the region $z > 0$ of the unit ball. A surface is of class $C^k$ if the diffeomorphisms $\phi_i$ are of class $C^k$. If $\phi_i \in C^\infty$, then we speak of a smooth surface.

The covering of $\Omega$ and the diffeomorphisms $\phi_i$ are called atlas and the pairs $(U_i, \phi_i)$ are called charts. If $\phi_i$ are Lipschitz functions, that is, there is a constant $M > 0$ such that

$$\left|\phi_i^{-1}(\boldsymbol{r}) - \phi_i^{-1}(\boldsymbol{r}')\right| \leq M\left|\boldsymbol{r} - \boldsymbol{r}'\right| \quad \text{for all } \boldsymbol{r}, \boldsymbol{r}' \in \mathbb{B}_1^3(\boldsymbol{0}) \tag{2.9}$$

holds, then $\Gamma$ is a Lipschitz surface.

*Remark.* These charts are not only useful for defining differentiable operators, but also for introducing Sobolev spaces on surfaces.

If $\Omega$ is multiply connected, then more than one set $U_0$ is needed to describe its interior [Néd01]. Since we are interested in the definition of surface operators and since their definition is the same for simply and for multiply connected geometries, we assume without loss of generality that $\Omega$ is simply connected (and thereby we do not make the mathematical framework unnecessarily complicated).

This section follows closely the definitions in [Néd01]. Thus, we avoid to introduce the language of differential forms and the framework of differential geometry. In the following, it is assumed that $\Omega$ is a bounded domain with a smooth surface. It is possible to extend the definitions of the mathematical operators to Lipschitz surfaces. While for scalar functions there is only little difference when dealing with a Lipschitz surface, the treatment of vector fields becomes more complicated since, for example, the surface normal is not defined on corners and edges of the surface. This thesis deals with vector fields and their corresponding function spaces in order to justify the choice of expansion and testing functions. For this justification, there is virtually no difference between smooth or Lipschitz surfaces. The objective at the heart of this thesis, however, is the introduction of new preconditioning paradigms. The novel formulations depend on scalar integral equations and by using quasi-Helmholtz decompositions we connect them to the electromagnetic integral equations (i.e., vector integral equations). Thus the benefit of discussing the general Lipschitz case is limited, in fact, due to the more intricate framework, it might even obfuscate the objective of this thesis. The interested reader may find more details on this general setting in [Cos88; BC01b; BC01a; BCS02b; Buf03].

The function

$$\delta(\boldsymbol{r}) = \inf_{\boldsymbol{r}' \in \Gamma} \left| \boldsymbol{r} - \boldsymbol{r}' \right| \tag{2.10}$$

denotes the minimal distance of the point $\boldsymbol{r}$ to the surface $\Gamma$. We define the tubular neighborhood of $\Gamma$ as

$$\Gamma_\varepsilon = \left\{ \boldsymbol{r} \,:\, \delta(\boldsymbol{r}) < \varepsilon \right\}. \tag{2.11}$$

If $\varepsilon$ is small enough, then all $\boldsymbol{r} \in \Gamma_\varepsilon$ have a unique projection $\mathcal{P}(\boldsymbol{r})$ onto $\Gamma$ such that

$$\left| \boldsymbol{r} - \mathcal{P}(\boldsymbol{r}) \right| = \delta(\boldsymbol{r}). \tag{2.12}$$

Since it is assumed that $\Gamma$ is smooth, every point on it admits a tangent plane and the vector $\boldsymbol{r} - \mathcal{P}(\boldsymbol{r})$ is normal to it. Furthermore, we choose the open cover of $\Gamma$ such that $U_i$, $i > 0$ are completely contained in $\Gamma_\varepsilon$. We can then define the unit normal directed to the exterior as

$$\hat{\boldsymbol{n}}(\mathcal{P}(\boldsymbol{r})) = \operatorname{grad} \delta(\boldsymbol{r}), \quad \forall \boldsymbol{r} \in \overline{\Omega}^{\mathrm{c}}, \tag{2.13}$$

$$\hat{\boldsymbol{n}}(\mathcal{P}(\boldsymbol{r})) = -\operatorname{grad} \delta(\boldsymbol{r}), \quad \forall \boldsymbol{r} \in \Omega. \tag{2.14}$$

where $\overline{\Omega}^{\mathrm{c}}$ is the complement of the closure of $\Omega$. The points $\boldsymbol{r} \in \Gamma_\varepsilon$ can be described using the orthogonal splitting

$$\boldsymbol{r} = \mathcal{P}(\boldsymbol{r}) + s\hat{\boldsymbol{n}}(\mathcal{P}(\boldsymbol{r})), \quad -\varepsilon < s < \varepsilon, \tag{2.15}$$

$$s = \begin{cases} +\delta(\boldsymbol{r}), & \forall \boldsymbol{r} \in \overline{\Omega}^{\mathrm{c}}, \\ -\delta(\boldsymbol{r}), & \forall \boldsymbol{r} \in \Omega. \end{cases} \tag{2.16}$$

We define the pieces of surface $\Gamma_i = U_i \cap \Gamma$ and note that each is parametrized by a diffeomorphism $\phi_i^{-1}$ which maps by definition from the two-dimensional unit ball $\mathbb{B}_1^2(\mathbf{0})$ to $\Gamma_i$. Let $\xi_1$ and $\xi_2$ be the variables associated with this diffeomorphism. Then we have the decomposition

$$\boldsymbol{r}(\xi_1, \xi_2, s) = \boldsymbol{r}'(\xi_1, \xi_2) + s\hat{\boldsymbol{n}}(\xi_1, \xi_2), \quad -\varepsilon < s < \varepsilon, \tag{2.17}$$

which is used throughout this section. This allows to define a lifting for scalar functions $u$ defined on $\Gamma$: we have a natural extension $\tilde{u}(\boldsymbol{r})$ into the three-dimensional space surrounding the surface by defining

$$\tilde{u}(\boldsymbol{r}) = u(\mathcal{P}(\boldsymbol{r})). \tag{2.18}$$

This lifting enables us to obtain the surface equivalences of operators such as the gradient or the curl operator.

**Definition 2.5** (Surface Gradient)**.** The surface gradient is defined as

$$\operatorname{grad}_\Gamma u := \operatorname{grad} \tilde{u}_{|\Gamma}\,. \tag{2.19}$$

**Definition 2.6** (Surface Curl)**.** The surface curl is

$$\mathbf{curl}_\Gamma u := \operatorname{curl}\big(\tilde{u}\hat{\boldsymbol{n}}\big)_{|\Gamma}\,. \tag{2.20}$$

**Definition 2.7** (Laplace-Beltrami Operator)**.** The Laplace-Beltrami operator is

$$\Delta_\Gamma u := \operatorname{div}_\Gamma \operatorname{grad}_\Gamma u = -\operatorname{curl}_\Gamma \mathbf{curl}_\Gamma u\,. \tag{2.21}$$

Given that $\hat{\boldsymbol{n}}$ is defined as the gradient of the distance function and given the vector calculus formula [Bro+08]

$$\operatorname{curl}(u\boldsymbol{v}) = \operatorname{grad} u \times \boldsymbol{v} + u \operatorname{curl} \boldsymbol{v} \tag{2.22}$$

we obtain

$$\mathbf{curl}_\Gamma u = \operatorname{grad}_\Gamma u \times \hat{\boldsymbol{n}}\,. \tag{2.23}$$

For defining the surface divergence and the surfacic curl, we need a lifting operator for vector fields. To this end, we first introduce the family of parallel surfaces

$$\Gamma_s = \left\{ \boldsymbol{r} \,:\, \boldsymbol{r} = \boldsymbol{r}' + s\hat{\boldsymbol{n}}(\boldsymbol{r}'); \boldsymbol{r}' \in \Gamma \right\}. \tag{2.24}$$

**Definition 2.8** (Curvature Operator)**.** The curvature operator is defined by

$$\boldsymbol{\mathcal{R}}_s = \operatorname{grad} \hat{\boldsymbol{n}}(\boldsymbol{r})\,. \tag{2.25}$$

It is a matrix-valued operator and we set, for notational convenience, $\boldsymbol{\mathcal{R}} := \boldsymbol{\mathcal{R}}_0$.

This allows us to define the transport of tangential vectors fields $\boldsymbol{v}$ into the tubular neighborhood $\Gamma_\varepsilon$ by defining

$$\widetilde{\boldsymbol{v}}(\boldsymbol{r}) = \boldsymbol{v}(\boldsymbol{r}') - s\boldsymbol{\mathcal{R}}_s(\boldsymbol{r})\boldsymbol{v}(\boldsymbol{r}')\,. \tag{2.26}$$

**Definition 2.9** (Surface Divergence)**.** The surface divergence of a tangent vector field $\boldsymbol{v}$ is

$$\operatorname{div}_\Gamma \boldsymbol{v} = \operatorname{div} \widetilde{\boldsymbol{v}}_{|\Gamma} \tag{2.27}$$

**Definition 2.10** (Surfacic Curl)**.** The surfacic curl of a tangent vector field $\boldsymbol{v}$ is

$$\operatorname{curl}_\Gamma \boldsymbol{v} = \left(\operatorname{curl} \widetilde{\boldsymbol{v}} \cdot \hat{\boldsymbol{n}}\right)_{|\Gamma} \tag{2.28}$$

**Definition 2.11** (Hodge Operator)**.** The Hodge operator (i.e., the vectorial Laplacian) of a tangent vector field $\boldsymbol{v}$ is

$$\Delta_\Gamma \boldsymbol{v} = \operatorname{grad}_\Gamma \operatorname{div}_\Gamma \boldsymbol{v} - \mathbf{curl}_\Gamma \operatorname{curl}_\Gamma \boldsymbol{v}\,. \tag{2.29}$$

Since we have diffeomorphisms $\phi_i$ with associated coordinates $\xi_1$ and $\xi_2$, we can also state more explicit forms of the surface operators. To this end, we need to define an explicit basis for the tangent plane at each point $\boldsymbol{r} \in \Gamma_s$. Such a basis is given by

$$\boldsymbol{e}_1(\boldsymbol{r}) = \boldsymbol{e}_1(\boldsymbol{r}', s) = \frac{\partial \boldsymbol{r}}{\partial \xi_1} + s\frac{\partial \hat{\boldsymbol{n}}}{\partial \xi_1} = \boldsymbol{e}_1(\boldsymbol{r}') + s\boldsymbol{\mathcal{R}}(\boldsymbol{r}')\boldsymbol{e}_1(\boldsymbol{r}')\,, \tag{2.30}$$

$$\boldsymbol{e}_2(\boldsymbol{r}) = \boldsymbol{e}_2(\boldsymbol{r}', s) = \frac{\partial \boldsymbol{r}'}{\partial \xi_2} + s\frac{\partial \hat{\boldsymbol{n}}}{\partial \xi_2} = \boldsymbol{e}_2(\boldsymbol{r}') + s\boldsymbol{\mathcal{R}}(\boldsymbol{r}')\boldsymbol{e}_2(\boldsymbol{r}')\,. \tag{2.31}$$

If $\boldsymbol{v}$ is a vector in the tangent plane, it can be written as

$$\boldsymbol{v} = v^1 \boldsymbol{e}_1 + v^2 \boldsymbol{e}_2\,. \tag{2.32}$$

This allows to introduce the metric tensor

$$g_{ij} = \boldsymbol{e}_i \cdot \boldsymbol{e}_j\,, \tag{2.33}$$

which links the tangent with the cotangent plane[9]. More precisely, the metric tensor can be written as a two by two matrix, and thus its inverse is $\boldsymbol{g}^{-1}$. The entries of this matrix are denoted as $g^{ij}$ and we can define the basis vectors of the cotangent plane as

$$\boldsymbol{e}^i = \sum_{j=1}^{2} g^{ij} \boldsymbol{e}_j\,. \tag{2.34}$$

9 The cotangent plane is the dual space of the tangent plane. For the definition of dual space, see Definition 2.13.

Then we have

$$(\boldsymbol{e}^i \cdot \boldsymbol{e}_j) = \delta^i_j\,, \tag{2.35}$$

where $\delta^i_j$ denotes the Kronecker delta and thus

$$\boldsymbol{v} = v_1 \boldsymbol{e}^1 + v_2 \boldsymbol{e}^2\,, \tag{2.36}$$

with

$$v_i = \sum_{j=1}^{2} g_{ij}\, v^j\,. \tag{2.37}$$

Using these definitions, explicit formulas of the surface operators are available: the surface gradient of the function $u$ is

$$\operatorname{grad}_\Gamma u = \frac{\partial u}{\partial \xi_1}\boldsymbol{e}^1 + \frac{\partial u}{\partial \xi_2}\boldsymbol{e}^2\,, \tag{2.38}$$

and the surface curl is

$$\mathbf{curl}_\Gamma u = \frac{1}{\sqrt{\det \boldsymbol{g}}}\left(\frac{\partial u}{\partial \xi_2}\boldsymbol{e}^1 - \frac{\partial u}{\partial \xi_1}\boldsymbol{e}^2\right). \tag{2.39}$$

We obtain for the surface divergence of a contravariant tangential vector field

$$\operatorname{div}_\Gamma \boldsymbol{v} = \frac{1}{\sqrt{\det \boldsymbol{g}}}\left(\frac{\partial}{\partial \xi_1}\sqrt{\det \boldsymbol{g}}\, v^1 + \frac{\partial}{\partial \xi_2}\sqrt{\det \boldsymbol{g}}\, v^2\right), \tag{2.40}$$

and the surfacic curl of a covariant tangential vector

$$\operatorname{curl}_\Gamma \boldsymbol{v} = \frac{1}{\sqrt{\det \boldsymbol{g}}}\left(\frac{\partial}{\partial x_1} v_2 - \frac{\partial}{\partial x_2} v_1\right). \tag{2.41}$$

For the Laplace-Beltrami operator, we obtain the expression

$$\begin{aligned}\Delta_\Gamma u = \operatorname{div}_\Gamma \operatorname{grad}_\Gamma u = -\operatorname{curl}_\Gamma \mathbf{curl}_\Gamma u \\ = \frac{1}{\sqrt{\det \boldsymbol{g}}}\left(\sum_{i,j=1}^{2} \frac{\partial}{\partial \xi_i}\sqrt{\det \boldsymbol{g}}\, g^{ij}\frac{\partial u}{\partial \xi_j}\right).\end{aligned} \tag{2.42}$$

These surfaces operators are related to each other, in fact, the surface divergence is the adjoint operator of the surface gradient, and likewise the surfacic curl is the adjoint operator of the surface curl.

**Theorem 2.1** ([Néd01]). *Let $u \in C^1(\Gamma)$ be a function and $\boldsymbol{v} \in \left(C^1(\Gamma)\right)^2$ a tangent vector field defined on the surface $\Gamma$. We have the following Stokes identities:*

$$\int_\Gamma \left(\operatorname{grad}_\Gamma u \cdot \boldsymbol{v}\right) \mathrm{d}S(\boldsymbol{r}) = -\int_\Gamma u \operatorname{div}_\Gamma \boldsymbol{v} \mathrm{d}S(\boldsymbol{r}), \tag{2.43}$$

$$\int_\Gamma (\mathbf{curl}_\Gamma u \cdot \boldsymbol{v}) \mathrm{d}S(\boldsymbol{r}) = +\int_\Gamma u \operatorname{curl}_\Gamma \boldsymbol{v} \mathrm{d}S(\boldsymbol{r}), \tag{2.44}$$

$$\operatorname{div}_\Gamma \mathbf{curl}_\Gamma u = 0, \tag{2.45}$$

$$\operatorname{curl}_\Gamma \operatorname{grad}_\Gamma = 0, \tag{2.46}$$

$$\operatorname{div}_\Gamma(\boldsymbol{v} \times \hat{\boldsymbol{n}}) = \operatorname{curl}_\Gamma \boldsymbol{v}. \tag{2.47}$$

## c) Sobolev Spaces

We have qualified surfaces by using the classical $C^k$-function spaces (i.e., by requiring that the diffeomorphisms $\phi_i$ are members of such a space). Correspondingly, one could presume that we use these function spaces to qualify the solution of the integral equations we are faced with. This, however, is not practical since these function spaces are defined by the strong derivative;[10] a first step to broaden the domain in which we search for a solution is to introduce the weak derivative. The function spaces associated with the weak derivative are the Sobolev spaces. What makes the Sobolev spaces we encounter in the description of the scattering and radiation problems particularly suitable is the fact they are Hilbert spaces, that is, they come with an inner product. This inner product corresponds to the physical energy of the solution, and by searching for a solution in a Sobolev space, we ask for a solution with finite energy [HK97], a result one would reasonably expect from a physical point of view. This section follows closely the treatment in [Ste10].

10 An example for the limitation imposed by the strong derivative is the one-dimensional scalar wave equation $c^2\partial^2 u/\partial x^2 - \partial^2 u/\partial t^2 = 0$, where in the distributional sense every function of the form $f(x \pm ct)$ is a solution even though the solution might not be twice continuously differentiable.

## $\alpha$) Generalized Derivatives, Distributions, and Sobolev Spaces

Let $u$ be a function $u : A \subset \mathbb{R}^3 \longrightarrow \mathbb{C}$. The support of $u$ is defined as

$$\operatorname{supp} u := \overline{\left\{ x \in A : u(x) \neq 0 \right\}}. \tag{2.48}$$

The set

$$\mathcal{D}(\Omega) = \left\{ u \in C^\infty(\Omega) : \operatorname{supp} u \subset \Omega \right\} \tag{2.49}$$

is the space of test functions, that is, the space of smooth functions with compact support.

In order to define the weak derivative, we need function spaces that take into account the integrability of a function; such spaces are the $L^p(\Omega)$-spaces, which simply speaking, contain all functions with bounded norm[11]

$$\|u\|_{L^p(\Omega)} := \left( \int_\Gamma |u(\boldsymbol{r})|^p \, \mathrm{d}V(\boldsymbol{r}) \right)^{1/p}, \quad \text{for } 1 \leq p < \infty. \tag{2.50}$$

The $L^2$-space is a Hilbert space equipped with the inner product

$$(u, v)_{L^2(\Omega)} = \int_\Omega \overline{u(\boldsymbol{r})} v(\boldsymbol{r}) \mathrm{d}V(\boldsymbol{r}), \tag{2.51}$$

where $\overline{u(\boldsymbol{r})}$ is the conjugate of $u(\boldsymbol{r})$. For defining the weak derivative in the broadest possible sense, we also need the space of locally integrable functions

$$L^1_{\mathrm{loc}}(\Omega) = \left\{ u : \int_K \left|u(\boldsymbol{r})\right| \mathrm{d}V(\boldsymbol{r}) < \infty, \text{for all compact subsets } K \subset \Omega \right\}. \tag{2.52}$$

**Definition 2.12** (Weak derivative)**.** A function $v \in L^1_{\mathrm{loc}}(\Omega)$ is the $\boldsymbol{\alpha}$th weak derivative of the function $u$ if for all test functions $\varphi \in \mathcal{D}(\Omega)$, we have

$$\int_\Omega v \varphi \mathrm{d}V(\boldsymbol{r}) = (-1)^{|\boldsymbol{\alpha}|} \int_\Omega u \mathrm{D}^{\boldsymbol{\alpha}} \varphi \mathrm{d}V(\boldsymbol{r}). \tag{2.53}$$

We denote the weak derivative as $\mathrm{D}^{\boldsymbol{\alpha}} u := v$.

11 Formally, we should write that the space $L^p(\Omega)$ contains all equivalence classes of measurable functions $u$ defined on $\Omega$ such that $|u|^p$ is integrable for $1 \leq p < \infty$. The introduction of equivalence classes is necessary to ensure that $L^p(\Omega)$ has only one element whose norm is zero. See [Rud91].

Not all functions possess a weak derivative, one just has to think of the step function. A further generalization of derivatives is possible by resorting to distribution theory.

**Definition 2.13** (Topological Dual Space)**.** Let $V$ be a topological vector space, that is, a vector space on which a topology is defined.[12] Then the set of all continuous and linear functionals on $V$ is denoted as $V'$.

*Remark.* When we speak of a dual space in this thesis, we always mean the topological dual space.

**Definition 2.14** ([Ste10])**.** A complex valued continuous linear functional $T$ acting on $\mathcal{D}(\Omega)$ is called a distribution. The functional $T$ is continuous on $\mathcal{D}(\Omega)$ if $\varphi_k \longrightarrow \varphi$ in $\mathcal{D}(\Omega)$ always implies $T(\varphi_k) \longrightarrow T(\varphi)$. The set of all distributions is denoted by $\mathcal{D}'(\Omega)$.

Any functional

$$T_u(\varphi) := \int_\Omega u(\boldsymbol{r})\varphi(\boldsymbol{r})\mathrm{d}V(\boldsymbol{r}) \quad \text{for } \varphi \in \mathcal{D}(\Omega) \tag{2.54}$$

with $u \in L^1_{\mathrm{loc}}(\Omega)$ is continuous and therefore a distribution. Distributions of the type $T_u$ are called regular. Distributions which cannot be expressed by such an integral are called singular. Since any function $u \in L^1_{\mathrm{loc}}(\Omega)$ can be associated with a distribution $T_u$, we follow the common practice and write $u$ instead of $T_u$.

**Definition 2.15** (Derivatives of Distributions)**.** Let $T \in \mathcal{D}'(\Omega)$ and $\boldsymbol{\alpha}$ be a multi-index. Then the distribution $\mathrm{D}^{\boldsymbol{\alpha}} T \in \mathcal{D}'(\Omega)$ is defined as

$$\langle \mathrm{D}^{\boldsymbol{\alpha}} T, \varphi \rangle = (-1)^{|\boldsymbol{\alpha}|} \langle T, \mathrm{D}^{\boldsymbol{\alpha}} \varphi \rangle \tag{2.55}$$

for all $\varphi \in \mathcal{D}(\Omega)$.

**Definition 2.16** (Schwartz Space, [Ste10])**.** The space $\mathcal{S}(\mathbb{R}^d)$ is the space of functions $\varphi \in C^\infty(\mathbb{R}^d)$ satisfying

$$\|\varphi\|_{k,l} := \sup_{\boldsymbol{r}\in\mathbb{R}^d} \left(|\boldsymbol{r}|^k + 1\right) \sum_{|\boldsymbol{\alpha}|\le l} \left|\mathrm{D}^{\boldsymbol{\alpha}} \varphi(\boldsymbol{r})\right| < \infty \quad \text{for all } k, l \in \mathbb{N}_0 \,. \tag{2.56}$$

12 Virtually any vector space we encounter in this thesis will at least be a normed or even be a Hilbert space (and so they are also topological vector spaces). The reason why we have to mention topological vector spaces here, is that $\mathcal{D}$ is not a normed space (in fact, it is not even a metric space).

Any function $\varphi \in \mathcal{S}(\mathbb{R}^d)$ and all of its derivatives decrease faster for $|\boldsymbol{r}| \longrightarrow \infty$ than any polynomial. This ensures that the Fourier transformation is well-defined for any function $\varphi \in \mathcal{S}(\mathbb{R}^d)$ and we denote its Fourier transform as $\widehat{\varphi}$, which we define as

$$\widehat{\varphi}(\boldsymbol{\xi}) := (\mathcal{F}\varphi)(\boldsymbol{\xi}) = (2\pi)^{-d/2} \int_{\mathbb{R}^d} \mathrm{e}^{-\mathrm{i}\boldsymbol{r}\cdot\boldsymbol{\xi}} \varphi(\boldsymbol{r}) \mathrm{d}V(\boldsymbol{r}) \quad \text{for } \boldsymbol{\xi} \in \mathbb{R}^d . \tag{2.57}$$

We could have defined the Fourier transformation also for functions residing in $\mathcal{D}(\mathbb{R}^d)$; the Fourier transformation of these functions, however, does not necessarily reside in $\mathcal{D}(\mathbb{R}^d)$. In contrast, the mapping $\mathcal{F} : \mathcal{S}(\mathbb{R}^d) \longrightarrow \mathcal{S}(\mathbb{R}^d)$ is invertible and the inverse Fourier transformation is [Ste10]

$$\left(\mathcal{F}^{-1}\widehat{\varphi}\right)(\boldsymbol{r}) = (2\pi)^{-d/2} \int_{\mathbb{R}^d} \mathrm{e}^{\mathrm{i}\boldsymbol{r}\cdot\boldsymbol{\xi}} \widehat{\varphi}(\boldsymbol{r}) \mathrm{d}V(\boldsymbol{\xi}) \quad \text{for } \boldsymbol{r} \in \mathbb{R}^d . \tag{2.58}$$

Due to the smoothness of the functions of $\mathcal{S}(\mathbb{R}^d)$, the derivative is well-defined for any multi-index $\boldsymbol{\alpha}$ by

$$\mathrm{D}^{\boldsymbol{\alpha}}\left(\mathcal{F}\varphi\right)(\xi) = (-\mathrm{i})^{|\boldsymbol{\alpha}|} \mathcal{F}\left(\boldsymbol{r}^{\boldsymbol{\alpha}}\varphi\right)(\xi) \tag{2.59}$$

and

$$\boldsymbol{\xi}^{\boldsymbol{\alpha}}\left(\mathcal{F}\varphi\right)(\xi) = (-\mathrm{i})^{|\boldsymbol{\alpha}|} \mathcal{F}\left(\mathrm{D}^{\boldsymbol{\alpha}}\varphi\right)(\xi) . \tag{2.60}$$

We denote its dual space $\mathcal{S}'(\mathbb{R}^d)$ following Definition 2.14, that is, it is the space of all linear and continuous complex valued functionals over $\mathcal{S}(\mathbb{R}^d)$. The elements $T \in \mathcal{S}'(\mathbb{R}^d)$ are called tempered distributions, and we define their Fourier transformation $\widehat{T} \in \mathcal{S}'(\mathbb{R}^d)$ as

$$\widehat{T}(\varphi) := T(\widehat{\varphi}) \quad \text{for } \varphi \in \mathcal{S}(\mathbb{R}^d) . \tag{2.61}$$

Also for tempered distributions, the mapping $\mathcal{F} : \mathcal{S}'(\mathbb{R}^d) \longrightarrow \mathcal{S}'(\mathbb{R}^d)$ is invertible and the inverse Fourier transformation is defined as

$$\left(\mathcal{F}^{-1}T\right)\varphi := T(\mathcal{F}^{-1}\varphi) \quad \text{for } \varphi \in \mathcal{S}(\mathbb{R}^d) . \tag{2.62}$$

The identities (2.59) and (2.60) hold for tempered distributions as well. As a final ingredient for the definition of Sobolev spaces, we need the Bessel potential operator, which is defined by

$$\left(\mathcal{J}^s u\right)(\boldsymbol{r}) := (2\pi)^{-d/2} \int_{\mathbb{R}^d} \left(1 + |\boldsymbol{\xi}|^2\right)^{s/2} \widehat{u}(\xi) \mathrm{e}^{\mathrm{i}\boldsymbol{r}\cdot\boldsymbol{\xi}} \mathrm{d}V(\boldsymbol{\xi}), \quad \xi \in \mathbb{R}^d \tag{2.63}$$

for $s \in \mathbb{R}$ and $u \in \mathcal{S}(\mathbb{R}^d)$. The operator $\mathcal{J}^s u : \mathcal{S}(\mathbb{R}^d) \longrightarrow \mathcal{S}(\mathbb{R}^d)$ is a bounded and linear operator. Thus we have

$$(\mathcal{J}^s u)(\boldsymbol{r}) \equiv \mathcal{F}^{-1}\left(\left(1+|\boldsymbol{\xi}|^2\right)^{s/2}(\mathcal{F}u)(\boldsymbol{\xi})\right)(\boldsymbol{r})\,. \tag{2.64}$$

If we compare this equation with (2.60), we find that $\mathcal{J}^s$ is a differential operator of order $s$ (and since we allowed $s$ to be a real number, we thereby obtain a notion of fractional derivatives). As we did it before with the derivative operator and the Fourier transformation operator, we can generalize the Bessel operator to tempered distributions $T \in \mathcal{S}'(\mathbb{R}^d)$ by defining

$$\left(\mathcal{J}^s T\right)(\varphi) := T\left(\mathcal{J}^s \varphi\right) \quad \text{for all } \varphi \in \mathcal{S}\left(\mathbb{R}^d\right). \tag{2.65}$$

The operator $\mathcal{J}^s : \mathcal{S}'(\mathbb{R}^d) \longrightarrow \mathcal{S}'(\mathbb{R}^d)$ is bounded and linear.

**Definition 2.17** (Sobolev space $H^s$)**.** The Sobolev space $H^s$, $s \in \mathbb{R}$, is defined as

$$H^s(\mathbb{R}^d) := \left\{ u \in \mathcal{S}'(\mathbb{R}^d) : \|u\|_{H^s(\mathbb{R}^d)} < \infty \right\} \tag{2.66}$$

where

$$\|u\|_{H^s(\mathbb{R}^d)} := \left\|J^s u\right\|^2_{L_2(\mathbb{R}^d)} = \int_{R^d}\left(1+|\boldsymbol{\xi}|^2\right)^s \left|\widehat{u}(\boldsymbol{\xi})\right| \mathrm{d}V(\boldsymbol{\xi})\,. \tag{2.67}$$

*Remark.* The space $H^s$ is a Hilbert space, where the inner product is defined as

$$(u,v)_{H^s(\mathbb{R}^d)} := \left(\mathcal{J}^s u, \mathcal{J}^s v\right)_{L^2(\mathbb{R}^d)}. \tag{2.68}$$

We note that we have $H^0 = L^2$.

Lastly, we need to define $H^s(\Omega)$, where $\Omega \subset \mathbb{R}^d$ is some bounded domain. We obtain this space by restriction, that is, we define

$$H^s(\Omega) := \left\{ v = \tilde{v}_{|\Omega} : \tilde{v} \in H^s(\mathbb{R}^d) \right\} \tag{2.69}$$

and we equip this set with the norm

$$\|v\|_{H^s(\Omega)} := \left\{ \inf_{\tilde{v} \in H^s(\mathbb{R}^d), \tilde{v}_{|\Omega} = v} \|\tilde{v}\|_{H^s(\mathbb{R}^d)} \right\} \tag{2.70}$$

If the domain $\Omega$ is unbounded (e.g., the exterior scattering scenario), then the appropriate function spaces are $H^s_{\mathrm{loc}}(\Omega)$, which are defined in the same fashion as $L^1_{\mathrm{loc}}(\Omega)$.

## $\beta$) Sobolev Spaces on Surfaces

For defining the Sobolev spaces on the boundary $\Gamma$, we have to remember that we are in the possession of an overlapping piecewise parametrization of $\Gamma$, where

$$\Gamma = \bigcup_{i=1}^{J} \Gamma_i\,, \quad \Gamma_i := \left\{ \boldsymbol{r} \in \mathbb{R}^3 \,:\, \boldsymbol{r} = \phi_i^{-1}(\boldsymbol{r'}) \text{ for } \boldsymbol{r'} \in \mathbb{B}_1^2(\mathbf{0}) \right\}. \tag{2.71}$$

As mentioned in Section 2.b, it is assumed that $\Gamma$ is smooth. In addition, we introduce the partition of unity of non-negative cutoff functions $\chi_i \in \mathcal{D}(\mathbb{R}^3)$ such that

$$\sum_{i=1}^{J} \chi_i(\boldsymbol{r}) = 1\,, \quad \text{for } \boldsymbol{r} \in \Gamma\,, \tag{2.72}$$

and

$$\chi_i = 0\,, \quad \text{for } \boldsymbol{r} \in \Gamma \setminus \Gamma_i\,. \tag{2.73}$$

For any function $v$ defined on $\Gamma$, we can define functions $v_i := \chi_i v$ such that

$$v(\boldsymbol{r}) = \sum_{i=1}^{J} v_i(\boldsymbol{r}) \quad \text{for } \boldsymbol{r} \in \Gamma\,. \tag{2.74}$$

Using the parametrization $\phi_i^{-1}$, we define

$$\tilde{v}_i(\boldsymbol{r'}) := v_i(\phi_i^{-1}(\boldsymbol{r'})) = v_i(\boldsymbol{r})\,, \quad \forall \boldsymbol{r'} \in \mathbb{B}_1^2(\mathbf{0})\,. \tag{2.75}$$

For the parameter domain $\mathbb{B}_1^2(\mathbf{0})$, we have the appropriate Sobolev spaces at hand so that

$$\|v\|_{L^2_\phi(\Gamma)} := \left( \sum_{i=1}^{J} \|\tilde{v}_i\|^2_{L^2(\mathbb{B}_1^2(\mathbf{0}))} \right)^{1/2} \tag{2.76}$$

and

$$\|v\|_{H^s_\phi(\Gamma)} := \left( \sum_{i=1}^{J} \|\tilde{v}_i\|^2_{H^s(\mathbb{B}_1^2(\mathbf{0}))} \right)^{1/2}. \tag{2.77}$$

Then the spaces $L^2_\phi(\Gamma)$ and $H^s_\phi(\Gamma)$ contain all functions defined on the surface $\Gamma$ for which the norm is bounded.

Equivalent norms[13], which are easier to use since the parametrization is not required explicitly, are

$$\|v\|_{L^2(\Gamma)} := \sqrt{(v, v)_{L^2(\Gamma)}} \tag{2.79}$$

induced by the inner product

$$(v, u)_{L^2(\Gamma)} = \int_\Gamma v(\boldsymbol{r}) u(\boldsymbol{r}) \mathrm{d}S(\boldsymbol{r}) , \tag{2.80}$$

and the Sobolev-Slobodeckii norm

$$\|v\|_{H^s(\Gamma)} := \left( \|v\|^2_{L^2(\Gamma)} + \int_\Gamma \int_\Gamma \frac{\left| v(\boldsymbol{r}) - v(\boldsymbol{r}') \right|^2}{\left| \boldsymbol{r} - \boldsymbol{r}' \right|^{2+2s}} \mathrm{d}S(\boldsymbol{r}') \mathrm{d}S(\boldsymbol{r}) . \right)^{1/2} \tag{2.81}$$

If $\Gamma$ is not smooth, the maximum number of allowed derivatives depends on $\phi$. If $\phi_i \in C^{k-1,1}$, then $|s| \leq k$. In particular for Lipschitz surfaces, we have $|s| \leq 1$.

## $\gamma$) Vector Sobolev Spaces

So far we have defined all the Sobolev spaces, which we would need to model electrostatic or acoustic problems, that is, problems that can be described with scalar functions. For electromagnetic problems, however, one is faced with vector functions and we need appropriate Sobolev spaces to accommodate these functions. We define

$$\boldsymbol{H}^s(\Omega) := \left( H^s(\Omega) \right)^3 := \left\{ \boldsymbol{u} : (\boldsymbol{u})_i \in H^s(\Omega) , i = 1, 2, 3 \right\} \tag{2.82}$$

equipped with the norm

$$\|\boldsymbol{u}\|_{\boldsymbol{H}^s(\Omega)} := \sqrt{\sum_{i=1}^{3} \|(\boldsymbol{u})_i\|^2_{H^s(\Omega)}} . \tag{2.83}$$

13 Two norms $\|x\|_U$ and $\|x\|_V$ are called equivalent if there are constants $c$ and $C$ such that

$$c\|x\|_U \leq \|x\|_V \leq C\|x\|_U . \tag{2.78}$$

All norms defined on a finite-dimensional space are equivalent, but for an infinite space, this is generally not true. And as a side note: while systems resulting from a discretization are finite-dimensional, the situation becomes interesting when the discretization is refined so that the dimensionality grows. While for a certain discretization all norms are equivalent, we might not be able to find constants independent from the discretization density.

This definition readily extends to the case of $\boldsymbol{H}^s(\Gamma)$, where $\Gamma$ is a surface, and in particular we note that we have for $\boldsymbol{H}^0(\Gamma) = \boldsymbol{L}^2(\Gamma)$ the norm

$$\|\boldsymbol{u}\|_{\boldsymbol{L}^2(\Gamma)} := \sqrt{(\boldsymbol{u}, \boldsymbol{u})_{\boldsymbol{L}^2(\Gamma)}} \tag{2.84}$$

induced by the inner product

$$(\boldsymbol{u}, \boldsymbol{v}) = \int_\Gamma \boldsymbol{u}(\boldsymbol{r}) \cdot \boldsymbol{v}(\boldsymbol{r}) \mathrm{d}S(\boldsymbol{r}) \,. \tag{2.85}$$

The spaces containing tangential vector fields are

$$\boldsymbol{H}_{\mathrm{t}}^s(\Gamma) := \left\{ \boldsymbol{u} \in \boldsymbol{H}^s(\Gamma) \,:\, \boldsymbol{u} \cdot \hat{\boldsymbol{n}} = 0 \right\} \tag{2.86}$$

where $\Gamma$ is a smooth surface. Furthermore, we need the spaces

$$\boldsymbol{H}^s(\mathrm{div}_\Gamma, \Gamma) = \left\{ \boldsymbol{u} \in \boldsymbol{H}_{\mathrm{t}}^s(\Gamma) \,:\, \mathrm{div}_\Gamma \, \boldsymbol{u} \in H^s(\Gamma) \right\} \tag{2.87}$$

and

$$\boldsymbol{H}^s(\mathrm{curl}_\Gamma, \Gamma) = \left\{ \boldsymbol{u} \in \boldsymbol{H}_{\mathrm{t}}^s(\Gamma) \,:\, \mathrm{curl}_\Gamma \, \boldsymbol{u} \in H^s(\Gamma) \right\} \tag{2.88}$$

equipped with the norms

$$\|\boldsymbol{u}\|_{\boldsymbol{H}^s(\mathrm{div}_\Gamma, \Gamma)} := \|\boldsymbol{u}\|_{\boldsymbol{H}^s(\Omega)} + \|\mathrm{div}_\Gamma \, \boldsymbol{u}\|_{H^s(\Omega)} \,, \tag{2.89}$$

$$\|\boldsymbol{u}\|_{\boldsymbol{H}^s(\mathrm{curl}_\Gamma, \Gamma)} := \|\boldsymbol{u}\|_{\boldsymbol{H}^s(\Omega)} + \|\mathrm{curl}_\Gamma \, \boldsymbol{u}\|_{H^s(\Omega)} \,. \tag{2.90}$$

$$\tag{2.91}$$

We note that the spaces $\boldsymbol{H}^s(\mathrm{div}_\Gamma, \Gamma)$ and $\boldsymbol{H}^s(\mathrm{curl}_\Gamma, \Gamma)$ are dual with respect to the $\boldsymbol{L}^2$-inner product [Néd01].

Chapter 3

# Electromagnetic Theory and Integral Equation Formulations of Scattering Problems

Maxwell's equations describe the scenario which shall be solved: the scattering of electromagnetic waves from PEC obstacles in frequency domain. This chapter reviews the background material: Section 3.a introduces the necessary electromagnetic theory and derives the mixed potential formulas, which allow to compute the electromagnetic field excited by electric and magnetic current distributions. In Section 3.b, it is shown how these formulas can be used to model a scattering scenario. This chapter is closed by briefly discussing the electrostatic case in Section 3.c and by showing how integral operators can be used to obtain a solution for Laplace's equation.

## a) Maxwell's Equations and Their Solution

Since the focus is on time-harmonic problems, we assume and suppress the time-dependency $\exp(-\mathrm{i}\omega t)$ in the following, where $t$ is the time and $\omega$ the angular frequency. How the electric current density $\boldsymbol{j}$ and charge distribution $\rho_\mathrm{e}$ excite the electric field $\boldsymbol{E}$ and the magnetic field $\boldsymbol{H}$ and how these fields interact is described by Maxwell's equations [Har01]

$$\operatorname{curl} \boldsymbol{E} = \mathrm{i}\omega \boldsymbol{B}\,, \tag{3.1}$$

$$\operatorname{curl} \boldsymbol{H} = -\mathrm{i}\omega \boldsymbol{D} + \boldsymbol{j}\,, \tag{3.2}$$

$$\operatorname{div} \boldsymbol{D} = \rho_{\mathrm{e}} \,, \tag{3.3}$$

$$\operatorname{div} \boldsymbol{B} = 0 \,, \tag{3.4}$$

where $\boldsymbol{D}$ is the electric and $\boldsymbol{B}$ the magnetic flux density. The current density $\boldsymbol{j}$ and the charge distribution $\rho_{\mathrm{e}}$ are not independent since the charge must be conserved, that is, they must satisfy[14]

$$\operatorname{div} \boldsymbol{j} = \mathrm{i}\omega\rho \,. \tag{3.5}$$

The fluxes $\boldsymbol{D}$ and $\boldsymbol{B}$ are related to $\boldsymbol{E}$ and $\boldsymbol{H}$ by the constitutive relations[15]

$$\boldsymbol{D} = \boldsymbol{D}(\boldsymbol{E}, \boldsymbol{H}) \,, \tag{3.7}$$

$$\boldsymbol{B} = \boldsymbol{B}(\boldsymbol{E}, \boldsymbol{H}) \,, \tag{3.8}$$

that is, the relationship between the fields can be non-linear, (bi-)anisotropic, and space and frequency dependent. Due to the scope of this thesis, it suffices to consider piecewise homogeneous and isotropic materials, where the difference between the fields is just a multiplicative factor, so that the constitutive relations read

$$\boldsymbol{D} = \varepsilon \boldsymbol{E} = \varepsilon_{\mathrm{r}} \varepsilon_0 \boldsymbol{E} \,, \tag{3.9}$$

$$\boldsymbol{B} = \mu \boldsymbol{H} = \mu_{\mathrm{r}} \mu_0 \boldsymbol{H} \,, \tag{3.10}$$

where $\varepsilon$ is the permittivity and $\mu$ is the permeability, $\varepsilon_{\mathrm{r}}$ is the relative permittivity and $\mu_{\mathrm{r}}$ is the relative permeability, and $\varepsilon_0$ is the electric and $\mu_0$ the magnetic constant. If $\varepsilon$ or $\mu$ are piecewise constant, Maxwell's equations do not hold (in a classical sense) on the material boundary since the fields are not continuous anymore. Instead, we need to introduce continuity conditions at the interfaces which the fields must satisfy. These conditions are discussed in the next section.

While magnetic charges and currents do not exist, or at least have not been observed in nature so far, their introduction to Maxwell's equations provides a

14 In fact, if we postulate charge conservation, then (3.3) and (3.4) are a consequence of this postulate.

15 Conducting materials, which are not considered in this thesis, are introduced by a third constitutive relation

$$\boldsymbol{j} = \boldsymbol{j}(\boldsymbol{E}, \boldsymbol{H}) \,. \tag{3.6}$$

useful mathematical tool. Together with the constitutive relations and a normalization of $\boldsymbol{H}$ and $\boldsymbol{j}$ by the wave impedance

$$\eta = \sqrt{\mu/\varepsilon}\,, \tag{3.11}$$

we can write Maxwell's equations as

$$\operatorname{curl} \boldsymbol{E} = \mathrm{i}k\boldsymbol{H} - \boldsymbol{m}\,, \tag{3.12}$$
$$\operatorname{curl} \boldsymbol{H} = -\mathrm{i}k\boldsymbol{E} + \boldsymbol{j}\,, \tag{3.13}$$
$$\operatorname{div} \boldsymbol{D} = \rho_{\mathrm{e}}\,, \tag{3.14}$$
$$\operatorname{div} \boldsymbol{B} = \rho_{\mathrm{m}}\,, \tag{3.15}$$

where

$$k = 2\pi/\lambda \tag{3.16}$$
$$= \omega\sqrt{\varepsilon\mu} \tag{3.17}$$
$$= 2\pi f\sqrt{\varepsilon\mu} \tag{3.18}$$

is the wavenumber, $\lambda$ is the wavelength, and $f$ is the frequency. In other words, if $\boldsymbol{H}^{\text{classic}}$ and $\boldsymbol{j}^{\text{classic}}$ are the classically defined magnetic field and the electric current density, we define $\boldsymbol{H}^{\text{new}} = \eta\boldsymbol{H}^{\text{classic}}$ and $\boldsymbol{j}^{\text{new}} = \eta\boldsymbol{j}^{\text{classic}}$ and insert $1/\eta\boldsymbol{H}^{\text{new}}$ and $1/\eta\boldsymbol{j}^{\text{new}}$ into Maxwell's equations. Using this normalized system, the electric and magnetic field have the same unit, which simplifies the formalism.

## $\alpha$) Continuity Conditions

Let $\Omega \subset \mathbb{R}^3$ be a domain with a smooth boundary $\Gamma$. The fields are subject to the continuity conditions [Har01]

$$\hat{\boldsymbol{n}} \times \boldsymbol{E}^{+} - \hat{\boldsymbol{n}} \times \boldsymbol{E}^{-} = -\boldsymbol{m}_{\Gamma}\,, \tag{3.19}$$
$$\hat{\boldsymbol{n}} \times \boldsymbol{H}^{+} - \hat{\boldsymbol{n}} \times \boldsymbol{H}^{-} = \boldsymbol{j}_{\Gamma}\,, \tag{3.20}$$
$$\hat{\boldsymbol{n}} \cdot \boldsymbol{D}^{+} - \hat{\boldsymbol{n}} \cdot \boldsymbol{D}^{-} = \rho_{\Gamma,\mathrm{e}}\,, \tag{3.21}$$
$$\hat{\boldsymbol{n}} \cdot \boldsymbol{B}^{+} - \hat{\boldsymbol{n}} \cdot \boldsymbol{B}^{-} = \rho_{\Gamma,\mathrm{m}}\,, \tag{3.22}$$

where we used the definition

$$\boldsymbol{U}^{+}(\boldsymbol{r}) = \lim_{\boldsymbol{r}' \to \boldsymbol{r}} \boldsymbol{U}(\boldsymbol{r}), \quad \forall \boldsymbol{r}' \in \overline{\Omega}^{\mathrm{c}}, \tag{3.23}$$

$$\boldsymbol{U}^{-}(\boldsymbol{r}) = \lim_{\boldsymbol{r}' \to \boldsymbol{r}} \boldsymbol{U}(\boldsymbol{r}), \quad \forall \boldsymbol{r}' \in \Omega, \tag{3.24}$$

and $\hat{\boldsymbol{n}}$ is the surface unit normal vector directed to the exterior. The $\Gamma$ symbol in the subscript of the currents and charges indicates that these are surface densities. These densities are rather a theoretical construct and for physical applications typically zero. If one considers, however, idealized materials such as perfect electric or magnetic conductors, then the right-hand sides do not vanish. In this thesis, $\Omega$ describes a PEC object and thus the continuity equations simplify to

$$\hat{\boldsymbol{n}} \times \boldsymbol{E}^{+} = \boldsymbol{0}, \tag{3.25}$$

$$\hat{\boldsymbol{n}} \times \boldsymbol{H}^{+} = \boldsymbol{j}_{\Gamma}, \tag{3.26}$$

$$\hat{\boldsymbol{n}} \cdot \boldsymbol{D}^{+} = \rho_{\Gamma,\mathrm{e}}, \tag{3.27}$$

$$\hat{\boldsymbol{n}} \cdot \boldsymbol{B}^{+} = 0. \tag{3.28}$$

## $\beta$) Equivalence Principle

Different source distributions can lead to the same fields, a circumstance that is the fundamental idea of the equivalence principle. Let $\boldsymbol{j}_{\Omega}$ and $\boldsymbol{m}_{\Omega}$ be source distributions inside $\Omega$ and $\boldsymbol{E}$ and $\boldsymbol{H}$ the generated fields. If we assume the existence of surface current densities

$$\boldsymbol{m}_{\Gamma} = -\hat{\boldsymbol{n}} \times \boldsymbol{E}, \quad \forall \boldsymbol{r} \in \Gamma, \tag{3.29}$$

$$\boldsymbol{j}_{\Gamma} = \hat{\boldsymbol{n}} \times \boldsymbol{H}, \quad \forall \boldsymbol{r} \in \Gamma, \tag{3.30}$$

then we obtain [Har01]

$$\boldsymbol{E} = \begin{cases} \boldsymbol{E}, & \forall \boldsymbol{r} \in \overline{\Omega}^{\mathrm{c}}, \\ \boldsymbol{0}, & \forall \boldsymbol{r} \in \Omega \end{cases} \tag{3.31}$$

and

$$\boldsymbol{H} = \begin{cases} \boldsymbol{H}, & \forall \boldsymbol{r} \in \overline{\Omega}^{\mathrm{c}}, \\ \boldsymbol{0}, & \forall \boldsymbol{r} \in \Omega. \end{cases} \tag{3.32}$$

This means that we can replace the original problem by solving Maxwell's equations only in $\overline{\Omega}^{\mathrm{c}}$ subject to the boundary conditions (3.29) and (3.30). Likewise, the internal problem can be solved (with zero fields outside) by enforcing the boundary condition

$$\boldsymbol{m}_\Gamma = \hat{\boldsymbol{n}} \times \boldsymbol{E}\,, \quad \forall \boldsymbol{r} \in \Gamma\,, \tag{3.33}$$

$$\boldsymbol{j}_\Gamma = -\hat{\boldsymbol{n}} \times \boldsymbol{H}\,, \quad \forall \boldsymbol{r} \in \Gamma\,. \tag{3.34}$$

## γ) Electromagnetic Potentials, Green's Function, and Mixed Potential Formulas

The introduction of electromagnetic potentials provides an elegant means to solve Maxwell's equations since instead of solving the four Maxwell's equations it suffices to solve two vector Helmholtz equations. To obtain the potential approach, we leverage the linearity of Maxwell's equations: we split the electric and magnetic field into

$$\boldsymbol{E} = \boldsymbol{E}_{\mathrm{e}} + \boldsymbol{E}_{\mathrm{m}}\,, \tag{3.35}$$

$$\boldsymbol{H} = \boldsymbol{H}_{\mathrm{e}} + \boldsymbol{H}_{\mathrm{m}}\,, \tag{3.36}$$

where the fields $\boldsymbol{E}_{\mathrm{e}}$ and $\boldsymbol{H}_{\mathrm{e}}$ are due to electric and $\boldsymbol{E}_{\mathrm{m}}$ and $\boldsymbol{H}_{\mathrm{m}}$ due to magnetic sources. This splitting of the fields is justified by the linearity of Maxwell's equations.

In the absence of magnetic sources, the magnetic field $\boldsymbol{H}$ is solenoidal, that is,

$$\operatorname{div} \boldsymbol{H} = 0\,. \tag{3.37}$$

Therefore, we can find a vector potential $\boldsymbol{A}_{\mathrm{e}}$ such that [Har01]

$$\boldsymbol{H}_{\mathrm{e}} = \operatorname{curl} \boldsymbol{A}_{\mathrm{e}}\,. \tag{3.38}$$

Inserting this into (3.12) yields

$$\operatorname{curl}(\boldsymbol{E}_{\mathrm{e}} - \mathrm{i}k\boldsymbol{A}_{\mathrm{e}}) = \boldsymbol{0}\,, \tag{3.39}$$

which means that the total vector field $\boldsymbol{E}_{\mathrm{e}} - \mathrm{i}k\boldsymbol{A}_{\mathrm{e}}$ is conservative. Hence, there must be a scalar potential such that

$$\boldsymbol{E}_{\mathrm{e}} - \mathrm{i}k\boldsymbol{A}_{\mathrm{e}} = -\operatorname{grad} \phi_{\mathrm{e}}\,. \tag{3.40}$$

Inserting (3.38) into (3.13) yields

$$\operatorname{curl}\operatorname{curl} \boldsymbol{A}_\mathrm{e} = -\mathrm{i}k\boldsymbol{E}_\mathrm{e} + \boldsymbol{j} \tag{3.41}$$

and applying the vector identity $\operatorname{curl}\operatorname{curl} \boldsymbol{A}_\mathrm{e} = \operatorname{grad}\operatorname{div} \boldsymbol{A}_\mathrm{e} - \Delta\boldsymbol{A}_\mathrm{e}$ [Bro+08], we obtain

$$\boldsymbol{j} - \operatorname{grad}\operatorname{div} \boldsymbol{A}_\mathrm{e} + \Delta\boldsymbol{A}_\mathrm{e} = \mathrm{i}k\boldsymbol{E}_\mathrm{e}\,. \tag{3.42}$$

Combining (3.40) and (3.42), we yield

$$\boldsymbol{j} + \operatorname{grad}\operatorname{div} \boldsymbol{A}_\mathrm{e} + \Delta\boldsymbol{A}_\mathrm{e} + k^2\boldsymbol{A}_\mathrm{e} = -\operatorname{grad}\phi_\mathrm{e}\,. \tag{3.43}$$

Equation (3.38) only defines the curl of $\boldsymbol{A}_\mathrm{e}$, so we are free to choose $\operatorname{div} \boldsymbol{A}_\mathrm{e} = \mathrm{i}k\phi_\mathrm{e}$; this choice is called the Lorenz gauge. Thus we get

$$\Delta\boldsymbol{A}_\mathrm{e} + k^2\boldsymbol{A}_\mathrm{e} = -\boldsymbol{j} \tag{3.44}$$

and we find for the electric field

$$\boldsymbol{E}_\mathrm{e} = \mathrm{i}k\boldsymbol{A}_\mathrm{e} - 1/(\mathrm{i}k)\operatorname{grad}\operatorname{div} \boldsymbol{A}_\mathrm{e}\,. \tag{3.45}$$

Dually, we define

$$\boldsymbol{E}_\mathrm{m} = -\operatorname{curl} \boldsymbol{A}_\mathrm{m}\,, \tag{3.46}$$

and obtain

$$\Delta\boldsymbol{A}_\mathrm{m} + k^2\boldsymbol{A}_\mathrm{m} = -\boldsymbol{m} \tag{3.47}$$

$$\boldsymbol{H}_\mathrm{m} = \mathrm{i}k\boldsymbol{A}_\mathrm{m} - 1/(\mathrm{i}k)\operatorname{grad}\operatorname{div} \boldsymbol{A}_\mathrm{m}\,. \tag{3.48}$$

Summarizing, we have

$$\boldsymbol{E} = \mathrm{i}k\boldsymbol{A}_\mathrm{e} - 1/(\mathrm{i}k)\operatorname{grad}\operatorname{div} \boldsymbol{A}_\mathrm{e} - \operatorname{curl} \boldsymbol{A}_\mathrm{m}\,, \tag{3.49}$$

$$\boldsymbol{H} = \operatorname{curl} \boldsymbol{A}_\mathrm{e} + \mathrm{i}k\boldsymbol{A}_\mathrm{m} - 1/(\mathrm{i}k)\operatorname{grad}\operatorname{div} \boldsymbol{A}_\mathrm{m}\,. \tag{3.50}$$

A solution to (3.44) and to (3.47) can be obtained by convolving the Green's function [Har01]

$$G^k(\boldsymbol{r}, \boldsymbol{r}') = \frac{\mathrm{e}^{\mathrm{i}k\left|\boldsymbol{r},\boldsymbol{r}'\right|}}{4\pi\left|\boldsymbol{r}, \boldsymbol{r}'\right|} \tag{3.51}$$

with the current densities resulting in

$$\boldsymbol{A}_{\mathrm{e}}(\boldsymbol{r}) = \int_{\mathbb{R}^3} G^k(\boldsymbol{r}, \boldsymbol{r}')\boldsymbol{j}(\boldsymbol{r}')\mathrm{d}V(\boldsymbol{r}') \tag{3.52}$$

and

$$\boldsymbol{A}_{\mathrm{m}}(\boldsymbol{r}) = \int_{\mathbb{R}^3} G^k(\boldsymbol{r}, \boldsymbol{r}')\boldsymbol{m}(\boldsymbol{r}')\mathrm{d}V(\boldsymbol{r}')\,. \tag{3.53}$$

Therefore, we find for the electric field

$$\boldsymbol{E}(\boldsymbol{r}) = \mathrm{i}k \int_{\mathbb{R}^3} G^k(\boldsymbol{r}, \boldsymbol{r}')\boldsymbol{j}(\boldsymbol{r}')\mathrm{d}V(\boldsymbol{r}') - 1/(\mathrm{i}k)\,\mathrm{grad}\,\mathrm{div} \int_{\mathbb{R}^3} G^k(\boldsymbol{r}, \boldsymbol{r}')\boldsymbol{j}(\boldsymbol{r}')\mathrm{d}V(\boldsymbol{r}') - \mathrm{curl} \int_{\mathbb{R}^3} G^k(\boldsymbol{r}, \boldsymbol{r}')\boldsymbol{m}(\boldsymbol{r}')\mathrm{d}V(\boldsymbol{r}')\,, \tag{3.54}$$

and for the magnetic field

$$\boldsymbol{H}(\boldsymbol{r}) = \mathrm{i}k \int_{\mathbb{R}^3} G^k(\boldsymbol{r}, \boldsymbol{r}')\boldsymbol{m}(\boldsymbol{r}')\mathrm{d}V(\boldsymbol{r}') - 1/(\mathrm{i}k)\,\mathrm{grad}\,\mathrm{div} \int_{\mathbb{R}^3} G^k(\boldsymbol{r}, \boldsymbol{r}')\boldsymbol{m}(\boldsymbol{r}')\mathrm{d}V(\boldsymbol{r}') + \mathrm{curl} \int_{\mathbb{R}^3} G^k(\boldsymbol{r}, \boldsymbol{r}')\boldsymbol{j}(\boldsymbol{r}')\mathrm{d}V(\boldsymbol{r}')\,. \tag{3.55}$$

These equations for $\boldsymbol{E}$ and $\boldsymbol{H}$ are called mixed potential formulas.

If $\boldsymbol{j}$ and $\boldsymbol{m}$ are surface current densities located on a closed smooth surface $\Gamma$, then (3.52) and (3.53) hold for all $\boldsymbol{r} \notin \Gamma$ so that we may write

$$\boldsymbol{E}(\boldsymbol{r}) = \mathrm{i}k \int_{\Gamma} G^k(\boldsymbol{r}, \boldsymbol{r}')\boldsymbol{j}_\Gamma(\boldsymbol{r}')\mathrm{d}S(\boldsymbol{r}') - 1/(\mathrm{i}k)\,\mathrm{grad}\,\mathrm{div} \int_{\Gamma} G^k(\boldsymbol{r}, \boldsymbol{r}')\boldsymbol{j}_\Gamma(\boldsymbol{r}')\mathrm{d}S(\boldsymbol{r}') - \mathrm{curl} \int_{\Gamma} G^k(\boldsymbol{r}, \boldsymbol{r}')\boldsymbol{m}_\Gamma(\boldsymbol{r}')\mathrm{d}S(\boldsymbol{r}')\,, \tag{3.56}$$

and for the magnetic field

$$\boldsymbol{H}(\boldsymbol{r}) = \mathrm{i}k \int_{\Gamma} G^k(\boldsymbol{r}, \boldsymbol{r}')\boldsymbol{m}_\Gamma(\boldsymbol{r}')\mathrm{d}S(\boldsymbol{r}') - 1/(\mathrm{i}k)\,\mathrm{grad}\,\mathrm{div} \int_{\Gamma} G^k(\boldsymbol{r}, \boldsymbol{r}')\boldsymbol{m}_\Gamma(\boldsymbol{r}')\mathrm{d}S(\boldsymbol{r}') + \mathrm{curl} \int_{\Gamma} G^k(\boldsymbol{r}, \boldsymbol{r}')\boldsymbol{j}_\Gamma(\boldsymbol{r}')\mathrm{d}S(\boldsymbol{r}')\,. \tag{3.57}$$

Since for the remainder of this thesis all currents appearing will be surface currents, we omit the subscript $\Gamma$. For the limiting case that $\boldsymbol{r}$ approaches $\Gamma$, one finds for the (rotated) tangential component of the electric and the magnetic field[16]

$$\hat{\boldsymbol{n}} \times \boldsymbol{E}^{\pm} = \mathcal{T}\boldsymbol{j} + (\mp\mathcal{I}/2 + \mathcal{K})\boldsymbol{m}\,, \tag{3.58}$$

$$\hat{\boldsymbol{n}} \times \boldsymbol{H}^{\pm} = (\pm\mathcal{I}/2 - \mathcal{K})\boldsymbol{j} + \mathcal{T}\boldsymbol{m}\,, \tag{3.59}$$

where $\mathcal{I}$ is the identity operator,

$$\mathcal{K}\boldsymbol{j} = -\hat{\boldsymbol{n}} \times \operatorname{curl} \int_{\Gamma} G^k(\boldsymbol{r}, \boldsymbol{r}')\boldsymbol{j}(\boldsymbol{r}')\mathrm{d}S(\boldsymbol{r})\,, \tag{3.60}$$

and

$$\mathcal{T}\boldsymbol{j} := \mathrm{i}k\mathcal{T}_{\mathrm{A}} + 1/(\mathrm{i}k)\mathcal{T}_{\Phi} \tag{3.61}$$

is the EFIE operator composed of the vector potential operator[17]

$$\mathcal{T}_{\mathrm{A}}\boldsymbol{j} := \hat{\boldsymbol{n}} \times \int_{\Gamma} G^k(\boldsymbol{r}, \boldsymbol{r}')\boldsymbol{j}(\boldsymbol{r}')\mathrm{d}S(\boldsymbol{r}') \tag{3.62}$$

and the scalar potential operator[18]

$$\mathcal{T}_{\Phi}\boldsymbol{j} = -\hat{\boldsymbol{n}} \times \operatorname{grad} \int_{\Gamma} G^k(\boldsymbol{r}, \boldsymbol{r}') \operatorname{div}'_{\Gamma} \boldsymbol{j}(\boldsymbol{r}')\mathrm{d}S(\boldsymbol{r}')\,. \tag{3.64}$$

16 The derivation is rather cumbersome and we want to spare the reader the details. The interested reader may find it in, for example, [Néd01].

17 In this thesis, we distinguish operators that map from a function space defined on $\Gamma$ to a function space defined on $\overline{\Omega}^{\mathrm{c}}$ and/or $\Omega$ from those that map from and to a function space defined on $\Gamma$. The first type of operator will be called potential while the second type will be called potential operator. For example, $\int_{\Gamma} G^k(\boldsymbol{r}, \boldsymbol{r}')\boldsymbol{j}(\boldsymbol{r}')\mathrm{d}S(\boldsymbol{r}')$ in (3.56) is the vector potential and $\mathcal{T}_{\mathrm{A}}$ the vector potential operator. In some cases, we will omit the expression "potential" in "potential operator" for the sake of brevity. For example, instead of speaking of the single layer potential operator, we speak of the single layer operator.

18 Where we implicitly used that

$$\begin{aligned}\int_{\Gamma} \operatorname{div}_{\Gamma}\Big(G^k(\boldsymbol{r}, \boldsymbol{r}')\boldsymbol{j}(\boldsymbol{r}')\Big)\mathrm{d}S(\boldsymbol{r}') &= \int_{\Gamma} \operatorname{grad}_{\Gamma} G^k(\boldsymbol{r}, \boldsymbol{r}')\boldsymbol{j}(\boldsymbol{r}')\mathrm{d}S(\boldsymbol{r}') \\ &= -\int_{\Gamma} \operatorname{grad}'_{\Gamma} G^k(\boldsymbol{r}, \boldsymbol{r}')\boldsymbol{j}(\boldsymbol{r}')\mathrm{d}S(\boldsymbol{r}') \overset{(2.43)}{=} \int_{\Gamma} G^k(\boldsymbol{r}, \boldsymbol{r}') \operatorname{div}'_{\Gamma} \boldsymbol{j}(\boldsymbol{r}')\mathrm{d}S(\boldsymbol{r}')\,. \end{aligned} \tag{3.63}$$

## b) Scattering by or Radiation from a PEC Object

This thesis deals with the scattering of electromagnetic of waves by or the radiation from a PEC object described by the domain $\Omega \subset \mathbb{R}^3$ embedded in a homogeneous medium with permittivity $\varepsilon$ and permeability $\mu$. For a scattering scenario, the tuple $(\boldsymbol{E}^{\mathrm{i}}, \boldsymbol{H}^{\mathrm{i}})$ describes an incident time-harmonic electromagnetic wave impinging on $\Omega$, and the scattered wave, which is the quantity to solve for, is described by the tuple $(\boldsymbol{E}^{\mathrm{s}}, \boldsymbol{H}^{\mathrm{s}})$. For a radiation scenario, it is typically assumed that

$$\left|\boldsymbol{E}^{\mathrm{i}}\right| = V_0/L \tag{3.65}$$

between two antenna terminals, where $L$ is the width of the gap and $V_0$ the voltage [Gib14].

In the exterior region $\overline{\Omega}^{\mathrm{c}}$, the total fields $(\boldsymbol{E}, \boldsymbol{H}) = (\boldsymbol{E}^{\mathrm{i}} + \boldsymbol{E}^{\mathrm{s}}, \boldsymbol{H}^{\mathrm{i}} + \boldsymbol{H}^{\mathrm{s}})$ are subject to the Maxwell's equations

$$\nabla \times \boldsymbol{E} = +\mathrm{i}k\boldsymbol{H}\,, \tag{3.66}$$

and

$$\nabla \times \boldsymbol{H} = -\mathrm{i}k\boldsymbol{E}\,, \tag{3.67}$$

they must satisfy the boundary conditions

$$\hat{\boldsymbol{n}} \times \boldsymbol{E} = \boldsymbol{0}\,, \tag{3.68}$$

$$\hat{\boldsymbol{n}} \times \boldsymbol{H}^{\mathrm{s}} = \boldsymbol{j} - \hat{\boldsymbol{n}} \times \boldsymbol{H}^{\mathrm{i}} \tag{3.69}$$

on $\Gamma$, and $(\boldsymbol{E}^{\mathrm{s}}, \boldsymbol{H}^{\mathrm{s}})$ must satisfy the Silver-Müller radiation condition [Sil84; Mül48][19]

$$\lim_{r \longrightarrow \infty} \left( \boldsymbol{H}^{\mathrm{s}} \times \boldsymbol{r} - r\boldsymbol{E}^{\mathrm{s}} \right) = 0\,, \tag{3.70}$$

where $r = \|\boldsymbol{r}\|$.

Instead of solving the partial differential equations (3.66) and (3.67) directly, we use the mixed potential formulas (3.58) and (3.59) and solve for the surface current density $\boldsymbol{j}$. The scattered wave $(\boldsymbol{E}^{\mathrm{s}}, \boldsymbol{H}^{\mathrm{s}})$ is obtained by evaluating (3.56) and (3.57). In the following sections, we discuss surface integral equation formulations commonly used in literature.

19 The radiation condition is necessary to enforce that only solutions are obtained which are waves traveling from a source to infinity, where the ratio of the electric and magnetic field is the wave impedance $\eta^2$, and where the electric field, the magnetic field, and propagation vector form a trihedron.

### $\alpha$) Electric Field Integral Equation

For PEC objects, the tangential component of $\boldsymbol{E} = \boldsymbol{E}^{\mathrm{i}} + \boldsymbol{E}^{\mathrm{s}}$ on $\Gamma$ must vanish. Equation (3.19) implies that $\boldsymbol{m} = \boldsymbol{0}$ and using (3.58), we obtain the EFIE

$$-\hat{\boldsymbol{n}} \times \boldsymbol{E}^{\mathrm{i}} = \boldsymbol{\mathcal{T}} \boldsymbol{j}\,. \tag{3.71}$$

Once this equation is solved for $\boldsymbol{j}$, (3.56) and (3.57) may be used to compute $\boldsymbol{E}^{\mathrm{s}}$ and $\boldsymbol{H}^{\mathrm{s}}$ everywhere in $\overline{\Omega}^{\mathrm{c}}$. We note that $\boldsymbol{\mathcal{T}} : H^{-1/2}(\mathrm{div}_\Gamma, \Gamma) \longrightarrow H^{-1/2}(\mathrm{div}_\Gamma, \Gamma)$ is invertible if $k^2$ is not an interior electric eigenvalue [Néd01].

So far we have assumed that $\Gamma$ is a smooth surface. This is a severe limitation since we could not even make a statement on such "simple" problems as the scattering from a cube. Fortunately, the presented theory can be generalized to Lipschitz surfaces. This, however, renders the mathematical theory more complex given that $\hat{\boldsymbol{n}}$ is not defined on the edges and corners of a Lipschitz surfaces. A modified version of $H^{-1/2}(\mathrm{div}_\Gamma, \Gamma)$ must be introduced which then allows to obtain a generalized Gårding inequality which implies existence of a unique solution of (3.71) [BH03]. To obtain this result, extensive preliminary work was necessary [Cos88; McL00; Buf01; BC01b; BC01a; BCS02a; BCS02b; Buf03]. Open surfaces (i.e., Lipschitz screens) require a further extension of the theory, and so do T-junctions. In this thesis, however, we obtain theoretical results only for the case that $\Gamma$ is closed, and hence, we do not present the mathematical theory of these problems.

### $\beta$) Magnetic Field Integral Equation

As an alternative to the ansatz for the EFIE, we can leverage on (3.26), that is, $\hat{\boldsymbol{n}} \times \boldsymbol{H}^{\mathrm{s}} = \boldsymbol{j} - \hat{\boldsymbol{n}} \times \boldsymbol{H}^{\mathrm{i}}$, resulting in

$$\hat{\boldsymbol{n}} \times \boldsymbol{H}^{\mathrm{i}} = (\boldsymbol{\mathcal{I}}/2 + \boldsymbol{\mathcal{K}})\boldsymbol{j}\,, \tag{3.72}$$

and in the case of an excitation located in $\Omega$ (interior problem), we find the MFIE

$$\hat{\boldsymbol{n}} \times \boldsymbol{H}^{\mathrm{i}} = (\boldsymbol{\mathcal{I}}/2 - \boldsymbol{\mathcal{K}})\boldsymbol{j}\,. \tag{3.73}$$

As abbreviation, we introduce the exterior MFIE operator

$$\boldsymbol{\mathcal{M}}^{+} = \boldsymbol{\mathcal{I}}/2 + \boldsymbol{\mathcal{K}} \tag{3.74}$$

and the interior MFIE operator

$$\mathcal{M}^- = \mathcal{I}/2 - \mathcal{K}\,. \tag{3.75}$$

which allows as to compactly write

$$\hat{\boldsymbol{n}} \times \boldsymbol{H}^{\mathrm{i}} = \mathcal{M}^{\pm}\boldsymbol{j}\,. \tag{3.76}$$

Since this thesis focuses on scattering problems, we only deal with the exterior problem and hence for the sake of simplicity we omit the plus symbol and use $\mathcal{M}$ for the exterior MFIE operator, though the theory presented in this thesis holds for the interior problem as well. We note that $\mathcal{M} : H^{-1/2}(\mathrm{div}_\Gamma, \Gamma) \longrightarrow H^{-1/2}(\mathrm{div}_\Gamma, \Gamma)$ is invertible if $k^2$ is not an interior electric eigenvalue and similarly to the EFIE the MFIE can be solved on Lipschitz surfaces [BH03].

### γ) Combined Field Integral Equation

For interior electric eigenvalues $k^2$ both the EFIE and the MFIE do not possess a unique solution due to interior resonances. These interior resonances are unphysical (i.e., they cannot be excited by an exterior source). The classic approach in the engineering community is to form the CFIE [MH78]

$$\mathcal{C}\boldsymbol{j} = -\alpha_{\mathrm{C}}\hat{\boldsymbol{n}} \times \hat{\boldsymbol{n}} \times \boldsymbol{E}^{\mathrm{i}} + (1 - \alpha_{\mathrm{C}})\hat{\boldsymbol{n}} \times \boldsymbol{H}^{\mathrm{i}} \tag{3.77}$$

where

$$\mathcal{C} = \alpha_{\mathrm{C}}\hat{\boldsymbol{n}} \times \mathcal{T} + (1 - \alpha_{\mathrm{C}})\mathcal{M} \tag{3.78}$$

is the CFIE operator with $\alpha_{\mathrm{C}} \in ]0, 1[$. In particular for Lipschitz surfaces, it has not been shown that the CFIE has a unique solution. To overcome this issue regularized CFIEs have been proposed in the past [BH04; ES07], though only in the case of [BH04] also the numerical solvability has been discussed. These approaches, however, have never been adopted widely. In the case of the approach in [BH04], a reason might be that the edges of the geometry should be known to the solver.[20] Since no numerical evidence has ever been presented that would

20 We note that the terminology of what is to be called CFIE is not consistent in literature. What is called CFIE in [BH04] is typically called combined source integral equation in the engineering community. Different from the CFIE, one does not solve directly for the (real) electric current, but for some equivalent current. The combined source integral equation was first presented for the Helmholtz equation in [BW65] and is therefore often referred to as the Brakhage-Werner trick.

imply that the CFIE admits non-unique solutions, we use the standard CFIE denoted in (3.77).

## c) Electrostatics: Laplace's Equation and Integral Equation Formulations

In this thesis, we will frequently encounter integral operators known from the solution of Laplace's equation. This equation is obtained by considering that for $k = 0$ the electric field is conservative. This allows to express the electric field as the gradient of a scalar potential, that is, $\boldsymbol{E} = -\operatorname{grad}\varphi_\mathrm{e}$. Combining $\boldsymbol{E} = -\operatorname{grad}\varphi_\mathrm{e}$ together with (3.3) and (3.9) and assuming $\rho_\mathrm{e} = 0$, we yield Laplace's equation

$$\Delta\varphi_\mathrm{e} = 0\,, \tag{3.79}$$

subject to the boundary condition

$$\varphi_\mathrm{e} = g\,, \quad \forall \boldsymbol{r} \in \Gamma \tag{3.80}$$

for the Dirichlet problem,

$$\frac{\partial}{\partial \hat{\boldsymbol{n}}}\varphi_\mathrm{e} = g\,, \quad \forall \boldsymbol{r} \in \Gamma \tag{3.81}$$

for the Neumann problem , and the decay condition [SS11]

$$\varphi_\mathrm{e}(\boldsymbol{r}) \leq C/\|\boldsymbol{r}\| \quad \text{for } \|\boldsymbol{r}\| \longrightarrow \infty\,. \tag{3.82}$$

A solution for the Dirichlet problem can be obtained by solving

$$\mathcal{V}p = g \tag{3.83}$$

on $\Gamma$, where

$$\mathcal{V}p \,:\, H^{-1/2}(\Gamma) \longrightarrow H^{1/2}(\Gamma) \,:=\, \int_\Gamma G^0(\boldsymbol{r},\boldsymbol{r}')p(\boldsymbol{r}')\mathrm{d}S(\boldsymbol{r}')\,, \tag{3.84}$$

is the single layer (potential) operator, and we find the electric potential $\varphi_\mathrm{e}(\boldsymbol{r}) = (\mathcal{S}p)(\boldsymbol{r})$, where

$$\mathcal{S}p \,:\, H^{-1/2}(\Gamma) \longrightarrow H^1_\mathrm{loc}\left(\overline{\Omega}^\mathrm{c}\right) \,:=\, \int_\Gamma G^0(\boldsymbol{r},\boldsymbol{r}')p(\boldsymbol{r}')\mathrm{d}S(\boldsymbol{r}')\,, \tag{3.85}$$

is the single layer potential.[21]

For the Neumann problem, we assume that $g$ satisfies the compatibility condition

$$\int_\Gamma g(\boldsymbol{r})\mathrm{d}S(\boldsymbol{r}) = 0\,. \tag{3.86}$$

By using the hypersingular operator

$$\mathcal{W}p \,:\, H^{1/2}(\Gamma)/\mathbb{R} \longrightarrow H^{-1/2}(\Gamma) \,:=\, \int_\Gamma \frac{\partial^2}{\partial\hat{\boldsymbol{n}}_{\boldsymbol{r}}\partial\hat{\boldsymbol{n}}_{\boldsymbol{r}'}} G^0(\boldsymbol{r},\boldsymbol{r}')p(\boldsymbol{r}')\mathrm{d}S(\boldsymbol{r}') \tag{3.87}$$

and solving

$$\mathcal{W}p = -g \tag{3.88}$$

the electric potential can be computed as $\varphi_\mathrm{e}(\boldsymbol{r}) = (\mathcal{D}p)(\boldsymbol{r})$, where

$$\mathcal{D}p \,:\, H^{1/2}(\Gamma)/\mathbb{R} \longrightarrow H^1_{\mathrm{loc}}\left(\overline{\Omega}^\mathrm{c}\right) \,:=\, \int_\Gamma \frac{\partial}{\partial\hat{\boldsymbol{n}}_{\boldsymbol{r}'}} G^0(\boldsymbol{r},\boldsymbol{r}')p(\boldsymbol{r}')\mathrm{d}S(\boldsymbol{r}') \tag{3.89}$$

is the double layer potential and $H^{1/2}(\Gamma)/\mathbb{R}$ is a quotient space[22], which is necessary to guarantee a unique solution of (3.88) due to the null space of $\mathcal{W}$. We note that the integral in (3.87) has to be understood in the Cauchy principal value sense. For practical implementations this is not relevant since one would solve the variational formulation [Ste10; Néd01]

$$(v, \mathcal{W}p)_{L^2(\Gamma)} = (v, p)_{L^2(\Gamma)} \tag{3.90}$$

for all $v \in H^{1/2}$, where we have

$$(v, \mathcal{W}p)_{L^2(\Gamma)} = \int_\Gamma\int_\Gamma \mathbf{curl}_\Gamma\, p(\boldsymbol{r}')\cdot\mathbf{curl}_\Gamma\, v(\boldsymbol{r})\, G^0(\boldsymbol{r},\boldsymbol{r}')\mathrm{d}S(\boldsymbol{r}')\mathrm{d}S(\boldsymbol{r})\,. \tag{3.91}$$

The operators $\mathcal{V}$ and $\mathcal{W}$ satisfy the so-called Calderón identities

$$\mathcal{V}\mathcal{W} = \mathcal{I}/4 - \mathcal{K}^2 \tag{3.92}$$

21 This is by no means the only ansatz for finding a solution of the Dirichlet problem. It is an example of the indirect approaches, where the quantity $p$, we solve for, has no physical meaning. For an overview of the different approaches, we refer the reader to [Ste10].

22 See [Rud91] for a definition of quotient space.

and

$$\mathcal{WV} = \mathcal{I}/4 - \mathcal{K}'^2 \tag{3.93}$$

where

$$\mathcal{K}p \,:\, H^{1/2}(\Gamma) \longrightarrow H^{1/2}(\Gamma) \,:=\, \int_\Gamma \frac{\partial}{\partial \hat{\boldsymbol{n}}_{\boldsymbol{r}'}} G^0(\boldsymbol{r}, \boldsymbol{r}')p(\boldsymbol{r}')\mathrm{d}S(\boldsymbol{r}') \tag{3.94}$$

is the double layer operator,

$$\mathcal{K}'p \,:\, H^{-1/2}(\Gamma) \longrightarrow H^{-1/2}(\Gamma) \,:=\, \int_\Gamma \frac{\partial}{\partial \hat{\boldsymbol{n}}_{\boldsymbol{r}'}} G^0(\boldsymbol{r}, \boldsymbol{r}')p(\boldsymbol{r}')\mathrm{d}S(\boldsymbol{r}') \tag{3.95}$$

is the adjoint double layer operator, and $\mathcal{I}$ is the identity operator.

Chapter 4

# Discretization of Boundary Integral Operators and Equations

Numerical formulations of the integral equations (3.71), (3.76), and (3.77) are necessary to find solutions for non-canonical scattering problems. This chapter introduces the classical numerical formulations based on Galerkin theory. First, it discusses this theory and possible basis functions. Then discretized counterparts of (3.71), (3.76), and (3.77) are derived. Lastly, it analyzes the ill-conditioning of the system matrices resulting from these discretizations and shows partial remedies in form of quasi-Helmholtz decompositions and projectors.

## a) Petrov-Galerkin Theory

Except for a few canonical objects (e.g., if $\Omega$ is a sphere), analytic solutions are not known for (3.71), (3.76), and (3.77), so one must resort to a numerical approximation and discretize these equations. Different approaches are available such as the Nyström or collocation method. In this thesis, we use the Petrov-Galerkin method, which can guarantee that the numerical solution converges to the analytical solution.

For describing the Petrov-Galerkin method, we consider the equation

$$\mathcal{A}u = f\,, \tag{4.1}$$

where $\mathcal{A} : X \longrightarrow Y'$ is a bounded linear operator and $X$ and $Y$ are Hilbert spaces. We can associate with $\mathcal{A}$ a bilinear form $a : X \times Y \longrightarrow \mathbb{R}$ that satisfies [Ste10]

$$\left|a(x,y)\right| \leq C\|x\|_X \|y\|_Y \tag{4.2}$$

with $C > 0$. We are faced with the variational problem to find $u \in X$ such that

$$a(u, v) = \langle f, v \rangle_{Y' \times Y} \quad \forall v \in Y \text{ with } f \in Y'. \tag{4.3}$$

Equation (4.1) (or equivalently (4.3)) has a unique solution if [23]

$$\sup_{u \in X} \left| a(u, v) \right| > 0\,, \quad \forall v \neq 0\,, \tag{4.5}$$

$$\inf_{u \in X} \sup_{v \in Y} \frac{a(u, v)}{\|u\|_X \|v\|_Y} \geq c_{\mathrm{ALBB}} > 0 \tag{4.6}$$

are satisfied, where $c_{\mathrm{ALBB}}$ is a positive constant. These conditions are referred to as inf-sup conditions for the analytic problem [Bab71; Bre74; XZ03].[24]

For a numerical approximation, we must use finite-dimensional subspaces of $X$ and $Y$, that is, we employ $X_N = \operatorname{span}\left\{ \varphi_k \right\}_{k=1}^{N} \subset X$ and $Y_N = \operatorname{span}\left\{ \psi_k \right\}_{k=1}^{N} \subset Y$ with $\dim(X_N) = \dim(Y_N) = N$. The task is to find $u_N \in X_N$ such that

$$a(u_N, v_N) = \langle f, v_N \rangle_{Y_N' \times Y_N} \tag{4.7}$$

for all $v_N \in Y_N$. This variational formulation in (4.7) is equivalent to

$$\boldsymbol{A}\boldsymbol{u} = \boldsymbol{f} \tag{4.8}$$

where

$$\left[\boldsymbol{A}\right]_{mn} = \left(\psi_m, \mathcal{A}\varphi_n\right)_{L^2} \tag{4.9}$$

and

$$\left[\boldsymbol{f}\right]_{m} = \left(\psi_m, f\right)_{L^2}. \tag{4.10}$$

Even though the inf-sup conditions for the analytic problem are satisfied, this does not imply that we can expect to obtain a unique solution of (4.7). In addition,

23 Equations (4.5) and (4.6) can also be expressed as

$$c_{\mathrm{ALBB}} \|u\|_X \leq \sup_{0 \neq v \in Y} \frac{a(u, v)}{\|v\|_Y}\,, \quad \forall u \in (\operatorname{null} \mathcal{A})^{\perp} \subset X\,. \tag{4.4}$$

Equation (4.5) implies that $u$ must not be in the null space of $\mathcal{A}$.

24 In literature, this is also known as the Ladyzhenskaya-Babuska-Brezzi (LBB) condition.

a discrete inf-sup condition must be satisfied, that is, we must have [Bab71; Bre74; XZ03]

$$\sup_{u \in X_N} \left| a(u, v) \right| > 0 \,, \quad \forall v \neq 0 \,, \tag{4.11}$$

$$\inf_{u \in X_N} \sup_{v \in Y_N} \frac{a(u, v)}{\|u\|_X \|v\|_Y} \geq c_{\mathrm{DLBB}} > 0 \,, \tag{4.12}$$

where $c_{\mathrm{DLBB}}$ is a positive constant. If this condition is satisfied, then the solution is unique. If, in addition, the trial space satisfies the approximation property

$$\lim_{N \to \infty} \inf_{v_N \in X_N} \|v - v_N\|_X = 0 \,, \quad \forall v \in X \,, \tag{4.13}$$

then we have $u_N \longrightarrow u$ for $N \longrightarrow \infty$, that is, the approximation converges to the analytical solution.

To correctly apply the Petrov-Galerkin method, it is decisive that the testing is always performed in the dual space of the range of $\mathcal{A}$, where we notice that $Y'' = Y$ when $Y$ is a Hilbert space. As discussed in the next section, this requirement has been ignored in the case of the discretization of the MFIE in the past.

## b) Basis Functions

For the numerical solution, it is assumed that $\Gamma$ is a Lipschitz polyhedral surface. If instead $\Gamma$ is a smooth surface, then we would need to approximate the surface by a polyhedral surface. We presume that this preprocessing step has happened at this point. The polyhedral surface $\Gamma$ is discretized with a mesh of triangular cells. For the discretization of the scalar operators $\mathcal{V}$ and $\mathcal{W}$, we use piecewise constant functions[25] $p_i \in X_p \subset H^{-1/2}(\Gamma)$ and piecewise linear functions[26] $\lambda_i \in X_\lambda \subset H^{1/2}(\Gamma)$. The piecewise constant functions are defined as

$$p_i(\boldsymbol{r}) = \begin{cases} 1/A_i \,, & \boldsymbol{r} \in c_i \,, \\ 0 \,, & \text{otherwise,} \end{cases} \tag{4.14}$$

25 In literature, they are also referred to as patch functions.

26 Often referred to as pyramid or nodal functions.

where $c_i$ denotes the domain of the $i$th cell of the mesh and $A_i$ its area. The piecewise linear functions $\lambda_i$ are defined as

$$\lambda_i(\boldsymbol{r}) = \begin{cases} 1 & \text{for } \boldsymbol{r} \in v_i\,, \\ 0 & \text{for } \boldsymbol{r} \in v_j \neq v_i\,, \\ \text{linear} & \text{elsewhere,} \end{cases} \tag{4.15}$$

where $v_i \in \Gamma$ is the $i$th vertex of the mesh.

For the discretization of vector integral operators, we need RWG functions $\boldsymbol{f}_n \in X_f$ (that are equivalent to the zeroth order Raviart-Thomas functions on a manifold [RWG82; RT77]), which we define as

$$\boldsymbol{f}_n = \begin{cases} \dfrac{\boldsymbol{r} - \boldsymbol{r}_n^+}{2A_{c_n^+}} & \text{for } \boldsymbol{r} \in c_n^+\,, \\ \dfrac{\boldsymbol{r}_n^- - \boldsymbol{r}}{2A_{c_n^-}} & \text{for } \boldsymbol{r} \in c_n^- \end{cases} \tag{4.16}$$

following the convention depicted in Figure 4.1, where the vector $\boldsymbol{e}_n$ denotes the $n$th directed edge, $c_n^+$ and $c_n^-$ denote the domains of the cells on which $\boldsymbol{f}_n$ has its support, $v_n^+$ and $v_n^-$ denote the vertices on the edge $\boldsymbol{e}_n$, and $\boldsymbol{r}_n^+$ and $\boldsymbol{r}_n^-$ are the vertices opposite to the edge $\boldsymbol{e}_n$. In a slight abuse of notation, $A_{c_n^+}$ and $A_{c_n^-}$ denote the cell area of $c_n^+$ and $c_n^-$, respectively. Different from [RWG82], we do not normalize $\boldsymbol{f}_n$ by the edge length. We note that $X_f \subset H^{-1/2}(\mathrm{div}_\Gamma, \Gamma)$: the RWG functions are divergence conforming; the application of the divergence operator on RWG functions is well-defined in the sense that unphysical line charges cannot appear. For the rotated $\hat{\boldsymbol{n}} \times \boldsymbol{f}_i \in X_{\hat{\boldsymbol{n}}\times f}$ on the other hand, we have the property $X_{\hat{\boldsymbol{n}}\times f} \subset H^{-1/2}(\mathrm{curl}_\Gamma, \Gamma)$.

Often we need to discretize the identity operator $\mathcal{I}$ (or $\boldsymbol{\mathcal{I}}$, depending on the context). The resulting matrix is called Gram matrix.[27] In order to avoid defining the Gram matrix for different basis functions every time, we stick to the following convention: let $f_n \in X_f$ and $g_n \in X_g$ be functions of the function spaces $X_f$ and $X_g$, respectively; the Gram matrix of these functions is defined and denoted as

$$\left[\boldsymbol{G}_{fg}\right]_{mn} := \left(f_n, g_n\right)_{L^2}\,. \tag{4.17}$$

Naturally, this definition extends to the case that functions are vector-valued.

27 In literature, the Gram matrix is also referred to as mass matrix.

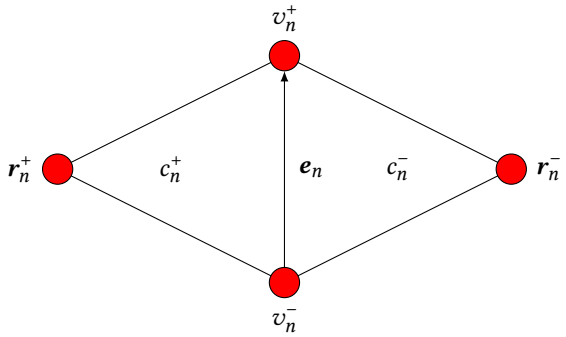


*Fig. 4.1.:* Definition of the RWG functions. The vector $\boldsymbol{e}_n$ denotes the directed edge, $c_n^+$ and $c_n^-$ denote the domains of the cells, $v_n^+$ and $v_n^-$ denote vertices on the edge $\boldsymbol{e}_n$, and $\boldsymbol{r}_n^+$ and $\boldsymbol{r}_n^-$ are the vertices opposite to the edge $\boldsymbol{e}_n$.

When the $L^2$-space is chosen as pivot space, the space $H^{-1/2}(\mathrm{curl}_\Gamma, \Gamma)$ is the dual space of $H^{-1/2}(\mathrm{div}_\Gamma, \Gamma)$ and vice versa. Unfortunately, $X_f$ and $X_{\hat{\boldsymbol{n}}\times f}$ are not dual to each other in the sense that they do not satisfy inf-sup conditions. This led to the development of the BC basis functions $\tilde{\boldsymbol{f}} \in X_{\tilde{f}}$. They are divergence conforming just as the RWG functions, but they allow to obtain a well-conditioned mixed Gram matrix $\boldsymbol{G}_{\hat{\boldsymbol{n}}\times\tilde{f},f}$, which means that inf-sup conditions are satisfied [BC07].[28]

28 The CW functions, which have been developed in a different context many years before the BC functions [CW90], could be used as well.

## c) Discretization of the Field Integral Equations

In order to apply the Petrov-Galerkin method to the EFIE, we need to obtain a bilinear form associated with $\mathcal{T}$. Such a variational formulation is given by [Rum54]

$$\begin{aligned}\left(\hat{\boldsymbol{n}} \times \boldsymbol{v}, \mathcal{T}\boldsymbol{u}\right)_{\boldsymbol{L}^2(\Gamma)} &:= \mathrm{i}k \int_\Gamma \boldsymbol{v}(\boldsymbol{r}) \cdot \int_\Gamma G^k(\boldsymbol{r}, \boldsymbol{r}')\boldsymbol{u}(\boldsymbol{r}')\mathrm{d}S(\boldsymbol{r}')\mathrm{d}S(\boldsymbol{r}) \\ &+ \frac{1}{\mathrm{i}k} \int_\Gamma \mathrm{div}_\Gamma\, \boldsymbol{v}(\boldsymbol{r}) \int_\Gamma G^k(\boldsymbol{r}, \boldsymbol{r}')\, \mathrm{div}'_\Gamma\, \boldsymbol{u}(\boldsymbol{r}')\mathrm{d}S(\boldsymbol{r}')\mathrm{d}S(\boldsymbol{r}), \\ &\forall \boldsymbol{u} \in H^{-1/2}(\mathrm{div}_\Gamma, \Gamma), \hat{\boldsymbol{n}} \times \boldsymbol{v} \in H^{-1/2}(\mathrm{curl}_\Gamma, \Gamma), \quad (4.18)\end{aligned}$$

where we used (2.43). Thus we obtain as Petrov-Galerkin discretization of (3.71)

$$\boldsymbol{T}^k \boldsymbol{j} = -\boldsymbol{e}, \quad (4.19)$$

where

$$\boldsymbol{T}^k = \mathrm{i}k\boldsymbol{T}^k_{\mathrm{A}} + 1/(\mathrm{i}k)\boldsymbol{T}^k_{\Phi} \quad (4.20)$$

with

$$\begin{aligned}\left[\boldsymbol{T}^k_{\mathrm{A}}\right]_{mn} &= \left(\hat{\boldsymbol{n}} \times \boldsymbol{f}_m, \mathcal{T}_{\mathrm{A}}\boldsymbol{f}_n\right)_{\boldsymbol{L}^2(\Gamma)} && (4.21)\\ &= \int_\Gamma \boldsymbol{f}_m(\boldsymbol{r}) \cdot \int_\Gamma G^k(\boldsymbol{r}, \boldsymbol{r}')\boldsymbol{f}_n(\boldsymbol{r}')\mathrm{d}S(\boldsymbol{r}')\mathrm{d}S(\boldsymbol{r}), && (4.22)\\ \left[\boldsymbol{T}^k_{\Phi}\right]_{mn} &= \left(\hat{\boldsymbol{n}} \times \boldsymbol{f}_m, \mathcal{T}_{\Phi}\boldsymbol{f}_n\right)_{\boldsymbol{L}^2(\Gamma)} && (4.23)\\ &= \int_\Gamma \mathrm{div}_\Gamma\, \boldsymbol{f}_m(\boldsymbol{r}) \int_\Gamma G^k(\boldsymbol{r}, \boldsymbol{r}')\, \mathrm{div}'_\Gamma\, \boldsymbol{f}_n(\boldsymbol{r}')\mathrm{d}S(\boldsymbol{r}')\mathrm{d}S(\boldsymbol{r}), && (4.24)\\ \left[\boldsymbol{e}\right]_n &= \left(\hat{\boldsymbol{n}} \times \boldsymbol{f}_m, \hat{\boldsymbol{n}} \times \boldsymbol{E}^{\mathrm{i}}\right)_{\boldsymbol{L}^2(\Gamma)}, && (4.25)\end{aligned}$$

where the electric current density is approximated by

$$\boldsymbol{j} \approx \sum_{n=1}^{N} \left[\boldsymbol{j}\right]_n \boldsymbol{f}_n. \quad (4.26)$$

An important requirement of the Petrov-Galerkin theory is that both analytic and discrete inf-sup conditions must be satisfied. That this requirement is satisfied

has been shown even for the case where $\Gamma$ is a Lipschitz surface [BH03]. For notational convenience, we will in general omit the superscript $k$ of $\boldsymbol{T}^k$.

The computation of the matrix elements of $\boldsymbol{T}_\mathrm{A}$ and $\boldsymbol{T}_\Phi$ is by no means trivial because of the singularity of the Green's function. If $\boldsymbol{r}$ and $\boldsymbol{r}'$ are sufficiently far away from each other, then Gaussian quadrature can be used for integration [Gau14; Dun85]. In the case that Gauss quadrature is not applicable, the singularity extraction method is employed in this thesis [Gra93].

For the MFIE, the situation is slightly different. Classically, the bilinear form

$$\begin{aligned}(\boldsymbol{v}, \mathcal{M}\boldsymbol{u})_{L^2(\Gamma)} &:= 1/2 \int_\Gamma \boldsymbol{v}(\boldsymbol{r}) \cdot \boldsymbol{u}(\boldsymbol{r}) \mathrm{d}S(\boldsymbol{r}) \\ &\quad - \int_\Gamma \boldsymbol{v}(\boldsymbol{r}) \cdot \hat{\boldsymbol{n}} \times \int_\Gamma \operatorname{grad} G^k(\boldsymbol{r}, \boldsymbol{r}') \times \boldsymbol{u}(\boldsymbol{r}') \mathrm{d}S(\boldsymbol{r}') \mathrm{d}S(\boldsymbol{r}), \\ &\qquad \forall \boldsymbol{u} \in H^{-1/2}(\operatorname{div}_\Gamma, \Gamma), \boldsymbol{v} \in H^{-1/2}(\operatorname{div}_\Gamma, \Gamma) \end{aligned} \tag{4.27}$$

has been used. Employing $\boldsymbol{f}_n$ as expansion and testing functions, we obtain the system

$$\boldsymbol{M}\boldsymbol{j} := \left(\boldsymbol{G}_{ff}/2 + \boldsymbol{K}\right)\boldsymbol{j} = \boldsymbol{h}, \tag{4.28}$$

where

$$\left[\boldsymbol{G}_{ff}\right]_{mn} = \left(\boldsymbol{f}_m, \boldsymbol{f}_n\right)_{L^2(\Gamma)} = \int_\Gamma \boldsymbol{f}_m(\boldsymbol{r}) \cdot \boldsymbol{f}_n(\boldsymbol{r}) \mathrm{d}S(\boldsymbol{r}), \tag{4.29}$$

$$\left[\boldsymbol{K}\right]_{mn} = \left(\boldsymbol{f}_m, \mathcal{K}\boldsymbol{f}_n\right)_{L^2(\Gamma)} \tag{4.30}$$

$$= - \int_\Gamma \boldsymbol{f}_m(\boldsymbol{r}) \cdot \hat{\boldsymbol{n}} \times \int_\Gamma \operatorname{grad} G^k(\boldsymbol{r}, \boldsymbol{r}') \times \boldsymbol{f}_n(\boldsymbol{r}') \mathrm{d}S(\boldsymbol{r}') \mathrm{d}S(\boldsymbol{r}), \tag{4.31}$$

$$\left[\boldsymbol{h}\right]_n = \left(\boldsymbol{f}_m, \hat{\boldsymbol{n}} \times \boldsymbol{H}^\mathrm{i}\right). \tag{4.32}$$

Such a discretization approach is, however, not conforming with Petrov-Galerkin theory. Just as in the case of the EFIE, the testing functions should belong to $H^{-1/2}(\operatorname{curl}_\Gamma, \Gamma)$. A discretization with $\hat{\boldsymbol{n}} \times \boldsymbol{f}_m$ is doomed to fail since discrete inf-sup conditions are not satisfied. Instead, a different set of basis functions must be used such that the discrete inf-sup conditions are satisfied. This issue was discussed in [Coo+11], where the use of BC functions was proposed. In this

case, the bilinear form reads

$$\begin{aligned}\left(\hat{\boldsymbol{n}} \times \boldsymbol{v}, \mathcal{M}\boldsymbol{u}\right)_{L^2(\Gamma)} &:= 1/2 \int_\Gamma \hat{\boldsymbol{n}} \times \boldsymbol{v}(\boldsymbol{r}) \cdot \boldsymbol{u}(\boldsymbol{r}) \mathrm{d}S(\boldsymbol{r}) \\ &\quad - \int_\Gamma \boldsymbol{v}(\boldsymbol{r}) \cdot \int_\Gamma \operatorname{grad} G^k(\boldsymbol{r}, \boldsymbol{r}') \times \boldsymbol{u}(\boldsymbol{r}') \mathrm{d}S(\boldsymbol{r}') \mathrm{d}S(\boldsymbol{r}) \,, \\ &\qquad \forall \boldsymbol{u} \in H^{-1/2}(\operatorname{div}_\Gamma, \Gamma), \hat{\boldsymbol{n}} \times \boldsymbol{v} \in H^{-1/2}(\operatorname{curl}_\Gamma, \Gamma) \,. \end{aligned} \tag{4.33}$$

Using $f_n$ as expansion and $\hat{\boldsymbol{n}} \times \tilde{\boldsymbol{f}}_n$ as testing functions, we obtain the system

$$\widetilde{\boldsymbol{M}}\boldsymbol{j} := \left(\boldsymbol{G}_{\hat{\boldsymbol{n}}\times\tilde{\boldsymbol{f}},\boldsymbol{f}}/2 + \widetilde{\boldsymbol{K}}\right)\boldsymbol{j} = \tilde{\boldsymbol{h}} \,, \tag{4.34}$$

where

$$\left[\boldsymbol{G}_{\hat{\boldsymbol{n}}\times\tilde{\boldsymbol{f}},\boldsymbol{f}}\right]_{mn} = \left(\hat{\boldsymbol{n}} \times \tilde{\boldsymbol{f}}_m, \boldsymbol{f}_n\right)_{L^2(\Gamma)} = \int_\Gamma \hat{\boldsymbol{n}} \times \tilde{\boldsymbol{f}}_m(\boldsymbol{r}) \cdot \boldsymbol{f}_n(\boldsymbol{r}) \mathrm{d}S(\boldsymbol{r}) \,, \tag{4.35}$$

$$\left[\widetilde{\boldsymbol{K}}\right]_{mn} = \left(\hat{\boldsymbol{n}} \times \tilde{\boldsymbol{f}}_m, \mathcal{K}\boldsymbol{f}_n\right)_{L^2(\Gamma)} \tag{4.36}$$

$$= -\int_\Gamma \tilde{\boldsymbol{f}}_m(\boldsymbol{r}) \cdot \int_\Gamma \operatorname{grad} G^k(\boldsymbol{r}, \boldsymbol{r}') \times \boldsymbol{f}_n(\boldsymbol{r}') \mathrm{d}S(\boldsymbol{r}') \mathrm{d}S(\boldsymbol{r}) \,, \tag{4.37}$$

$$\left[\tilde{\boldsymbol{h}}\right]_n = \left(\hat{\boldsymbol{n}} \times \tilde{\boldsymbol{f}}_m, \hat{\boldsymbol{n}} \times \boldsymbol{H}^{\mathrm{i}}\right) . \tag{4.38}$$

We refer to $\widetilde{\boldsymbol{M}}$ as conformingly discretized MFIE.

The classical discretization of the CFIE follows immediately as

$$\boldsymbol{C}\boldsymbol{j} = -\alpha_{\mathrm{C}}\boldsymbol{e} + (1 - \alpha_{\mathrm{C}})\boldsymbol{h} \,, \tag{4.39}$$

where

$$\boldsymbol{C} := \alpha_{\mathrm{C}}\boldsymbol{T} + (1 - \alpha_{\mathrm{C}})\boldsymbol{M} \,. \tag{4.40}$$

For the conformingly discretized system, however, we have

$$\widetilde{\boldsymbol{C}}\boldsymbol{j} = -\alpha_{\mathrm{C}}\boldsymbol{e} + (1 - \alpha_{\mathrm{C}})\boldsymbol{G}_{\boldsymbol{f}\boldsymbol{f}}\boldsymbol{G}^{-1}_{\hat{\boldsymbol{n}}\times\tilde{\boldsymbol{f}},\boldsymbol{f}}\tilde{\boldsymbol{h}} \,, \tag{4.41}$$

where

$$\widetilde{\boldsymbol{C}} = \alpha_{\mathrm{C}}\boldsymbol{T} + (1 - \alpha_{\mathrm{C}})\boldsymbol{G}_{\boldsymbol{f}\boldsymbol{f}}\boldsymbol{G}^{-1}_{\hat{\boldsymbol{n}}\times\tilde{\boldsymbol{f}},\boldsymbol{f}}\widetilde{\boldsymbol{M}} \,. \tag{4.42}$$

The Gram matrices are necessary to ensure that the CFIE is consistently tested [Beg+13].

Lastly, we need to discretize the scalar operators $\mathcal{V}$ and $\mathcal{W}$. Here, we obtain the system matrices

$$\left[\boldsymbol{V}\right]_{ij} = \left(p_i, \mathcal{V} p_j\right)_{L^2(\Gamma)} \tag{4.43}$$

and

$$\left[\boldsymbol{W}\right]_{ij} := \left(\lambda_i, \mathcal{W} \lambda_j\right)_{L^2(\Gamma)} \tag{4.44}$$

where for the latter we use the variational formulation of (3.91).

## d) On the Ill-Conditioning of System Matrices

We have pointed out in Chapter 1 that equations such as the discretized EFIE in (4.19) are typically solved with an iterative solver belonging to the family of Krylov subspace methods. The overall computational complexity in time then depends on the fast method used (a fast method such as the MLFMM or ACA) and the number of iterations required by the solver to converge.

If we consider the system $\boldsymbol{A}\boldsymbol{x} = \boldsymbol{b}$ where $\boldsymbol{A}$ is a symmetric, positive definite matrix and if we apply the CG method, we have the upper bound for the number of iterations

$$N_{\text{iter}} \leq \left\lceil \frac{1}{2} \sqrt{\operatorname{cond} \boldsymbol{A}} \log \frac{2}{\epsilon} \right\rceil \tag{4.45}$$

with the condition number

$$\operatorname{cond} \boldsymbol{A} = \|\boldsymbol{A}\| \left\|\boldsymbol{A}^{-1}\right\| = \frac{s_{\max}(\boldsymbol{A})}{s_{\min}(\boldsymbol{A})}, \tag{4.46}$$

where $s_{\max}(\boldsymbol{A})$ is the largest singular value and $s_{\min}(\boldsymbol{A})$ the smallest singular value of $\boldsymbol{A}$, and where $\epsilon$ is the relative residual error that serves as stopping criterion, that is, if $\|\boldsymbol{A}\boldsymbol{x} - \boldsymbol{b}\| \leq \epsilon \|\boldsymbol{b}\|$, then the CG solver stops.

Clearly, if cond $\boldsymbol{A}$ is large, then the CG solver will require many iterations to converge and one would say that $\boldsymbol{A}$ is ill-conditioned. There are many factors that can contribute to a large condition number, for example, a complicated geometry or a distorted mesh [Ste10]. These effects are, however, not on the focus of this thesis. Instead, the main attention is on the question how the condition number behaves if the mesh is refined, that is, the average edge length $h \longrightarrow 0$.

Why can a decreasing $h$ lead to an ill-conditioned system? For a symmetric, positive definite matrix, eigenvalues and singular values as well as eigenvectors and singular vectors coincide. If an operator with eigenvalues growing to infinity or accumulating at zero is discretized, then it comes at no surprise that such a behavior is observable in the corresponding system matrix: when the mesh is refined, the infinite spectrum of the respective operator is better captured and thus also the system matrix has growing or decreasing eigenvalues, at least under the condition that an $L^2$-stable basis is used, that is, the Gram matrix of this basis is well-conditioned.

By introducing the weak and distributional derivative, the concept of derivatives was generalized. Closely linked to this generalization are pseudo-differential operators. The Laplace-Beltrami operator is a pseudo-differential operator of order +2, while the hypersingular operator $\mathcal{W}$ is of order +1, and the single layer operator $\mathcal{V}$ is of order −1. Operators of negative order have eigenvalues clustering around zero, while operators of positive order have eigenvalues growing to infinity. The rate at which they grow or decrease corresponds to the order of the operator.

In general, if an $L^2$-stable basis is used for the discretization of an operator with non-zero order, then the resulting matrix is ill-conditioned. For integral operators, two of the most popular remedies are either the use of a basis, which is itself $L^2$-unstable, these are the hierarchical basis preconditioners, or to use an operator of opposite order as preconditioner. For a hierarchical basis preconditioner, it is typical that these bases are constructed on classical function spaces such as $X_p$ or $X_\lambda$. This allows to reuse the standard discretization and to apply the basis as a preconditioner in form of a transformation matrix. That is, instead of solving the system

$$\boldsymbol{A}\boldsymbol{x} = \boldsymbol{b} \tag{4.47}$$

we solve a system of the form

$$\boldsymbol{B}^{\mathrm{T}}\boldsymbol{A}\boldsymbol{B}\boldsymbol{y} = \boldsymbol{B}^{\mathrm{T}}\boldsymbol{b} \tag{4.48}$$

so that in the best case

$$\operatorname{cond}\left(\boldsymbol{B}^{\mathrm{T}}\boldsymbol{A}\boldsymbol{B}\right) \lesssim 1 \tag{4.49}$$

would hold, where the expression $a \lesssim b$ means that there is a constant $C$, independent of the average edge length $h$, such that $a \leq Cb$ holds. In addition, we will frequently use $a \eqsim b$ meaning that both inequalities $a \lesssim b$ and $b \lesssim a$ hold.

The approach to use an operator of the opposite order can be motivated by the Calderón identities, which we introduced in (3.92) and (3.93). By applying $\mathcal{V}$ to $\mathcal{W}$ (or vice versa), an integral equation of the second kind is obtained, that is, the identity operator plus a compact operator. Since the eigenvalues of a compact operator cluster around zero, the eigenvalues $\mathcal{I}/4 - \mathcal{K}^2$ accumulate at 1/4. When an iterative solver such as the CG method is used, the number of iterations to converge are bounded from above with a constant independent of the discretization density [SW98; Hip06; AK01]. In the case of the Calderón preconditioners, we solve a system of the form

$$\boldsymbol{P}\boldsymbol{A}\boldsymbol{x} = \boldsymbol{P}\boldsymbol{b} \tag{4.50}$$

and have

$$\operatorname{cond}(\boldsymbol{P}\boldsymbol{A}) \lesssim 1\,. \tag{4.51}$$

The preconditioner in (4.48) is referred to as split preconditioner, and the one in (4.51) as left preconditioner. In order to find new preconditioners, we will frequently use Rayleigh quotients. If $\boldsymbol{A} \in \mathbb{R}^{n\times n}$ is symmetric, positive definite, then we have

$$s_{\max}(\boldsymbol{A}) = \max_{\boldsymbol{x}} \frac{\boldsymbol{x}^{\mathrm{T}}\boldsymbol{A}\boldsymbol{x}}{\boldsymbol{x}^{\mathrm{T}}\boldsymbol{x}} \tag{4.52}$$

and

$$s_{\min}(\boldsymbol{A}) = \min_{\boldsymbol{x}} \frac{\boldsymbol{x}^{\mathrm{T}}\boldsymbol{A}\boldsymbol{x}}{\boldsymbol{x}^{\mathrm{T}}\boldsymbol{x}}\,. \tag{4.53}$$

For our analysis, we will use the notation

$$s_{\min}(\boldsymbol{A})\,\boldsymbol{x}^{\mathrm{T}}\boldsymbol{x} \le \boldsymbol{x}^{\mathrm{T}}\boldsymbol{A}\boldsymbol{x} \le s_{\max}(\boldsymbol{A})\,\boldsymbol{x}^{\mathrm{T}}\boldsymbol{x}\,, \quad \forall \boldsymbol{x} \in \mathbb{R}^n\,. \tag{4.54}$$

If, for example, the inequality

$$\boldsymbol{x}^{\mathrm{T}}\boldsymbol{A}\boldsymbol{x} \asymp \boldsymbol{x}^{\mathrm{T}}\boldsymbol{F}^{-1}\boldsymbol{x}\,, \quad \forall \boldsymbol{x} \in \mathbb{R}^n\,. \tag{4.55}$$

holds, then

$$\operatorname{cond}(\boldsymbol{F}\boldsymbol{A}) \lesssim 1 \tag{4.56}$$

follows.[29] The EFIE is not directly applicable to such an analysis since it is not a symmetric, positive definite matrix. This is mainly due to the frequency

29 Consider that in this case also

$$\boldsymbol{x}^{T}\boldsymbol{A}^2\boldsymbol{x} \asymp \boldsymbol{x}^{\mathrm{T}}\boldsymbol{F}^{-2}\boldsymbol{x}\,, \quad \forall \boldsymbol{x} \in \mathbb{R}^n \tag{4.57}$$

dependency of the Green's function $G^k(\boldsymbol{r}, \boldsymbol{r}')$. We are not, however, able to consider the case $k \longrightarrow 0$ due to the $1/k$ scaling of the scalar potential operator part of the EFIE. This observation, in fact, leads to another form of ill-conditioning particular to the EFIE: the low-frequency breakdown.

A close look at (4.20) reveals that $\boldsymbol{T}$ is ill-conditioned in $k$, that is, the condition number of $\boldsymbol{T}$ grows as $1/k^2$ for $k \longrightarrow 0$: the scalar potential operator $\boldsymbol{T}_\Phi$ has a null space spanned by a solenoidal subspace of the RWG functions. Hence, the spectrum of $\boldsymbol{T}$ consists of two branches, the spectrum of $\boldsymbol{T}_\Phi$ and of $\boldsymbol{T}_\mathrm{A}$. Due to the scaling of the vector and the scalar potential operator with $1/k$ and $k$, respectively, the two branches are driven apart leading to the ill-conditioning.

The $h$-dependency of the condition number $\boldsymbol{T}$ is more difficult to establish than the frequency dependency. In this case it is helpful to use a (quasi-)-Helmholtz decomposition to make the transition to scalar quantities and to consider the contribution from $\boldsymbol{T}_\mathrm{A}$ separately from $\boldsymbol{T}_\Phi$ so that well-established inverse inequalities can be used (see, for example, [ATV10].) A relatively general framework for assessing the ill-conditioning of an operator was shown in [Kir10]. Summarizing, one obtains for the EFIE

$$\mathrm{cond}(\boldsymbol{T}) \lesssim 1/(kh)^2 \,. \tag{4.60}$$

For $\boldsymbol{M}$ and $\widetilde{\boldsymbol{M}}$, we obtain that the condition number can be bounded independently from $k$ or $h$ on simply connected geometries, but on topologically non-trivial structures, we obtain [Bog+11]

$$\mathrm{cond}(\widetilde{\boldsymbol{M}}) \lesssim 1/k^2 \,. \tag{4.61}$$

The CFIE inherits these properties, and we have on simply connected geometries

$$\mathrm{cond}\, \widetilde{\boldsymbol{C}} = 1/h \tag{4.62}$$

and

$$\mathrm{cond}\, \widetilde{\boldsymbol{C}} = 1/(k^2 h) \tag{4.63}$$

---

holds and by using the substitution $\boldsymbol{y} = \boldsymbol{F}^{-1}\boldsymbol{x}$, we obtain

$$\boldsymbol{y}^T \boldsymbol{F}\boldsymbol{A}^2\boldsymbol{F}\boldsymbol{y} \asymp \boldsymbol{y}^\mathrm{T}\boldsymbol{y} \,, \quad \forall \boldsymbol{y} \in \mathbb{R}^n \,. \tag{4.58}$$

Given that $\boldsymbol{F}\boldsymbol{A}^2\boldsymbol{F} = \boldsymbol{F}^\mathrm{T}\boldsymbol{A}^\mathrm{T}\boldsymbol{A}\boldsymbol{F}$ and the definition of the singular value decomposition (SVD), we find

$$\mathrm{cond}(\boldsymbol{A}\boldsymbol{F}) = \sqrt{\mathrm{cond}\left(\boldsymbol{F}^\mathrm{T}\boldsymbol{A}^\mathrm{T}\boldsymbol{A}\boldsymbol{F}\right)} \,. \tag{4.59}$$

on multiply connected. The reduction in the ill-conditioning from $h^{-2}$ to $h^{-1}$ results from the identity operator in $\widetilde{\boldsymbol{C}}$: it introduces a lower bound of the spectrum so that the singular values of $\boldsymbol{T}_{\mathrm{A}}$ are shifted and bounded away from zero.

This dissertation introduces new paradigms for curing the dense-discretization breakdown of the EFIE and the CFIE. A tool that will be used throughout the following chapters are quasi-Helmholtz decompositions: they allow for a separate preconditioning of $\boldsymbol{T}_{\mathrm{A}}$ and $\boldsymbol{T}_{\Phi}$, and they can be used to consider equivalent problems linked to scalar integral operators, which makes it, for example, easier to devise a new basis.

## $\alpha$) Quasi-Helmholtz Decompositions

Quasi-Helmholtz decomposition have a long history, as pointed out in Chapter 1, since they were originally used to cure the low-frequency breakdown of the EFIE. Two families of basis functions, a solenoidal basis complemented with a non-solenoidal basis that can represent the charge, are employed. By rescaling these bases in $k$, the low-frequency breakdown is prevented.

Examples for classical quasi-Helmholtz decompositions are the loop-star and the loop-tree decomposition [WGK95; BK95; Vec99]. While for practical purposes the loop-tree decomposition works better than the loop-star decomposition, we show in this section that the latter is a better foundation for the development of new preconditioning strategies. Different from a real Helmholtz decomposition, where we would have a solenoidal and an irrotational basis, both the loop-star and the loop-tree decomposition provide a quasi-Helmholtz decomposition: instead of forming an irrotational basis, the star and the tree functions are only non-solenoidal. In fact, there is no real Helmholtz decomposition available for the RWG function space and thus we will frequently omit the word "quasi" and only use it if we want to stress the nature of the decomposition.

In more detail, let $\boldsymbol{\Lambda}_n \in X_{\boldsymbol{\Lambda}}$ be loop functions, $\boldsymbol{H}_n \in X_{\boldsymbol{H}}$ be global loops and $\boldsymbol{\Sigma}_n \in X_{\boldsymbol{\Sigma}}$ be star functions [WGK95; Vec99]. The global loops $\boldsymbol{H}_n$ are the discrete counterpart of the quasi-harmonic Helmholtz subspace. Their definition, however, is subtle and cannot be treated here (see, for example, [WG81; Coo+09]). As $X_{\boldsymbol{f}} = X_{\boldsymbol{\Lambda}} \oplus X_{\boldsymbol{H}} \oplus X_{\boldsymbol{\Sigma}}$, there are transformation matrices $\boldsymbol{\Lambda} \in \mathbb{R}^{N \times N_{\mathrm{V}}}$, $\boldsymbol{H} \in \mathbb{R}^{N \times N_{\mathrm{H}}}$, and $\boldsymbol{\Sigma} \in \mathbb{R}^{N \times N_{\mathrm{C}}}$ that link the expansion coefficients of the current in the loop-star

basis to the expansion coefficients in the RWG basis, that is, we have

$$\boldsymbol{j} = \boldsymbol{\Lambda}\boldsymbol{j}_{\Lambda} + \boldsymbol{H}\boldsymbol{j}_{H} + \boldsymbol{\Sigma}\boldsymbol{j}_{\Sigma} \tag{4.64}$$

and

$$\sum_{n=1}^{N} \left[\boldsymbol{j}\right]_n \boldsymbol{f}_n = \sum_{n=1}^{N_{\mathrm{V}}} \left[\boldsymbol{j}_{\Lambda}\right]_n \boldsymbol{\Lambda}_n + \sum_{n=1}^{N_{\mathrm{H}}} \left[\boldsymbol{j}_{H}\right]_n \boldsymbol{H}_n + \sum_{n=1}^{N_{\mathrm{C}}} \left[\boldsymbol{j}_{\Sigma}\right]_n \boldsymbol{\Sigma}_n\,, \tag{4.65}$$

where $\boldsymbol{j}_{\Lambda}$, $\boldsymbol{j}_{H}$, and $\boldsymbol{j}_{\Sigma}$ are the unknown vectors in the loop-star basis, $N_{\mathrm{V}}$ is the number of vertices (inner vertices, when $\Gamma$ is an open surface), $N_{\mathrm{C}}$ the number of cells, and $N_{\mathrm{H}} = 2g$, where $g$ is the genus of $\Gamma$. Given the convention depicted in Figure 4.1, the loop transformation matrix is defined as

$$\left[\boldsymbol{\Lambda}\right]_{ij} = \begin{cases} 1 & \text{for } v_j = v_i^+\,, \\ -1 & \text{for } v_j = v_i^-\,, \\ 0 & \text{otherwise,} \end{cases} \tag{4.66}$$

where $v_j$ is the $j$th vertex of the mesh. When the surface is open, $v_j$ are the inner vertices of the mesh and $N_{\mathrm{V}}$ is the number of inner vertices. Following the convention in Figure 4.1, the star transformation matrix is defined as

$$\left[\boldsymbol{\Sigma}\right]_{ij} = \begin{cases} 1 & \text{for } c_j = c_i^+\,, \\ -1 & \text{for } c_j = c_i^-\,, \\ 0 & \text{otherwise,} \end{cases} \tag{4.67}$$

where $c_j$ is the domain of the $j$th cell of the mesh. In other words, the $j$th column of $\boldsymbol{\Lambda}$ and $\boldsymbol{\Sigma}$ carries the coefficients with which the $j$th loop and star function, respectively, can be expressed as a linear combination of RWG functions.

We define the loop-star preconditioner as

$$\boldsymbol{Q} = \begin{bmatrix} \boldsymbol{\Lambda}/\sqrt{\mathrm{i}k} & \boldsymbol{H}/\sqrt{\mathrm{i}k} & \boldsymbol{\Sigma}\sqrt{\mathrm{i}k} \end{bmatrix}. \tag{4.68}$$

The discretization with the loop-star basis leads to the system matrix $\boldsymbol{T}_{\boldsymbol{Q}}$, which is related to $\boldsymbol{T}$ by

$$\boldsymbol{T}_{\boldsymbol{Q}} = \boldsymbol{Q}^{\mathrm{T}}\boldsymbol{T}\boldsymbol{Q} = \begin{bmatrix} \boldsymbol{T}_{\Lambda\Lambda} & \boldsymbol{T}_{\Lambda\Sigma} \\ \boldsymbol{T}_{\Sigma\Lambda} & \boldsymbol{T}_{\Sigma\Sigma} \end{bmatrix} \tag{4.69}$$

if $\Gamma$ is simply connected.[30]

The loop-star decomposition has some interesting properties. First, we can relate the loop-loop and the star-star part of $\boldsymbol{T}_{\boldsymbol{Q}}$ to system matrices stemming from the discretization of scalar integral operators: we define the functions

$$\phi_i(\boldsymbol{r}) = \begin{cases} 3/A_i & \text{for } \boldsymbol{r} \in c_i\,, \\ -1/A_j & \text{for } \boldsymbol{r} \in c_j \text{ and } c_j \text{ is adjacent to } c_i\,, \\ 0 & \text{otherwise,} \end{cases} \tag{4.71}$$

which are the divergence of the star functions. Then we have [ATV10; Néd01]

$$\left[\boldsymbol{T}^0_{\Lambda\Lambda}\right]_{ij} = (\lambda_i, \mathcal{W}\lambda_j)_{L^2(\Gamma)}\,, \tag{4.72}$$

and

$$\left[\boldsymbol{T}^0_{\Sigma\Sigma}\right]_{ij} = (\phi_i, \mathcal{V}\phi_j)_{L^2(\Gamma)}\,. \tag{4.73}$$

At this point, we should comment on the fact that the loop and the star functions are not independent if $\Gamma$ is closed; the all-one vectors

$$\left[\boldsymbol{1}_\Lambda\right]_n = 1\,, \quad n = 1, \dots, N_\mathrm{V} \tag{4.74}$$

and

$$\left[\boldsymbol{1}_\Sigma\right]_n = 1\,, \quad n = 1, \dots, N_\mathrm{C} \tag{4.75}$$

are in the null spaces of $\boldsymbol{\Lambda}$ and $\boldsymbol{\Sigma}$, that is, $\boldsymbol{\Lambda}\boldsymbol{1}_\Lambda = \boldsymbol{0}$ and $\boldsymbol{\Sigma}\boldsymbol{1}_\Sigma = \boldsymbol{0}$. If $\Gamma$ is open, the loop functions are linearly independent, but since the overall charge is zero, the star functions remain linearly dependent. The consequence for the classical loop-star preconditioner is that if $\Gamma$ is closed, then a loop and a star function must be eliminated, and if $\Gamma$ is open, then only a star function must be eliminated resulting in transformation matrices $\boldsymbol{\Lambda} \in \mathbb{R}^{N \times N_\Lambda}$ and $\boldsymbol{\Sigma} \in \mathbb{R}^{N \times N_\Sigma}$, where $N_\Lambda$ and $N_\Sigma$ are the dimensions such that the loop and star functions are linearly independent and we have $N = N_\Lambda + N_\mathrm{H} + N_\Sigma$ [Vec99].

30 In the multiply connected case, it reads

$$\boldsymbol{T}_{\boldsymbol{Q}} = \boldsymbol{Q}^\mathrm{T}\boldsymbol{T}\boldsymbol{Q} = \begin{bmatrix} \boldsymbol{T}_{\Lambda\Lambda} & \boldsymbol{T}_{\Lambda\mathrm{H}} & \boldsymbol{T}_{\Lambda\Sigma} \\ \boldsymbol{T}_{\mathrm{H}\Lambda} & \boldsymbol{T}_{\mathrm{H}\mathrm{H}} & \boldsymbol{T}_{\mathrm{H}\Sigma} \\ \boldsymbol{T}_{\Sigma\Lambda} & \boldsymbol{T}_{\Sigma\mathrm{H}} & \boldsymbol{T}_{\Sigma\Sigma} \end{bmatrix} \tag{4.70}$$

.

For the preconditioning schemes we are developing in this thesis, this is not a customary choice. For example, the equality in (4.72) only holds if we do not eliminate a loop function since $\boldsymbol{W}$ has a null space spanned by $\mathbf{1}_\Lambda$ (and in the end, we are developing a preconditioner for $\boldsymbol{W}$, which we can then only apply to $\boldsymbol{T}_\mathrm{A}$ if this equality holds). Another issue by eliminating a function is that the matrices $\boldsymbol{\Lambda}$ and $\boldsymbol{\Sigma}$ become even more ill-conditioned [And12a]. For the (quasi-)Helmholtz projectors, we are introducing in Section 4.d.$\beta$, it is necessary to solve the systems $\boldsymbol{\Lambda}^\mathrm{T}\boldsymbol{\Lambda}\boldsymbol{x} = \boldsymbol{b}$ and $\boldsymbol{\Sigma}^\mathrm{T}\boldsymbol{\Sigma}\boldsymbol{x} = \boldsymbol{b}$. It turns out that if the functions are not eliminated, then it is easier to precondition these systems. Depending on the preconditioner used, however, a deflection of the null spaces might be necessary (see Section 4.d.$\beta$). The overall Helmholtz projectors are, however, identical, regardless whether we eliminate a function or not. We leverage this fact in Chapter 6 in order to keep the notation concise.

## $\beta$) Quasi-Helmholtz Projectors

We have seen that the loop-star basis allows to link $\boldsymbol{T}_\mathrm{A}$ to $\boldsymbol{W}$ and $\boldsymbol{T}_\Phi$ to $\boldsymbol{V}$. Another important property of the loop-star decomposition is the orthogonality between the transformation matrices: we have $\boldsymbol{\Lambda}^\mathrm{T}\boldsymbol{\Sigma} = \mathbf{0}$, $\boldsymbol{\Lambda}^\mathrm{T}\boldsymbol{H} = \mathbf{0}$, and $\boldsymbol{H}^\mathrm{T}\boldsymbol{\Sigma} = \mathbf{0}$. The orthogonality can be used to recover the loop or the star components of $\boldsymbol{j}$. The right-inverses of $\boldsymbol{\Lambda}$ and $\boldsymbol{\Sigma}$ are given by $(\boldsymbol{\Lambda}^\mathrm{T}\boldsymbol{\Lambda})^+\boldsymbol{\Lambda}^\mathrm{T}$ and $(\boldsymbol{\Sigma}^\mathrm{T}\boldsymbol{\Sigma})^+\boldsymbol{\Sigma}^\mathrm{T}$. If, for example, $(\boldsymbol{\Lambda}^\mathrm{T}\boldsymbol{\Lambda})^+\boldsymbol{\Lambda}^\mathrm{T}$ is applied to (4.64), then we obtain the loop expansion coefficients, that is, $\boldsymbol{j}_\Lambda = (\boldsymbol{\Lambda}^\mathrm{T}\boldsymbol{\Lambda})^+\boldsymbol{\Lambda}^\mathrm{T}\boldsymbol{j}$. The symbol "+" denotes the Moore-Penrose pseudo-inverse, which is necessary due to the linear dependency of the loop and the star functions.

This motivates the definition of quasi-Helmholtz projectors

$$\boldsymbol{P}_\Lambda := \boldsymbol{\Lambda}\left(\boldsymbol{\Lambda}^\mathrm{T}\boldsymbol{\Lambda}\right)^+\boldsymbol{\Lambda}^\mathrm{T} \tag{4.76}$$

and

$$\boldsymbol{P}_\Sigma := \boldsymbol{\Sigma}\left(\boldsymbol{\Sigma}^\mathrm{T}\boldsymbol{\Sigma}\right)^+\boldsymbol{\Sigma}^\mathrm{T} \tag{4.77}$$

where $\boldsymbol{P}_\Lambda$ projects to the solenoidal and $\boldsymbol{P}_\Sigma$ to the non-solenoidal Helmholtz subspace (for a detailed discussion and derivation of the Helmholtz projectors, see [And12a; And+13]). When the geometry is multiply connected, there is the projector $\boldsymbol{P}_\mathrm{H}$ that projects to the harmonic subspace. We can implicitly obtain this projector as

$$\boldsymbol{P}_\mathrm{H} = \boldsymbol{I} - \boldsymbol{P}_\Lambda - \boldsymbol{P}_\Sigma\,. \tag{4.78}$$

The matrices $\boldsymbol{\Sigma}^{\mathrm{T}}\boldsymbol{\Sigma}$ and $\boldsymbol{\Lambda}^{\mathrm{T}}\boldsymbol{\Lambda}$ are graph Laplacians and thus ill-conditioned. Standard techniques, such as algebraic multigrid preconditioners, allow an efficient inversion [LB12; NN12; Not]. In practice, the null spaces of $\boldsymbol{\Sigma}^{\mathrm{T}}\boldsymbol{\Sigma}$ and $\boldsymbol{\Lambda}^{\mathrm{T}}\boldsymbol{\Lambda}$ can prevent convergence when the residual error is low. To stabilize the iterative solver, we deflect the null space as follows. For a single body problem, we can invert the matrix $\boldsymbol{\Sigma}^{\mathrm{T}}\boldsymbol{\Sigma} + \hat{\mathbf{1}}_{\Sigma}\hat{\mathbf{1}}_{\Sigma}^{\mathrm{T}}$, where $\hat{\mathbf{1}}_{\Sigma} \in \mathbb{R}^{N_{\mathrm{C}}}$ is the normalized all-one vector (i.e., $\hat{\mathbf{1}}_{\Sigma} = \mathbf{1}_{\Sigma}/\|\mathbf{1}_{\Sigma}\|_2$) spanning the null space of $\boldsymbol{\Sigma}^{\mathrm{T}}\boldsymbol{\Sigma}$. We note that

$$\left(\boldsymbol{\Sigma}^{\mathrm{T}}\boldsymbol{\Sigma} + \hat{\mathbf{1}}_{\Sigma}\hat{\mathbf{1}}_{\Sigma}^{\mathrm{T}}\right)^{-1} = \left(\boldsymbol{\Sigma}^{\mathrm{T}}\boldsymbol{\Sigma}\right)^{+} + \hat{\mathbf{1}}_{\Sigma}\hat{\mathbf{1}}_{\Sigma}^{\mathrm{T}} \tag{4.79}$$

holds (see [And+13]). Other normalizations may be used as well. The best performance of the iterative solver can be expected when the singular value associated with $\hat{\mathbf{1}}_{\Sigma}\hat{\mathbf{1}}_{\Sigma}^{\mathrm{T}}$ is shifted into the spectrum of $\boldsymbol{\Sigma}^{\mathrm{T}}\boldsymbol{\Sigma}$. For a multibody problem, the dimensionality of the null space is the number of bodies $N_{\mathrm{B}}$. For the $i$th body, the $i$th vector $\hat{\mathbf{1}}_{\Sigma,i}$ is defined as

$$\left[\hat{\mathbf{1}}_{\Sigma,i}\right]_j = \begin{cases} 1/\sqrt{N_{\mathrm{C},i}}\,, & \text{when } c_j \in \Gamma_i \\ 0\,, & \text{else,} \end{cases} \tag{4.80}$$

where $N_{\mathrm{C},i}$ is the number of cells and $\Gamma_i$ is the surface of the $i$th body, respectively, and $c_j$ denotes the $j$th cell of the entire surface $\Gamma = \cup_{i=1}^{N_{\mathrm{B}}}\Gamma_i$. We define the matrix $\hat{\hat{\mathbf{1}}}_{\Sigma} \in \mathbb{R}^{N_{\mathrm{C}} \times N_{\mathrm{B}}}$ as

$$\left[\hat{\hat{\mathbf{1}}}_{\Sigma}\right]_{ji} = \left[\hat{\mathbf{1}}_{\Sigma,i}\right]_j \tag{4.81}$$

and then the matrix $\boldsymbol{\Sigma}^{\mathrm{T}}\boldsymbol{\Sigma} + \hat{\hat{\mathbf{1}}}_{\Sigma}\hat{\hat{\mathbf{1}}}_{\Sigma}^{\mathrm{T}}$ is invertible.

Similarly, we can deal with $\boldsymbol{\Lambda}^{\mathrm{T}}\boldsymbol{\Lambda}$. Different from $\boldsymbol{\Sigma}^{\mathrm{T}}\boldsymbol{\Sigma}$ though, the graph Laplacian $\boldsymbol{\Lambda}^{\mathrm{T}}\boldsymbol{\Lambda}$ has a null space only when the surface is closed. For stabilizing the inversion of $\boldsymbol{\Lambda}^{\mathrm{T}}\boldsymbol{\Lambda}$ in the presence of a null space, we can invert the matrix $\boldsymbol{\Lambda}^{\mathrm{T}}\boldsymbol{\Lambda}+\hat{\mathbf{1}}_{\Lambda}\hat{\mathbf{1}}_{\Lambda}^{\mathrm{T}}$ (i.e., using the same strategy, as we did in the case of $\boldsymbol{\Sigma}^{\mathrm{T}}\boldsymbol{\Sigma}$), where $\hat{\mathbf{1}}_{\Lambda}$ is the normalized all-one vector (i.e., $\hat{\mathbf{1}}_{\Lambda} = \mathbf{1}_{\Lambda}/\|\mathbf{1}_{\Lambda}\|_2$) spanning the null space of $\boldsymbol{\Lambda}^{\mathrm{T}}\boldsymbol{\Lambda}$. For a multibody problem, the dimensionality of the null space is the number of closed bodies $N_{\mathrm{B_C}}$. For the $i$th closed body, we have the vector $\hat{\mathbf{1}}_{\Lambda,i}$ with entries

$$\left[\hat{\mathbf{1}}_{\Lambda,i}\right]_j = \begin{cases} 1/\sqrt{N_{\mathrm{V},i}}\,, & \text{when } v_j \in \Gamma_i \\ 0\,, & \text{else,} \end{cases} \tag{4.82}$$

where $\Gamma_i$ is the surface of the $i$th closed body, $N_{\mathrm{V},i}$ is the number of vertices on this surface, and $v_j$ denotes the $j$th vertex of the entire surface $\Gamma$. We define the matrix $\boldsymbol{O}_\Lambda \in \mathbb{R}^{N_\Lambda \times N_{\mathrm{B_C}}}$ as

$$\left[\hat{\hat{\mathbf{1}}}_\Lambda\right]_{ji} = \left[\hat{\mathbf{1}}_{\Lambda,i}\right]_j \tag{4.83}$$

and then the matrix $\boldsymbol{\Lambda}^{\mathrm{T}}\boldsymbol{\Lambda} + \hat{\hat{\mathbf{1}}}_\Lambda \hat{\hat{\mathbf{1}}}_\Lambda^{\mathrm{T}}$ is invertible.

As demonstrated in [And+13], the projectors are an ideal means to cure the low-frequency breakdown. We define $\boldsymbol{P}_{\Lambda\mathrm{H}} = \boldsymbol{P}_\Lambda + \boldsymbol{P}_\mathrm{H}$. Applying the projectors to the system matrix, we find

$$\begin{aligned}(\boldsymbol{P}_{\Lambda\mathrm{H}} + \boldsymbol{P}_\Sigma)\boldsymbol{T}(\boldsymbol{P}_{\Lambda\mathrm{H}} + \boldsymbol{P}_\Sigma)&\\ = (\boldsymbol{P}_{\Lambda\mathrm{H}} + \boldsymbol{P}_\Sigma)\left(\mathrm{i}k\boldsymbol{T}_\mathrm{A} + 1/(\mathrm{i}k)\boldsymbol{T}_\Phi\right)(\boldsymbol{P}_{\Lambda\mathrm{H}} + \boldsymbol{P}_\Sigma)&\\ = (\mathrm{i}k)\boldsymbol{P}_{\Lambda\mathrm{H}}\boldsymbol{T}_\mathrm{A}\boldsymbol{P}_{\Lambda\mathrm{H}} + (\mathrm{i}k)\boldsymbol{P}_{\Lambda\mathrm{H}}\boldsymbol{T}_\mathrm{A}\boldsymbol{P}_\Sigma + (\mathrm{i}k)\boldsymbol{P}_\Sigma\boldsymbol{T}_\mathrm{A}\boldsymbol{P}_{\Lambda\mathrm{H}}&\\ + (\mathrm{i}k)\boldsymbol{P}_\Sigma\boldsymbol{T}_\mathrm{A}\boldsymbol{P}_\Sigma + 1/(\mathrm{i}k)\boldsymbol{P}_\Sigma\boldsymbol{T}_\Phi\boldsymbol{P}_\Sigma\,.&\end{aligned} \tag{4.84}$$

To prevent the low-frequency breakdown, we rescale the projectors with the square root of the wavenumber resulting in the preconditioner

$$\boldsymbol{P} = \left(1/\sqrt{k}\right)\boldsymbol{P}_{\Lambda\mathrm{H}} + \mathrm{i}\sqrt{k}\boldsymbol{P}_\Sigma\,. \tag{4.85}$$

Considering (4.20) and (4.84), it is evident that

$$\boldsymbol{P}\boldsymbol{T}\boldsymbol{P} \tag{4.86}$$

is free from the low-frequency breakdown.The imaginary unit +i is used to prevent the numerical cancellation due to the different scaling of the solenoidal and non-solenoidal components in the right-hand side and the current vector (for an exhaustive discussion, we refer the reader to [And+13]).

While (4.86) is free from the low-frequency breakdown, its condition number still grows with $1/h^2$. In the following parts, new paradigms in preconditioning are introduced to handle the dense-discretization breakdown.

# Part II.

# Hierarchical Bases on Structured and Unstructured Meshes

Chapter 5

# Primal and Dual Haar Bases on Unstructured Meshes for the EFIE

*A new hierarchical basis preconditioner for the EFIE operator is introduced. In contrast to other hierarchical basis preconditioners, it works on arbitrary meshes and preconditions both the vector and the scalar potential within the EFIE operator. This is achieved by taking into account that the vector and the scalar potential operator discretized with loop-star basis functions are related to the hypersingular and the single layer operator (i.e., the well known integral operators from electrostatics). The strategy proposed in this chapter for preconditioning the EFIE is the transformation of the scalar and the vector potential operator into operators equivalent to the single layer operator and to its inverse. Further mathematical considerations show that this allows to use generalized primal and dual Haar functions as preconditioner. It turns out though that in the case of the dual Haar wavelets, the inverse transformation matrix must be used. The numerical results show the effectiveness of the proposed preconditioner and the practical impact of theoretical developments in real case scenarios. This chapter is based on [AAE17].*

Quasi-Helmholtz decompositions—as we have seen in Chapter 4—are commonly used to cure the low-frequency breakdown. Typical examples are the loop-star and the loop-tree basis preconditioners, where the loop functions form a set of solenoidal functions and the star/tree functions form a set of non-solenoidal functions. With such a Helmholtz decomposed basis, the solenoidal null space of the scalar potential is exploited to separate the vector from the scalar potential operator allowing to rescale them in frequency [BK95; WGK95].

While loop-star and loop-tree preconditioners tackle the low-frequency breakdown, they do not cure the dense-discretization breakdown. The dense-discretization breakdown is due to the integrative and derivative strength of the vector and of the scalar potential operator giving rise to a condition number of the EFIE system matrix which scales with $1/h^2$, where $h$ is the average edge length of the mesh. Hierarchical basis preconditioners cure the dense-discretization breakdown when the basis is constructed such that it reflects the Sobolev norm induced by the EFIE operator [ATV10].

They are, however, not a panacea. In fact, the construction of a hierarchical basis for the discretization of vector operators such as the EFIE is far from being trivial, in particular, when three constraints are applied: (i) it should be possible to apply the hierarchical basis multiplicatively to an EFIE that is discretized with RWG functions (so that the hierarchical preconditioner can easily be integrated into existing codes), (ii) the construction and application of the hierarchical basis should have at most a quasilinear complexity (i.e., linear up to logarithmically growing multiplicative terms) so that the advantage of using fast matrix-vector multiplication algorithms is not jeopardized), and (iii) the hierarchical basis should be applicable to unstructured meshes. An unstructured mesh is the output of a mesher where, given a spline geometry, an optimized triangulation subject to a certain average edge length $h$ is generated. A structured mesh, on the other hand, is generated from a (usually coarse) unstructured mesh by sequentially refining it, for example, dyadically (i.e., the midpoints of the three edges of a cell are connected resulting in four smaller, new cells) until the desired average edge length $h$ is obtained.

While the first and second condition are met by virtually all hierarchical basis preconditioners [VPV05; ATV07; And12b; ATV10; Che+09; HM12], there have been only few hierarchical bases reported for the EFIE that work on unstructured meshes as well [AVV08]. The satisfaction of the third criterion, however, is decisive for the practicality of the hierarchical basis preconditioner. Structured meshes are, in industrial applications, rarely used for two reasons. Usually one cannot start from a coarse mesh and perform a structured refinement. Most of the time, one has to start with a mesh that is relatively fine since only then the details of the spline geometry can be captured. In addition, the hierarchical basis only reduces the condition number to one obtained by a discretization of the EFIE on coarsest mesh. This condition number can still be prohibitively large so that the effectiveness of the hierarchical basis preconditioner is insufficient.

Currently available hierarchical basis preconditioners for unstructured meshes only precondition the scalar potential operator [AVV08; DJC11]. As part of the underlying quasi-Helmholtz decomposition, loop functions are used for the solenoidal basis which, however, do not cure the dense-discretization breakdown of the vector potential operator [And12a]. Thus the condition number of the entire system matrix still grows with $1/h$ and we face the open task to find a hierarchical basis that preconditions the vector potential operator on unstructured meshes.

The reason why there is a hierarchical basis preconditioner available for the scalar potential operator but not for the vector potential operator can be explained as follows. When the EFIE operator is discretized with RWG functions as expansion and testing functions, the scalar potential operator is a single layer operator discretized with piecewise constant basis functions related to the two divergence terms of the current basis functions. This allows, once these divergence terms are resolved, to reuse a hierarchical basis defined on the space of piecewise constant functions [AVV08].

The vector potential operator, on the other hand, is a single layer operator on the vector function space of the electric surface current density $\boldsymbol{j}$. Unlike the scalar potential operator, we cannot turn it directly into a scalar single layer operator. Yet, there is an important property of the vector potential operator: we have seen in Chapter 4 that when loop functions are used, the discretized vector potential operator is equivalent to the hypersingular operator $\mathcal{W}$ discretized with scalar piecewise linear functions. This simplifies our task of preconditioning the vector potential operator since we do not have to deal with a vector but a scalar operator, that is, we "only" have to find a hierarchical basis for a scalar function space.

In this chapter, a provable hierarchical preconditioning strategy for the vector potential operator is reported. The three criteria (i)-(iii) for a good hierarchical basis preconditioner stated before are satisfied. Both the scalar and the vector potential operator are preconditioned in this work by generalized primal and dual Haar bases (i.e. generalized Haar bases defined on the standard and dual mesh respectively). In order to precondition the scalar potential operator with the primal Haar basis, we use graph Laplacians to transform it into the single layer operator $\mathcal{V}$. For the vector potential operator instead, which relates to the hypersingular operator $\mathcal{W}$, we exploit the spectral equivalency of the latter to the inverse single layer operator to precondition it with a linear-in-complexity,

closed-form inverse of the dual Haar basis. Since the generalized Haar basis is easy to construct and the same code can be used for the generation of the primal and the dual Haar bases, the implementational effort of using the preconditioner is minimal.

The chapter is structured as follows: in Section 5.a, we comment on the scattering scenario. Section 5.b introduces the primal and the dual Haar basis. In Section 5.c, we show how the vector and the scalar potential operator can be transformed into operators spectrally equivalent to the single layer operator and its inverse and how they can be preconditioned with a generalized Haar bases in these representations. In Section 5.d, we present numerical results that demonstrate the effectiveness of the proposed approach.

## a) Background

As required in Chapter 4, the scatterer $\Omega \subset \mathbb{R}^3$ is Lipschitz polyhedral, we constrain ourselves, however, to the discussion of simply connected geometries to keep the notation concise. For multiply connected geometries, the hierarchical basis can be complemented with global loops as discussed in Section 4.d.$\alpha$. If the number of global functions is large, or even scales with $N$, this is not efficient anymore. Chapter 6 discusses how hierarchical basis preconditioners can be combined with a Helmholtz projector approach, where the quasi-harmonic Helmholtz subspace is only recovered implicitly. Whenever relevant for the implementation of the hierarchical basis preconditioner, we will point out to the reader the necessary modifications to apply the technique to multi-body problems, both closed and open.

## b) Construction of the Generalized Haar Basis

Generalized Haar bases have been constructed before, also for the case of unstructured meshes (see, for example, [HKS05], where an octree was used for the partitioning of the mesh). Classically, a Haar basis would be constructed on the space of piecewise constant functions $X_p$. As it turns out in Section 5.c, we also need a Haar basis for the piecewise constant functions defined on the dual mesh, which we denote as $\tilde{p}_i \in X_{\tilde{p}}$. Different from the standard piecewise

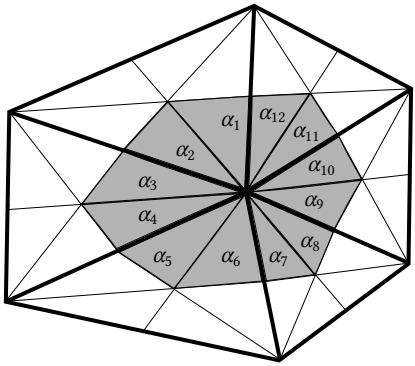


*Fig. 5.1.:* The standard (thick lines) and the barycentrically refined (thin lines) mesh. The grey shaded area is a dual cell.

constant functions, which are defined on the cells of the mesh, these functions are associated with the vertices of the mesh. We can define the dual piecewise constant functions by using a barycentric mesh refinement. The support of the dual piecewise constant function $\tilde{p}_j$ is given by the cells on the barycentrically refined mesh that are attached to the $j$th vertex (Figure 5.1 shows the support of a dual piecewise constant function). When $\boldsymbol{r}$ is in the support of $\tilde{p}_j$, the function value $\tilde{p}_j(\boldsymbol{r}) = 1/\widetilde{A}_j$, where $\widetilde{A}_j$ is the area of the support of $p_j$, and is zero when $\boldsymbol{r}$ is not in the support of $\tilde{p}_j$. Let $p_i^{\text{bar}}$ be the standard piecewise constant functions defined on the barycentrically refined mesh. For the example given in Figure 5.1, we find

$$\tilde{p}_j = \sum_{i=1}^{12} \alpha_i p_i^{\text{bar}}, \tag{5.1}$$

where $\alpha_i = A_i^{\text{bar}}/\widetilde{A}_j$ for all $i = 1, \dots, 12$ with $A_i^{\text{bar}}$ being the area of the support of $p_i^{\text{bar}}$ and $\widetilde{A}_j = \sum_{i=1}^{12} A_i^{\text{bar}}$ is the area of the support of $\tilde{p}_j$. Now we have all the functions spaces necessary to construct the primal and dual Haar bases.

The Haar bases are obtained in the form of transformation matrices $\hat{\boldsymbol{H}}_\Sigma$ and $\hat{\boldsymbol{H}}_\Lambda$. The columns of the matrices $\hat{\boldsymbol{H}}_\Sigma$ and $\hat{\boldsymbol{H}}_\Lambda$ carry the expansion coefficients of the Haar functions in terms of piecewise constant $p_i$ and dual piecewise constant

functions $\tilde{p}_i$, respectively. We refer to the generalized Haar bases $\hat{\boldsymbol{H}}_\Sigma$ and $\hat{\boldsymbol{H}}_\Lambda$ as primal and dual generalized Haar basis.

We start with the construction of $\hat{\boldsymbol{H}}_\Sigma$. The construction algorithm requires as input the cell-based graph Laplacian $\boldsymbol{\Sigma}^\mathrm{T}\boldsymbol{\Sigma}$ and the areas $A_i$ of the cells $c_i$ of the mesh. The construction of the Haar basis begins with defining the entire mesh as a macro cell (see Figure 5.2a). On this macro cell, the first generalized Haar function is defined as the constant function

$$p_{\mathrm{H},0} = 1/A_\Gamma\,, \quad \boldsymbol{r} \in \Gamma\,, \tag{5.2}$$

where $A_\Gamma$ is the area of the surface $\Gamma$. Eventually, we seek to obtain a multiplicative preconditioner in the form of a matrix $\hat{\boldsymbol{H}}_\Sigma$ that maps from the generalized Haar functions to the piecewise constant functions $p_i \in X_p$. We have the relationship

$$p_{\mathrm{H},0} = 1/A_\Gamma \sum_{i=1}^{N_\mathrm{C}} A_i p_i \tag{5.3}$$

between the first generalized Haar function and the functions $p_i \in X_p$. We insert the expansion coefficients for $p_{\mathrm{H},0}$, which are

$$\left[\hat{\boldsymbol{H}}_\Sigma\right]_{i1} = A_i/A_\Gamma \tag{5.4}$$

with $i = 1, \ldots, N_\mathrm{C}$, in the first column of $\hat{\boldsymbol{H}}_\Sigma$.

The next Haar functions are obtained by dividing the mesh into $N_\mathrm{m} = 4$ macro cells. Although alternative strategies are possible [MA14], in our implementation, we have used the graph partitioning algorithms made available by the METIS library [KK98]. Other graph partitioning algorithms could be used as well as long as they can ensure that the macro cells have (approximately) the same area and that the cells in a macro cell are all connected by their edges. An example for the division is shown in Figure 5.2.

We denote the domains of the thereby generated macro cells by $c_{\mathrm{m},i}, i = 1, \ldots, N_\mathrm{m}$ and define macro piecewise constant functions

$$p_{\mathrm{m},i} = \begin{cases} \dfrac{1}{A(c_{\mathrm{m},i})} & \boldsymbol{r} \in c_{\mathrm{m},i}\,, \\ 0 & \boldsymbol{r} \notin c_{\mathrm{m},i}\,, \end{cases} \tag{5.5}$$

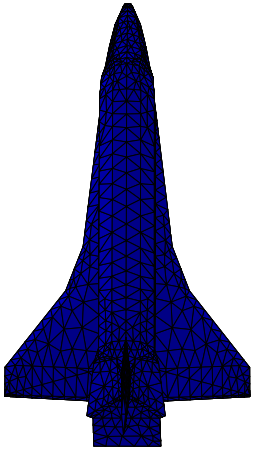

*(a)* The initial macro cell.

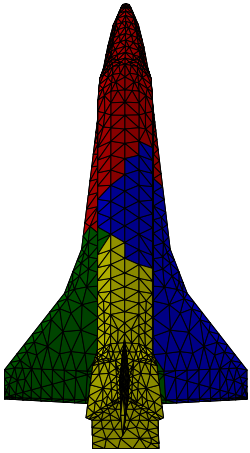

*(b)* The macro cells after the first partitioning using METIS.

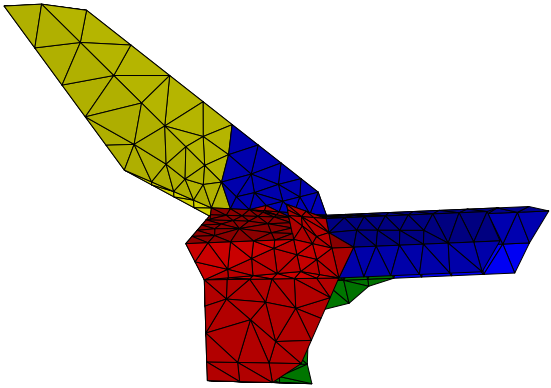

*(c)* The next macro cells after the application of METIS to a macro cell from Figure 5.2b.

*Fig. 5.2.:* Space Shuttle: macro cells generated by using METIS.

where $A(c_{\mathrm{m},i})$ is the area of the macro cell $c_{\mathrm{m},i}$. Notice, that these functions are normalized such that $\int_\Gamma p_{\mathrm{m},i}\mathrm{d}S(\boldsymbol{r}) = 1$. The functions $p_{\mathrm{m},i}$ are given in terms of $p_j$ as

$$p_{\mathrm{m},i} = 1/A(c_{\mathrm{m},i}) \sum_{i \in \left\{ n \in N \mid c_n \subset c_{\mathrm{m},i} \right\}} A_i p_i \,. \tag{5.6}$$

With this relationship, we obtain the vectors

$$\left[\boldsymbol{b}_i\right]_n = \begin{cases} A_n/A(c_{\mathrm{m},i}) & \text{when } c_n \subset c_{\mathrm{m},i}\,, \\ 0 & \text{otherwise,} \end{cases} \tag{5.7}$$

and we can combine them columnwise in the matrix $\boldsymbol{B} = \begin{bmatrix} \boldsymbol{b}_1 & \dots & \boldsymbol{b}_{N_\mathrm{m}} \end{bmatrix}$.

The functions $p_{\mathrm{m},i}$ with $i = 1, \dots, N_\mathrm{m}$ and $p_{\mathrm{H},0}$ are linearly dependent, and they are not orthogonal to $p_{\mathrm{H},0}$. Therefore, we need to form $N_\mathrm{m} - 1$ linear combinations of macro piecewise constant functions $p_{\mathrm{H},j}$ such that $\left(p_{\mathrm{H},0}, p_{\mathrm{H},j}\right)_{L^2} = 0$ for $j = 1, \dots, N_\mathrm{m} - 1$. There is not a unique solution, and so we strive to orthogonalize the Haar functions of the same group as well, which we obtain in the case of uniform meshes by considering the unweighted cell-based graph Laplacian $\boldsymbol{L}$ defined by the $N_\mathrm{m}$ macro cells $c_{\mathrm{m},i}$ and apply the SVD, that is, we have $\boldsymbol{U}\boldsymbol{S}\boldsymbol{U}^\mathrm{T} = \boldsymbol{L}$. Then we define the matrix $\boldsymbol{R} = \boldsymbol{U}(1 : \mathrm{end}, 1 : \mathrm{end} - 1)$ (Matlab notation). Using this matrix, we define the Haar functions as

$$p_{\mathrm{H},j} = \sum_{i=1}^{N_\mathrm{m}} p_{\mathrm{m},i} \left[\boldsymbol{R}\right]_{ij}, \quad j = 1, \dots, N_\mathrm{m} - 1 \tag{5.8}$$

noting that $\sum_i \boldsymbol{R}(i,j) = 0$ which ensures the orthogonality of the Haar wavelets to $p_{\mathrm{H},0}$. Given these definitions, the matrix $\boldsymbol{B}\boldsymbol{R}$ is the transformation matrix that maps from the Haar functions to the piecewise constant functions $p_i \in X_p$. The matrix $\boldsymbol{B}\boldsymbol{R}$ is added to the matrix $\hat{\boldsymbol{H}}_\Sigma$, which at this point consists of a single column associated with $p_{\mathrm{H},0}$.

The remaining generalized Haar functions are obtained recursively: each macro cell, when it contains more than one cell, is subject to a further division into $N_\mathrm{m}$ cells (as it is depicted in Figure 5.2b and Figure 5.2c). This gives rise to new macro cells, on which we define new macro piecewise constant functions; we obtain a new matrix $\boldsymbol{B}$ and a new matrix $\boldsymbol{R}$, and every time the new matrix $\boldsymbol{B}\boldsymbol{R}$ is added to $\hat{\boldsymbol{H}}_\Sigma$. In this way, we obtain $N_\mathrm{C}$ generalized Haar functions.

Since the primal generalized Haar basis is used for representing the electric charge and since the total charge is zero, we discard the function $p_{\mathrm{H},0}$ and denote the resulting matrix as $\boldsymbol{H}_\Sigma \in \mathbb{R}^{N_\mathrm{C} \times N_\Sigma}$.

Analogously, the dual generalized Haar basis $\hat{\boldsymbol{H}}_\Lambda$ can be constructed. As input, we now need the vertex-based graph Laplacian matrix $\boldsymbol{\Lambda}^\mathrm{T}\boldsymbol{\Lambda}$ and the areas $\widetilde{A}_i$ of the dual cells $\tilde{c}_i$, where $\tilde{c}_i$ denotes the support of the $i$th dual piecewise constant function. The definition of $p_{\mathrm{H},0}$ stays the same as in (5.2), and we represent it as a linear combination of dual piecewise constant functions

$$p_{\mathrm{H},0} = 1/A_\Gamma \sum_{i=1}^{N_\mathrm{V}} \widetilde{A}_i \tilde{p}_i \,. \tag{5.9}$$

Therefore, the first column of $\hat{\boldsymbol{H}}_\Lambda$ is given by

$$\left[\hat{\boldsymbol{H}}_\Lambda\right]_{i1} = \widetilde{A}_i / A_\Gamma \tag{5.10}$$

with $i = 1, \dots, N_\mathrm{V}$.

On each of these dual macro cells we define a dual macro piecewise constant function

$$\tilde{p}_{\mathrm{m},i} = \begin{cases} \dfrac{1}{\widetilde{A}(c_{\mathrm{m},i})} & \boldsymbol{r} \in \tilde{c}_{\mathrm{m},i} \,, \\ 0 & \boldsymbol{r} \notin \tilde{c}_{\mathrm{m},i} \,, \end{cases} \tag{5.11}$$

where $\widetilde{A}(c_{\mathrm{m},i})$ is the area of the dual macro cell $\tilde{c}_{\mathrm{m},i}$. Notice, that these functions are normalized such that $\int_\Gamma \tilde{p}_{\mathrm{m},i} \mathrm{d}S(\boldsymbol{r}) = 1$. We define the vectors

$$\left[\tilde{\boldsymbol{b}}_i\right]_n = \begin{cases} \widetilde{A}_n / \widetilde{A}(\tilde{c}_{\mathrm{m},i}) & \text{when } \tilde{c}_n \subset \tilde{c}_{\mathrm{m},i} \,, \\ 0 & \text{otherwise,} \end{cases} \tag{5.12}$$

and we combine them columnwise in the matrix $\widetilde{\boldsymbol{B}} = \begin{bmatrix} \tilde{\boldsymbol{b}}_1 & \dots & \tilde{\boldsymbol{b}}_{N_\mathrm{m}} \end{bmatrix}$.

The dual macro functions are combined to the dual generalized Haar functions

$$\tilde{p}_{\mathrm{H},j} = \sum_{i=1}^{N_\mathrm{m}} \tilde{p}_{\mathrm{m},i} \left[\widetilde{\boldsymbol{R}}\right]_{ij} \,, \quad j = 1, \dots, N_\mathrm{m} - 1 \tag{5.13}$$

such that $\left(p_{\mathrm{H},0}, \tilde{p}_{\mathrm{H},j}\right)_{L^2} = 0$ and where $\widetilde{\boldsymbol{R}}$ is obtained analogously to $\boldsymbol{R}$ by using the SVD applied to the cell-based graph Laplacian of the $N_\mathrm{m}$ dual macro cells $\tilde{c}_{\mathrm{m},i}$.

The matrix $\widetilde{\boldsymbol{B}}\widetilde{\boldsymbol{R}}$ is the transformation matrix that maps from the Haar functions to the dual piecewise constant functions $\tilde{p}_i \in X_{\tilde{p}}$. The matrix $\widetilde{\boldsymbol{B}}\widetilde{\boldsymbol{R}}$ is added to $\hat{\boldsymbol{H}}_\Lambda$, which at this point consists of a single column which is associated with $p_{\mathrm{H},0}$. Then the algorithm continues recursively by further dividing the dual macro cells and generating for each new division step the matrices $\widetilde{\boldsymbol{B}}\widetilde{\boldsymbol{R}}$.

When the surface is closed, the function $p_{\mathrm{H},0}$ and the associated column in $\hat{\boldsymbol{H}}_\Lambda$ are discarded. We denote the resulting matrix as $\boldsymbol{H}_\Lambda$. Different from the generation of $\boldsymbol{H}_\Sigma$, special care must be taken when the surface is open. First of all, only the dual piecewise constant functions associated with the inner vertices of the mesh are considered. Secondly, the function $p_{\mathrm{H},0}$ must not be discarded (i.e., $\boldsymbol{H}_\Lambda := \hat{\boldsymbol{H}}_\Lambda$) as in this case the loop functions are a set of linearly independent functions and thus $\boldsymbol{\Lambda}^{\mathrm{T}}\boldsymbol{T}_{\mathrm{A}}\boldsymbol{\Lambda}$ has full rank.

## c) New Hierarchical Basis

In the following, we transform the vector and the scalar potential operator such that we can apply a generalized Haar basis for preconditioning.

### $\alpha$) Scalar Potential Operator

It is known that $\boldsymbol{V}$ can be preconditioned by applying the Haar basis transformation matrix $\hat{\boldsymbol{H}}_\Sigma$—at least on structured meshes—followed by the diagonal rescaling matrix [Osw94; Osw98; HKS05]

$$\left[\hat{\boldsymbol{D}}_\Sigma\right]_{ii} = 2^{-\hat{l}_\Sigma(i)/2}\,, \tag{5.14}$$

where the function $\hat{l}_\Sigma(i)$, $i \in \{1, \dots, N_{\mathrm{C}}\}$, returns the level on which the associated Haar function is defined, so that the condition number bound

$$\mathrm{cond}\left(\hat{\boldsymbol{D}}_\Sigma \hat{\boldsymbol{H}}_\Sigma^{\mathrm{T}} \boldsymbol{V} \hat{\boldsymbol{H}}_\Sigma \hat{\boldsymbol{D}}_\Sigma\right) \lesssim \log^2(1/h) \tag{5.15}$$

holds [Osw98]. The numerical results show that such a basis is an effective preconditioner even for unstructured meshes.

The divergence of $\boldsymbol{f}_n$ is given by [RWG82]

$$\operatorname{div}_\Gamma \boldsymbol{f}_n = \begin{cases} 1/A_n^+, & \boldsymbol{r} \in c_n^+, \\ -1/A_n^-, & \boldsymbol{r} \in c_n^-, \\ 0, & \text{otherwise.} \end{cases} \tag{5.16}$$

Since the functions $\operatorname{div}_\Gamma \boldsymbol{f}_n$ are piecewise constant, they can be defined as a linear combination of $p_i$ functions, thereby giving rise to a transformation matrix $\boldsymbol{X}$. Then we have

$$\left[\boldsymbol{T}_\Phi\right]_{ij} := -\left(\hat{\boldsymbol{n}} \times \boldsymbol{f}_i, \boldsymbol{\mathcal{T}}_\Phi \boldsymbol{f}_j\right)_\Gamma = \boldsymbol{X}^{\mathrm{T}} \boldsymbol{V} \boldsymbol{X}\,, \tag{5.17}$$

where the matrix $\boldsymbol{X} \in \mathbb{R}^{N_\mathrm{C} \times N}$ is defined as

$$\left[\boldsymbol{X}\right]_{ij} = \begin{cases} 1 & \text{for } c_i = c_j^+\,, \\ -1 & \text{for } c_i = c_j^-\,, \\ 0 & \text{otherwise.} \end{cases} \tag{5.18}$$

Comparing (5.18) with (4.67), we see that $\boldsymbol{X} = \boldsymbol{\Sigma}^{\mathrm{T}}$, and another application of $\boldsymbol{\Sigma}$ yields

$$\boldsymbol{T}^0_{\Sigma\Sigma} = \boldsymbol{\Sigma}^{\mathrm{T}} \boldsymbol{\Sigma} \boldsymbol{V} \boldsymbol{\Sigma}^{\mathrm{T}} \boldsymbol{\Sigma}\,. \tag{5.19}$$

To apply the generalized Haar basis to the scalar potential operator, we must remove the star transformation matrices $\boldsymbol{\Sigma}^{\mathrm{T}}\boldsymbol{\Sigma}$ in (5.19). We apply from left and right $(\boldsymbol{\Sigma}^{\mathrm{T}}\boldsymbol{\Sigma})^+$, where the "+"-symbol denotes the Moore-Penrose pseudo-inverse, and find

$$\left(\boldsymbol{\Sigma}^{\mathrm{T}}\boldsymbol{\Sigma}\right)^+ \boldsymbol{\Sigma}^{\mathrm{T}} \boldsymbol{\Sigma} \boldsymbol{V} \boldsymbol{\Sigma}^{\mathrm{T}} \boldsymbol{\Sigma} \left(\boldsymbol{\Sigma}^{\mathrm{T}}\boldsymbol{\Sigma}\right)^+ = \left(\boldsymbol{\Sigma}^{\mathrm{T}}\boldsymbol{\Sigma}\right)^+ \boldsymbol{T}^0_{\Sigma\Sigma} \left(\boldsymbol{\Sigma}^{\mathrm{T}}\boldsymbol{\Sigma}\right)^+ . \tag{5.20}$$

The pseudo-inverse is necessary since there are only $N_\Sigma = N_\mathrm{C} - 1$ linearly independent star functions as the total charge is always zero [Vec99].

We take this latter fact into account by using $\boldsymbol{H}_\Sigma \in \mathbb{R}^{N_\mathrm{C} \times N_\Sigma}$, which is obtained from $\hat{\boldsymbol{H}}_\Sigma$ by discarding the constant Haar function (see Section 5.b). In order to apply $\boldsymbol{H}_\Sigma \boldsymbol{D}_\Sigma$ to (5.20), we must have

$$\boldsymbol{D}_\Sigma \boldsymbol{H}_\Sigma^{\mathrm{T}} \left(\boldsymbol{\Sigma}^{\mathrm{T}}\boldsymbol{\Sigma}\right)^+ \boldsymbol{\Sigma}^{\mathrm{T}} \boldsymbol{\Sigma} \boldsymbol{V} \boldsymbol{\Sigma}^{\mathrm{T}} \boldsymbol{\Sigma} \left(\boldsymbol{\Sigma}^{\mathrm{T}}\boldsymbol{\Sigma}\right)^+ \boldsymbol{H}_\Sigma \boldsymbol{D}_\Sigma = \boldsymbol{D}_\Sigma \boldsymbol{H}_\Sigma^{\mathrm{T}} \boldsymbol{V} \boldsymbol{H}_\Sigma \boldsymbol{D}_\Sigma\,, \tag{5.21}$$

where $\left[\boldsymbol{D}_\Sigma\right]_{ii} = 2^{-l_\Sigma(i)/2}$ with $i \in \{1, \dots, N_\Sigma\}$ and $l_\Sigma(i) = \hat{l}_\Sigma(i+1)$. That (5.21) holds can be seen as follows: the system $\boldsymbol{\Sigma}^{\mathrm{T}}\boldsymbol{\Sigma}\boldsymbol{x} = \boldsymbol{y}$ is solvable only when $\boldsymbol{y}$ is in the range of $\boldsymbol{\Sigma}^{\mathrm{T}}\boldsymbol{\Sigma}$. It is easy to see that

$$\left[\boldsymbol{\Sigma}^{\mathrm{T}}\boldsymbol{\Sigma}\right]_{ij} = \begin{cases} \deg c_i & \text{if } i = j\,, \\ -1 & \text{if } i \neq j \text{ and } c_i \text{ is adjacent to } c_j\,, \\ 0 & \text{otherwise,} \end{cases} \tag{5.22}$$

where $\deg c_i$ is the degree of $c_i$ (i.e., the number of cells attached to $i$th cell). In other words $\boldsymbol{\Sigma}^{\mathrm{T}}\boldsymbol{\Sigma}$ is the graph Laplacian matrix associated with the cell-based graph. From this definition it follows that the left null space of $\boldsymbol{\Sigma}^{\mathrm{T}}\boldsymbol{\Sigma}$ is spanned by the all-one vector. Only vectors whose row sum is zero are orthogonal to this vector. Hence, the row sum of $\boldsymbol{y} = \boldsymbol{H}_\Sigma\boldsymbol{x}$ must be zero for all $\boldsymbol{x}$, as $\boldsymbol{y}$ must be in the range of $\boldsymbol{\Sigma}^{\mathrm{T}}\boldsymbol{\Sigma}$. That the row sum is zero for all $\boldsymbol{x}$, can be seen from the definition of $\boldsymbol{H}_\Sigma$ (see (5.7) and (5.8) in Section 5.b).

We define

$$\widehat{\boldsymbol{\Sigma}} := \left[\boldsymbol{\Sigma}\left(\boldsymbol{\Sigma}^{\mathrm{T}}\boldsymbol{\Sigma}\right)^{+}\boldsymbol{H}_\Sigma\right], \tag{5.23}$$

where the wide hat symbol "$\widehat{\ }$" signifies that we deal with a hierarchical basis. Then we have

$$\operatorname{cond}\left(\boldsymbol{D}_\Sigma\widehat{\boldsymbol{\Sigma}}^{\mathrm{T}}\boldsymbol{T}_\Phi^0\widehat{\boldsymbol{\Sigma}}\boldsymbol{D}_\Sigma\right) \lesssim \log^2(1/h) \tag{5.24}$$

since

$$\begin{aligned} \boldsymbol{D}_\Sigma\widehat{\boldsymbol{\Sigma}}^{\mathrm{T}}\boldsymbol{T}_\Phi^0\widehat{\boldsymbol{\Sigma}}\boldsymbol{D}_\Sigma &= \boldsymbol{D}_\Sigma\boldsymbol{H}_\Sigma^{\mathrm{T}}\left(\boldsymbol{\Sigma}^{\mathrm{T}}\boldsymbol{\Sigma}\right)^{+}\boldsymbol{\Sigma}^{\mathrm{T}}\boldsymbol{T}_{\Sigma\Sigma}^0\boldsymbol{\Sigma}\left(\boldsymbol{\Sigma}^{\mathrm{T}}\boldsymbol{\Sigma}\right)^{+}\boldsymbol{H}_\Sigma\boldsymbol{D}_\Sigma \\ &\overset{(5.20)}{=} \boldsymbol{D}_\Sigma\boldsymbol{H}_\Sigma^{\mathrm{T}}\left(\boldsymbol{\Sigma}^{\mathrm{T}}\boldsymbol{\Sigma}\right)^{+}\boldsymbol{\Sigma}^{\mathrm{T}}\boldsymbol{\Sigma}\boldsymbol{V}\boldsymbol{\Sigma}^{\mathrm{T}}\boldsymbol{\Sigma}\left(\boldsymbol{\Sigma}^{\mathrm{T}}\boldsymbol{\Sigma}\right)^{+}\boldsymbol{H}_\Sigma\boldsymbol{D}_\Sigma \\ &\overset{(5.21)}{=} \boldsymbol{D}_\Sigma\boldsymbol{H}_\Sigma^{\mathrm{T}}\boldsymbol{V}\boldsymbol{H}_\Sigma\boldsymbol{D}_\Sigma \end{aligned} \tag{5.25}$$

and

$$\operatorname{cond}\left(\boldsymbol{D}_\Sigma\boldsymbol{H}_\Sigma^{\mathrm{T}}\boldsymbol{V}\boldsymbol{H}_\Sigma\boldsymbol{D}_\Sigma\right) \lesssim \operatorname{cond}\left(\hat{\boldsymbol{D}}_\Sigma\hat{\boldsymbol{H}}_\Sigma^{\mathrm{T}}\boldsymbol{V}\hat{\boldsymbol{H}}_\Sigma\hat{\boldsymbol{D}}_\Sigma\right) \overset{(5.15)}{\lesssim} \log^2(1/h)\,, \tag{5.26}$$

where we used that for any symmetric, positive definite (SPD) matrix the symmetric elimination of a row and column leads to a smaller or at most equal condition number than the original matrix.

### $\beta$) Vector Potential Operator

According to (4.72), the loop-loop block matrix $\boldsymbol{T}^0_{\Lambda\Lambda}$ is identical to the discretization of the hypersingular operator with piecewise linear functions, that is,

$$\left[\boldsymbol{W}\right]_{ij} = \left[\boldsymbol{T}^0_{\Lambda\Lambda}\right]_{ij}. \tag{5.27}$$

Since a set of hierarchical piecewise linear functions for unstructured meshes is not available, we must resort to a strategy that does not explicitly require such a set of hierarchical functions.

To simplify the following analysis, we consider a modified hypersingular operator. Without the modification, the operator $\mathcal{W}$ is not $H^{1/2}(\Gamma)$-elliptic, and its discretization possesses a null space spanned by the constant functions. Following a standard approach [Ste10], we introduce the deflected operator

$$\hat{\mathcal{W}} : H^{1/2}(\Gamma) \longrightarrow H^{-1/2}(\Gamma) \tag{5.28}$$

defined by the bilinear form

$$\left(v, \hat{\mathcal{W}} w\right)_{L^2(\Gamma)} := (v, \mathcal{W} w)_{L^2(\Gamma)} + (1, w)_{L^2(\Gamma)}(1, v)_{L^2(\Gamma)} \tag{5.29}$$

for all $w, v \in H^{1/2}(\Gamma)$. We note that the unique solution $w$ of $\hat{\mathcal{W}} w = g$ is also a solution of $\mathcal{W} w = g$ when $g$ satisfies the solvability condition $\int_\Gamma g \mathrm{d}S(\boldsymbol{r}') = 0$. This can be seen when $v = 1$ in (5.29), which reduces to $(w, 1)_{L^2(\Gamma)}(1, 1)_{L^2(\Gamma)} = 0$ which implies $(w, 1)_{L^2(\Gamma)} = 0$. The discretization of $\hat{\mathcal{W}}$ is given by

$$\left[\hat{\boldsymbol{W}}\right]_{ij} = \left(\lambda_i, \hat{\mathcal{W}} \lambda_j\right)_{L^2(\Gamma)}. \tag{5.30}$$

With the dual piecewise constant functions we can discretize the single layer resulting in the matrix $\left[\widetilde{\boldsymbol{V}}\right]_{ij} = \left(\tilde{p}_i, \mathcal{V} \tilde{p}_j\right)_{L^2(\Gamma)}$. It should be noticed that by using dual piecewise constant functions, we obtain system matrices $\widetilde{\boldsymbol{V}}$ and $\boldsymbol{W}$ with equal dimensionality.

**Proposition 5.1.** *Let $\boldsymbol{H}_\Lambda$ be the transformation matrix from the dual generalized Haar basis to the dual piecewise constant functions as defined in Section 5.b, and let*

$$\left[\boldsymbol{D}_\Lambda\right]_{ii} = 2^{-l_\Lambda(i)/2}, \tag{5.31}$$

*where the function $l_\Lambda(i)$, $i \in \{1, \dots, N_\Lambda\}$ returns the level on which the associated Haar function is defined with $N_\Lambda = N_\mathrm{V} - 1$ the number of linearly independent loop functions. Then we have*

$$\mathrm{cond}\left( \boldsymbol{D}_\Lambda^{-1} \boldsymbol{H}_\Lambda^{\ddagger} \boldsymbol{G}_{\lambda\tilde{p}}^{-1} \boldsymbol{W} \boldsymbol{G}_{\lambda\tilde{p}}^{-\mathrm{T}} \left( \boldsymbol{H}_\Lambda^{\ddagger} \right)^{\mathrm{T}} \boldsymbol{D}_\Lambda^{-1} \right) \lesssim \log^2(1/h)\,, \tag{5.32}$$

*where $\left[\boldsymbol{G}_{\lambda\tilde{p}}\right]_{ij} = \left(\lambda_i, \tilde{p}_j\right)_{L^2(\Gamma)}$ and $\boldsymbol{H}_\Lambda^{\ddagger}$ is an $L^2$-generalized inverse matrix defined as*

$$\boldsymbol{H}_\Lambda^{\ddagger} = \left( \boldsymbol{H}_\Lambda^{\mathrm{T}} \boldsymbol{G}_{\tilde{p}\tilde{p}} \boldsymbol{H}_\Lambda \right)^{-1} \boldsymbol{H}_\Lambda^{\mathrm{T}} \boldsymbol{G}_{\tilde{p}\tilde{p}}\,. \tag{5.33}$$

*Proof.* From (5.15), we have

$$\mathrm{cond}\left( \hat{\boldsymbol{D}}_\Lambda \hat{\boldsymbol{H}}_\Lambda^{\mathrm{T}} \widetilde{\boldsymbol{V}} \hat{\boldsymbol{H}}_\Lambda \hat{\boldsymbol{D}}_\Lambda \right) \lesssim \log^2(1/h)\,, \tag{5.34}$$

where $\hat{\boldsymbol{H}}_\Lambda$ is defined in Section 5.b and $\left[\hat{\boldsymbol{D}}_\Lambda\right]_{ii} = 2^{-\hat{l}_\Lambda(i)/2}$ with $i \in \{0 \dots, N_\mathrm{V}\}$. Based on the scalar Calderón identities (see Section 3.c and [SW98; Hip06]), we have the spectral equivalence

$$\boldsymbol{x}^{\mathrm{T}} \widetilde{\boldsymbol{V}} \boldsymbol{x} \eqsim \boldsymbol{x}^{\mathrm{T}} \boldsymbol{G}_{\lambda\tilde{p}}^{\mathrm{T}} \hat{\boldsymbol{W}}^{-1} \boldsymbol{G}_{\lambda\tilde{p}} \boldsymbol{x}\,, \quad \forall \boldsymbol{x} \in \mathbb{R}^{N_\mathrm{V}} \tag{5.35}$$

and therefore obtain

$$\mathrm{cond}\left( \hat{\boldsymbol{D}}_\Lambda \hat{\boldsymbol{H}}_\Lambda^{\mathrm{T}} \boldsymbol{G}_{\lambda\tilde{p}}^{\mathrm{T}} \hat{\boldsymbol{W}}^{-1} \boldsymbol{G}_{\lambda\tilde{p}} \hat{\boldsymbol{H}}_\Lambda \hat{\boldsymbol{D}}_\Lambda \right) \lesssim \log^2(1/h) \tag{5.36}$$

from which

$$\mathrm{cond}\left( \hat{\boldsymbol{D}}_\Lambda^{-1} \hat{\boldsymbol{H}}_\Lambda^{-1} \boldsymbol{G}_{\lambda\tilde{p}}^{-1} \hat{\boldsymbol{W}} \boldsymbol{G}_{\lambda\tilde{p}}^{-\mathrm{T}} \hat{\boldsymbol{H}}_\Lambda^{-\mathrm{T}} \hat{\boldsymbol{D}}_\Lambda^{-1} \right) \lesssim \log^2(1/h) \tag{5.37}$$

holds, since all matrices appearing are invertible. We should now make the transition from $\hat{\boldsymbol{W}}$ to $\boldsymbol{W}$. It follows from (5.30), that $\hat{\boldsymbol{W}}\boldsymbol{x}$ can be replaced by $\boldsymbol{W}\boldsymbol{x}$ when the associated function $\lambda_{\boldsymbol{x}} := \sum_i \left[\boldsymbol{x}\right]_i \lambda_i$ satisfies $(\lambda_{\boldsymbol{x}}, 1)_{L^2(\Gamma)} = 0$. In matrix form, this can be expressed as

$$\tilde{\boldsymbol{a}}^{\mathrm{T}} \boldsymbol{G}_{\tilde{p}\lambda} \boldsymbol{x} = 0\,, \tag{5.38}$$

where $\left[\tilde{\boldsymbol{a}}\right]_i = \widetilde{A}_i$. Any preconditioner $\boldsymbol{X} \in \mathbb{R}^{N_\mathrm{V} \times N_\Lambda}$ applicable to $\boldsymbol{W}$ such that $\boldsymbol{X}^{\mathrm{T}} \boldsymbol{W} \boldsymbol{X}$ is well-conditioned must ensure for any $\boldsymbol{y} \in \mathbb{R}^{N_\Lambda}$ that the expansion coefficients $\boldsymbol{x} = \boldsymbol{X}\boldsymbol{y}$ satisfy the discrete solvability condition (5.38).

First, we note that $\hat{\boldsymbol{H}}_\Lambda^{-1} = (\hat{\boldsymbol{H}}_\Lambda^{\mathrm{T}} \boldsymbol{G}_{\tilde{p}\tilde{p}} \hat{\boldsymbol{H}}_\Lambda)^{-1} \hat{\boldsymbol{H}}_\Lambda^{\mathrm{T}} \boldsymbol{G}_{\tilde{p}\tilde{p}}$. Since $\boldsymbol{H}_\Lambda$ is obtained by eliminating the first column of $\hat{\boldsymbol{H}}_\Lambda$, we use as left inverse of $\boldsymbol{H}_\Lambda$ the matrix $\boldsymbol{H}_\Lambda^{\ddagger}$, which is obtained from $\hat{\boldsymbol{H}}_\Lambda^{-1}$ by eliminating the first row, and which we can write explicitly as $\hat{\boldsymbol{H}}_\Lambda^{\ddagger} = (\boldsymbol{H}_\Lambda^{\mathrm{T}} \boldsymbol{G}_{\tilde{p}\tilde{p}} \boldsymbol{H}_\Lambda)^{-1} \boldsymbol{H}_\Lambda^{\mathrm{T}} \boldsymbol{G}_{\tilde{p}\tilde{p}}$. Then we have

$$\mathrm{cond}\left( \boldsymbol{D}_\Lambda^{-1} \boldsymbol{H}_\Lambda^{\ddagger} \boldsymbol{G}_{\lambda\tilde{p}}^{-1} \hat{\boldsymbol{W}} \boldsymbol{G}_{\lambda\tilde{p}}^{-\mathrm{T}} \left( \hat{\boldsymbol{H}}_\Lambda^{\ddagger} \right)^{\mathrm{T}} \boldsymbol{D}_\Lambda^{-1} \right) \lesssim \log^2(1/h)\,, \tag{5.39}$$

since the matrix in (5.39) is symmetric, positive definite and for any such matrix the elimination of the $i$th row and column yields a condition number bounded by the condition number of the original matrix. In addition, by the definition of $\boldsymbol{H}^{\ddagger}$, we satisfy (5.38): for any $\boldsymbol{y} \in \mathbb{R}^{N_\Lambda}$, we find a $\boldsymbol{z} \in \mathbb{R}^{N_\Lambda}$ such that

$$\boldsymbol{y} = (\boldsymbol{H}_\Lambda^{\mathrm{T}} \boldsymbol{G}_{\tilde{p}\tilde{p}} \boldsymbol{H}_\Lambda)^{-1} \boldsymbol{D}_\Lambda^{-1} \boldsymbol{z}\,. \tag{5.40}$$

Defining $\boldsymbol{x} = \boldsymbol{G}_{\lambda\tilde{p}}^{-\mathrm{T}} \boldsymbol{G}_{\tilde{p}\tilde{p}} \boldsymbol{H}_\Lambda \boldsymbol{y}$ and inserting in (5.38), we obtain

$$\tilde{\boldsymbol{a}} \boldsymbol{G}_{\tilde{p}\lambda} \boldsymbol{x} = \tilde{\boldsymbol{a}} \boldsymbol{G}_{\tilde{p}\lambda} \boldsymbol{G}_{\lambda\tilde{p}}^{-\mathrm{T}} \boldsymbol{G}_{\tilde{p}\tilde{p}} \boldsymbol{H}_\Lambda \boldsymbol{y} = \tilde{\boldsymbol{a}} \boldsymbol{G}_{\tilde{p}\tilde{p}} \boldsymbol{H}_\Lambda \boldsymbol{y}\,. \tag{5.41}$$

Since $\left[ \boldsymbol{G}_{\tilde{p}\tilde{p}} \right]_{ii} = 1/\widetilde{A}_i$, eq. (5.41) can be written as

$$\mathbf{1}_\Lambda^{\mathrm{T}} \boldsymbol{H}_\Lambda \boldsymbol{y} = 0\,, \tag{5.42}$$

where $\mathbf{1}_\Lambda \in \mathbb{R}^{N_\mathrm{V}}$ is the all-one vector and the equality results from the definition of $\boldsymbol{H}_\Lambda$, where we notice that the column vectors of $\boldsymbol{H}_\Lambda$ have a zero mean value (see Section 5.b). □

Summarizing, we define the transformation matrix for the new solenoidal basis as

$$\widehat{\boldsymbol{\Lambda}} := \boldsymbol{\Lambda} \boldsymbol{G}_{\lambda\tilde{p}}^{-\mathrm{T}} \boldsymbol{G}_{\tilde{p}\tilde{p}} \boldsymbol{H}_\Lambda \left( \boldsymbol{H}_\Lambda^{\mathrm{T}} \boldsymbol{G}_{\tilde{p}\tilde{p}} \boldsymbol{H}_\Lambda \right)^{-1}. \tag{5.43}$$

The Gram matrix $\boldsymbol{G}_{\lambda\tilde{p}}$ can be computed analytically. We have

$$\left[ \boldsymbol{G}_{\lambda\tilde{p}} \right]_{ij} = \begin{cases} \dfrac{11}{18} & \text{when } i = j\,, \\ \dfrac{7}{18} \dfrac{A_{ij}^{+} + A_{ij}^{-}}{6} \dfrac{1}{\widetilde{A}_j}\,, & \text{when } i \in Adj(j)\,, \\ 0\,, & \text{otherwise,} \end{cases} \tag{5.44}$$

where $Adj(i)$ is the set of vertices adjoint to vertex $i$, $A_{ij}^{+}$ and $A_{ij}^{-}$ are the areas of the cells attached to the edge that connect the vertices $i$ and $j$, and $\widetilde{A}_i$ is the area of the dual cell attached to vertex $i$ (see Figure 5.1 for an example of a dual cell). Since this Gram matrix is well-conditioned and sparse, iterative solvers can be used for computing the application of $\boldsymbol{G}_{\lambda\tilde{p}}^{-1}$ to a vector.

We note that $\boldsymbol{H}_{\Lambda}^{\mathrm{T}}\boldsymbol{G}_{\tilde{p}\tilde{p}}\boldsymbol{H}_{\Lambda}$ is the Gram matrix of the Haar functions, that is,

$$\left[\boldsymbol{H}_{\Lambda}^{\mathrm{T}}\boldsymbol{G}_{\tilde{p}\tilde{p}}\boldsymbol{H}_{\Lambda}\right]_{ij} = \left(\tilde{p}_{H,i}, \tilde{p}_{H,j}\right)_{L^2} \tag{5.45}$$

(for an explicit definition of the Haar functions $\tilde{p}_{H,i}$, see Section 5.b). The inverse of the matrix $\boldsymbol{H}_{\Lambda}^{\mathrm{T}}\boldsymbol{G}_{\tilde{p}\tilde{p}}\boldsymbol{H}_{\Lambda}$ can be computed fast (i.e., in $\mathcal{O}(N_{\mathrm{V}})$ complexity). This can be seen by considering the structure of this Gram matrix: the only Haar functions which are not orthogonal to a Haar function $\tilde{p}_{\mathrm{H},i}$ in the $L^2$-sense are the Haar functions defined on the same macro cell as $\tilde{p}_{\mathrm{H},i}$; by construction of the Haar functions, we have ensured that the functions from different levels are $L^2(\Gamma)$-orthogonal. Haar functions on the same level but defined on different macro cells have orthogonal supports and thus are orthogonal in the $L^2(\Gamma)$-sense. As outlined in Section 5.b, every macro cell is split in (at most) four smaller macro cells, and hence, there are at most three Haar functions defined on a macro cell. Then for each Haar function there are at most only two other non-orthogonal Haar functions. Thus $\boldsymbol{H}_{\Lambda}^{\mathrm{T}}\boldsymbol{G}_{\tilde{p}\tilde{p}}\boldsymbol{H}_{\Lambda}$ is a block diagonal matrix with blocks of at most size $3 \times 3$ (i.e., to be precisely, it is block diagonal when the non-orthogonal Haar functions are grouped together). Clearly, this matrix is sparse with the number of elements scaling as $\mathcal{O}(N_{\mathrm{V}})$ and its inverse is given by the inversion of each of the matrix blocks. Since the costs for inverting a single block is independent from $N_{\mathrm{V}}$ and the number of blocks are scaling linearly in $N_{\mathrm{V}}$, the complexity for finding the inverse is $\mathcal{O}(N_{\mathrm{V}})$.

### $\gamma$) Proposed Preconditioner for the EFIE Operator

We define the overall basis transformation matrix as

$$\widehat{\boldsymbol{Q}} = \begin{bmatrix} \widehat{\boldsymbol{\Lambda}} & \widehat{\boldsymbol{\Sigma}} \end{bmatrix}, \tag{5.46}$$

where $\widehat{\boldsymbol{\Lambda}}$ was defined in (5.43) and $\widehat{\boldsymbol{\Sigma}}$ in (5.23), and the rescaling matrix as

$$\boldsymbol{D} = \begin{bmatrix} \boldsymbol{D}_\Lambda^{-1}/\sqrt{\mathrm{i}k} & \\ & \boldsymbol{D}_\Sigma\sqrt{\mathrm{i}k} \end{bmatrix}, \tag{5.47}$$

where $\boldsymbol{D}_\Lambda$ was defined in (5.31) and $\boldsymbol{D}_\Sigma$ in (5.14). We observe for the static limit

$$\lim_{k\to 0} \boldsymbol{D}\widehat{\boldsymbol{Q}}^{\mathrm{T}}\boldsymbol{T}^k\widehat{\boldsymbol{Q}}\boldsymbol{D} = \begin{bmatrix} \boldsymbol{D}_\Lambda^{-1}\widehat{\boldsymbol{\Lambda}}^{\mathrm{T}}\boldsymbol{T}_{\mathrm{A}}^0\widehat{\boldsymbol{\Lambda}}\boldsymbol{D}_\Lambda^{-1} & \\ & \boldsymbol{D}_\Sigma\widehat{\boldsymbol{\Sigma}}^{\mathrm{T}}\boldsymbol{T}_\Phi^0\widehat{\boldsymbol{\Sigma}}\boldsymbol{D}_\Sigma \end{bmatrix} \tag{5.48}$$

and because of (5.24) and (5.32), we have

$$\operatorname{cond}\left(\lim_{k\to 0} \boldsymbol{D}\widehat{\boldsymbol{Q}}^{\mathrm{T}}\boldsymbol{T}^k\widehat{\boldsymbol{Q}}\boldsymbol{D}\right) \lesssim \log^2(1/h)\,. \tag{5.49}$$

Since the dynamic kernel only introduces a compact perturbation, we conclude that $\boldsymbol{D}\widehat{\boldsymbol{Q}}^{\mathrm{T}}\boldsymbol{T}\widehat{\boldsymbol{Q}}\boldsymbol{D}$ is well-conditioned up to a logarithmic perturbation.

As a side note, we also consider multiply connected geometries. Similar to loop-star or loop-tree quasi-Helmholtz preconditioners (see also Section 4.d.$\alpha$), we add the global loops transformation matrix $\boldsymbol{H}$ to $\widehat{\boldsymbol{Q}}$ resulting in

$$\widehat{\boldsymbol{Q}} = \begin{bmatrix} \widehat{\boldsymbol{\Lambda}} & \boldsymbol{H} & \widehat{\boldsymbol{\Sigma}} \end{bmatrix} \tag{5.50}$$

and use

$$\boldsymbol{D} = \begin{bmatrix} \boldsymbol{D}_\Lambda^{-1}/\sqrt{\mathrm{i}k} & & \\ & \boldsymbol{D}_{\mathrm{H}}/\sqrt{ik} & \\ & & \boldsymbol{D}_\Sigma\sqrt{\mathrm{i}k} \end{bmatrix}, \tag{5.51}$$

where

$$\left[\boldsymbol{D}_{\mathrm{H}}\right]_{ii} = 1/\sqrt{\left[\boldsymbol{H}^{\mathrm{T}}\boldsymbol{T}_{\mathrm{A}}^0\boldsymbol{H}\right]_{ii}}\,. \tag{5.52}$$

Then we have

$$\lim_{k\to 0} \boldsymbol{D}\widehat{\boldsymbol{Q}}^{\mathrm{T}}\boldsymbol{T}^k\widehat{\boldsymbol{Q}}\boldsymbol{D} = \begin{bmatrix} \boldsymbol{D}_\Lambda^{-1}\widehat{\boldsymbol{\Lambda}}^{\mathrm{T}}\boldsymbol{T}_{\mathrm{A}}^0\widehat{\boldsymbol{\Lambda}}\boldsymbol{D}_\Lambda^{-1} & \boldsymbol{D}_\Lambda^{-1}\widehat{\boldsymbol{\Lambda}}^{\mathrm{T}}\boldsymbol{T}_{\mathrm{A}}^0\boldsymbol{H}\boldsymbol{D}_{\mathrm{H}} & \\ \boldsymbol{D}_{\mathrm{H}}\boldsymbol{H}^{\mathrm{T}}\boldsymbol{T}_{\mathrm{A}}^0\widehat{\boldsymbol{\Lambda}}\boldsymbol{D}_\Lambda^{-1} & \boldsymbol{D}_{\mathrm{H}}\boldsymbol{H}^{\mathrm{T}}\boldsymbol{T}_{\mathrm{A}}^0\boldsymbol{H}\boldsymbol{D}_{\mathrm{H}} & \\ & & \boldsymbol{D}_\Sigma\widehat{\boldsymbol{\Sigma}}^{\mathrm{T}}\boldsymbol{T}_\Phi^0\widehat{\boldsymbol{\Sigma}}\boldsymbol{D}_\Sigma \end{bmatrix}. \tag{5.53}$$

The analysis of the conditioning is more complicated than for (5.48) due to the off-diagonal block matrices. First, we note that $\boldsymbol{D}_\mathrm{H}\boldsymbol{H}^\mathrm{T}\boldsymbol{T}_\mathrm{A}^0\boldsymbol{H}\boldsymbol{D}_\mathrm{H}$ is well-conditioned since mesh refinements do not change the global loops. Thus all the block matrices on the main diagonal are well-conditioned. The transformation matrix $\boldsymbol{H}$ has no preconditioning strength, which would indicate that the matrices $\boldsymbol{D}_\Lambda^{-1}\widehat{\boldsymbol{\Lambda}}^\mathrm{T}\boldsymbol{T}_\mathrm{A}^0\boldsymbol{H}\boldsymbol{D}_\mathrm{H}$ and $\boldsymbol{D}_\mathrm{H}\boldsymbol{H}^\mathrm{T}\boldsymbol{T}_\mathrm{A}^0\widehat{\boldsymbol{\Lambda}}\boldsymbol{D}_\Lambda^{-1}$ are only "half preconditioned" so that we have for their singular values an upper bound. We note that by adding the global loops, we cannot exclude the case that some eigenvalues of $\lim_{k\to 0}\boldsymbol{D}\widehat{\boldsymbol{Q}}^\mathrm{T}\boldsymbol{T}^k\widehat{\boldsymbol{Q}}\boldsymbol{D}$ are shifted closer to zero, but since the basis transformation matrix $\widehat{\boldsymbol{Q}}$ has full rank, we can exclude that a real null space is introduced. Numerical evidence suggests that even a shifting of eigenvalues closer to zero does not occur (see Chapter 6). Thus it seems that we can safely assume that the logarithmic bound persists in the presence of global loops.

Obtaining $\boldsymbol{H}$ explicitly is, however, not a trivial task and using global loops explicitly can be a costly operation. Therefore, we present a scheme in the next chapter that allows to use hierarchical basis preconditioners for the EFIE such that a search for the global loops is not required.

Returning to the simply connected case, better results are observed in practice when a normalization is used for curing the low-frequency breakdown, that is, we use

$$\boldsymbol{D} = \begin{bmatrix} \boldsymbol{D}_\Lambda^{-1}/\sqrt{\sigma_\Lambda} & \\ & \boldsymbol{D}_\Sigma/\sqrt{\sigma_\Sigma} \end{bmatrix}, \tag{5.54}$$

where $\sigma_\Lambda$ and $\sigma_\Sigma$ are the largest singular values of $\boldsymbol{D}_\Lambda^{-1}\widehat{\boldsymbol{\Lambda}}^\mathrm{T}\boldsymbol{T}\widehat{\boldsymbol{\Lambda}}\boldsymbol{D}_\Lambda^{-1}$ and $\boldsymbol{D}_\Sigma\widehat{\boldsymbol{\Sigma}}^\mathrm{T}\boldsymbol{T}\widehat{\boldsymbol{\Sigma}}\boldsymbol{D}_\Sigma$, respectively. The difference in the norm of these two matrices is properly taken into account in (5.54) by the rescaling of $\boldsymbol{D}_\Lambda$ and $\boldsymbol{D}_\Sigma$. Note that $\sigma_\Lambda$ and $\sigma_\Sigma$ can be obtained in linear complexity by using, for example, a power iteration method [Gol13].

The matrices $\boldsymbol{D}_\Lambda$ and $\boldsymbol{D}_\Sigma$ where defined by simply taking into account the level on which the respective Haar function is defined (see (5.14) and (5.31)). This works well when partitions on a level have all the same area. Since graph partitioning schemes are usually heuristic this is only approximately ensured. For this reason it is typically proposed to compute

$$\left[\boldsymbol{D}\right]_{ii} = 1/\sqrt{\left[\widehat{\boldsymbol{Q}}^\mathrm{T}\boldsymbol{T}\widehat{\boldsymbol{Q}}\right]_{ii}}, \tag{5.55}$$

where $\boldsymbol{T}$ is usually replaced by the near-interaction part of the system matrix in order to compute the matrix-matrix products rapidly. In our scheme, it is not possible to compute $\boldsymbol{D}$ in this manner due to the inverse matrices appearing in the definition of $\widehat{\boldsymbol{\Lambda}}$ and $\widehat{\boldsymbol{\Sigma}}$. However, we have an alternative by leveraging on the fact the Haar functions we are using are not $L^2$-stable, so that the Gram matrices of the primal and the dual Haar bases scale as

$$\left[\boldsymbol{H}_\Lambda^{\mathrm{T}} \boldsymbol{G}_{pp} \boldsymbol{H}_\Lambda\right]_{ii} \asymp 2^{2l_\Lambda(i)}, \tag{5.56}$$

and

$$\left[\boldsymbol{H}_\Sigma^{\mathrm{T}} \boldsymbol{G}_{pp} \boldsymbol{H}_\Sigma\right]_{ii} \asymp 2^{2l_\Sigma(i)}. \tag{5.57}$$

Hence, we can use the diagonal of their Gram matrices to obtain $\boldsymbol{D}_\Lambda$ and $\boldsymbol{D}_\Sigma$, that is, we define

$$\left[\boldsymbol{D}_\Lambda\right]_{ii} = \left(\left[\boldsymbol{H}_\Lambda^{\mathrm{T}} \boldsymbol{G}_{\tilde{p}\tilde{p}} \boldsymbol{H}_\Lambda\right]_{ii}\right)^{-0.25}, \tag{5.58}$$

$$\left[\boldsymbol{D}_\Sigma\right]_{ii} = \left(\left[\boldsymbol{H}_\Sigma^{\mathrm{T}} \boldsymbol{G}_{pp} \boldsymbol{H}_\Sigma\right]_{ii}\right)^{-0.25}. \tag{5.59}$$

## d) Numerical Results

We begin with studying the spectral properties of the new formulation by using a cube with side length 1 m. We have generated a regular sequence of meshes, for different values of the average edge length $h$, resulting in numbers of unknowns ranging from 18 to 18 432.

At first, we analyze how well the dense-discretization breakdown is prevented by the proposed preconditioner. This is done by computing the condition number for different values of the spectral index $1/h$. We begin our analysis by comparing the preconditioned scalar potential operator in (5.24) with a star, a tree, and a standard hierarchical non-solenoidal basis preconditioner (like the non-solenoidal part of the method used in [ATV10]). Figure 5.3a shows that both hierarchical preconditioners have the same qualitative behavior, whereas the star and tree preconditioner result in ill-conditioned system matrices.

Next, we analyze the effectiveness of our proposed preconditioning strategy of the vector potential operator in (5.32). We compare it with a vector potential operator that is discretized with loop functions, the modified hierarchical loop

functions proposed in [ATV10], and with hierarchical loop functions. The latter are constructed by adding the loop functions defined on all the new vertices of each refinement step. This construction does not enforce an orthogonality between the levels, and thus we cannot expect it to show any sign of preconditioning effectiveness. Figure 5.3b) displays the condition number as a function of the spectral index $1/h$. The modified hierarchical loops compare well with our proposed method. This can be expected from the theory presented in [ATV10]. The modified hierarchical loops lead to a discretization where the condition number of the matrix is bounded by a constant, whereas for the proposed preconditioner the condition number is still growing logarithmically. Different from the proposed preconditioner, the modified hierarchical loops are limited to structured meshes and lack, therefore, the necessary flexibility for practical applications.

Figure 5.3c shows the results when the entire EFIE operator is preconditioned with our new method, with the preconditioner presented in [ATV10], and with a standard hierarchical basis preconditioner. The standard hierarchical basis preconditioner consists of loop functions and a hierarchical non-solenoidal basis. This preconditioner is representative of the state of the art, since it is applicable to structured and unstructured meshes. In Figure 5.3c, the condition number is shown as a function of the spectral index $1/h$. These results show that the new preconditioner presented in this work compares favorably with previously proposed techniques. In fact, it has a performance which is comparable with the preconditioner in [ATV10], which however is applicable only to structured meshes. Since the standard hierarchical basis preconditioner employs loop functions, the vector potential operator is not effectively preconditioned; it is for this reason that in Figure 5.3c we observe the growth in the number of iterations for this preconditioner. In Figure 5.3d, the condition number of the system matrix is shown as a function of the frequency $f$. The frequency $f$ is related to the wavenumber by $k = 2\pi f/c$, where $c$ is the speed of light. The results show that the new preconditioner effectively cures the low-frequency breakdown.

Finally, we have tested the new preconditioner on more realistic geometries. The proposed preconditioner requires the inversion of the mixed Gram matrix $\boldsymbol{G}_{\lambda\tilde{p}}$ and the graph Laplacian $\boldsymbol{\Sigma}^{\mathrm{T}}\boldsymbol{\Sigma}$. In general, we are going to use the conjugate gradient squared (CGS) method as iterative solver with the exception of our treatment of $\boldsymbol{\Sigma}^{\mathrm{T}}\boldsymbol{\Sigma}$ (other Krylov subspace methods could be used as well). The matrix $\boldsymbol{G}_{\lambda\tilde{p}}$ is sparse and well-conditioned, hence one can easily use a solver

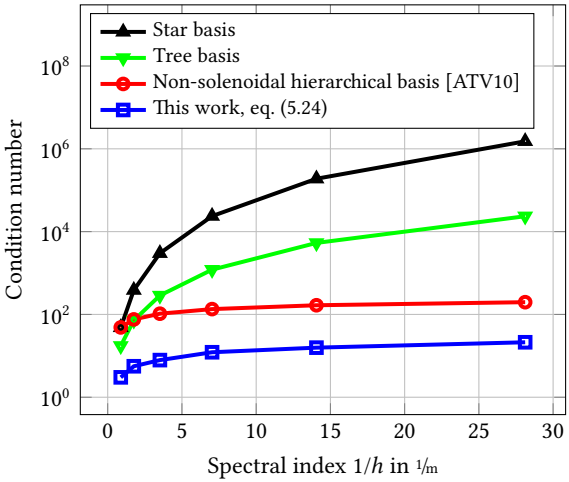


*(a)* Condition number of preconditioned $\boldsymbol{T}_{\Phi}$.

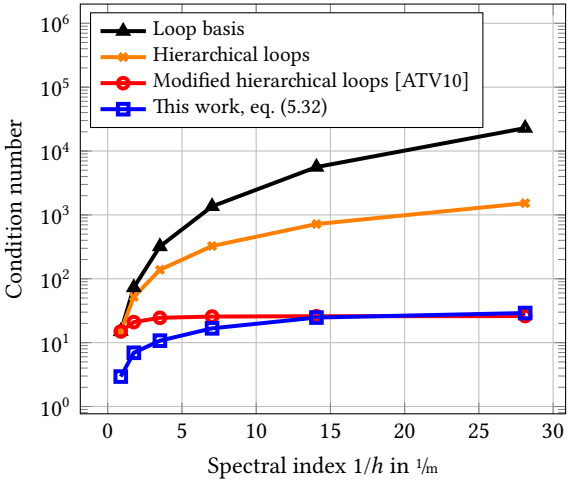


*(b)* Condition number of preconditioned $\boldsymbol{T}_{\mathrm{A}}$.

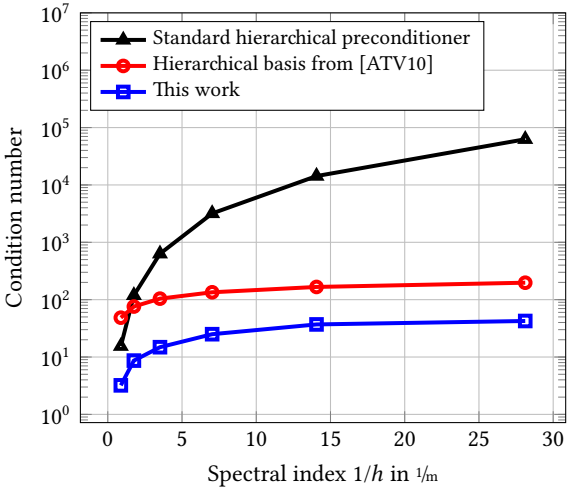


*(c)* Condition number of preconditioned $\boldsymbol{T}$.

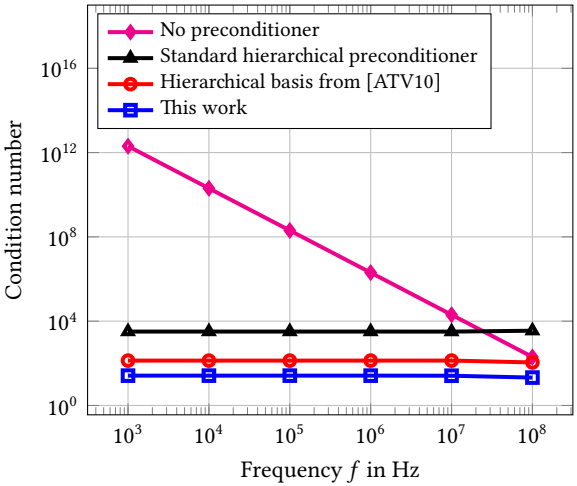


*(d)* Verification of the low-frequency stability of (preconditioned) $\boldsymbol{T}$.

*Fig. 5.3.:* Cube: spectral analysis of the different preconditioners for varying $h$ and $f$.

tolerance close to machine precision. As $\boldsymbol{\Sigma}^{\mathrm{T}}\boldsymbol{\Sigma}$ is a graph Laplacian, the matrix is ill-conditioned and a preconditioner necessary. We are using the aggregation-based algebraic multigrid preconditioner AGMG presented in [NN12; Not]. As solver tolerances, we use $1 \cdot 10^{-14}$ for the AGMG solver and $1 \cdot 10^{-16}$ for the CGS for $\boldsymbol{G}_{\lambda\tilde{p}}$, thereby showing that even for small tolerances our method remains practical.

As closed realistic structure, we use a model of a Space Shuttle discretized with 1 148 400 basis functions. The length of the Space Shuttle is $\lambda/20$. We compared the preconditioner proposed in this work with a classical loop-tree preconditioner [WGK95] and the case that a hierarchical non-solenoidal basis is complemented by loop functions (denoted as "standard hierarchical preconditioner"). For obtaining the numerical results, we used the CGS solver with tolerance $1 \cdot 10^{-4}$. To accelerate the computation, we employed the ACA with precision $1 \cdot 10^{-4}$. As excitation, we used a plane wave and a voltage gap, respectively. The results, summarized in Table 5.1, show clearly the improvements that the preconditioner proposed in this work presents over the state of the art. Figure 5.4 shows a good agreement of the bistatic scattering cross sections.

Like other hierarchical preconditioner schemes or Calderón preconditioners, the new preconditioner was derived under the assumption that the structures are closed. In practice, we find that the new preconditioner can be used on open structures as well. We simulated the scattering problem for the model of a MiG-15 with 306 036 unknowns. We used the same ACA precision and solver tolerance as for the Space Shuttle, and we studied the effect of a plane wave and a voltage gap excitation. Table 5.2 shows the number of iterations and the timings, and Figure 5.5 shows the bistatic scattering cross section. Clearly, the new preconditioner remains effective for open structures.

## e) Conclusion

We presented a hierarchical basis preconditioner, which works on structured and on unstructured meshes. Different from other hierarchical basis preconditioners with comparable applicability, it preconditions the electric field integral equation operator completely. The numerical results do not only confirm the theoretical predictions but also show that the presented preconditioner outperforms standard methods for real case scenarios.

*Tab. 5.1.:* Space Shuttle: the number of iterations and the time used by the solver to obtain a residual error below $1 \cdot 10^{-4}$.

| Preconditioner | Iterations | $l_2$-relativ error* | Time | | |
|---|---|---|---|---|---|
| | | (%) | Setup preconditioner (h:m:s) | CGS (h:m:s) | Total† (h:m:s) |
| *Plane wave excitation* | | | | | |
| Loop-tree preconditioner | 5370 | 0 | 00:04:48 | 97:26:04 | 99:42:36 |
| Standard hierarchical pre. | 154 | 0.26 | 00:11:18 | 08:57:17 | 11:37:04 |
| This work | 27 | 0.14 | 00:19:29 | 01:25:27 | 03:49:15 |
| *Voltage gap excitation* | | | | | |
| Loop-tree preconditioner | 4602 | 0 | 00:04:51 | 85:37:55 | 87:41:22 |
| Standard hierarchical pre. | 518 | 0.012 | 00:10:07 | 26:18:46 | 28:47:02 |
| This work | 32 | 0.009 | 00:19:31 | 01:37:52 | 04:01:41 |

* The relative error is with respect to the solution obtained by using the loop-tree preconditioner.

† This includes also the time for constructing the matrix $\boldsymbol{T}$ using the ACA.

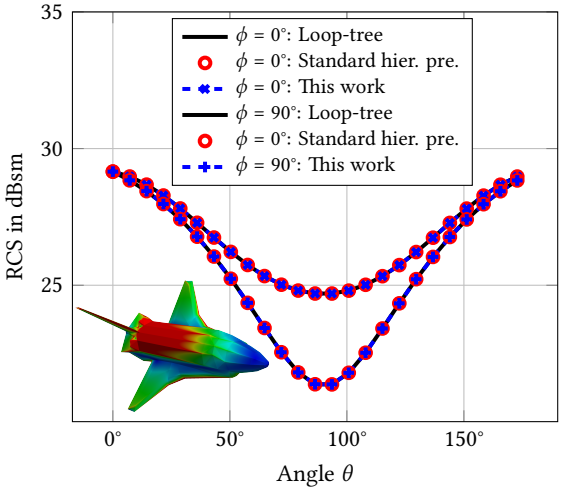


*(a)* Plane wave excitation.

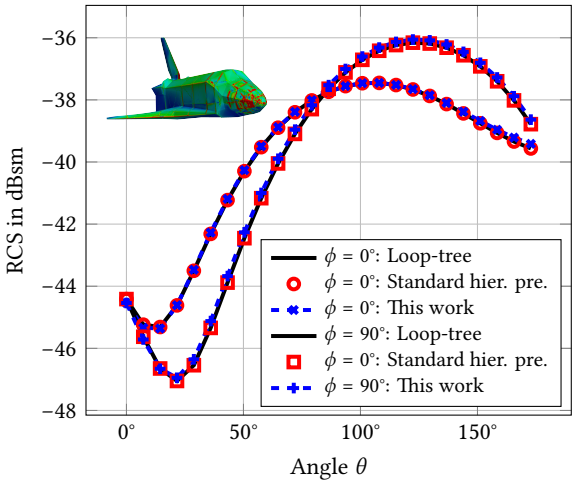


*(b)* Voltage gap excitation.

*Fig. 5.4.:* Space Shuttle: bistatic scattering cross section. The system matrix is compressed with the ACA (precision $1 \cdot 10^{-4}$).

*Tab. 5.2.:* MiG-15: the number of iterations and the time used by the solver to obtain a residual error below $1 \cdot 10^{-4}$.

| Preconditioner | Iterations | $l_2$-relativ error* | Time | | |
|---|---|---|---|---|---|
| | | (%) | Setup preconditioner (h:m:s) | CGS (h:m:s) | Total† (h:m:s) |
| *Plane wave excitation* | | | | | |
| Loop-tree preconditioner | 2814 | 0 | 00:01:36 | 14:10:38 | 14:21:28 |
| Standard hierarchical pre. | 166 | 1.05 | 00:03:10 | 01:57:44 | 02:10:04 |
| This work | 33 | 0.47 | 00:06:10 | 00:24:00 | 00:39:21 |
| *Voltage gap excitation* | | | | | |
| Loop-tree preconditioner | 926 | 0 | 00:01:37 | 04:40:38 | 04:51:23 |
| Standard hierarchical pre. | 175 | 0.001 | 00:03:10 | 02:05:09 | 02:17:26 |
| This work | 31 | 0.006 | 00:06:10 | 00:23:02 | 00:38:23 |

* The relative error is with respect to the solution obtained by using the loop-tree preconditioner.

† This includes also the time for constructing the matrix $\boldsymbol{T}$ using the ACA.

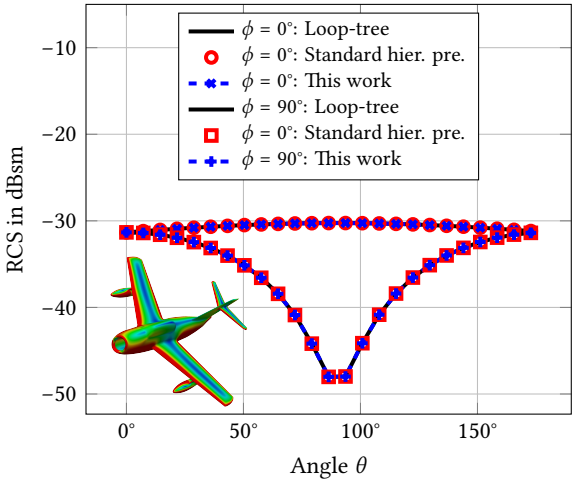


*(a)* Plane wave excitation.

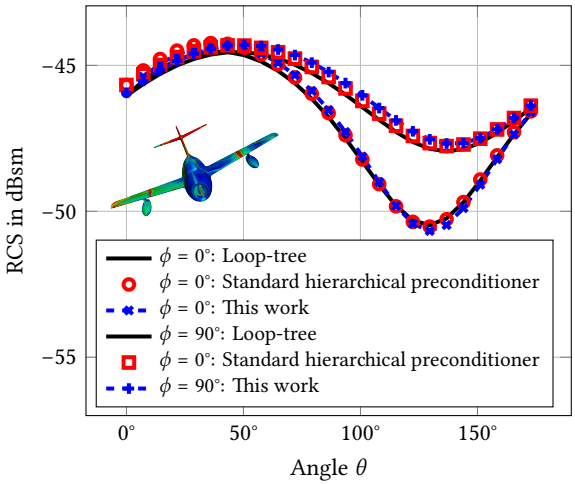


*(b)* Voltage gap excitation.

*Fig. 5.5.:* MiG-15: bistatic scattering cross section. The system matrix is compressed with the ACA (precision $1 \cdot 10^{-4}$).

Chapter 6

# Hierarchical Bases on Multiply Connected Objects for the EFIE

*This chapter extends hierarchical basis preconditioners applicable to the EFIE such that on multiply connected geometries no search for global loops is required. Currently available hierarchical basis preconditioners need an explicit representation of global loops. Finding these requires a computational complexity exceeding the linearithmic complexity of fast matrix-vector multiplication methods. Instead of using an explicit representation of global loops, quasi-Helmholtz projectors are utilized to precondition the EFIE separately on the solenoidal, non-solenoidal, and quasi-harmonic Helmholtz subspace. Thereby, we avoid the explicit recovery of the global loops and maintain the leading complexity of fast multiplication methods. Numerical results prove the effectiveness of the proposed approach. This chapter is based on [AAE14b].*

Hierarchical basis preconditioners, as discussed in Chapter 1 and in Chapter 5, can cure the ill-conditioning of the EFIE up to a logarithmic perturbation. Various bases have been presented for the EFIE operator and their effectiveness has been demonstrated in the past [VPV05; ATV07; Che+09; ATV10; AVV08; HM12; AAE17]. A hierarchical basis for the EFIE operator must precondition both the vector and the scalar potential operator. The separate preconditioning of the vector and the scalar potential operator is usually achieved by using a set of hierarchical solenoidal and non-solenoidal basis functions. This enforces a quasi-Helmholtz decomposition that exploits the solenoidal null space of the scalar potential operator in order to split it off from the vector potential operator.

On multiply connected geometries, however, the hierarchical bases share the same issue as the classical loop-star/tree quasi-Helmholtz decompositions: they require an explicit representation of the quasi-harmonic subspace. This subspace is spanned by the so-called global loops, which are associated with the handles and holes of the geometry [Ces96; Vec99].

The explicit representation of the quasi-harmonic subspace requires to find the global loops of the geometry. Existing loop-finding algorithms have at least a complexity of $\mathcal{O}(gN)$, where $g$ is the genus of the geometry [VY90; Laz+01]. When $g \propto N$, the loop-finding algorithms cannot have a complexity less than quadratic [EH04].

For a convenient application of the hierarchical preconditioner, it is desirable that the hierarchical basis can be applied multiplicatively. In standard codes the EFIE is discretized with RWG basis functions and the preconditioner is a sparse basis transformation matrix applied from left and right to the system matrix. Standard loop-finding algorithms do not generally find the shortest loops, so that the transformation matrix mapping the global loops to RWG functions is dense. Algorithms that do ensure to find the shortest loops (and thereby avoid a dense transformation matrix) have at least a cubic complexity [EH04; DFW13].

As the leading complexity set by the fast multiplication methods is at most linearithmic [CRW93; ZVL05], the use of loop-finding algorithms is unattractive. Considering that the implementation of such an algorithm is cumbersome and their application is only satisfactory for certain classes of geometries, it is desirable to find a general purpose formulation where the search for global loops is unnecessary, that can be integrated easily into existing codes, and that does not jeopardize the effectiveness of the fast multiplication method.

In this chapter, we present such a formulation applicable to hierarchical bases for the EFIE operator meeting these criteria. To this end, we leverage quasi-Helmholtz projectors allowing for an implicit representation of the quasi-harmonic Helmholtz subspace. Helmholtz projectors were first introduced in [And12a], where the projectors were used for stabilizing the Calderón preconditioned EFIE in the static limit. We show that we cannot directly integrate these Helmholtz projectors in a hierarchical preconditioning scheme to bypass the search for the global loops. Instead, it turns out that the standard split preconditioning formulation must be abandoned in favor of a left preconditioning formulation. The numerical results corroborate the effectiveness of the presented theory.

# a) Background

In this chapter, we allow $\Omega$ to be a multiply connected Lipschitz polyhedral domain. Available hierarchical bases rest upon a quasi-Helmholtz decomposition [VPV05; ATV07; Che+09; ATV10; AVV08; AAE17] as the scalar potential operator must be preconditioned separately from the vector potential operator. For any hierarchical basis that shall be applicable to the formulation presented in this work, we require that the space of hierarchical functions is equal to the space of RWG functions: $X_f = X_{\widehat{\Lambda}} \oplus X_H \oplus X_{\widehat{\Sigma}}$, where $X_f$ is the space of RWG basis functions, $X_{\widehat{\Lambda}}$ the space of hierarchical solenoidal functions, $X_H$ is the space of quasi-harmonic global loop functions, and $X_{\widehat{\Sigma}}$ the space of hierarchical non-solenoidal basis functions. This allows us to define linear mappings $\widehat{\boldsymbol{\Lambda}} \in \mathbb{R}^{N \times N_\Lambda}$, $\boldsymbol{H} \in \mathbb{R}^{N \times N_\mathrm{H}}$, and $\widehat{\boldsymbol{\Sigma}} \in \mathbb{R}^{N \times N_\Sigma}$ from the hierarchical solenoidal and non-solenoidal functions to the RWG basis functions. We do not give an explicit representation of $\widehat{\boldsymbol{\Lambda}}$ and $\widehat{\boldsymbol{\Sigma}}$, as our scheme is not limited to a specific hierarchical basis.

In other words, we can express the system matrix $\boldsymbol{T}_{\widehat{\boldsymbol{Q}}}$ which is obtained by using the hierarchical basis in terms of a linear mapping

$$\widehat{\boldsymbol{Q}} = \begin{bmatrix} \widehat{\boldsymbol{\Lambda}} & \boldsymbol{H} & \widehat{\boldsymbol{\Sigma}} \end{bmatrix} \tag{6.1}$$

applied to $\boldsymbol{T}$ as $\boldsymbol{T}_{\widehat{\boldsymbol{Q}}} = \widehat{\boldsymbol{Q}}^{\mathrm{T}} \boldsymbol{T} \widehat{\boldsymbol{Q}}$. In general for the hierarchical basis preconditioner to be effective, the matrix has to be rescaled by using the diagonal preconditioner

$$\left[\boldsymbol{D}\right]_{ii} = 1/\sqrt{\left[\boldsymbol{T}_{\widehat{\boldsymbol{Q}}}\right]_{ii}}\,. \tag{6.2}$$

This diagonal preconditioner is necessary for both curing the low-frequency and the dense-discretization breakdown. Summarizing, the preconditioned system matrix is

$$\boldsymbol{D}\boldsymbol{T}_{\widehat{\boldsymbol{Q}}}\boldsymbol{D}\,. \tag{6.3}$$

Given the discussion in the previous chapter on the conditioning of the matrix (5.53), we assume that we have condition number bound

$$\mathrm{cond}\left(\boldsymbol{D}\boldsymbol{T}_{\widehat{\boldsymbol{Q}}}\boldsymbol{D}\right) \lesssim \log^2\left(1/h^2\right). \tag{6.4}$$

## b) New Formulation Without the Search for Global Loops

Since the explicit construction of $X_H$ is computationally expensive, the new formulation presented in this chapter uses an implicit representation of the quasi-harmonic subspace. To this end, we use projectors that allow us to obtain the solenoidal, non-solenoidal, and quasi-harmonic part of the current density $\boldsymbol{j}$ in terms of RWG functions so that we can precondition the EFIE operator on each Helmholtz subspace separately [AEA13]. These projectors have been recently introduced [And12a; And+13]. They are based on the classical loop and star functions [Wil83; WGK95; BK95].

It remains to link the projectors to the hierarchical basis preconditioner. Inspired by (4.85), a first idea would be to use

$$\hat{\dot{\boldsymbol{P}}} = \widehat{\boldsymbol{\Lambda}}\boldsymbol{D}_{\widehat{\boldsymbol{\Lambda}}}\boldsymbol{X}_{\widehat{\boldsymbol{\Lambda}}} + \boldsymbol{P}_{\mathrm{H}}\sqrt{\gamma} + \widehat{\boldsymbol{\Sigma}}\boldsymbol{D}_{\widehat{\boldsymbol{\Sigma}}}\boldsymbol{X}_{\widehat{\boldsymbol{\Sigma}}}\,, \tag{6.5}$$

requiring that

$$\hat{\dot{\boldsymbol{P}}}^{\mathrm{T}}\boldsymbol{T}\hat{\dot{\boldsymbol{P}}} \tag{6.6}$$

is well-conditioned. The matrices $\boldsymbol{D}_{\widehat{\boldsymbol{\Lambda}}}$ and $\boldsymbol{D}_{\widehat{\boldsymbol{\Sigma}}}$ are the diagonal preconditioners of $\widehat{\boldsymbol{\Lambda}}^{\mathrm{T}}\boldsymbol{T}\widehat{\boldsymbol{\Lambda}}$ and $\widehat{\boldsymbol{\Sigma}}^{\mathrm{T}}\boldsymbol{T}\widehat{\boldsymbol{\Sigma}}$, respectively. The matrices $\boldsymbol{X}_{\widehat{\boldsymbol{\Lambda}}} \in \mathbb{C}^{N_\Lambda \times N}$ and $\boldsymbol{X}_{\widehat{\boldsymbol{\Sigma}}} \in \mathbb{C}^{N_\Sigma \times N}$ are necessary to match the column dimensionality of $\boldsymbol{P}_{\mathrm{H}}$ since $\boldsymbol{D}_{\widehat{\boldsymbol{\Lambda}}} \in \mathbb{C}^{N_\Lambda \times N_\Lambda}$ and $\boldsymbol{D}_{\widehat{\boldsymbol{\Sigma}}} \in \mathbb{C}^{N_\Sigma \times N_\Sigma}$ but $\boldsymbol{P}_{\mathrm{H}} \in \mathbb{R}^{N \times N}$. The parameter $\gamma$ (instead of $1/\sqrt{k}$ as in (6.5)) is necessary, because the diagonal preconditioning of $\boldsymbol{D}_{\widehat{\boldsymbol{\Lambda}}}$ might have an effect different from a mere rescaling with $1/\sqrt{k}$ (the choice of $\gamma$ is discussed in Section 6.c). All in all, the projector-based preconditioning of the quasi-harmonic subspace becomes more complicated than in (6.5) or in [And+13].

It might seem that $\boldsymbol{\Lambda}^{\mathrm{T}}$ and $\boldsymbol{\Sigma}^{\mathrm{T}}$ are natural choices for $\boldsymbol{X}_{\widehat{\boldsymbol{\Lambda}}}$ and $\boldsymbol{X}_{\widehat{\boldsymbol{\Sigma}}}$. But these matrices are ill-conditioned, as they have a derivative strength [And12a]. Applying an ill-conditioned matrix from left and right to a well-conditioned matrix results, in general, in an ill-conditioned matrix and so (6.6) is not well-conditioned.[31]

31 Alternatively, we could resort to the hierarchical basis transformation matrices $\widehat{\boldsymbol{\Lambda}}^{\mathrm{T}}$ and $\widehat{\boldsymbol{\Sigma}}^{\mathrm{T}}$ and rescale them such that they become $\boldsymbol{L}^2$-stable transformations, that is that the discretization of the identity operator $\widehat{\boldsymbol{\Lambda}}^{\mathrm{T}}\boldsymbol{G}_{ff}\widehat{\boldsymbol{\Lambda}}$ and $\widehat{\boldsymbol{\Sigma}}^{\mathrm{T}}\boldsymbol{G}_{ff}\widehat{\boldsymbol{\Sigma}}$ is well-conditioned. However, both the solenoidal and the non-solenoidal hierarchical basis should be $\boldsymbol{L}^2(\Gamma)$-stable, which they not necessarily are (e.g.,

Instead of choosing $\boldsymbol{\Lambda}$ and $\boldsymbol{\Sigma}$ for $\boldsymbol{X}_{\widehat{\boldsymbol{\Lambda}}}^{\mathrm{T}}$ and $\boldsymbol{X}_{\widehat{\boldsymbol{\Sigma}}}^{\mathrm{T}}$, one might consider using the transformation matrices $\boldsymbol{\Gamma}$ and $\boldsymbol{\Theta}$ of cotree and tree functions, respectively, since $\boldsymbol{\Gamma}$ and $\boldsymbol{\Theta}$ do not possess a derivative (or integrative) strength. For the definition of tree/cotree functions see [Sun+95] (what we call tree functions in this chapter, is referred to as cotree function in [Sun+95] and vice versa; they can be obtained in linear complexity by a depth-first search). The dimensionality of the tree functions $N_\Sigma$ (as they must span the charge space), and thus, the dimensionality of the cotree space is $N - N_\Sigma = N_\Lambda + N_\mathrm{H}$, where $N_\mathrm{H}$ is the dimensionality of the quasi-harmonic subspace. To match the dimensionality of $X_{\widehat{\boldsymbol{\Lambda}}}$, we must eliminate $N_\mathrm{H}$ cotree functions resulting in the reduced cotree transformation matrix $\boldsymbol{\Gamma}$.

Despite their well-conditionedness, $\boldsymbol{\Gamma}$ and $\boldsymbol{\Theta}$ may not be used, because their null spaces are not orthogonal to the null space of $\boldsymbol{P}_\mathrm{H}$. The non-orthogonality of the null spaces induces a new form of ill-conditioning. To illustrate this effect, we used a cube with a hole on each side so that the cube has five global loops (this cube is shown in Figure 6.1; there are five and not six global loops, because one hole makes the cube an open but still simply connected structure). A plane wave with frequency 1 MHz impinges on this cube with side length $\lambda/150$, where $\lambda$ is the wavelength. Figure 6.4 shows the spectrum of the system matrix. When we use the cotree/tree formulation, five isolated singular values appear. These are the singular values associated with the global loops. These singular values are not clustered meaning that the quasi-harmonic subspace has become ill-conditioned.

Hence, we need matrices that have null spaces that are orthogonal to the null space of $\boldsymbol{P}_\mathrm{H}$, but which are, in contrast to $\boldsymbol{\Lambda}^{\mathrm{T}}$ and $\boldsymbol{\Sigma}^{\mathrm{T}}$, well-conditioned. The following lemma provides us with matrices having the desired properties.

**Lemma 6.1.** *The first $N_\Lambda$ ($N_\Sigma$) singular values of $(\boldsymbol{\Lambda}^{\mathrm{T}}\boldsymbol{\Lambda})^{-1/2}\boldsymbol{\Lambda}^{\mathrm{T}}$ ($(\boldsymbol{\Sigma}^{\mathrm{T}}\boldsymbol{\Sigma})^{-1/2}\boldsymbol{\Sigma}^{\mathrm{T}}$) are equal to one, the rest of the singular values are zero.*

*Proof.* We proof this for $(\boldsymbol{\Lambda}^{\mathrm{T}}\boldsymbol{\Lambda})^{-1/2}\boldsymbol{\Lambda}^{\mathrm{T}}$. The proof for $(\boldsymbol{\Sigma}^{\mathrm{T}}\boldsymbol{\Sigma})^{-1/2}\boldsymbol{\Sigma}^{\mathrm{T}}$ follows analogously. Let

$$\boldsymbol{U}\boldsymbol{\Xi}\boldsymbol{R}^{\mathrm{T}} \tag{6.7}$$

the hierarchical solenoidal functions from the previous chapter would when applied to $\boldsymbol{G}_{ff}$ lead to a condition number scaling like $\mathcal{O}(\log^4(1/h))$ as discussed in Section 7.b), and even if they are $\boldsymbol{L}^2(\Gamma)$-stable, then the upper bound of the condition number of $\widehat{\boldsymbol{\Lambda}}^{\mathrm{T}}\boldsymbol{G}_{ff}\widehat{\boldsymbol{\Lambda}}$ or $\widehat{\boldsymbol{\Sigma}}^{\mathrm{T}}\boldsymbol{G}_{ff}\widehat{\boldsymbol{\Sigma}}$ can still be prohibitively large for practical applications.

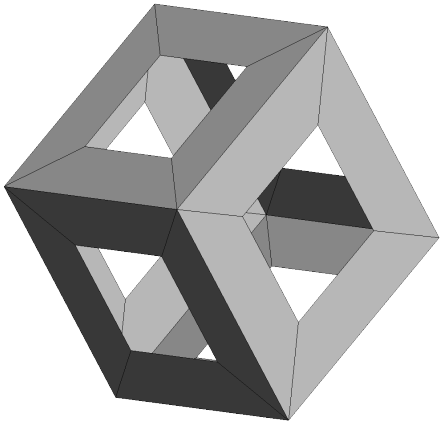

*Fig. 6.1.:* Cube with six holes: open surface with five global loops.

be the singular value decomposition of $\boldsymbol{\Lambda}$ and let $\xi_i = \left[\boldsymbol{\Xi}\right]_{ii}$ be the singular values. Notice that $\boldsymbol{U}$ and $\boldsymbol{R}^{\mathrm{T}}$ are unitarian matrices. Then it follows that the eigenvalue and singular value decomposition of $\boldsymbol{\Lambda}^{\mathrm{T}}\boldsymbol{\Lambda}$ is $\boldsymbol{R}\boldsymbol{\Pi}\boldsymbol{R}^{\mathrm{T}}$, where $\left[\boldsymbol{\Pi}\right]_{ii} = \xi_i^2$ for $i = 1, \ldots, N_\Lambda$ and $\boldsymbol{\Pi} \in \mathbb{R}^{N_\Lambda \times N_\Lambda}$. The inverse square root of $\boldsymbol{\Lambda}^{\mathrm{T}}\boldsymbol{\Lambda}$ is given by the decomposition $\boldsymbol{R}\boldsymbol{\Pi}^{-1/2}\boldsymbol{R}^{\mathrm{T}}$. We then find

$$\left(\boldsymbol{\Lambda}^{\mathrm{T}}\boldsymbol{\Lambda}\right)^{-1/2}\boldsymbol{\Lambda}^{\mathrm{T}} = \boldsymbol{R}\boldsymbol{\Pi}^{-1/2}\underbrace{\boldsymbol{R}^{\mathrm{T}}\boldsymbol{R}}_{\boldsymbol{I}}\boldsymbol{\Xi}\boldsymbol{U}^{\mathrm{T}} = \boldsymbol{R}\boldsymbol{\Psi}\boldsymbol{U}^{\mathrm{T}}, \tag{6.8}$$

where $\boldsymbol{\Psi} = \boldsymbol{\Pi}^{-1/2}\boldsymbol{\Xi}$, $\boldsymbol{\Psi} \in \mathbb{R}^{N_\Lambda \times N}$ with $\left[\boldsymbol{\Psi}\right]_{ii} = 1$, $i = 1, \ldots, N_\Lambda$ and zero otherwise. It follows from (6.7) and (6.8) that the range and null spaces of $\boldsymbol{\Lambda}^{\mathrm{T}}$ and $(\boldsymbol{\Lambda}^{\mathrm{T}}\boldsymbol{\Lambda})^{-1/2}\boldsymbol{\Lambda}^{\mathrm{T}}$ are identical. □

Lemma 6.1 infers that the matrices $(\boldsymbol{\Lambda}^{\mathrm{T}}\boldsymbol{\Lambda})^{-1/2}\boldsymbol{\Lambda}$ and $(\boldsymbol{\Sigma}^{\mathrm{T}}\boldsymbol{\Sigma})^{-1/2}\boldsymbol{\Sigma}$ are well-conditioned up to the null space of $\boldsymbol{\Lambda}$ and $\boldsymbol{\Sigma}$, respectively, and that they, because of their range and null space matching those of $\boldsymbol{P}_{\mathrm{H}}$, can be used instead of $\boldsymbol{\Lambda}^{\mathrm{T}}$ and $\boldsymbol{\Sigma}^{\mathrm{T}}$.

Modifying the preconditioner proposed in (6.5) to

$$\widehat{\boldsymbol{P}} = \widehat{\boldsymbol{\Lambda}}\boldsymbol{D}_{\widehat{\boldsymbol{\Lambda}}}\left(\boldsymbol{\Lambda}^{\mathrm{T}}\boldsymbol{\Lambda}\right)^{-1/2}\boldsymbol{\Lambda}^{\mathrm{T}} + \boldsymbol{P}_{\mathrm{H}}\sqrt{\gamma} + \widehat{\boldsymbol{\Sigma}}\boldsymbol{D}_{\widehat{\boldsymbol{\Sigma}}}\left(\boldsymbol{\Sigma}^{\mathrm{T}}\boldsymbol{\Sigma}\right)^{-1/2}\boldsymbol{\Sigma}^{\mathrm{T}}, \tag{6.9}$$

we obtain a hierarchical preconditioner, which takes implicitly care of the quasi-harmonic Helmholtz subspace. Figure 6.4 demonstrates the correctness of this square root based approach. We see that all the singular values are clustered for a suitably chosen $\gamma$ as described in Section 6.c.

The downside of this approach is obvious: we have to compute the inverse square root of a matrix. To avoid this, we propose a left preconditioner instead of this split preconditioner: instead of

$$\widehat{\boldsymbol{P}}^{\mathrm{T}}\boldsymbol{T}\widehat{\boldsymbol{P}} \tag{6.10}$$

we suggest to use

$$\widehat{\boldsymbol{P}}\widehat{\boldsymbol{P}}^{\mathrm{T}}\boldsymbol{T}, \tag{6.11}$$

where we note that $\widehat{\boldsymbol{P}}\widehat{\boldsymbol{P}}^{\mathrm{T}}$ does not contain inverse square roots anymore, as we have

$$\widehat{\boldsymbol{P}}\widehat{\boldsymbol{P}}^{\mathrm{T}} = \widehat{\boldsymbol{\Lambda}}\boldsymbol{D}^2_{\widehat{\boldsymbol{\Lambda}}}\widehat{\boldsymbol{\Lambda}}^{\mathrm{T}} + \boldsymbol{P}_{\mathrm{H}}\gamma + \widehat{\boldsymbol{\Sigma}}\boldsymbol{D}^2_{\widehat{\boldsymbol{\Sigma}}}\widehat{\boldsymbol{\Sigma}}^{\mathrm{T}}. \tag{6.12}$$

We note that the matrices $\widehat{\boldsymbol{P}}\widehat{\boldsymbol{P}}^{\mathrm{T}}\boldsymbol{T}$ and $\widehat{\boldsymbol{P}}^{\mathrm{T}}\boldsymbol{T}\widehat{\boldsymbol{P}}$ are similar, since

$$\widehat{\boldsymbol{P}}^{-1}\left(\widehat{\boldsymbol{P}}\widehat{\boldsymbol{P}}^{\mathrm{T}}\boldsymbol{T}\right)\widehat{\boldsymbol{P}} = \widehat{\boldsymbol{P}}^{\mathrm{T}}\boldsymbol{T}\widehat{\boldsymbol{P}}. \tag{6.13}$$

and thus they have the same eigenvalue spectrum, which typically results in a convergence behavior of the iterative solver comparable to the split preconditioned case.

For extremely low frequencies this approach needs a slight modification: since the solenoidal/quasi-harmonic and the non-solenoidal part of the current, $\boldsymbol{P}_{\Lambda\mathrm{H}}\boldsymbol{j}$ and $\boldsymbol{P}_{\Sigma}\boldsymbol{j}$, scale differently in frequency, numerical cancellation appears in $\boldsymbol{j}$, which would render it impossible to compute the electric and magnetic field (see [And+13] for more details). In this case, one should apply the low-frequency preconditioner from Section 4.d.$\beta$ and replace $\boldsymbol{T}$ by $-\mathrm{i}\boldsymbol{P}^{\mathrm{T}}\boldsymbol{T}\boldsymbol{P}$ so that $\hat{\boldsymbol{P}}$ does not have to take care of the low-frequency breakdown anymore. In more detail, the preconditioned matrix would read

$$\widehat{\boldsymbol{P}}\widehat{\boldsymbol{P}}^{\mathrm{T}}\left(-\mathrm{i}\boldsymbol{P}^{\mathrm{T}}\boldsymbol{T}\boldsymbol{P}\right) \tag{6.14}$$

where the diagonal preconditioners should be obtained from the frequency independent system matrices

$$\left[\boldsymbol{D}_{\widehat{\boldsymbol{\Lambda}}}\right]_{ii} = 1/\sqrt{\left[\widehat{\boldsymbol{\Lambda}}^{\mathrm{T}}\boldsymbol{T}_{\mathrm{A}}^{0}\widehat{\boldsymbol{\Lambda}}\right]_{ii}} \tag{6.15}$$

and

$$\left[\boldsymbol{D}_{\widehat{\boldsymbol{\Sigma}}}\right]_{ii} = 1/\sqrt{\left[\widehat{\boldsymbol{\Sigma}}^{\mathrm{T}}\boldsymbol{T}_{\Phi}^{0}\widehat{\boldsymbol{\Sigma}}\right]_{ii}} \tag{6.16}$$

since $-\mathrm{i}\boldsymbol{P}^{\mathrm{T}}\boldsymbol{T}\boldsymbol{P}$ is well-conditioned in frequency. If the basis from the previous chapter is used, then (5.58) and (5.59) can be used to determine $\boldsymbol{D}_{\widehat{\boldsymbol{\Lambda}}}$ and $\boldsymbol{D}_{\widehat{\boldsymbol{\Sigma}}}$.

We note that $-\mathrm{i}\boldsymbol{P}^{\mathrm{T}}\boldsymbol{T}\boldsymbol{P}$ and $\widehat{\boldsymbol{P}}^{\mathrm{T}}(-\mathrm{i}\boldsymbol{P}^{\mathrm{T}}\boldsymbol{T}\boldsymbol{P})\widehat{\boldsymbol{P}}$ become SPD for $k \longrightarrow 0$. This allows to obtain an upper bound for the condition number of $\widehat{\boldsymbol{P}}\widehat{\boldsymbol{P}}^{\mathrm{T}}(-\mathrm{i}\boldsymbol{P}^{\mathrm{T}}\boldsymbol{T}\boldsymbol{P})$ in the static limit.

**Lemma 6.2.** *If we have a hierarchical basis such that*

$$\boldsymbol{x}^{\mathrm{T}}\boldsymbol{x} \lesssim \lim_{k\longrightarrow 0} \boldsymbol{x}^{\mathrm{T}}\widehat{\boldsymbol{P}}^{\mathrm{T}}\left(-\mathrm{i}\boldsymbol{P}^{\mathrm{T}}\boldsymbol{T}^{k}\boldsymbol{P}\right)\widehat{\boldsymbol{P}}x \lesssim \log^2(1/h)\boldsymbol{x}^{\mathrm{T}}\boldsymbol{x}\,, \quad \forall \boldsymbol{x} \in \mathbb{R}^N \lesssim \log^2(1/h) \tag{6.17}$$

*is satisfied, then*

$$\mathrm{cond}\left(\lim_{k\longrightarrow 0} \widehat{\boldsymbol{P}}\widehat{\boldsymbol{P}}^{\mathrm{T}}\left(-\mathrm{i}\boldsymbol{P}^{\mathrm{T}}\boldsymbol{T}^{k}\boldsymbol{P}\right)\right) \lesssim \log^2(1/h) \tag{6.18}$$

*holds.*

*Proof.* In the following, we assume $k \longrightarrow 0$ and suppress the limit. Using Rayleigh quotients, we have

$$\boldsymbol{x}^{\mathrm{T}}\boldsymbol{x} \lesssim \boldsymbol{x}^{\mathrm{T}}\widehat{\boldsymbol{P}}^{\mathrm{T}}\left(-\mathrm{i}\boldsymbol{P}^{\mathrm{T}}\boldsymbol{T}\boldsymbol{P}\right)\widehat{\boldsymbol{P}}\boldsymbol{x} \lesssim \log^2(1/h)\boldsymbol{x}^{\mathrm{T}}\boldsymbol{x}\,, \quad \forall \boldsymbol{x} \in \mathbb{R}^N\,. \tag{6.19}$$

Using the substitution $\widehat{\boldsymbol{P}}\boldsymbol{x} = \boldsymbol{y}$, we have

$$\boldsymbol{y}^{\mathrm{T}}\widehat{\boldsymbol{P}}^{-\mathrm{T}}\widehat{\boldsymbol{P}}^{-1}\boldsymbol{y} \lesssim \boldsymbol{y}^{\mathrm{T}} - \mathrm{i}\boldsymbol{P}^{\mathrm{T}}\boldsymbol{T}\boldsymbol{P}\boldsymbol{y} \lesssim \log^2(1/h)\boldsymbol{y}^{\mathrm{T}}\widehat{\boldsymbol{P}}^{-\mathrm{T}}\widehat{\boldsymbol{P}}^{-1}\boldsymbol{y}\,, \quad \forall \boldsymbol{y} \in \mathbb{R}^N \tag{6.20}$$

and thus

$$\begin{aligned}\boldsymbol{y}^{\mathrm{T}}\left(\widehat{\boldsymbol{P}}^{-\mathrm{T}}\widehat{\boldsymbol{P}}^{-1}\right)^2\boldsymbol{y} &\lesssim \boldsymbol{y}^{\mathrm{T}}\left(-\mathrm{i}\boldsymbol{P}^{\mathrm{T}}\boldsymbol{T}\boldsymbol{P}\right)^2\boldsymbol{y} \\ &\lesssim \log^4(1/h)\boldsymbol{y}^{\mathrm{T}}\left(\widehat{\boldsymbol{P}}^{-\mathrm{T}}\widehat{\boldsymbol{P}}^{-1}\right)^2\boldsymbol{y}\,, \quad \forall \boldsymbol{y} \in \mathbb{R}^N\,.\end{aligned} \tag{6.21}$$

Using the substitution $\widehat{\boldsymbol{P}}^{-\mathrm{T}}\widehat{\boldsymbol{P}}^{-1}\boldsymbol{y} = \boldsymbol{x}$, we obtain

$$\boldsymbol{x}^{\mathrm{T}}\boldsymbol{x} \lesssim \boldsymbol{x}^{\mathrm{T}}\widehat{\boldsymbol{P}}\widehat{\boldsymbol{P}}^{\mathrm{T}}\left(-\mathrm{i}\boldsymbol{P}^{\mathrm{T}}\boldsymbol{T}\boldsymbol{P}\right)^{2}\widehat{\boldsymbol{P}}\widehat{\boldsymbol{P}}^{\mathrm{T}}\boldsymbol{x} \lesssim \log^{4}(1/h)\boldsymbol{x}^{\mathrm{T}}\boldsymbol{x}\,, \quad \forall \boldsymbol{y} \in \mathbb{R}^{N}\,. \tag{6.22}$$

This implies

$$\mathrm{cond}\left(\widehat{\boldsymbol{P}}\widehat{\boldsymbol{P}}^{\mathrm{T}}\left(-\mathrm{i}\boldsymbol{P}^{\mathrm{T}}\boldsymbol{T}\boldsymbol{P}\right)^{2}\widehat{\boldsymbol{P}}\widehat{\boldsymbol{P}}^{\mathrm{T}}\right) \lesssim \log^{4}(1/h) \tag{6.23}$$

and hence

$$\mathrm{cond}\left(\widehat{\boldsymbol{P}}\widehat{\boldsymbol{P}}^{\mathrm{T}}\left(-\mathrm{i}\boldsymbol{P}^{\mathrm{T}}\boldsymbol{T}\boldsymbol{P}\right)\right) \lesssim \log^{2}(1/h)\,. \tag{6.24}$$

□

Considering that the effect of the non-dynamic kernel is only a compact perturbation, we do not expect a significant impact on the employed method. The numerical results shown in Section 6.d confirm our expectations and demonstrate the legitimacy of (6.11).

## c) Implementational Issues

Since we were not interested in extremely low-frequencies, we used (6.11) to demonstrate the applicability of our approach. So far it has not been discussed, how to select the scaling parameter $\gamma$. The spectrum of the global loops scales linearly in frequency. For that reason, the preconditioner in (4.85) rescales both the solenoidal and quasi-harmonic subspace with the same factor $1/k$. When we use the hierarchical basis and a diagonal preconditioner is obtained by using (6.2), one could simply use the average factor by which the spectrum is shifted, that is,

$$\gamma = \frac{N_{\Lambda}}{\sum_{i=1}^{N_{\Lambda}}\left[\widehat{\boldsymbol{\Lambda}}^{\mathrm{T}}(\mathrm{i}k\boldsymbol{T}_{\mathrm{A}})\widehat{\boldsymbol{\Lambda}}\right]_{ii}}\,. \tag{6.25}$$

For the numerical results in this chapter, we have used this approach.[32]

32 If the preconditioner from Chapter 5 is applied, where the power iteration method is used to cure the low-frequency breakdown, it is more customary to employ the power iteration method for the quasi-harmonic part of the spectrum as well.

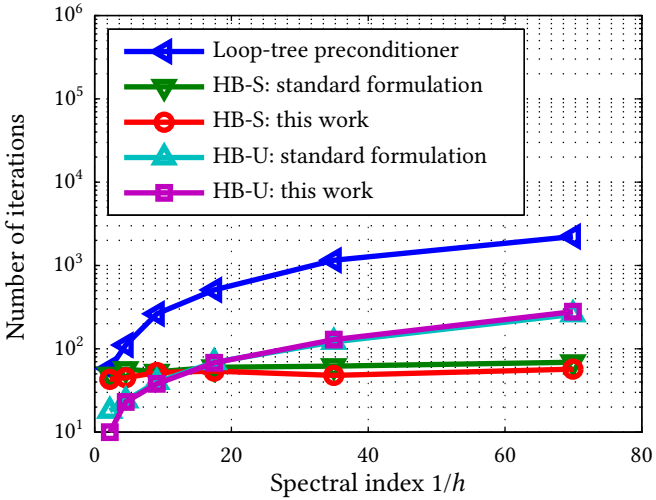


*Fig. 6.2.:* Cube: number of iterations for a CGS solver with precision $1 \cdot 10^{-6}$ and ACA accuracy $1 \cdot 10^{-7}$.

Albeit (6.11) is a significant improvement compared with (6.10), further enhancements are possible. If a hierarchical basis is used, where it is advisable to use the diagonal preconditioner to obtain $\boldsymbol{D}$, then numerical results show that it suffices to compute $\boldsymbol{D}_{\widehat{\boldsymbol{\Lambda}}}$ and $\boldsymbol{D}_{\widehat{\boldsymbol{\Sigma}}}$ as the diagonal preconditioners of $\widehat{\boldsymbol{\Lambda}}^{\mathrm{T}}\boldsymbol{T}^{\mathrm{near}}\widehat{\boldsymbol{\Lambda}}$ and $\widehat{\boldsymbol{\Sigma}}^{\mathrm{T}}\boldsymbol{T}^{\mathrm{near}}\widehat{\boldsymbol{\Sigma}}$, where $\boldsymbol{T}^{\mathrm{near}}$ is the near-interaction part of the system matrix as defined in the ACA scheme. This matrix is sparse and hence the products can be formed explicitly. As $\boldsymbol{D} = \left[\boldsymbol{D}_{\widehat{\boldsymbol{\Lambda}}} \quad \boldsymbol{D}_{\widehat{\boldsymbol{\Sigma}}}\right]$, $\boldsymbol{D}_{\widehat{\boldsymbol{\Lambda}}}$ and $\boldsymbol{D}_{\widehat{\boldsymbol{\Sigma}}}$ can be obtained without modification of an existing hierarchical basis preconditioner code.

## d) Numerical Results

To prove the general effectiveness of (6.11), we tested it with both kinds of hierarchical bases: a hierarchical basis for unstructured meshes (HB-U) [And12b] (which in this case preconditions only the scalar potential operator) and a hierarchical basis for structured meshes (HB-S) [ATV10] (which preconditions in this case the vector and the scalar potential operator).

In the first test, we verified the applicability of the new formulation with a simply connected geometry. A plane wave with frequency 1 MHz impinges on a cube with side length $\lambda/300$. In order to use the HB-S, we used a dyadic mesh refinement. To accelerate the computation, we compressed the system matrix, compression precision $1 \cdot 10^{-7}$, with the adaptive cross approximation (ACA), which reduces the cost of a single matrix-vector product to $\mathcal{O}(N \log N)$ [ZVL05]. We compared the new formulation from (6.11) with the loop-tree preconditioner and with the standard formulation of each hierarchical basis preconditioner as it is denoted in (6.3). From Figure 6.2, we can see that the proposed formulation has a comparable efficacy as the standard formulation of (6.3) in terms of number of iterations. In fact, for some cases the left preconditioning formulation outperforms the standard split preconditioning formulation in terms of number of iterations. The better performance of the HB-S compared with the HB-U stems from the fact that the used HB-U only preconditions the scalar potential operator.

As a second example, we verified the low-frequency stability. We used the multiply connected cube with six holes (see Figure 6.1). For the generation of the results we used the HB-U. We compared the proposed method with the case where $\gamma = 1$ independent from the frequency. One can see in Figure 6.3 that the condition number remains constant, while when $\gamma = 1$ the condition number changes with the frequency. Figure 6.4 shows the spectrum for the case when $f = 1\,\mathrm{kHz}$. One can see that the part of the spectrum associated with the global loops is well-contained in the rest of the spectrum, while for $\gamma = 1$ the singular values associated with the global loops are separated from the rest of the spectrum. In comparison with Figure 6.4, we can see the integrity of the preconditioner: the singular values associated with the global loops are clustered.

As a third example, we tested the HB-U on a plate with an increasing amount of holes (as an example, a plate with 64 holes is shown in Figure 6.6). A plane wave with frequency 1 MHz impinges on the plate. We compared the HB-U in the new formulation with a classical loop-tree preconditioner that does not take into account the global loops. Figure 6.5 shows the relative error. The CGS precision was $1 \cdot 10^{-6}$. The large and with the number of holes growing error shows the importance of including the global loops—explicitly or implicitly.

Lastly, we were interested in the performance when we deal with more complex structures. To evaluate the performance, we used the model of a MiG-15 as shown in Figure 6.7. This model is an open geometry with one hole. We tested the proposed preconditioner with the HB-U. The precision of the iterative solver

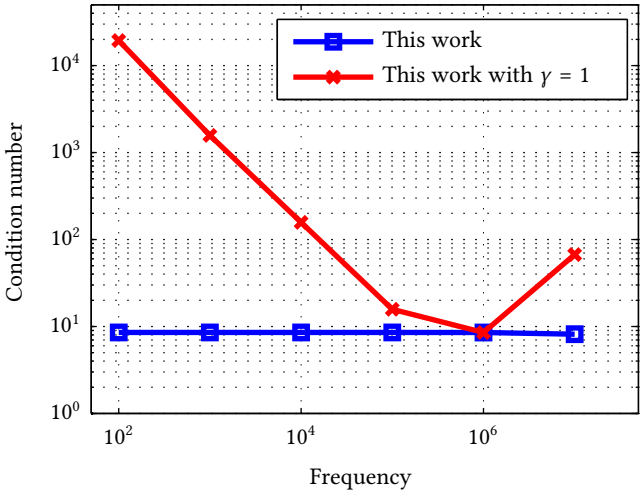


*Fig. 6.3.:* Cube with six holes: the condition number as a function of the frequency.

is $1 \cdot 10^{-6}$ and the precision of the ACA is $1 \cdot 10^{-7}$. Figure 6.9 shows the number of iterations. We observe that the number of iterations needed by the new formulation is in the same order as the number of iterations needed by the standard formulation of hierarchical basis preconditioners. This demonstrates that the optimality effect of the hierarchical basis—that the number of iterations grows at most logarithmically—is maintained.

## e) Conclusion

We presented a formulation that allows to apply hierarchical bases for preconditioning the EFIE on multiply connected geometries without searching for global loops—a search which has, in general, a quadratic cost. Instead, the quasi-harmonic subspace is preserved by implicitly recovering the global loops using a left preconditioning formulation instead of the standard split preconditioning formulation of the hierarchical bases preconditioner. Thereby, the leading complexity $\mathcal{O}(N \log N)$ set by the fast multiplication method is maintained regardless of the

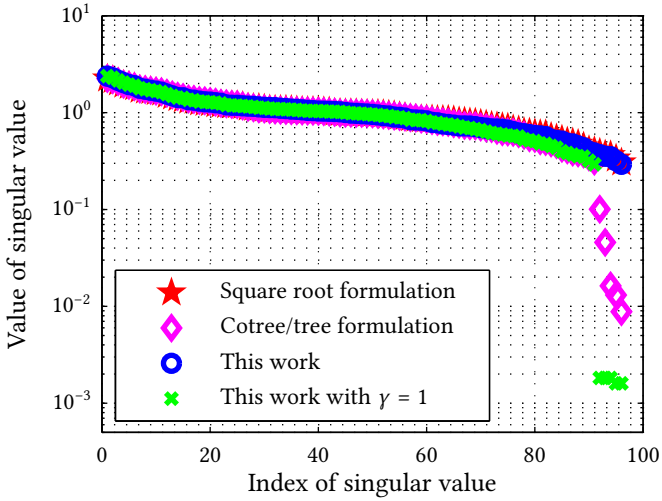


*Fig. 6.4.:* Cube with six holes: the singular value spectrum using cotree/tree functions (formulation of (6.5) with $\boldsymbol{X}_{\hat{\boldsymbol{\Lambda}}} = \boldsymbol{\Gamma}^{\mathrm{T}}$ and $\boldsymbol{X}_{\hat{\boldsymbol{\Sigma}}} = \boldsymbol{\Theta}^{\mathrm{T}}$) and preconditioned loop/star functions (formulation of (6.8)), and the singular value spectrum of the proposed method (formulation of (6.11) with $\gamma$ chosen as in (6.25) and with $\gamma = 1$). The frequency is 1 kHz. The plot of the square root formulation is hidden behind the plot of "This work".

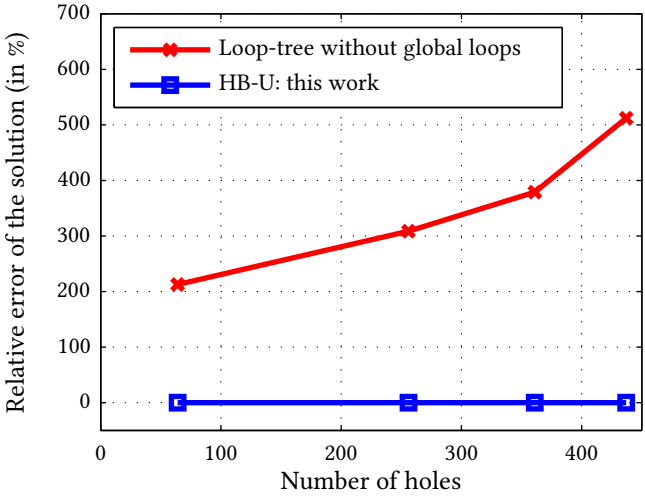


*Fig. 6.5.:* Plates: relative error of the iteratively obtained solutions compared with the solution obtained by a direct inversion of the matrix.

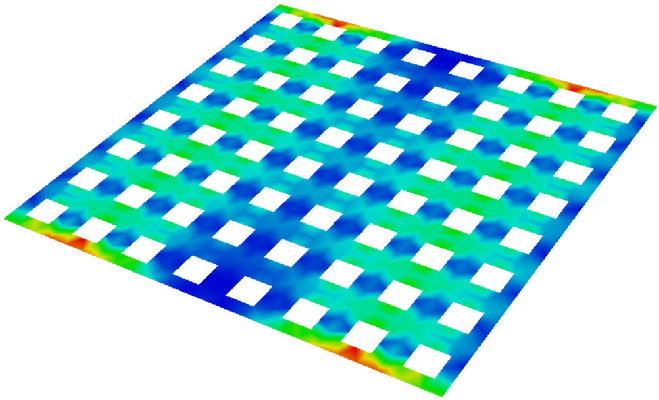

*Fig. 6.6.:* Plate: model with 64 holes. The surface current density excited by a plane wave with frequency 1 MHz is shown. © IEEE 2014.

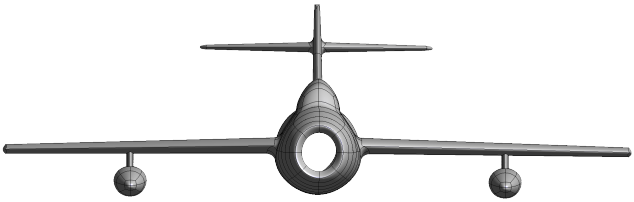

*Fig. 6.7.:* MiG-15: open surface with one hole.

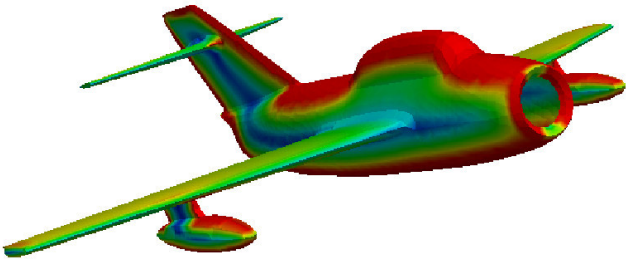

*Fig. 6.8.:* MiG-15: current density for a plane wave impinging when the frequency is 1 MHz. © IEEE 2014.

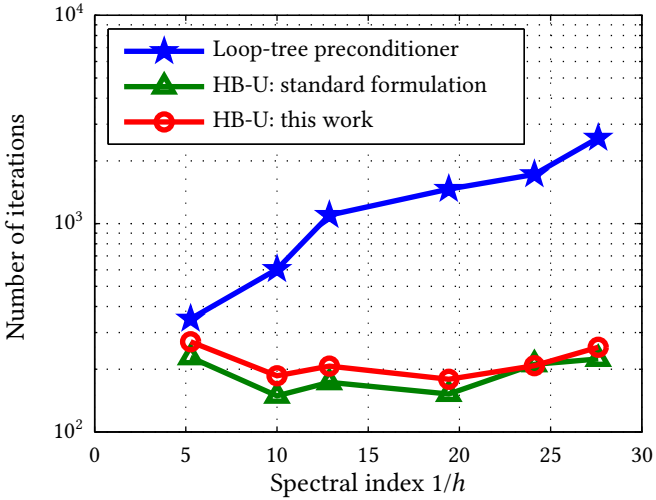


*Fig. 6.9.:* MiG-15: number of iterations for a CGS solver with precision $1 \cdot 10^{-6}$ and ACA accuracy $1 \cdot 10^{-7}$.

number of global loops. The proposed formulation was evaluated with different hierarchical bases and for all bases the results demonstrate a performance comparable with the results obtained by the standard formulation of the hierarchical bases preconditioners, where a loop-finding algorithm had been employed to construct the quasi-harmonic subspace explicitly.

Chapter 7

# On the Hierarchical Preconditioning of the CFIE

*This chapter analyzes how hierarchical bases preconditioners constructed for the EFIE can be effectively applied to the CFIE. In addition, a new scheme is proposed: the CFIE is implicitly preconditioned on the solenoidal Helmholtz subspace by using a Helmholtz projector, while a hierarchical non-solenoidal basis is used for the non-solenoidal Helmholtz subspace. Numerical results corroborate the effectiveness of the new formulation. This chapter is based on [AAE16b].*

At resonance frequencies, the EFIE and the MFIE are not uniquely solvable (see the discussion in Section 4.c), an issue that has been overcome by solving the CFIE [MH78]. Since, however, the CFIE is a combination of the EFIE and of the MFIE, it is not free from the low-frequency and the dense-discretization breakdown. For this reason, efforts have been made to extend the hierarchical basis preconditioners to the CFIE [Fra+14].

The conference contribution [Fra+14] reported on the fact that the application of a hierarchical loop/hierarchical non-solenoidal basis preconditioner to the CFIE resulted in a well-conditioned equation. Given that the hierarchical loop preconditioner is not capable of preconditioning the EFIE [ATV10; LO98], we found the result surprising and decided to perform a theoretical investigation of the problem.

This leads to this chapter whose novelty content is twofold: (i) we show on a theoretically sound basis that a direct application of the hierarchical basis preconditioner to the CFIE is possible when the hierarchical loop [VPV05] or the three-point hierarchical loop functions [ATV10] are used as solenoidal basis. Beyond the discussion in [AAE16b], we discuss the applicability of the new dual

Haar basis developed in Chapter 5. (ii) We propose a new hierarchical left preconditioning scheme that different from any other hierarchical approach for the preconditioning of the CFIE (including those communicated in [Fra+14] and detailed in [Rig+16]) can provide optimal (up to a logarithmic term) preconditioning *both* on structured and unstructured meshes. Numerical results will show the effectiveness of the new scheme for canonical and realistic examples.

## a) Spectral Analysis of the EFIE

We assume in this analysis that $\Omega$ is simply connected. The operators $\mathcal{W}$ and $\mathcal{V}$ are known to suffer from the dense-discretization breakdown [ATV10]. If we precondition these operators successfully, we can precondition the EFIE (see also Chapter 5). Different hierarchical bases have been introduced in the past. For preconditioning $\mathcal{T}_\Phi$, the bases developed are all equivalent, and we choose as a representative the basis from [AVV08].

For $\mathcal{T}_\mathrm{A}$, two hierarchical bases have been commonly used until the publication of [AAE17]: the hierarchical loops $\widehat{\boldsymbol{\Lambda}}_{\mathrm{H}i}$ [VPV05] (the subscript "H" denotes that we deal with hierarchical loops. It has nothing to do with global loops, which are denoted as $\boldsymbol{H}_i$ in this thesis) and the three-point hierarchical loops $\widehat{\boldsymbol{\Lambda}}_{\mathrm{T}i}$ [ATV10].[33] Only the latter can cure, however, the dense-discretization breakdown of the EFIE [ATV10]. Both $\widehat{\boldsymbol{\Lambda}}_{\mathrm{H}i}$ and $\widehat{\boldsymbol{\Lambda}}_{\mathrm{T}i}$ require a structured mesh: a mesh that is obtained by iteratively refining, for example dyadically, $J$ times a coarse mesh. Accordingly, $\widehat{\boldsymbol{\Lambda}}_{\mathrm{H}i}$ and $\widehat{\boldsymbol{\Lambda}}_{\mathrm{T}i}$ are defined on $J$ hierarchical levels (for details, see [ATV10]). These functions are related to scalar functions by

$$\widehat{\boldsymbol{\Lambda}}_{\mathrm{H}i} = \nabla \times \hat{\boldsymbol{n}}\hat{\lambda}_{\mathrm{H}i} \tag{7.1}$$

and

$$\widehat{\boldsymbol{\Lambda}}_{\mathrm{T}i} = \nabla \times \hat{\boldsymbol{n}}\hat{\lambda}_{\mathrm{T}i}\,, \tag{7.2}$$

where $\hat{\lambda}_{\mathrm{H}i}$ are the hierarchical nodal functions presented by Yserentant [Yse86] and $\hat{\lambda}_{\mathrm{T}i}$ are the three-point hierarchical nodal functions by Stevenson [Ste98]. As

33 Due to the relationship of loop functions with the piecewise linear functions, as will be outlined in this section, it should be possible to generate further hierarchical solenoidal bases by using, for example, a basis as presented in [DS99]. This would, however, not impact the discussion in this chapter since $\widehat{\boldsymbol{\Lambda}}_{\mathrm{H}i}$ are $H^s$-stable, $0 \le s \le 1$, that is, they are optimal for preconditioning in the relevant range of $s$ (and for any other hierarchical basis the analysis could be adapted).

we did for the loop basis, we can define transformation matrices $\widehat{\boldsymbol{\Lambda}}_{\mathrm{H}}$ and $\widehat{\boldsymbol{\Lambda}}_{\mathrm{T}}$ for the hierarchical loop and three-point hierarchical loop functions, respectively. In this chapter we assume, following the discussion in Section 4.d.$\alpha$, that the bases are all linearly independent, that is, a loop function has been eliminated so that $\boldsymbol{\Lambda}, \widehat{\boldsymbol{\Lambda}}_{\mathrm{H}}, \widehat{\boldsymbol{\Lambda}}_{\mathrm{T}} \in R^{N \times N_\Lambda}$.

In addition, we consider the new solenoidal hierarchical basis introduced in Chapter 5, where we denote the transformation matrix as $\widehat{\boldsymbol{\Lambda}}$. For notational convenience, we assume that these functions have been rescaled as explained in Chapter 5 such that $\operatorname{cond}(\widehat{\boldsymbol{\Lambda}}^{\mathrm{T}} \boldsymbol{T}_{\mathrm{A}} \widehat{\boldsymbol{\Lambda}}) \lesssim \log^2\left(1/h^2\right)$, thus there is no need for an additional diagonal preconditioner matrix in order to precondition the EFIE.

The operator $\mathcal{W}$ maps from the Sobolev space $H^{1/2}(\Gamma)$ to $H^{-1/2}(\Gamma)$ and induces an inner product on $H^{1/2}/\mathbb{R}$ [Néd01]. The three-point hierarchical nodal functions $\lambda_{\mathrm{T}i}$ are $H^{1/2}$-stable, that is, when rescaled appropriately, the three-point hierarchical loop functions can precondition the vector potential operator [ATV10] resulting in

$$\operatorname{cond}\left( \boldsymbol{D}_\Lambda^1 \widehat{\boldsymbol{\Lambda}}_{\mathrm{T}}^{\mathrm{T}} \boldsymbol{T}_{\mathrm{A}} \widehat{\boldsymbol{\Lambda}}_{\mathrm{T}} \boldsymbol{D}_\Lambda^1 \right) \lesssim 1\,, \tag{7.3}$$

with

$$\left[ \boldsymbol{D}_\Lambda^s \right]_{ii} = 2^{(1-s) l_\Lambda(j)}\,, \tag{7.4}$$

where $l_\Lambda(i)$, $i \in \{1, \ldots, N_\Lambda\}$, is the number of the level of the $i$th three-point hierarchical loop function. We note that $\boldsymbol{D}_\Lambda^1$ makes the three-point hierarchical nodal functions $H^{1/2}$-stable, while $\boldsymbol{D}_\Lambda^0$ results in $L^2$-stable and $\boldsymbol{D}_\Lambda^2$ in $H^1$-stable three-point hierarchical nodal functions.[34] The hierarchical nodal functions, on the other hand, are not $H^{1/2}$-stable [LO98], and thus, the hierarchical loop functions fail to precondition $\boldsymbol{\mathcal{T}}_{\mathrm{A}}$. Likewise, the nodal functions are not $H^{1/2}$-stable resulting in [ATV10][35]

$$\operatorname{cond}\left( \boldsymbol{\Lambda}^{\mathrm{T}} \boldsymbol{T}_{\mathrm{A}} \boldsymbol{\Lambda} \right) \lesssim 1/h\,. \tag{7.5}$$

We note that an application of a Jacobi preconditioner can improve the behavior quantitatively but not qualitatively (see Fig. 7.1a).

34 This means that for $\boldsymbol{D}_\Lambda^1$ the three-point hierarchical loop functions are $\boldsymbol{H}(\operatorname{div}_\Gamma 0, \Gamma)$-stable and for $\boldsymbol{D}_\Lambda^2$ they are $\boldsymbol{L}^2(\Gamma)$-stable, where $\boldsymbol{H}(\operatorname{div}_\Gamma 0, \Gamma) = \left\{ \boldsymbol{u} \in \boldsymbol{H}(\operatorname{div}_\Gamma, \Gamma) \,:\, \operatorname{div}_\Gamma \boldsymbol{u} = 0 \right\}$. The definition of $\boldsymbol{D}_\Lambda$ always depends on the definition of the hierarchical basis. Naturally, one could have tailored the hierarchical basis such that it is $\boldsymbol{L}^2$-stable without the application of a diagonal preconditioner.

35 Due to the elimination of a loop function, the conditioning is actually worse: there is an isolated singular value going astray [And12a]. In order not to complicate the situation, we ignore this effect.

Let $\widehat{\Sigma}_i$ be the hierarchical non-solenoidal functions for which we define the transformation matrix $\widehat{\boldsymbol{\Sigma}}$. Since $\mathcal{V}$ is inducing an $H^{-1/2}$ inner product, we need a rescaling defined by $\left[\boldsymbol{D}_\Sigma\right]_{ii} = 2^{+l_\Sigma(i)/2}$ to make div $\widehat{\Sigma}_i$ stable in $H^{-1/2}$, where $l_\Sigma(i)$, $i \in \{1 \ldots, N_\Sigma\}$, is the number of the level of the $i$th hierarchical non-solenoidal function. Then it can be proved that (see [ATV10] and references therein)

$$\operatorname{cond}\left(\boldsymbol{D}_\Sigma \widehat{\boldsymbol{\Sigma}}^{\mathrm{T}} \boldsymbol{T}_\Phi \widehat{\boldsymbol{\Sigma}} \boldsymbol{D}_\Sigma\right) \lesssim \log^2\left(1/h^2\right). \tag{7.6}$$

We define the overall transformation matrix

$$\boldsymbol{Q}^s_{\boldsymbol{X}/k,\widehat{\boldsymbol{\Sigma}}k} := \left[\boldsymbol{X}\boldsymbol{D}^s_\Lambda/\sqrt{k} \quad \widehat{\boldsymbol{\Sigma}}\boldsymbol{D}_\Sigma\sqrt{k}\right], \tag{7.7}$$

where $\boldsymbol{X}$ can be $\boldsymbol{\Lambda}$, $\widehat{\boldsymbol{\Lambda}}_{\mathrm{H}}$, or $\widehat{\boldsymbol{\Lambda}}_{\mathrm{T}}$. Summarizing, we find for the preconditioned EFIE that the loop/hierarchical non-solenoidal basis yields

$$\operatorname{cond}\left(\left(\boldsymbol{Q}^0_{\boldsymbol{\Lambda}/k,\widehat{\boldsymbol{\Sigma}}k}\right)^{\mathrm{T}} \boldsymbol{T} \boldsymbol{Q}^0_{\boldsymbol{\Lambda}/k,\widehat{\boldsymbol{\Sigma}}k}\right) \lesssim 1/h \tag{7.8}$$

and that the three-point hierarchical loops/hierarchical non-solenoidal basis yields

$$\operatorname{cond}\left(\left(\boldsymbol{Q}^1_{\widehat{\boldsymbol{\Lambda}}_{\mathrm{T}}/k,\widehat{\boldsymbol{\Sigma}}k}\right)^{\mathrm{T}} \boldsymbol{T} \boldsymbol{Q}^1_{\widehat{\boldsymbol{\Lambda}}_{\mathrm{T}}/k,\widehat{\boldsymbol{\Sigma}}k}\right) \lesssim \log^2\left(1/h^2\right). \tag{7.9}$$

## b) Spectral Analysis and Preconditioning of the CFIE

Following these considerations, we study the CFIE. For the sake of brevity, the analysis is carried out only for the conformingly discretized CFIE. The findings are, however, the same as for the standard CFIE. Because of the identity operator of the MFIE, the conditioning of the CFIE is better than that of the EFIE with

$$\operatorname{cond}\left(\widetilde{\boldsymbol{C}}\right) \lesssim 1/h\,. \tag{7.10}$$

While the largest singular value of $\mathcal{T}_\Phi$ still grows to infinity, the singular values of $\mathcal{T}_\mathrm{A}$ are shifted from 0 to 1/2 by $\mathcal{I}/2$. Next, we have to study a Helmholtz-decomposed CFIE. Following the argumentation in [And12a], the compact operator $\mathcal{K}$ (i.e., $\mathcal{K}$ is compact on smooth surfaces; the numerical results imply that

the spectral properties hold for non-smooth surfaces as well) can be neglected and it suffices to analyze how $\boldsymbol{G}_{ff}$ changes the EFIE behavior.

We notice that when $\boldsymbol{\mathcal{I}}$ is discretized with loop, hierarchical loop, and three-point hierarchical loop functions, the resulting matrix is equivalent to the discretization of the Laplace operator in its weak formulation with nodal, hierarchical nodal, and three-point hierarchical nodal functions since [And12a]

$$\left(\nabla \times \hat{\boldsymbol{n}} f_i, \nabla \times \hat{\boldsymbol{n}} f_j\right)_{L^2} = \left(\nabla f_i, \nabla f_j\right)_{L^2} . \tag{7.11}$$

The Laplace operator induces an inner product on $H^1/\mathbb{R}$, and hence, we need $H^1$-stable basis functions.

It is well-known that the nodal functions are not $H^1$-stable [LO98]; the condition number grows with $O(1/h^2)$, and given that the Laplace operator $\Delta_\Gamma$ is a pseudo-differential operator of order +2 and $\mathcal{W}$ is a pseudo-differential operator of order +1, the total order of $\mathcal{W} + \Delta_\Gamma$ is +2, and hence, we have

$$\operatorname{cond}\left(\boldsymbol{\Lambda}^{\mathrm{T}} \widetilde{\boldsymbol{C}} \boldsymbol{\Lambda}\right) \lesssim 1/h^2 . \tag{7.12}$$

In other words, loop functions applied to the CFIE result in a conditioning worse than when they are applied to the EFIE.

Similar to [And12a], we ignore $\boldsymbol{\mathcal{K}}$ for the condition number analysis since its eigenvalues cluster around zero. Hence, we only consider $\boldsymbol{\mathcal{I}}$ and $\boldsymbol{\mathcal{T}}$. We note that on multiply connected geometries, we cannot neglect $\boldsymbol{\mathcal{K}}$ [Bog+11].

The hierarchical nodal functions are not $H^1$-stable. Yet, for $H^1$ and when rescaled appropriately, they result in a condition number that grows with [Yse86]

$$\mathcal{O}\left(\log^2\left(1/h^2\right)\right), \tag{7.13}$$

and thus, we have

$$\operatorname{cond}\left(\widehat{\boldsymbol{\Lambda}}_{\mathrm{H}}^{\mathrm{T}} \widetilde{\boldsymbol{C}} \widehat{\boldsymbol{\Lambda}}_{\mathrm{H}}\right) \lesssim 1/h^2 . \tag{7.14}$$

The three-point hierarchical nodal functions are $H^1$-stable [Ste98], and thus, we have

$$\operatorname{cond}\left(\boldsymbol{D}_\Lambda^2 \widehat{\boldsymbol{\Lambda}}_{\mathrm{T}}^{\mathrm{T}} \widetilde{\boldsymbol{C}} \widehat{\boldsymbol{\Lambda}}_{\mathrm{T}} \boldsymbol{D}_\Lambda^2\right) \asymp 1 . \tag{7.15}$$

Notice that the matrix $\boldsymbol{D}_\Lambda^2 \widehat{\boldsymbol{\Lambda}}_{\mathrm{T}}^{\mathrm{T}} \boldsymbol{T} \widehat{\boldsymbol{\Lambda}}_{\mathrm{T}} \boldsymbol{D}_\Lambda^2$ is ill-conditioned; since we use $H^1$-stable functions, the singular values are now accumulating at zero. This does not destroy the well-conditioning as $\boldsymbol{D}_\Lambda^2 \widehat{\boldsymbol{\Lambda}}_{\mathrm{T}}^{\mathrm{T}} \boldsymbol{G}_{ff} \widehat{\boldsymbol{\Lambda}}_{\mathrm{T}} \boldsymbol{D}_\Lambda^2$ is spectrally equivalent to $\boldsymbol{I}$, that is,

$$\boldsymbol{x}^{\mathrm{T}} \boldsymbol{D}_\Lambda^2 \widehat{\boldsymbol{\Lambda}}_{\mathrm{T}}^{\mathrm{T}} \boldsymbol{G}_{ff} \widehat{\boldsymbol{\Lambda}}_{\mathrm{T}} \boldsymbol{D}_\Lambda^2 \boldsymbol{x} \asymp \boldsymbol{x}^{\mathrm{T}} \boldsymbol{x}, \quad \forall \boldsymbol{x} \in \mathbb{R}^{N_\Lambda}, \tag{7.16}$$

and thus the spectrum is bounded from below. Since $\boldsymbol{\mathcal{T}}_\Phi$ is a derivate operator, the Gram matrix $\boldsymbol{D}_\Sigma \widehat{\boldsymbol{\Sigma}}^{\mathrm{T}} \boldsymbol{G}_{ff} \widehat{\boldsymbol{\Sigma}} \boldsymbol{D}_\Sigma$ of the rescaled $\widehat{\Sigma}_i$ must have integrative strength to precondition $\boldsymbol{\mathcal{T}}_\Phi$. As it is true for integrative operators, the singular values of this Gram matrix cluster around zero, and since $\boldsymbol{D}_\Sigma \widehat{\boldsymbol{\Sigma}}^{\mathrm{T}} \boldsymbol{T} \widehat{\boldsymbol{\Sigma}} \boldsymbol{D}_\Sigma$ is spectrally equivalent (up to a logarithmic term) to $\boldsymbol{I}$, we can conclude that

$$\operatorname{cond}\left( \boldsymbol{D}_\Sigma \widehat{\boldsymbol{\Sigma}}^{\mathrm{T}} \widetilde{\boldsymbol{C}} \widehat{\boldsymbol{\Sigma}} \boldsymbol{D}_\Sigma \right) \lesssim \log^2\left(1/h^2\right). \tag{7.17}$$

Summarizing, we have for the loop/hierarchical non-solenoidal basis preconditioner

$$\operatorname{cond}\left( \left( \boldsymbol{Q}^0_{\boldsymbol{\Lambda}, \widehat{\boldsymbol{\Sigma}} k} \right)^{\mathrm{T}} \widetilde{\boldsymbol{C}} \boldsymbol{Q}^0_{\boldsymbol{\Lambda}, \widehat{\boldsymbol{\Sigma}} k} \right) \lesssim 1/h^2, \tag{7.18}$$

for the hierarchical loop/hierarchical non-solenoidal basis preconditioner

$$\operatorname{cond}\left( \left( \boldsymbol{Q}^2_{\widehat{\boldsymbol{\Lambda}}_{\mathrm{H}}, \widehat{\boldsymbol{\Sigma}} k} \right)^{\mathrm{T}} \widetilde{\boldsymbol{C}} \boldsymbol{Q}^2_{\widehat{\boldsymbol{\Lambda}}_{\mathrm{H}}, \widehat{\boldsymbol{\Sigma}} k} \right) \lesssim \log^2\left(1/h^2\right), \tag{7.19}$$

and for the three-point hierarchical loop/hierarchical non-solenoidal basis preconditioner

$$\operatorname{cond}\left( \left( \boldsymbol{Q}^2_{\widehat{\boldsymbol{\Lambda}}_{\mathrm{T}}, \widehat{\boldsymbol{\Sigma}} k} \right)^{\mathrm{T}} \widetilde{\boldsymbol{C}} \boldsymbol{Q}^2_{\widehat{\boldsymbol{\Lambda}}_{\mathrm{T}}, \widehat{\boldsymbol{\Sigma}} k} \right) \lesssim \log^2\left(1/h^2\right). \tag{7.20}$$

Equivalently said, the combination loop/hierarchical non-solenoidal functions does not precondition the CFIE, while both combinations hierarchical loop/hierarchical non-solenoidal and three-point hierarchical loop/hierarchical non-solenoidal basis are a valid preconditioner for the CFIE.

Both the hierarchical loops and the three-point hierarchical loops only operate on structured meshes. The hierarchical solenoidal basis $\widehat{\boldsymbol{\Lambda}}$ presented in Chapter 5 might be an interesting alternative since it can be defined on unstructured meshes as well. It is based on an explicit inversion of the dual Haar basis transformation matrix and stability results for the $H^{1/2}$-space were obtained by using Oswald's

result that the (dual) Haar basis is $H^{-1/2}$-stable [Osw98] and by leveraging a discrete Calderón identity.

When it comes to the Laplace operator it is not immediately clear whether or not the dual Haar basis is applicable since there is no formal proof available that the Haar basis is $H^{-1}$-stable. By anticipating a result from the next chapter, we assume that we have

$$\boldsymbol{x}^{\mathrm{T}}\boldsymbol{\Delta}\boldsymbol{x} \asymp \boldsymbol{x}^{\mathrm{T}}\boldsymbol{W}\boldsymbol{G}_{\lambda\lambda}^{-1}\boldsymbol{W}\boldsymbol{x} \asymp \boldsymbol{x}^{\mathrm{T}}\boldsymbol{W}\boldsymbol{W}\boldsymbol{x}/h^2\,, \quad \forall \boldsymbol{x} \in \mathbb{R}^N\,. \tag{7.21}$$

As shown in Chapter 5, the matrix

$$\boldsymbol{D}_\Lambda^{-1}\boldsymbol{H}_\Lambda^{\ddagger}\boldsymbol{G}_{\lambda\tilde{p}}^{-1}\boldsymbol{W}\boldsymbol{G}_{\lambda\tilde{p}}^{-\mathrm{T}}\left(\boldsymbol{H}_\Lambda^{\ddagger}\right)^{\mathrm{T}}\boldsymbol{D}_\Lambda^{-1} \tag{7.22}$$

is well-conditioned up to the $\log^2(1/h)$ perturbation and we note that the left preconditioned version

$$\boldsymbol{W}\boldsymbol{G}_{\lambda\tilde{p}}^{-\mathrm{T}}\left(\boldsymbol{H}_\Lambda^{\ddagger}\right)^{\mathrm{T}}\boldsymbol{D}_\Lambda^{-2}\boldsymbol{H}_\Lambda^{\ddagger}\boldsymbol{G}_{\lambda\tilde{p}}^{-1} \tag{7.23}$$

has the same eigenvalue spectrum due to the matrix similarity. Then clearly, we have

$$\operatorname{cond}\left(\boldsymbol{G}_{\lambda\tilde{p}}^{-\mathrm{T}}\left(\boldsymbol{H}_\Lambda^{\ddagger}\right)^{\mathrm{T}}\boldsymbol{D}_\Lambda^{-2}\boldsymbol{H}_\Lambda^{\ddagger}\boldsymbol{G}_{\lambda\tilde{p}}^{-1}\boldsymbol{W}\boldsymbol{W}\boldsymbol{G}_{\lambda\tilde{p}}^{-\mathrm{T}}\left(\boldsymbol{H}_\Lambda^{\ddagger}\right)^{\mathrm{T}}\boldsymbol{D}_\Lambda^{-2}\boldsymbol{H}_\Lambda^{\ddagger}\boldsymbol{G}_{\lambda\tilde{p}}^{-1}\right) \lesssim \log^4(1/h) \tag{7.24}$$

and by using (7.21), we find

$$\operatorname{cond}\left(\boldsymbol{G}_{\lambda\tilde{p}}^{-\mathrm{T}}\left(\boldsymbol{H}_\Lambda^{\ddagger}\right)^{\mathrm{T}}\boldsymbol{D}_\Lambda^{-2}\boldsymbol{H}_\Lambda^{\ddagger}\boldsymbol{G}_{\lambda\tilde{p}}^{-1}\boldsymbol{\Delta}\boldsymbol{G}_{\lambda\tilde{p}}^{-\mathrm{T}}\left(\boldsymbol{H}_\Lambda^{\ddagger}\right)^{\mathrm{T}}\boldsymbol{D}_\Lambda^{-2}\boldsymbol{H}_\Lambda^{\ddagger}\boldsymbol{G}_{\lambda\tilde{p}}^{-1}\right) \lesssim \log^4(1/h) \tag{7.25}$$

Consequently, we can use

$$\boldsymbol{G}_{\lambda\tilde{p}}^{-\mathrm{T}}\left(\boldsymbol{H}_\Lambda^{\ddagger}\right)^{\mathrm{T}}\boldsymbol{D}_\Lambda^{-2}\boldsymbol{H}_\Lambda^{\ddagger}\boldsymbol{G}_{\lambda\tilde{p}}^{-1} \tag{7.26}$$

as split preconditioner for $\boldsymbol{\Delta}$ resulting in a condition number that grows with $\log^4(1/h)$. The message from this consideration is that it might be possible to modify $\widehat{\boldsymbol{\Lambda}}$ such that it becomes applicable to the CFIE, but at the price that the

upper bound of $\mathcal{O}(\log^2(1/h))$ on the condition number set by the Haar basis preconditioner for $\boldsymbol{T}_\Phi$ is deteriorated. Since we are interested in maintaining this bound, we do not further consider this basis.

In practical scenarios, the mesh is typically unstructured and thus hierarchical loop and three-point hierarchical loop functions are not available; yet, from the presented theory it is clear that the use of loop functions is not effective and a different strategy is necessary. To this end, we define the transformation matrix

$$\sqrt{\boldsymbol{\Lambda}} := \boldsymbol{\Lambda}\left(\boldsymbol{\Lambda}^{\mathrm{T}}\boldsymbol{\Lambda}\right)^{-1/2}. \tag{7.27}$$

The Gram matrix of these new loop functions is well-conditioned since

$$\boldsymbol{x}^{\mathrm{T}}\sqrt{\boldsymbol{\Lambda}}^{\mathrm{T}}\boldsymbol{G}_{ff}\sqrt{\boldsymbol{\Lambda}}\boldsymbol{x} \asymp \boldsymbol{x}^{\mathrm{T}}\left(\boldsymbol{\Lambda}^{\mathrm{T}}\boldsymbol{\Lambda}\right)^{-1/2}\boldsymbol{\Lambda}^{\mathrm{T}}\boldsymbol{\Lambda}\left(\boldsymbol{\Lambda}^{\mathrm{T}}\boldsymbol{\Lambda}\right)^{-1/2}\boldsymbol{x} = \boldsymbol{x}^{\mathrm{T}}\boldsymbol{x}, \quad \forall \boldsymbol{x} \in \mathbb{R}^{N_\Lambda}. \tag{7.28}$$

Using these orthogonalized loop functions, we obtain as hierarchically preconditioned system

$$\left(\boldsymbol{Q}^0_{\sqrt{\boldsymbol{\Lambda}},\widehat{\boldsymbol{\Sigma}}k}\right)^{\mathrm{T}}\widetilde{\boldsymbol{C}}\boldsymbol{Q}^0_{\sqrt{\boldsymbol{\Lambda}},\widehat{\boldsymbol{\Sigma}}k}\boldsymbol{j} = \left(\boldsymbol{Q}^0_{\sqrt{\boldsymbol{\Lambda}},\widehat{\boldsymbol{\Sigma}}k}\right)^{\mathrm{T}}\left(-\alpha_{\mathrm{C}}\boldsymbol{e} + (1-\alpha_{\mathrm{C}})\boldsymbol{G}_{ff}\boldsymbol{G}^{-1}_{\hat{\boldsymbol{n}}\times\tilde{f},f}\tilde{\boldsymbol{h}}\right), \tag{7.29}$$

with

$$\operatorname{cond}\left(\left(\boldsymbol{Q}^0_{\sqrt{\boldsymbol{\Lambda}},\widehat{\boldsymbol{\Sigma}}k}\right)^{\mathrm{T}}\widetilde{\boldsymbol{C}}\boldsymbol{Q}^0_{\sqrt{\boldsymbol{\Lambda}},\widehat{\boldsymbol{\Sigma}}k}\right) \lesssim \log^2\left(1/h^2\right). \tag{7.30}$$

While this approach is theoretically sound, it lacks practical applicability due to the presence of square root matrices. Following the strategy outlined in Chapter 6, we modify the approach by considering a left instead of the split preconditioner in (7.29). Thereby, we obtain

$$\boldsymbol{Q}^0_{\sqrt{\boldsymbol{\Lambda}},\widehat{\boldsymbol{\Sigma}}k}\left(\boldsymbol{Q}^0_{\sqrt{\boldsymbol{\Lambda}},\widehat{\boldsymbol{\Sigma}}k}\right)^{\mathrm{T}} = \boldsymbol{\Lambda}\left(\boldsymbol{\Lambda}^{\mathrm{T}}\boldsymbol{\Lambda}\right)^{-1}\boldsymbol{\Lambda}^{\mathrm{T}} + \widehat{\boldsymbol{\Sigma}}\boldsymbol{D}^2_{\Sigma}\widehat{\boldsymbol{\Sigma}}^{\mathrm{T}}. \tag{7.31}$$

As discussed in Section 4.d.$\beta$, the matrix $\boldsymbol{\Lambda}(\boldsymbol{\Lambda}^{\mathrm{T}}\boldsymbol{\Lambda})^{-1}\boldsymbol{\Lambda}^{\mathrm{T}} \equiv \boldsymbol{P}_\Lambda$ is a projector to the solenoidal Helmholtz subspace [And+13] and compared with $(\boldsymbol{\Lambda}^{\mathrm{T}}\boldsymbol{\Lambda})^{1/2}\boldsymbol{x} = \boldsymbol{b}$, the system $(\boldsymbol{\Lambda}^{\mathrm{T}}\boldsymbol{\Lambda})\boldsymbol{x} = \boldsymbol{b}$ can be solved more rapidly [HHT08]. The left preconditioner is motivated by the same argument as in Chapter 6: the left preconditioned system matrix is similar to the split precondition system matrix, so that they have the

same eigenvalue spectrum and the preconditioned conjugate gradient method would show the same iterative behavior if it were applicable. The conjugate gradient method is not applicable since $\widetilde{\boldsymbol{C}}$ is not HPD. But as in Chapter 6, we still expect a reasonable behavior of the iterative method given that the eigenvalue spectrum is the same. Albeit there is not strict proof for the well-conditioning, the numerical results corroborate our expectations.

Usually, best results are obtained when the (hierarchical) functions are rescaled by leveraging on a Jacobi preconditioner, that is, we use

$$\left[\boldsymbol{D}_\Sigma\right]_{ii} = 1/\sqrt{\left[\widehat{\boldsymbol{\Sigma}}^{\mathrm{T}}\widetilde{\boldsymbol{C}}\widehat{\boldsymbol{\Sigma}}\right]_{ii}}. \tag{7.32}$$

For a fair comparison of the different bases discussed, solenoidal and non-solenoidal alike, each basis is rescaled by using such a Jacobi preconditioner.

When the conforming CFIE is used, the Gram matrices prohibit to obtain the Jacobi preconditioner efficiently in a direct manner. For the preconditioner presented in this work, this problem can be avoided by using

$$\left[\boldsymbol{D}_\Sigma\right]_{ii} = 1/\sqrt{\left[\widehat{\boldsymbol{\Sigma}}^{\mathrm{T}}\boldsymbol{T}\widehat{\boldsymbol{\Sigma}}\right]_{ii}} \tag{7.33}$$

that is, the same procedure as for the EFIE can be used. If the basis from Chapter 5 is used, then (5.59) can be employed. This choice cures the low-frequency breakdown (i.e., the condition is independent of the frequency); however, a further alignment of the singular value branches associated with the solenoidal and the non-solenoidal Helmholtz subspace improves the condition number. To this end, by selecting $\beta = \left\|\boldsymbol{P}_\Lambda\widetilde{\boldsymbol{C}}\right\|_2$ and $\gamma = \left\|\widehat{\boldsymbol{\Sigma}}\boldsymbol{D}_\Sigma^2\widehat{\boldsymbol{\Sigma}}^{\mathrm{T}}\widetilde{\boldsymbol{C}}\right\|_2$, we can define

$$\widehat{\boldsymbol{P}} := \boldsymbol{P}_\Lambda/\beta + \widehat{\boldsymbol{\Sigma}}\boldsymbol{D}_\Sigma^2\widehat{\boldsymbol{\Sigma}}^{\mathrm{T}}/\gamma \tag{7.34}$$

resulting in the system

$$\widehat{\boldsymbol{P}}\widetilde{\boldsymbol{C}}\boldsymbol{j} = \widehat{\boldsymbol{P}}\left(-\alpha_{\mathrm{C}}\boldsymbol{e} + (1-\alpha_{\mathrm{C}})\boldsymbol{G}_{ff}\boldsymbol{G}^{-1}_{\hat{\boldsymbol{n}}\times\tilde{f},f}\tilde{\boldsymbol{h}}\right). \tag{7.35}$$

The norms can be estimated rapidly by using a power iteration method.

While the CFIE is typically not used for extremely low frequencies, for such a scenario it would be necessary to apply the new preconditioner to the frequency

preconditioned $\boldsymbol{P}^{\mathrm{T}}\widetilde{\boldsymbol{C}}\boldsymbol{P}$, where $\boldsymbol{P}$ was defined in (4.85), in order to avoid numerical cancellation in the current and in the right-hand side. The reader should note, however, two obstacles: such a low-frequency scheme is only applicable when the MFIE is conformingly and carefully discretized. The reason is that for a standard MFIE the loop-loop part of the system matrix is not scaling in frequency. It does so for a conformingly discretized MFIE, but it requires a meticulous discretization [Bog+11].

## c) Numerical Results

In the following, we compare our new formulation (7.35) with the unpreconditioned CFIE and when standard hierarchical basis preconditioners are applied. The standard hierarchical preconditioners we use always consist of the same hierarchical non-solenoidal basis complemented by loop, hierarchical loop, or three-point hierarchical loop functions, respectively. We do this for the conformingly discretized CFIE operator $\widetilde{\boldsymbol{C}}$, and the standard CFIE $\boldsymbol{C}$ (denoted as S-CFIE). Furthermore, we used $\alpha_{\mathrm{C}} = 0.9$ for the CFIE parameter. By this choice we profit from the fact that the EFIE usually yields a higher accuracy compared with the MFIE [OCE15].

First, we analyzed the dense-discretization stability by using a cube with side length 1 m. We used a plane wave excitation and fixed the frequency at $f = 1\,\mathrm{MHz}$ with $f = kc/(2\pi)$, where $c$ is the speed of light. We varied the average edge length $h$ from 1.13 m to 0.07 m, and the number of iterations is displayed as a function of the spectral index $1/h$ in Fig. 7.1a. The results confirm the presented theory: in particular, we can conclude from the figure that loop functions should not be used with the CFIE, and that hierarchical loops can safely be used with the CFIE but not with the EFIE. The new formulation (7.35) performs well both when applied to a conformingly discretized CFIE as well as a standard CFIE.

Next, we verified the frequency stability. Figure 7.1b displays the condition number as a function of the frequency $f$. We see that all preconditioned formulations are free from the low-frequency breakdown. Figure 7.1c shows that all preconditioned CFIEs are resonance-free. We also see that in terms of the condition number, the unpreconditioned CFIE works better than the preconditioned counterparts. This is not unexpected since hierarchical basis preconditioners need to be adapted to high-frequency problems.

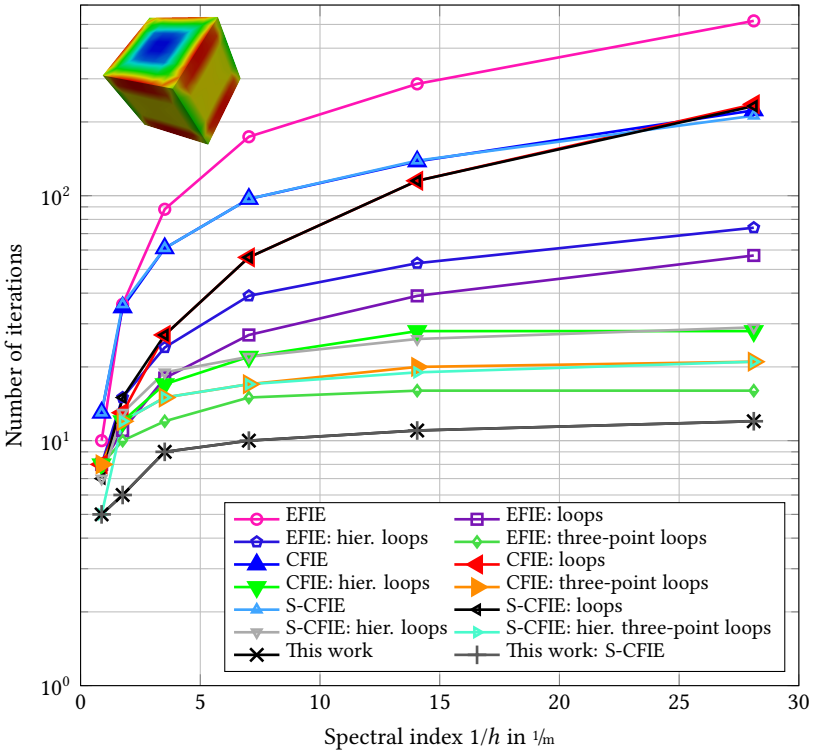


*(a)* Dense-discretization stability.

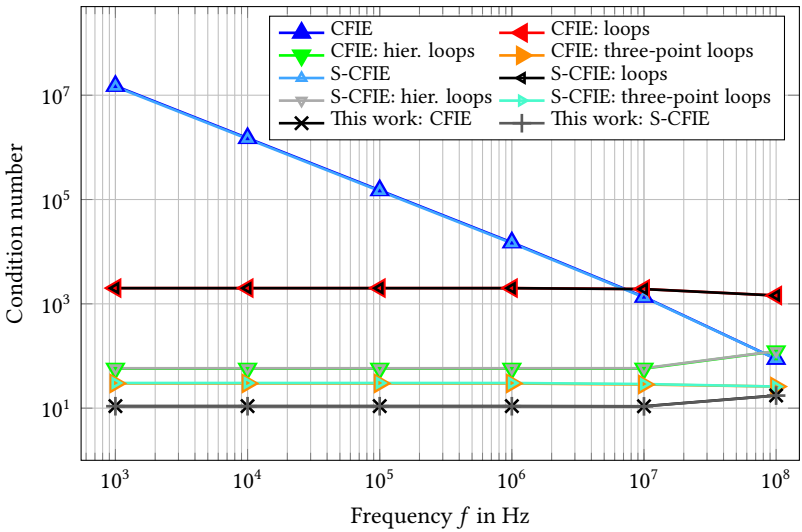


*(b)* Low-frequency stability.

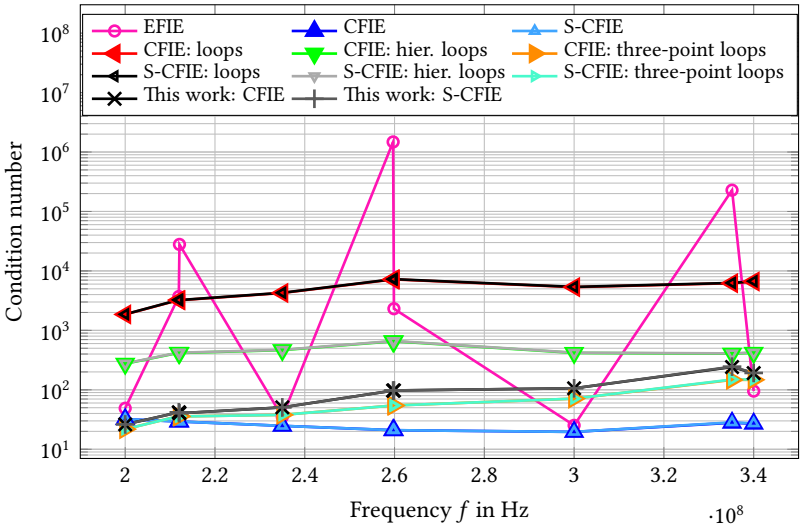


*(c)* Resonance-freeness.

*Fig. 7.1.:* Cube: spectral analysis.

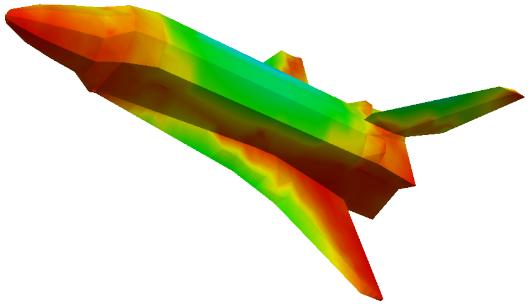

*Fig. 7.2.:* Space Shuttle. © IEEE 2016.

| Formulation | Iterations | Formulation | Iterations |
|---|---|---|---|
| CFIE | 436 | S-CFIE | 417 |
| CFIE: loops | 199 | S-CFIE: loops | 198 |
| This work: CFIE | 39 | This work: S-CFIE | 37 |

*Tab. 7.1.:* Space Shuttle: the number of iterations for the different formulations with solver tolerance $1 \cdot 10^{-6}$.

To apply our new method to a more realistic structure, we employed the model of a Space Shuttle shown in Fig. 7.2. The electric size of the Space Shuttle is $1/2\lambda$, where $\lambda$ is the wavelength. Table 7.1 summarizes our results, where the solver tolerance was $1 \cdot 10^{-6}$.

## d) Conclusion

First, we can conclude that the hierarchical loop functions, which fail to precondition the vector potential operator $\mathcal{T}_{\mathrm{A}}$ of the EFIE, can be successfully applied to the CFIE (though the results obtained by using three-point hierarchical loop functions are usually better, and they work for the EFIE as well). The best results were obtained with our new formulation in (7.35), which different from all other hierarchical preconditioners, works on both structured and unstructured meshes. It is part of ongoing research to obtain a hierarchical preconditioner which remains efficient for electrically large problems.

# Part III.

# Calderón Multiplicative Preconditioners

Chapter 8

# On a Refinement-Free Calderón Multiplicative Preconditioner for the EFIE

*This chapter presents a Calderón preconditioner for the EFIE, which does not require a barycentric refinement of the mesh, where the condition number can be bounded independently from the frequency and average edge length of the mesh, and which yields an Hermitian, positive definite (HPD) system matrix allowing for the usage of the CG solver. Different from existing Calderón preconditioners, no second discretization of the EFIE operator with BC functions is necessary. We obtain this preconditioner by leveraging spectral equivalences between (scalar) integral operators, namely the single layer and hypersingular operator, and the Laplace-Beltrami operator. Since our approach incorporates Helmholtz projectors, there is no search for global loops necessary and our method remains stable on multiply connected geometries. The numerical results demonstrate the effectiveness of our approach for both canonical and realistic (multi-scale) problems. Preliminary results have been presented at conferences [AAE14a; AAE15].*

Calderón identity based preconditioners, unlike the hierarchical basis preconditioners, allow to obtain an EFIE, where the condition number has an upper bound independent from $h$ [CN02; BC07; And+08; Con+02; Ada04]. In the static limit, however, the Calderón strategies stop working due to numerical cancellation in both the right-hand side excitation vector and the unknown current since solenoidal and non-solenoidal components scale differently in $k$ [Zha+03]. Explicit quasi-Helmholtz decompositions do not suffer from this cancellation since the solenoidal and non-solenoidal components are

stored separately. To make Calderón preconditioners stable in the static limit, one could combine the Calderón multiplicative preconditioner (CMP) with an explicit quasi-Helmholtz decomposition.

These approaches suffer, however, from the same defect that explicit quasi-Helmholtz decompositions share: if the geometry is multiply connected, then the quasi-harmonic global loop functions have to be added to the basis of the decomposition [Vec99]. Different from loop, star, or tree functions, (or any of the hierarchical bases mentioned in this thesis) the construction of the global loops is, in general, a costly operation making the overall problem $\mathcal{O}(N^2 \log(N))$, where $N$ is the number of unknowns [AAE14b] (see also Chapter 6).

In order to avoid the construction of the global loops, a modified CMP has been presented which leverages an implicit quasi-Helmholtz decomposition based on projectors [And12a; And+13]. These projectors require the application of the inverse primal (i.e., cell-based) and the inverse dual (i.e., vertex-based) graph Laplacian, a task for which blackbox-like preconditioners such as algebraic multigrid methods can be used for obtaining the inverse rapidly. We note that a scheme based on an explicit loop-star quasi-Helmholtz decomposition does not offer an alternative since the inverse Gram matrices appearing therein are all spectrally equivalent to discretized Laplace-Beltrami operators, however, with the additional challenge that the Gram matrices are not symmetric since the loop-star basis is applied to a mixed Gram matrix, that is, BC functions are used as expansion and rotated RWG functions are used as testing functions [And12a; And+13].

The work in [And+08; And+13] demonstrated a Calderón scheme that can be integrated relatively easily in existing codes. Instead of discretizing the operator on the standard mesh with RWG and BC functions, only a single discretization with RWG functions on the barycentrically refined mesh is necessary. Yet, there are caveats: (i) the memory consumption as well as the costs for a single-matrix vector product are increased by a factor of six and (ii) for open structures the codes must be modified such that half-RWG functions on the boundary edges are included for the discretization of the EFIE.

In this work, we propose a refinement-free Calderón multiplicative preconditioner (RF-CMP) for the EFIE. Different from existing Calderón preconditioners, no BC functions are employed, so that a standard discretization of the EFIE with RWG functions can be used. No modifications for open structures are necessary, though similar to the CMP, we do not have a constant upper bound of the

condition number. What is more, we get a system matrix, which is HPD. We obtain this result by leveraging spectral equivalences between the single layer and hypersingular operator known from electrostatics and the Laplace-Beltrami operator. Similar to [And+13], graph Laplacians need to be inverted. Since the new system matrix is HPD, we are allowed to employ the CG solver. In contrast to other Krylov subspace methods, it guarantees convergence and has the least computational overhead. The numerical results corroborate the new formulation.

The chapter is structured as follows. Section 8.a discusses the background; Section 8.b introduces the new formulation and provides implementational details, while Section 8.c provides the theoretical apparatus behind the new formulation. For the implementation of the new preconditioner, it is not necessary to study Section 8.c. Numerical results demonstrating the effectiveness of the new approach are shown in Section 8.d.

# a) Background

The matrix $\boldsymbol{T}$ is ill-conditioned both in $k$ and $h$ [CN02]. An optimal preconditioner is given by $\boldsymbol{\mathcal{T}}$ itself: the Calderón identity

$$\boldsymbol{\mathcal{T}}^2 = -\boldsymbol{\mathcal{I}}/4 + \boldsymbol{\mathcal{K}}^2\,, \tag{8.1}$$

where $\boldsymbol{\mathcal{K}}$ is a compact operator, dictates that its discretization

$$\boldsymbol{G}^{-\mathrm{T}}_{\hat{\boldsymbol{n}}\times f,\tilde{f}}\widetilde{\boldsymbol{T}}\boldsymbol{G}^{-1}_{\hat{\boldsymbol{n}}\times f,\tilde{f}}\boldsymbol{T} \tag{8.2}$$

is well-conditioned with $\left[\widetilde{\boldsymbol{T}}\right]_{mn} = (\hat{\boldsymbol{n}}\times\tilde{f}_m, \boldsymbol{\mathcal{T}}\tilde{f}_n)_{L^2}$, where $\tilde{f}\in X_{\tilde{f}}$ are functions dual to $f$ such as the BC functions [BC07].

The matrix in (8.2) is, however, not numerically stable down to the static limit due to numerical cancellation in the excitation $\boldsymbol{e}$ and the unknown current vector $\boldsymbol{j}$, and on multiply connected geometries it comprises a null space associated with the harmonic Helmholtz subspace [Coo+09]. A first approach to overcome the numerical cancellation could be to use an explicit quasi-Helmholtz decomposition. While this could succeed in preventing the numerical cancellation and in preserving the quasi-harmonic Helmholtz subspace, it also comes with several drawbacks as will be discussed in the following.

In more detail, let $\boldsymbol{Q} = \begin{bmatrix}\boldsymbol{\Lambda}/\sqrt{\mathrm{i}k} & \boldsymbol{H}/\sqrt{\mathrm{i}k} & \boldsymbol{\Sigma}\sqrt{\mathrm{i}k}\end{bmatrix}$ (as defined in Section 4.d.$\beta$). If we were to eliminate loop and star functions so that $\boldsymbol{Q} \in \mathbb{C}^{N\times N}$ has full rank (i.e., this follows the classical loop-star preconditioner approach), then $\boldsymbol{Q}^{\mathrm{T}}\boldsymbol{T}\boldsymbol{Q}$ is well-conditioned in frequency and hence

$$\left(\boldsymbol{Q}^{\mathrm{T}}\boldsymbol{G}_{\hat{\boldsymbol{n}}\times f,\tilde{f}}\boldsymbol{Q}\right)^{-\mathrm{T}}\boldsymbol{Q}^{\mathrm{T}}\widetilde{\boldsymbol{T}}\boldsymbol{Q}\left(\boldsymbol{Q}^{\mathrm{T}}\boldsymbol{G}_{\hat{\boldsymbol{n}}\times f,\tilde{f}}\boldsymbol{Q}\right)^{-1}\boldsymbol{Q}^{\mathrm{T}}\boldsymbol{T}\boldsymbol{Q} \tag{8.3}$$

is stable in frequency down to the static limit.

There are two drawbacks: First, the global loops $\boldsymbol{H}_n$ have to be constructed, where currently available algorithms have, in general, a complexity of $\mathcal{O}(N^2)$ for $N \asymp g$, where $g$ is the genus of geometry, and $\boldsymbol{H}$ is dense (a sparse matrix $\boldsymbol{H}$ can be obtained, but then the costs for finding the global loop is $\mathcal{O}(N^3)$, see Chapter 6 and references therein). Second, the Gram matrix $\boldsymbol{Q}^{\mathrm{T}}\boldsymbol{G}_{\hat{\boldsymbol{n}}\times f,\tilde{f}}\boldsymbol{Q}$ is ill-conditioned with a condition number that grows as $\mathcal{O}(1/h^2)$. The reason for this is that loop and star functions are not $\boldsymbol{L}^2$-stable, their Gram matrices are spectrally equivalent to discretized Laplace-Beltrami operators, for which the condition number grows with $1/h^2$, that is, we have for the Gram matrices [And12a]

$$\boldsymbol{\Lambda}^{\mathrm{T}}\boldsymbol{G}_{ff}\boldsymbol{\Lambda} = \boldsymbol{\Delta} \tag{8.4}$$

and

$$\boldsymbol{\Sigma}^{\mathrm{T}}\boldsymbol{G}_{\tilde{f}\tilde{f}}\boldsymbol{\Sigma} = \widetilde{\boldsymbol{\Delta}}, \tag{8.5}$$

where

$$\left[\boldsymbol{\Delta}\right]_{nm} = (\nabla_\Gamma\lambda_n, \nabla_\Gamma\lambda_m)_{L^2} \tag{8.6}$$

is the Laplace-Beltrami operator discretized with piecewise linear nodal functions

$$\lambda_n(\boldsymbol{r}) = \begin{cases} 1 & \text{for } \boldsymbol{r} \in \upsilon_n\,, \\ 0 & \text{for } \boldsymbol{r} \in \upsilon_m \neq \upsilon_n\,, \\ \text{linear} & \text{elsewhere,} \end{cases} \tag{8.7}$$

where $\upsilon_n \in \Gamma$ is the $n$th vertex of mesh, and

$$\left[\widetilde{\boldsymbol{\Delta}}\right]_{nm} = \left(\nabla_\Gamma\tilde{\lambda}_n, \nabla_\Gamma\tilde{\lambda}_m\right)_{L^2} \tag{8.8}$$

is the Laplace-Beltrami operator discretized with dual piecewise linear nodal functions as defined in [BC07]. The matrix $\boldsymbol{Q}^{\mathrm{T}}\boldsymbol{G}_{\hat{\boldsymbol{n}}\times f,\tilde{f}}\boldsymbol{Q}$ is even more difficult to invert since unlike $\boldsymbol{\Delta}$ it is not a symmetric matrix anymore due to $\boldsymbol{G}_{\hat{\boldsymbol{n}}\times f,\tilde{f}}$.

Recently, a scheme has been presented that leverages the quasi-Helmholtz projectors [And+13], which we have discussed in Section 4.d.$\beta$. In addition to the projectors that were defined therein, we also need $\boldsymbol{P}_{\Sigma\mathrm{H}} := \boldsymbol{I} - \boldsymbol{P}_{\Lambda}$. This allows to define the primal $\boldsymbol{P} := \boldsymbol{P}_{\Lambda\mathrm{H}}/\sqrt{k} + \mathrm{i}\boldsymbol{P}_{\Sigma}\sqrt{k}$ and the dual decomposition operator $\widetilde{\boldsymbol{P}} := \boldsymbol{P}_{\Sigma\mathrm{H}}/\sqrt{k} + \mathrm{i}\boldsymbol{P}_{\Lambda}\sqrt{k}$. Then the matrix

$$\boldsymbol{G}^{-\mathrm{T}}_{\hat{\boldsymbol{n}}\times f,\tilde{f}}\big(\widetilde{\boldsymbol{P}}\widetilde{\boldsymbol{T}}\widetilde{\boldsymbol{P}}\big)\boldsymbol{G}^{-1}_{\hat{\boldsymbol{n}}\times f,\tilde{f}}(\boldsymbol{P}\boldsymbol{T}\boldsymbol{P}) \tag{8.9}$$

is well-conditioned [And+13]. Different from (8.3), the costly global loop finding and construction of the (dense) matrix $\boldsymbol{H}$ is avoided. Instead of dealing with the non-symmetric matrix $\boldsymbol{Q}^{\mathrm{T}}\boldsymbol{G}_{\hat{\boldsymbol{n}}\times f,\tilde{f}}\boldsymbol{Q}$, in (8.9) only symmetric, positive semi-definite graph Laplacians $\boldsymbol{\Lambda}^{\mathrm{T}}\boldsymbol{\Lambda}$ (vertex-based) and $\boldsymbol{\Sigma}^{\mathrm{T}}\boldsymbol{\Sigma}$ (cell-based) appear. As pointed out in [And+13], a plethora of (black box) algorithms exists for inverting these matrices efficiently.

## b) New Formulation

This section introduces and motivates the new formulation and provides the implementational details. For the interested reader, a theoretical derivation of this formulation is provided in the next section.

Similar to the formulation in (8.9), the new formulation uses quasi-Helmholtz projectors. Different from (8.9), no second discretization of $\boldsymbol{\mathcal{T}}$ with dual functions $\widetilde{f}_n$ is required and thus no (barycentric) refinement of the mesh. Instead, we exploit the fact that $\boldsymbol{\Lambda}$ and $\boldsymbol{\Sigma}$ are ill-conditioned and use them to precondition $\boldsymbol{T}$.

We propose the new formulation

$$\boldsymbol{P}_{\mathrm{o}}^{\dagger}\boldsymbol{T}^{\dagger}\boldsymbol{P}_{\mathrm{m}}\boldsymbol{T}\boldsymbol{P}_{\mathrm{o}}\boldsymbol{i} = -\boldsymbol{P}_{\mathrm{o}}^{\dagger}\boldsymbol{T}^{\dagger}\boldsymbol{P}_{\mathrm{m}}\boldsymbol{e}\,, \tag{8.10}$$

where

$$\boldsymbol{P}_{\mathrm{o}} = \boldsymbol{P}_{\Lambda\mathrm{H}}/\alpha + \mathrm{i}\boldsymbol{P}_{\Sigma}/\beta\,, \tag{8.11}$$

$$\boldsymbol{P}_{\mathrm{m}} = \boldsymbol{P}_{\mathrm{m}\Lambda} + \boldsymbol{P}_{\mathrm{m}\Sigma}\,, \tag{8.12}$$

$$\boldsymbol{P}_{\mathrm{m}\Lambda} = \boldsymbol{\Lambda}\boldsymbol{G}_{\lambda\lambda}^{-1}\boldsymbol{\Lambda}^{\mathrm{T}}/\alpha^2 + \boldsymbol{P}_{\Lambda\mathrm{H}}/\gamma\,, \tag{8.13}$$

$$\boldsymbol{P}_{\mathrm{m}\Sigma} = \boldsymbol{\Sigma}\left(\boldsymbol{\Sigma}^{\mathrm{T}}\boldsymbol{\Sigma}\right)^{+}\boldsymbol{G}_{pp}^{\ddagger}\left(\boldsymbol{\Sigma}^{\mathrm{T}}\boldsymbol{\Sigma}\right)^{+}\boldsymbol{\Sigma}^{\mathrm{T}}/\beta^2\,, \tag{8.14}$$

$$\boldsymbol{G}_{pp}^{\ddagger} = \boldsymbol{G}_{pp}^{-1} - \boldsymbol{G}_{pp}^{-1}\mathbf{1}_{\Sigma}\mathbf{1}_{\Sigma}^{\mathrm{T}}\boldsymbol{G}_{pp}^{-1}/\left(\mathbf{1}_{\Sigma}^{\mathrm{T}}\boldsymbol{G}_{pp}^{-1}\mathbf{1}_{\Sigma}\right) \tag{8.15}$$

with $\boldsymbol{j} = \boldsymbol{P}_{\mathrm{o}}\boldsymbol{i}$, and the coefficients

$$\alpha = \sqrt[4]{\left\|\boldsymbol{P}_{\Lambda\mathrm{H}}\boldsymbol{T}_{\mathrm{A}}^{\dagger}\boldsymbol{\Lambda}\boldsymbol{G}_{\lambda\lambda}^{-1}\boldsymbol{\Lambda}^{\mathrm{T}}\boldsymbol{T}_{\mathrm{A}}\boldsymbol{P}_{\Lambda\mathrm{H}}\right\|_2}\,, \tag{8.16}$$

$$\beta = \sqrt[4]{\left\|\boldsymbol{P}_{\Sigma}\boldsymbol{T}_{\Phi}^{\dagger}\boldsymbol{P}_{\mathrm{m}\Sigma}\boldsymbol{T}_{\Phi}\boldsymbol{P}_{\Sigma}\right\|_2}\,, \tag{8.17}$$

$$\gamma = \left\|(\boldsymbol{P}_{\Lambda\mathrm{H}}/\alpha)\boldsymbol{T}_{\mathrm{A}}^{\dagger}\boldsymbol{P}_{\Lambda\mathrm{H}}\boldsymbol{T}_{\mathrm{A}}(\boldsymbol{P}_{\Lambda\mathrm{H}}/\alpha)\right\|_2\,. \tag{8.18}$$

These coefficients are necessary to cure the low-frequency breakdown. A power iteration method can be used to compute the norms. The coefficients could be replaced by functions of $k$ as shown in Section 8.c, that is, we could have used

$$\alpha = \sqrt{k}\,, \tag{8.19}$$

$$\beta = 1/\sqrt{k}\,, \tag{8.20}$$

$$\gamma = k\,, \tag{8.21}$$

but typically the condition number obtained by using norms is lower; thereby, the number of iterations used by a Krylov subspace method is reduced (and this saving usually outweighs the costs for estimating the norms).

The use of the imaginary unit +i in the definition $\boldsymbol{P}_{\mathrm{o}}$ is motivated for the same reason as it was for $\boldsymbol{P}$: to prevent the numerical cancellation due to different scaling of the solenoidal and non-solenoidal components in $\boldsymbol{e}$ and $\boldsymbol{j}$ (for a detailed analysis, see [And+13]).

In Section 8.c, we derive the new formulation in a rigorous way. Given that this section is rather technical, we shall provide some intuitive ideas about the

approach. In a first step, we decompose the EFIE into two scalar operators as shown in Chapter 4.

Equation (8.1) is not the only Calderòn identity that exists. For the single layer operator $\mathcal{V}$ and the hypersingular operator $\mathcal{W}$, we have the identities [SS11] (see also Section 3.c)

$$\mathcal{W}\circ\mathcal{V} = -\mathcal{I}/4 + \mathcal{K}_1\,, \tag{8.22}$$

$$\mathcal{V}\circ\mathcal{W} = -\mathcal{I}/4 + \mathcal{K}_2\,. \tag{8.23}$$

Here, and in the following, $\mathcal{K}_n$, $n \in \mathbb{N}$, denotes operators, which are compact on a smooth geometry. These two equations imply that the hypersingular operator can be used as preconditioner for the single layer potential and vice versa [SW98]. We are, however, not interested in doing this, since we would still need to use dual basis functions so that there is no real advantage compared with the standard Calderón techniques. By combining (8.22) and (8.23), we yield

$$\mathcal{V}\circ\mathcal{W}\circ\mathcal{W}\circ\mathcal{V} = \mathcal{I}/16 + \mathcal{K}_3\,, \tag{8.24}$$

$$\mathcal{W}\circ\mathcal{V}\circ\mathcal{V}\circ\mathcal{W} = \mathcal{I}/16 + \mathcal{K}_4\,. \tag{8.25}$$

These expressions can be simplified, if we take into account the identities [Néd01]

$$-\mathcal{W} = (-\Delta_\Gamma)^{1/2} + \mathcal{K}_5\,, \tag{8.26}$$

$$\mathcal{V} = (-\Delta_\Gamma)^{-1/2} + \mathcal{K}_6\,, \tag{8.27}$$

where $\Delta_\Gamma$ is the Laplace-Beltrami operator. Combining (8.24) with (8.26) and (8.25) with (8.27), we obtain

$$\mathcal{V}\circ(-\Delta_\Gamma)\circ\mathcal{V} = \mathcal{I}/16 + \mathcal{K}_7\,, \tag{8.28}$$

$$\mathcal{W}\circ(-\Delta_\Gamma)^{-1}\circ\mathcal{W} = \mathcal{I}/16 + \mathcal{K}_8\,. \tag{8.29}$$

Then we could consider

$$\boldsymbol{G}_{p\tilde{p}}^{-1}\boldsymbol{V}\boldsymbol{G}_{\tilde{\lambda}p}^{-1}\widetilde{\boldsymbol{\Delta}}\boldsymbol{G}_{p\tilde{\lambda}}^{-1}\boldsymbol{V} \tag{8.30}$$

and

$$\boldsymbol{G}_{\lambda\tilde{\lambda}}^{-1}\boldsymbol{W}\boldsymbol{\Delta}^{+}\boldsymbol{W} \tag{8.31}$$

as discretizations of (8.28) and (8.29). For deriving the final formulation, it is better to use symmetric, positive definite versions of these matrices, that is, we use

$$\boldsymbol{G}_{pp}^{-1/2}\boldsymbol{V}\boldsymbol{G}_{\tilde{\lambda}p}^{-1}\widetilde{\boldsymbol{\Delta}}\boldsymbol{G}_{p\tilde{\lambda}}^{-1}\boldsymbol{V}\boldsymbol{G}_{pp}^{-1/2} \tag{8.32}$$

and

$$\boldsymbol{G}_{\lambda\lambda}^{-1/2}\boldsymbol{W}\boldsymbol{\Delta}^{+}\boldsymbol{W}\boldsymbol{G}_{\lambda\lambda}^{-1/2}\,, \tag{8.33}$$

which are well-conditioned as well since they are similar matrices.

The RWG and BC functions are $L^2$-stable so the discretization of the identity operator is well-conditioned, that is, we have [And12a]

$$\boldsymbol{x}^{\mathrm{T}}\boldsymbol{G}_{ff}\boldsymbol{x} \asymp \boldsymbol{x}^{\mathrm{T}}\boldsymbol{G}_{\tilde{f}\tilde{f}}\boldsymbol{x} \asymp \boldsymbol{x}^{\mathrm{T}}\boldsymbol{x}\,, \quad \forall \boldsymbol{x} \in \mathbb{R}^{N}\,, \tag{8.34}$$

and thus

$$\boldsymbol{x}^{\mathrm{T}}\widetilde{\boldsymbol{\Delta}}\boldsymbol{x} \asymp \boldsymbol{x}^{\mathrm{T}}\boldsymbol{\Sigma}^{\mathrm{T}}\boldsymbol{\Sigma}\boldsymbol{x}\,, \quad \forall \boldsymbol{x} \in \mathbb{R}^{N_{\mathrm{C}}}\,, \tag{8.35}$$

and

$$\boldsymbol{x}^{\mathrm{T}}\boldsymbol{\Delta}\boldsymbol{x} \asymp \boldsymbol{x}^{\mathrm{T}}\boldsymbol{\Lambda}^{\mathrm{T}}\boldsymbol{\Lambda}\boldsymbol{x}\,, \quad \forall \boldsymbol{x} \in \mathbb{R}^{N_{\mathrm{V}}}\,. \tag{8.36}$$

While the mixed Gram matrix is necessary to obtain a rigorous proof for the well-conditioning, numerical evidence suggests that it has no practical impact. Since its omission allows numerical savings, we leave it out. Then (8.32) simplifies to

$$\boldsymbol{G}_{pp}^{-1/2}\boldsymbol{V}\boldsymbol{\Sigma}^{\mathrm{T}}\boldsymbol{\Sigma}\boldsymbol{V}\boldsymbol{G}_{pp}^{-1/2} \tag{8.37}$$

and (8.33) simplifies to

$$\boldsymbol{G}_{\lambda\lambda}^{-1/2}\boldsymbol{W}\left(\boldsymbol{\Lambda}^{\mathrm{T}}\boldsymbol{\Lambda}\right)^{+}\boldsymbol{W}\boldsymbol{G}_{\lambda\lambda}^{-1/2}\,. \tag{8.38}$$

Considering the definition of $\boldsymbol{P}_{\Sigma}$ and substituting back from $\boldsymbol{V}$ to $\boldsymbol{T}_{\Phi}$, then (8.37) reads

$$\boldsymbol{G}_{pp}^{-1/2}\left(\boldsymbol{\Sigma}^{\mathrm{T}}\boldsymbol{\Sigma}\right)\boldsymbol{\Sigma}^{\mathrm{T}}\boldsymbol{T}_{\Phi}^{0}\boldsymbol{P}_{\Sigma}\boldsymbol{T}_{\Phi}^{0}\boldsymbol{\Sigma}\left(\boldsymbol{\Sigma}^{\mathrm{T}}\boldsymbol{\Sigma}\right)\boldsymbol{G}_{pp}^{-1/2}\,. \tag{8.39}$$

If a matrix $\boldsymbol{A}^{\mathrm{T}}\boldsymbol{A}$ is well-conditioned, then so is $\boldsymbol{A}\boldsymbol{A}^{\mathrm{T}}$, which can be seen by considering the SVD of $\boldsymbol{A}$. Hence, the matrix

$$\boldsymbol{P}_{\Sigma}\boldsymbol{T}_{\Phi}^{0}\boldsymbol{\Sigma}\left(\boldsymbol{\Sigma}^{\mathrm{T}}\boldsymbol{\Sigma}\right)\boldsymbol{G}_{pp}^{-1}\left(\boldsymbol{\Sigma}^{\mathrm{T}}\boldsymbol{\Sigma}\right)\boldsymbol{\Sigma}^{\mathrm{T}}\boldsymbol{T}_{\Phi}^{0}\boldsymbol{P}_{\Sigma} \tag{8.40}$$

is well-conditioned on the non-solenoidal Helmholtz subspace, where we used that $\boldsymbol{P}_\Sigma^2 = \boldsymbol{P}_\Sigma$. Likewise, we find for (8.38)

$$\boldsymbol{G}_{\lambda\lambda}^{-1/2}\boldsymbol{\Lambda}^{\mathrm{T}}\boldsymbol{T}_{\mathrm{A}}^{0}\boldsymbol{\Lambda}\Big(\boldsymbol{\Lambda}^{\mathrm{T}}\boldsymbol{\Lambda}\Big)^{+}\boldsymbol{\Lambda}^{\mathrm{T}}\boldsymbol{T}_{\mathrm{A}}^{0}\boldsymbol{\Lambda}\boldsymbol{G}_{\lambda\lambda}^{-1/2} \tag{8.41}$$

and using the definition of $\boldsymbol{P}_\Lambda$, we obtain

$$\boldsymbol{G}_{\lambda\lambda}^{-1/2}\boldsymbol{\Lambda}^{\mathrm{T}}\boldsymbol{T}_{\mathrm{A}}^{0}\boldsymbol{P}_\Lambda\boldsymbol{T}_{\mathrm{A}}^{0}\boldsymbol{\Lambda}\boldsymbol{G}_{\lambda\lambda}^{-1/2}\,. \tag{8.42}$$

If this matrix is well-conditioned on the solenoidal Helmholtz subspace, then so is

$$\boldsymbol{P}_\Lambda\boldsymbol{T}_{\mathrm{A}}^{0}\boldsymbol{\Lambda}\boldsymbol{G}_{\lambda\lambda}^{-1}\boldsymbol{\Lambda}^{\mathrm{T}}\boldsymbol{T}_{\mathrm{A}}^{0}\boldsymbol{P}_\Lambda\,. \tag{8.43}$$

On the other hand, for $k \longrightarrow 0$, (8.10) reduces to

$$\boldsymbol{P}_\Lambda\boldsymbol{T}_{\mathrm{A}}^{0}\boldsymbol{\Lambda}\boldsymbol{G}_{\lambda\lambda}^{-1}\boldsymbol{\Lambda}^{\mathrm{T}}\boldsymbol{T}_{\mathrm{A}}^{0}\boldsymbol{P}_\Lambda + \boldsymbol{P}_\Sigma^{\dagger}\boldsymbol{T}_{\Phi}^{0}\boldsymbol{\Sigma}\Big(\boldsymbol{\Sigma}^{\mathrm{T}}\boldsymbol{\Sigma}\Big)^{+}\boldsymbol{G}_{pp}^{\ddagger}\Big(\boldsymbol{\Sigma}^{\mathrm{T}}\boldsymbol{\Sigma}\Big)^{+}\boldsymbol{T}_{\Phi}^{0}\boldsymbol{P}_\Sigma\,. \tag{8.44}$$

The matrix $\boldsymbol{G}_{pp}^{\ddagger}$ is a variant of $\boldsymbol{G}_{pp}^{-1}$, where we introduced a null space to match with the null space of $\boldsymbol{\Sigma}^{\mathrm{T}}\boldsymbol{\Sigma}$ (this results in a better conditioning for non-uniform meshes, which is motivated in Section 8.c.$\beta$). We see that (8.10) is the sum of (8.42) and (8.41), it is therefore well-conditioned, and it can be interpreted as discretization of the scalar Calderón identities. The dynamic kernel introduces a compact perturbation, and so we can conclude that for $k \neq 0$ the formulation of (8.10) is still well-conditioned. In addition, since any matrix of the form $\boldsymbol{A}^{\dagger}\boldsymbol{A}$ is HPD, then so is (8.10).

This derivation has, however, some caveats and due to these we provide a different derivation in Section 8.c, a derivation which is alas less intuitive and more complicated. For example, (8.27) and (8.26) were derived in [Néd01] under the assumption that the surface $\Gamma$ is smooth (this is a considerable limitation, a simple cube is not a smooth geometry). This means that for the case that $\Omega$ is a Lipschitz polyhedral domain, we cannot prove that (8.28) and (8.29) hold.

So far, we have only discussed simply connected geometries. For multiply connected ones, we note that $\boldsymbol{H}^{\mathrm{T}}\boldsymbol{T}_{\mathrm{A}}^{0}\boldsymbol{H}$ is well-conditioned since the global loops are associated with the geometry of $\Gamma$ and hence $\boldsymbol{H}_n$ and subsequently $\big(\boldsymbol{H}_m, \boldsymbol{\mathcal{T}}_{\mathrm{A}}^{\kappa}\boldsymbol{H}_n\big)_{L^2}$ remains the same when $h \longrightarrow 0$. Thus we have

$$\boldsymbol{x}^{\mathrm{T}}\boldsymbol{H}^{\mathrm{T}}\boldsymbol{T}_{\mathrm{A}}^{0}\boldsymbol{H}\boldsymbol{x} \asymp \boldsymbol{x}^{\mathrm{T}}\boldsymbol{H}^{\mathrm{T}}\boldsymbol{H}\boldsymbol{x} \asymp \boldsymbol{x}^{\mathrm{T}}\boldsymbol{x}\,, \quad \forall \boldsymbol{x} \in \mathbb{R}^{N_{\mathrm{H}}} \tag{8.45}$$

and since $\boldsymbol{H} = \boldsymbol{P}_{\Lambda\mathrm{H}}\boldsymbol{H}$, we have

$$\boldsymbol{x}^{\mathrm{T}}\boldsymbol{P}_{\Lambda\mathrm{H}}\boldsymbol{T}_{\mathrm{A}}^{0}\boldsymbol{P}_{\Lambda\mathrm{H}}\boldsymbol{x} \asymp \boldsymbol{x}^{\mathrm{T}}\boldsymbol{x}\,, \tag{8.46}$$

for all $\boldsymbol{x} \in X_{\mathrm{H}} := \left\{ \boldsymbol{x} \in \mathbb{R}^{n} \mid \exists \boldsymbol{y} \in \mathbb{R}^{N_{\mathrm{H}}} \,:\, \boldsymbol{x} = \boldsymbol{H}\boldsymbol{y} \right\}$, and thus

$$\boldsymbol{x}^{\mathrm{T}}\boldsymbol{P}_{\Lambda\mathrm{H}}\boldsymbol{T}_{\mathrm{A}}^{0}\boldsymbol{P}_{\Lambda\mathrm{H}}\boldsymbol{T}_{\mathrm{A}}^{0}\boldsymbol{P}_{\Lambda\mathrm{H}}\boldsymbol{x} \asymp \boldsymbol{x}^{\mathrm{T}}\boldsymbol{x}\,, \quad \forall \boldsymbol{x} \in X_{\mathrm{H}}\,. \tag{8.47}$$

## c) Theoretical Apparatus

The formulation for which we are going to show the well-conditioning in the static limit reads

$$\check{\boldsymbol{P}}_{\mathrm{o}}^{\dagger}\boldsymbol{T}^{\dagger}\check{\boldsymbol{P}}_{\mathrm{m}}\boldsymbol{T}\check{\boldsymbol{P}}_{\mathrm{o}}\check{\boldsymbol{\imath}} = -\check{\boldsymbol{P}}_{\mathrm{o}}^{\dagger}\boldsymbol{T}^{\dagger}\check{\boldsymbol{P}}_{\mathrm{m}}\boldsymbol{e}\,, \tag{8.48}$$

where

$$\check{\boldsymbol{P}}_{\mathrm{o}} = \boldsymbol{P}_{\Lambda\mathrm{H}}/\sqrt{k} + \mathrm{i}\boldsymbol{P}_{\mathrm{g}\Sigma}\sqrt{k}\,, \tag{8.49}$$

$$\boldsymbol{P}_{\mathrm{g}\Sigma} = \boldsymbol{\Sigma}\left(\boldsymbol{\Sigma}^{\mathrm{T}}\boldsymbol{\Sigma}\right)^{+}\boldsymbol{G}_{\tilde{\lambda}p}^{-1}\boldsymbol{\Sigma}^{\mathrm{T}}\,, \tag{8.50}$$

$$\check{\boldsymbol{P}}_{\mathrm{m}} = \check{\boldsymbol{P}}_{\mathrm{m}\Lambda}/k + \check{\boldsymbol{P}}_{\mathrm{m}\Sigma}k\,, \tag{8.51}$$

$$\check{\boldsymbol{P}}_{\mathrm{m}\Lambda} = \boldsymbol{\Lambda}\boldsymbol{G}_{\lambda\lambda}^{-1}\boldsymbol{\Lambda}^{\mathrm{T}} + \boldsymbol{P}_{\Lambda\mathrm{H}}\,, \tag{8.52}$$

$$\check{\boldsymbol{P}}_{\mathrm{m}\Sigma} = \boldsymbol{\Sigma}\left(\boldsymbol{\Sigma}^{\mathrm{T}}\boldsymbol{\Sigma}\right)^{+}\boldsymbol{G}_{p\tilde{p}}^{-1}\left(\boldsymbol{\Sigma}^{\mathrm{T}}\boldsymbol{\Sigma}\right)^{+}\boldsymbol{\Sigma}^{\mathrm{T}}\,. \tag{8.53}$$

Two differences compared with the formulation in (8.10) are noticable: (i) instead of using the norms, we make the frequency treatment explicit by using the wavenumber $k$, (ii) and we use $\boldsymbol{P}_{\mathrm{g}\Sigma}$ and not $\boldsymbol{P}_{\Sigma}$. For obtaining a rigorous statement on the conditioning, we cannot omit the Gram matrix in $\boldsymbol{P}_{\mathrm{g}\Sigma}$. In terms of the number of iterations used by a Krylov subspace method, there is only a minor difference observable between using $\boldsymbol{P}_{\mathrm{g}\Sigma}$ or $\boldsymbol{P}_{\Sigma}$. Since the usage of $\boldsymbol{P}_{\mathrm{g}\Sigma}$ is computationally more expensive, we recommend to use $\boldsymbol{P}_{\Sigma}$. If, however, the implementation of (8.48) is desired, then this can still be trivially achieved since

we have the analytic formula

$$\left[\boldsymbol{G}_{\tilde{\lambda}p}\right]_{mn} = \begin{cases} \dfrac{2}{18}\left(\dfrac{9}{2} + \displaystyle\sum_{i=1}^{3} \dfrac{1}{NoC(VoC(m,i))}\right), & \text{if } m = n\,, \\ \dfrac{2}{18}\left(\dfrac{1}{2} + \dfrac{1}{NoC(e^+)} + \dfrac{1}{NoC(e^-)}\right), & \text{if cells } m \text{ and } n\,, \\ & \text{share edge } e, \\ 0\,, & \text{otherwise,} \end{cases}$$

where the function $NoC(v)$ returns the number of cells attached to $v$th vertex of the mesh, the function $VoC(c,i)$ returns the global index of the $i$th vertex of the $c$th cell, and $e^+$ and $e^-$ are the indices of the vertices of the $e$th edge.

In order to show the well-conditioning of (8.48) in the static limit, we need to establish spectral equivalences between $\boldsymbol{W}$ and $\boldsymbol{\Delta}$ as well as $\boldsymbol{V}$ and $\widetilde{\boldsymbol{\Delta}}$. These equivalences will be established by using Rayleigh quotients. What makes it difficult is that for example $\boldsymbol{W}$ possesses a null space and if we need to form the inverse of a product of matrices where some matrices have a null space and some matrices have not, then the inverse of such a product cannot be simplified easily. To avoid the null space issue, we follow a standard approach (as we have done already in Chapter 5) by defining operators that are identical to $\mathcal{W}$ and $\Delta_\Gamma$ for mean-value free functions, but have no null space [Ste10]: we introduce the operator $\hat{\mathcal{W}} : H^{1/2} \longrightarrow H^{-1/2}$ defined by the bilinear form

$$\left(v, \hat{\mathcal{W}} w\right)_{L^2(\Gamma)} := (v, \mathcal{W} w)_{L^2(\Gamma)} + (1, w)_{L^2(\Gamma)}(1, v)_{L^2(\Gamma)} \tag{8.54}$$

for all $w, v \in H^{1/2}(\Gamma)$. We note that the unique solution $w$ of $\hat{\mathcal{W}} w = g$ is also a solution of $\mathcal{W} w = g$ when $g$ satisfies the solvability condition $\int_\Gamma g \mathrm{d}S(\boldsymbol{r}') = 0$. This can be seen when $v = 1$ in (8.54), which reduces to $(1, w)_{L^2(\Gamma)}(1, 1)_{L^2(\Gamma)} = 0$. Likewise, let $\Delta_\Gamma : H^1/\mathbb{R} \longrightarrow H^{-1}$ be the Laplace-Beltrami operator [Néd01]; we consider the $H^1$-elliptic modified Laplace-Beltrami operator $\hat{\Delta}_\Gamma$ defined by the bilinear form

$$\left(v, \hat{\Delta}_\Gamma w\right)_{L^2(\Gamma)} := (\nabla_\Gamma w, \nabla_\Gamma v)_{L^2(\Gamma)} + (1, w)_{L^2(\Gamma)}(1, v)_{L^2(\Gamma)}\,. \tag{8.55}$$

When $\lambda_i$ are used for the discretization of $\hat{\mathcal{W}}$ and $\hat{\Delta}_\Gamma$, the resulting matrices are

$$\hat{\boldsymbol{W}} = \boldsymbol{W} + \boldsymbol{G}_{\lambda\lambda}^{\mathrm{T}} \mathbf{1}_\Lambda \mathbf{1}_\Lambda^{\mathrm{T}} \boldsymbol{G}_{\lambda\lambda} \tag{8.56}$$

and

$$\hat{\boldsymbol{\Delta}} = \boldsymbol{\Delta} + \boldsymbol{G}_{\lambda\lambda}^{\mathrm{T}} \mathbf{1}_{\Lambda} \mathbf{1}_{\Lambda}^{\mathrm{T}} \boldsymbol{G}_{\lambda\lambda} \,. \tag{8.57}$$

If $\tilde{\lambda}_i$ are used for the discretization, the resulting matrices read

$$\hat{\widetilde{\boldsymbol{W}}} = \widetilde{\boldsymbol{W}} + \boldsymbol{G}_{\tilde{\lambda}\tilde{\lambda}}^{\mathrm{T}} \mathbf{1}_{\Sigma} \mathbf{1}_{\Sigma}^{\mathrm{T}} \boldsymbol{G}_{\tilde{\lambda}\tilde{\lambda}} \tag{8.58}$$

and

$$\hat{\widetilde{\boldsymbol{\Delta}}} = \widetilde{\boldsymbol{\Delta}} + \boldsymbol{G}_{\tilde{\lambda}\tilde{\lambda}}^{\mathrm{T}} \mathbf{1}_{\Sigma} \mathbf{1}_{\Sigma}^{\mathrm{T}} \boldsymbol{G}_{\tilde{\lambda}\tilde{\lambda}} \,. \tag{8.59}$$

In addition, we define

$$\check{\boldsymbol{W}} := \boldsymbol{W} + \mathbf{1}_{\Lambda} \mathbf{1}_{\Lambda}^{\mathrm{T}} h^4 \tag{8.60}$$

and

$$\check{\boldsymbol{\Delta}} := \boldsymbol{\Delta} + \mathbf{1}_{\Lambda} \mathbf{1}_{\Lambda}^{\mathrm{T}} h^4 \,. \tag{8.61}$$

In the following, we assume the spectral equivalences

$$\boldsymbol{x}^{\mathrm{T}} \hat{\boldsymbol{W}} \boldsymbol{G}_{\lambda\lambda}^{-1} \hat{\boldsymbol{W}} \boldsymbol{x} \asymp \boldsymbol{x}^{\mathrm{T}} \hat{\boldsymbol{\Delta}} \boldsymbol{x} \,, \quad \forall \boldsymbol{x} \in \mathbb{R}^{N_{\mathrm{V}}} \tag{8.62}$$

and

$$\boldsymbol{x}^{\mathrm{T}} \hat{\widetilde{\boldsymbol{W}}} \boldsymbol{G}_{\tilde{\lambda}\tilde{\lambda}}^{-1} \hat{\widetilde{\boldsymbol{W}}} \boldsymbol{x} \asymp \boldsymbol{x}^{\mathrm{T}} \hat{\widetilde{\boldsymbol{\Delta}}} \boldsymbol{x} \,, \quad \forall \boldsymbol{x} \in \mathbb{R}^{N_{\mathrm{C}}} \,. \tag{8.63}$$

As shown in the Appendix for (8.62), such a spectral equivalence can be established when we have a nested sequence of function spaces. Similarly to preconditioning strategies such as algebraic multigrid, the new formulation remains effective as can be seen from the numerical results in Section 8.d.

### $\alpha$) Vector Potential Operator

Here, we prove for the case of a simply connected geometry that

$$\boldsymbol{P}_{\Lambda} \left( \boldsymbol{T}_{\mathrm{A}}^{k} \right)^{\dagger} \boldsymbol{\Lambda} \boldsymbol{G}_{\lambda\lambda}^{-1} \boldsymbol{\Lambda}^{\mathrm{T}} \boldsymbol{T}_{\mathrm{A}}^{k} \boldsymbol{P}_{\Lambda} \tag{8.64}$$

is well-conditioned up to its null space. To this end, we first need to establish several spectral equivalences.

**Lemma 8.1.** *We have the spectral equivalences*

$$\boldsymbol{x}^{\mathrm{T}}\hat{\boldsymbol{\Delta}}\boldsymbol{x} \asymp \boldsymbol{x}^{\mathrm{T}}\check{\boldsymbol{\Delta}}\boldsymbol{x}\,, \quad \forall \boldsymbol{x} \in \mathbb{R}^{N_{\mathrm{V}}}\,, \tag{8.65}$$

*and*

$$\boldsymbol{x}^{\mathrm{T}}\hat{\boldsymbol{W}}\boldsymbol{x} \asymp \boldsymbol{x}^{\mathrm{T}}\check{\boldsymbol{W}}\boldsymbol{x}\,, \quad \forall \boldsymbol{x} \in \mathbb{R}^{N_{\mathrm{V}}}\,. \tag{8.66}$$

*Proof.* Here we prove (8.65); the proof for (8.66) follows analogously. We note that the null space of $\boldsymbol{\Delta}$ is spanned by $\mathbf{1}_\Lambda$. Furthermore, we note

$$\mathbf{1}_\Lambda^{\mathrm{T}}\boldsymbol{G}_{\lambda\lambda}^{\mathrm{T}}\mathbf{1}_\Lambda\mathbf{1}_\Lambda^{\mathrm{T}}\boldsymbol{G}_{\lambda\lambda}\mathbf{1}_\Lambda = A_\Gamma^2 \asymp 1\,, \tag{8.67}$$

where $A_\Gamma$ is the area of $\Gamma$, and $\|\mathbf{1}_\Lambda\|_2 = \sqrt{N_{\mathrm{V}}} \asymp 1/h$ and thus

$$\mathbf{1}_\Lambda^{\mathrm{T}}\mathbf{1}_\Lambda\mathbf{1}_\Lambda^{\mathrm{T}}\mathbf{1}_\Lambda h^4 \asymp 1\,. \tag{8.68}$$

First, consider that we have

$$\boldsymbol{x}^{\mathrm{T}}\mathbf{1}_\Lambda\mathbf{1}_\Lambda^{\mathrm{T}}h^4\boldsymbol{x} \lesssim \boldsymbol{x}^{\mathrm{T}}\boldsymbol{x}h^2\,, \quad \forall \boldsymbol{x} \in \mathbb{R}^{N_{\mathrm{V}}}\,, \tag{8.69}$$

and

$$\boldsymbol{x}^{\mathrm{T}}\boldsymbol{G}_{\lambda\lambda}^{\mathrm{T}}\mathbf{1}_\Lambda\mathbf{1}_\Lambda^{\mathrm{T}}\boldsymbol{G}_{\lambda\lambda}\boldsymbol{x} \lesssim \boldsymbol{x}^{\mathrm{T}}\boldsymbol{x}h^2\,, \quad \forall \boldsymbol{x} \in \mathbb{R}^{N_{\mathrm{V}}}\,, \tag{8.70}$$

where the last inequality follows from the well-known equivalence

$$\boldsymbol{x}^{\mathrm{T}}\boldsymbol{G}_{\lambda\lambda}\boldsymbol{x} \asymp \boldsymbol{x}^{\mathrm{T}}\boldsymbol{x}h^2\,, \quad \forall \boldsymbol{x} \in \mathbb{R}^{N_{\mathrm{V}}}\,, \tag{8.71}$$

and the submultiplicativity of the matrix norm, that is,

$$\left\|\boldsymbol{G}_{\lambda\lambda}^{\mathrm{T}}\mathbf{1}_\Lambda\mathbf{1}_\Lambda^{\mathrm{T}}\boldsymbol{G}_{\lambda\lambda}\right\|_2 \leq \left\|\boldsymbol{G}_{\lambda\lambda}^{\mathrm{T}}\right\|_2\left\|\mathbf{1}_\Lambda\mathbf{1}_\Lambda^{\mathrm{T}}\right\|_2\|\boldsymbol{G}_{\lambda\lambda}\|_2 \lesssim h^2\,. \tag{8.72}$$

Let $\boldsymbol{x} = \boldsymbol{x}_\parallel + \boldsymbol{x}_\perp$ be an orthogonal splitting with $\boldsymbol{x}_\parallel \in \operatorname{span}\mathbf{1}_\Lambda$. If $\boldsymbol{x}_\perp = \mathbf{0}_\Lambda$, then

$$\boldsymbol{x}^{\mathrm{T}}\hat{\boldsymbol{\Delta}}\boldsymbol{x} = \boldsymbol{x}^{\mathrm{T}}\boldsymbol{G}_{\lambda\lambda}^{\mathrm{T}}\mathbf{1}_\Lambda\mathbf{1}_\Lambda^{\mathrm{T}}\boldsymbol{G}_{\lambda\lambda}\boldsymbol{x} \asymp \boldsymbol{x}^{\mathrm{T}}\mathbf{1}_\Lambda\mathbf{1}_\Lambda^{\mathrm{T}}h^4\boldsymbol{x} = \boldsymbol{x}^{\mathrm{T}}\check{\boldsymbol{\Delta}}\boldsymbol{x} \tag{8.73}$$

due to (8.67), (8.68) (noting that $\boldsymbol{x}_\parallel$ is a multiple of $\mathbf{1}_\Lambda$). Since we have [And12a]

$$\boldsymbol{x}^{\mathrm{T}}\boldsymbol{x}h^2 \lesssim \boldsymbol{x}^{\mathrm{T}}\boldsymbol{\Delta}\boldsymbol{x} \lesssim \boldsymbol{x}^{\mathrm{T}}\boldsymbol{x}\,, \quad \forall \boldsymbol{x} \in \left(\operatorname{span}\mathbf{1}_\Lambda\right)^\perp\,, \tag{8.74}$$

we note that for $\boldsymbol{x}_\perp \neq \mathbf{0}_\Lambda$ the leading contribution $\boldsymbol{x}^\mathrm{T}\boldsymbol{\Delta}\boldsymbol{x}$ scales at least $\mathcal{O}(h^2)$ and at most $\mathcal{O}(1)$. The contribution from $\boldsymbol{x}^\mathrm{T}\boldsymbol{G}_{\lambda\lambda}^\mathrm{T}\mathbf{1}_\Lambda\mathbf{1}_\Lambda^\mathrm{T}\boldsymbol{G}_{\lambda\lambda}\boldsymbol{x}$ and $\boldsymbol{x}^\mathrm{T}\mathbf{1}_\Lambda\mathbf{1}_\Lambda^\mathrm{T}\boldsymbol{x}$ adds a positive quantity that scales at most $\mathcal{O}(h^2)$ due to (8.70), (8.71), and the fact that $\boldsymbol{G}_{\lambda\lambda}^\mathrm{T}\mathbf{1}_\Lambda\mathbf{1}_\Lambda^\mathrm{T}\boldsymbol{G}_{\lambda\lambda}$ and $\mathbf{1}_\Lambda\mathbf{1}_\Lambda^\mathrm{T}$ are positive semi-definite rank-1 matrices. Hence for $h \longrightarrow 0$, we can conclude that the eigenvalues of $\hat{\boldsymbol{\Delta}}$ and $\check{\boldsymbol{\Delta}}$ which scale with $\mathcal{O}(h^\alpha)$, $0 \leq \alpha < 2$ (and their associated eigenvectors) are spectrally identical and the eigenvalues scaling by $\mathcal{O}(h^2)$ are shifted at most by a constant factor. Thus (8.65) follows.

For (8.66), the same argumentation can be used noting that

$$\boldsymbol{x}^\mathrm{T}\boldsymbol{x}h^2 \lesssim \boldsymbol{x}^\mathrm{T}\boldsymbol{W}\boldsymbol{x} \lesssim \boldsymbol{x}^\mathrm{T}\boldsymbol{x}h\,, \quad \forall \boldsymbol{x} \in \left(\operatorname{span}\mathbf{1}_\Lambda\right)^\perp, \tag{8.75}$$

holds. □

*Remark.* This lemma will be frequently used in order to replace $\boldsymbol{G}_{\lambda\lambda}^\mathrm{T}\mathbf{1}_\Lambda\mathbf{1}_\Lambda^\mathrm{T}\boldsymbol{G}_{\lambda\lambda}$ by $\mathbf{1}_\Lambda\mathbf{1}_\Lambda^\mathrm{T}$. In essence, we are allowed to do so if the matrix accompanying $\boldsymbol{G}_{\lambda\lambda}^\mathrm{T}\mathbf{1}_\Lambda\mathbf{1}_\Lambda^\mathrm{T}\boldsymbol{G}_{\lambda\lambda}$ has a null space spanned by $\mathbf{1}_\Lambda$ and where the smallest non-zero singular value scales as $\mathcal{O}(h^s)$ with $s \leq 2$.

**Lemma 8.2.** *We have the spectral equivalences*

$$\begin{aligned}\boldsymbol{x}^\mathrm{T}\hat{\boldsymbol{W}}\boldsymbol{G}_{\lambda\lambda}^{-1}\hat{\boldsymbol{W}}\boldsymbol{x} &\asymp \boldsymbol{x}^\mathrm{T}\left(\boldsymbol{W}\boldsymbol{G}_{\lambda\lambda}^{-1}\boldsymbol{W} + \boldsymbol{G}_{\lambda\lambda}^\mathrm{T}\mathbf{1}_\Lambda\mathbf{1}_\Lambda^\mathrm{T}\boldsymbol{G}_{\lambda\lambda}\right)\boldsymbol{x} \\ &\asymp \boldsymbol{x}^\mathrm{T}\left(\boldsymbol{W}\boldsymbol{G}_{\lambda\lambda}^{-1}\boldsymbol{W} + \mathbf{1}_\Lambda\mathbf{1}_\Lambda^\mathrm{T}h^4\right)\boldsymbol{x}\,, \quad \forall \boldsymbol{x} \in \mathbb{R}^{N_\mathrm{V}}\,. \end{aligned} \tag{8.76}$$

*Proof.* We have

$$\begin{aligned}\hat{\boldsymbol{W}}\boldsymbol{G}_{\lambda\lambda}^{-1}\hat{\boldsymbol{W}} &= \left(\boldsymbol{W}\boldsymbol{G}_{\lambda\lambda}^{-1} + \boldsymbol{G}_{\lambda\lambda}\mathbf{1}_\Lambda\mathbf{1}_\Lambda^\mathrm{T}\right)\left(\boldsymbol{W} + \boldsymbol{G}_{\lambda\lambda}\mathbf{1}_\Lambda\mathbf{1}_\Lambda^\mathrm{T}\boldsymbol{G}_{\lambda\lambda}\right) \\ &= \boldsymbol{W}\boldsymbol{G}_{\lambda\lambda}^{-1}\boldsymbol{W} + \boldsymbol{G}_{\lambda\lambda}\mathbf{1}_\Lambda\mathbf{1}_\Lambda^\mathrm{T}\boldsymbol{G}_{\lambda\lambda}\mathbf{1}_\Lambda\mathbf{1}_\Lambda^\mathrm{T}\boldsymbol{G}_{\lambda\lambda} \end{aligned} \tag{8.77}$$

using $\boldsymbol{W}\mathbf{1}_\Lambda = \mathbf{0}$ and $\mathbf{1}_\Lambda^\mathrm{T}\boldsymbol{W} = \mathbf{0}^\mathrm{T}$. Since $\mathbf{1}_\Lambda^\mathrm{T}\boldsymbol{G}_{\lambda\lambda}\mathbf{1}_\Lambda = \int_\Gamma \mathrm{d}S(\boldsymbol{r}) = A_\Gamma$ is a constant, we yield

$$\boldsymbol{x}^\mathrm{T}\hat{\boldsymbol{W}}\boldsymbol{G}_{\lambda\lambda}^{-1}\hat{\boldsymbol{W}}\boldsymbol{x} \asymp \boldsymbol{x}^\mathrm{T}\left(\boldsymbol{W}\boldsymbol{G}_{\lambda\lambda}^{-1}\boldsymbol{W} + \boldsymbol{G}_{\lambda\lambda}\mathbf{1}_\Lambda\mathbf{1}_\Lambda^\mathrm{T}\boldsymbol{G}_{\lambda\lambda}\right)\boldsymbol{x}\,, \quad \forall \boldsymbol{x} \in \mathbb{R}^{N_\mathrm{V}}\,, \tag{8.78}$$

which proves the first equivalence. For the second equivalence, we have due to (8.71)

$$\boldsymbol{x}^{\mathrm{T}}\boldsymbol{W}\boldsymbol{G}_{\lambda\lambda}^{-1}\boldsymbol{W}\boldsymbol{x} \asymp \boldsymbol{x}^{\mathrm{T}}\boldsymbol{W}\boldsymbol{W}\boldsymbol{x}/h^2\,, \quad \forall \boldsymbol{x} \in \mathbb{R}^{N_{\mathrm{V}}} \tag{8.79}$$

and using (8.75), we have

$$\boldsymbol{x}^{\mathrm{T}}\boldsymbol{x}h^2 \lesssim \boldsymbol{x}^{\mathrm{T}}\boldsymbol{W}\boldsymbol{W}\boldsymbol{x}/h^2 \lesssim \boldsymbol{x}^{\mathrm{T}}\boldsymbol{x}\,, \quad \forall \boldsymbol{x} \in \left(\operatorname{span}\mathbf{1}_\Lambda\right)^{\perp}. \tag{8.80}$$

Then using the argumentation of Lemma 8.1, we obtain

$$\begin{aligned}\boldsymbol{x}^{\mathrm{T}}\Big(\boldsymbol{W}\boldsymbol{G}_{\lambda\lambda}^{-1}\boldsymbol{W} + \boldsymbol{G}_{\lambda\lambda}^{\mathrm{T}}\mathbf{1}_\Lambda\mathbf{1}_\Lambda^{\mathrm{T}}\boldsymbol{G}_{\lambda\lambda}\Big)\boldsymbol{x} \\ \asymp \boldsymbol{x}^{\mathrm{T}}\Big(\boldsymbol{W}\boldsymbol{G}_{\lambda\lambda}^{-1}\boldsymbol{W} + \mathbf{1}_\Lambda\mathbf{1}_\Lambda^{\mathrm{T}}h^4\Big)\boldsymbol{x}\,, \quad \forall \boldsymbol{x} \in \mathbb{R}^{N_{\mathrm{V}}}\,.\end{aligned} \tag{8.81}$$

□

**Lemma 8.3.** *We have the spectral equivalence*

$$\boldsymbol{x}^{\mathrm{T}}\check{\boldsymbol{\Delta}}\boldsymbol{x} \asymp \boldsymbol{x}^{\mathrm{T}}\Big(\boldsymbol{\Lambda}^{\mathrm{T}}\boldsymbol{\Lambda} + \mathbf{1}_\Lambda\mathbf{1}_\Lambda^{\mathrm{T}}h^4\Big)\boldsymbol{x}\,, \in \mathbb{R}^{N_{\mathrm{V}}}\,. \tag{8.82}$$

*Proof.* Since $\boldsymbol{\Delta} = \boldsymbol{\Lambda}^{\mathrm{T}}\boldsymbol{G}_{ff}\boldsymbol{\Lambda}$ and [And12a]

$$\boldsymbol{x}^{\mathrm{T}}\boldsymbol{G}_{ff}\boldsymbol{x} \asymp \boldsymbol{x}^{\mathrm{T}}\boldsymbol{x} \quad \forall \boldsymbol{x} \in \mathbb{R}^{N}\,, \tag{8.83}$$

we have

$$x^{\mathrm{T}}\boldsymbol{\Delta}\boldsymbol{x} \asymp \boldsymbol{x}^{\mathrm{T}}\boldsymbol{\Lambda}^{\mathrm{T}}\boldsymbol{\Lambda}\boldsymbol{x}\,, \quad \forall \boldsymbol{x} \in \mathbb{R}^{N_{\mathrm{V}}}\,. \tag{8.84}$$

Equation (8.84) remains true when we add $\mathbf{1}_\Lambda\mathbf{1}_\Lambda^{\mathrm{T}}h^4$ to the matrices since all matrices appearing are positive, semi-definite. □

**Proposition 8.1.** *We have the spectral equivalence*

$$\boldsymbol{x}^{\mathrm{T}}\boldsymbol{P}_\Lambda\Big(\boldsymbol{T}_{\mathrm{A}}^{k}\Big)^{\dagger}\boldsymbol{\Lambda}\boldsymbol{G}_{\lambda\lambda}^{-1}\boldsymbol{\Lambda}^{\mathrm{T}}\boldsymbol{T}_{\mathrm{A}}^{k}\boldsymbol{P}_\Lambda\boldsymbol{x} \asymp \boldsymbol{x}^{\mathrm{T}}\boldsymbol{P}_\Lambda\boldsymbol{x}\,, \quad \forall \boldsymbol{x} \in \mathbb{R}^{N}\,. \tag{8.85}$$

*Proof.* By combining the previous lemmas we can establish

$$\boldsymbol{x}^{\mathrm{T}}\Big(\boldsymbol{W}\boldsymbol{G}_{\lambda\lambda}^{-1}\boldsymbol{W} + \mathbf{1}_\Lambda\mathbf{1}_\Lambda^{\mathrm{T}}h^4\Big)\boldsymbol{x} \asymp \boldsymbol{x}^{\mathrm{T}}\Big(\boldsymbol{\Lambda}^{\mathrm{T}}\boldsymbol{\Lambda} + \mathbf{1}_\Lambda\mathbf{1}_\Lambda^{\mathrm{T}}h^4\Big)\boldsymbol{x}\,, \quad \forall \boldsymbol{x} \in \mathbb{R}^{N_{\mathrm{V}}}\,, \tag{8.86}$$

that is in more detail, we have

$$\begin{aligned}
\boldsymbol{x}^{\mathrm{T}}\Big(\boldsymbol{W}\boldsymbol{G}_{\lambda\lambda}^{-1}\boldsymbol{W} + \mathbf{1}_\Lambda\mathbf{1}_\Lambda^{\mathrm{T}}h^4\Big)\boldsymbol{x} & \\
&\overset{\text{Lemma 8.2}}{\asymp} \boldsymbol{x}^{\mathrm{T}}\hat{\boldsymbol{W}}\boldsymbol{G}_{\lambda\lambda}^{-1}\hat{\boldsymbol{W}}\boldsymbol{x} \\
&\overset{\text{Proposition A.1}}{\asymp} \boldsymbol{x}^{\mathrm{T}}\hat{\boldsymbol{\Delta}}\boldsymbol{x} \\
&\overset{\text{Lemma 8.1}}{\asymp} \boldsymbol{x}^{\mathrm{T}}\check{\boldsymbol{\Delta}}\boldsymbol{x} \\
&\overset{\text{Lemma 8.3}}{\asymp} \boldsymbol{x}^{\mathrm{T}}\Big(\boldsymbol{\Lambda}^{\mathrm{T}}\boldsymbol{\Lambda} + \mathbf{1}_\Lambda\mathbf{1}_\Lambda^{\mathrm{T}}h^4\Big)\boldsymbol{x}\,, \quad \forall \boldsymbol{x} \in \mathbb{R}^{N_{\mathrm{V}}}\,. \qquad (8.87)
\end{aligned}$$

We apply the substitution $\boldsymbol{x} = (\boldsymbol{\Lambda}^{\mathrm{T}}\boldsymbol{\Lambda})^{+}\boldsymbol{\Lambda}^{\mathrm{T}}\boldsymbol{y}$ and obtain

$$\boldsymbol{y}^{\mathrm{T}}\boldsymbol{\Lambda}\Big(\boldsymbol{\Lambda}^{\mathrm{T}}\boldsymbol{\Lambda}\Big)^{+}\boldsymbol{W}\boldsymbol{G}_{\lambda\lambda}^{-1}\boldsymbol{W}\Big(\boldsymbol{\Lambda}^{\mathrm{T}}\boldsymbol{\Lambda}\Big)^{+}\boldsymbol{\Lambda}^{\mathrm{T}}\boldsymbol{y} \asymp \boldsymbol{y}^{\mathrm{T}}\boldsymbol{P}_\Lambda\boldsymbol{y}\,, \quad \forall \boldsymbol{y} \in \mathbb{R}^{N}\,, \qquad (8.88)$$

where $\boldsymbol{P}_\Lambda \equiv \boldsymbol{\Lambda}(\boldsymbol{\Lambda}^{\mathrm{T}}\boldsymbol{\Lambda})^{+}\boldsymbol{\Lambda}^{\mathrm{T}}$. We note that $\boldsymbol{\Lambda}^{\mathrm{T}}\boldsymbol{T}_{\mathrm{A}}^{0}\boldsymbol{\Lambda} = \boldsymbol{W} = \boldsymbol{W}^{\dagger}$; for $k \neq 0$, the dynamic kernel introduces a compact perturbation, which does not affect the $h$-conditioning, and we can freely choose $\boldsymbol{T}_{\mathrm{A}}^{\dagger}$ instead of $\boldsymbol{T}_{\mathrm{A}}$ resulting in (8.85). □

*Remark.* The matrix $\boldsymbol{P}_\Lambda(\boldsymbol{T}_{\mathrm{A}}^{k})^{\dagger}\boldsymbol{\Lambda}\boldsymbol{G}_{\lambda\lambda}^{-1}\boldsymbol{\Lambda}^{\mathrm{T}}\boldsymbol{T}_{\mathrm{A}}^{k}\boldsymbol{P}_\Lambda$ is Hermitian and positive semi-definite, which can be seen by considering

$$\boldsymbol{P}_\Lambda\Big(\boldsymbol{T}_{\mathrm{A}}^{k}\Big)^{\dagger}\boldsymbol{\Lambda}\boldsymbol{G}_{\lambda\lambda}^{-1}\boldsymbol{\Lambda}^{\mathrm{T}}\boldsymbol{T}_{\mathrm{A}}^{k}\boldsymbol{P}_\Lambda = \Big(\boldsymbol{G}_{\lambda\lambda}^{-1/2}\boldsymbol{\Lambda}^{\mathrm{T}}\boldsymbol{T}_{\mathrm{A}}^{k}\boldsymbol{P}_\Lambda\Big)^{\dagger}\boldsymbol{G}_{\lambda\lambda}^{-1/2}\boldsymbol{\Lambda}^{\mathrm{T}}\boldsymbol{T}_{\mathrm{A}}^{k}\boldsymbol{P}_\Lambda\,. \qquad (8.89)$$

Now, we are ready to consider the case that $\Gamma$ is multiply connected: we have to establish that

$$\boldsymbol{P}_{\Lambda\mathrm{H}}\Big(\boldsymbol{T}_{\mathrm{A}}^{k}\Big)^{\dagger}\Big(\boldsymbol{\Lambda}\boldsymbol{G}_{\lambda\lambda}^{-1}\boldsymbol{\Lambda}^{\mathrm{T}} + \boldsymbol{P}_{\Lambda\mathrm{H}}\Big)\boldsymbol{T}_{\mathrm{A}}^{k}\boldsymbol{P}_{\Lambda\mathrm{H}} \qquad (8.90)$$

is well-conditioned up to its null space. For deriving this result some preliminary considerations are necessary, and again, we start with considering the static limit $k \longrightarrow 0$.

**Proposition 8.2.** *We have the spectral equivalence*

$$\boldsymbol{x}^{\mathrm{T}}\Big(\check{\boldsymbol{\Lambda}}^{\mathrm{T}}\check{\boldsymbol{\Lambda}}\Big)^{-1/4}\check{\boldsymbol{\Lambda}}^{\mathrm{T}}\boldsymbol{T}_{\mathrm{A}}^{0}\check{\boldsymbol{\Lambda}}\Big(\check{\boldsymbol{\Lambda}}^{\mathrm{T}}\check{\boldsymbol{\Lambda}}\Big)^{-1/4}\boldsymbol{x} \asymp \boldsymbol{x}^{\mathrm{T}}\boldsymbol{x}\,, \quad \forall \boldsymbol{x} \in \big(\operatorname{span}\mathbf{1}_\Lambda\big)^{\perp}\,, \qquad (8.91)$$

*where we used the substitution* $\check{\boldsymbol{\Lambda}} := \boldsymbol{\Lambda}/h$.

*Proof.* Proposition 8.1 states that

$$\boldsymbol{x}^{\mathrm{T}}\boldsymbol{P}_{\Lambda}\left(\boldsymbol{T}_{\mathrm{A}}^{0}\right)^{\dagger}\boldsymbol{\Lambda}\boldsymbol{G}_{\lambda\lambda}^{-1}\boldsymbol{\Lambda}^{\mathrm{T}}\boldsymbol{T}_{\mathrm{A}}^{0}\boldsymbol{P}_{\Lambda}\boldsymbol{x} \asymp \boldsymbol{x}^{\mathrm{T}}\boldsymbol{P}_{\Lambda}\boldsymbol{x}\,, \quad \forall \boldsymbol{x} \in X_{\Lambda} \tag{8.92}$$

with

$$X_{\Lambda} := \left\{ \boldsymbol{x} \in \mathbb{R}^{n} \mid \boldsymbol{x} = \boldsymbol{P}_{\Lambda}\boldsymbol{x} \right\} \tag{8.93}$$

holds. We apply the substitution $\boldsymbol{y} = (\boldsymbol{\Lambda}^{\mathrm{T}}\boldsymbol{\Lambda})^{-1/2}\boldsymbol{\Lambda}^{\mathrm{T}}\boldsymbol{x}$ noting that $(\boldsymbol{\Lambda}^{\mathrm{T}}\boldsymbol{\Lambda})^{-1/2}\boldsymbol{\Lambda}^{\mathrm{T}} : X_{\Lambda} \longrightarrow \left(\operatorname{span}\mathbf{1}_{\Lambda}\right)^{\perp}$ is one-to-one and onto and that $\boldsymbol{P}_{\Lambda} = \boldsymbol{\Lambda}(\boldsymbol{\Lambda}^{\mathrm{T}}\boldsymbol{\Lambda})^{-1/2}(\boldsymbol{\Lambda}^{\mathrm{T}}\boldsymbol{\Lambda})^{-1/2}\boldsymbol{\Lambda}^{\mathrm{T}}$ so we obtain

$$\begin{aligned}\boldsymbol{y}^{\mathrm{T}}\left(\boldsymbol{\Lambda}^{\mathrm{T}}\boldsymbol{\Lambda}\right)^{-1/2}\boldsymbol{\Lambda}^{\mathrm{T}}\left(\boldsymbol{T}_{\mathrm{A}}^{k}\right)^{\dagger}\boldsymbol{\Lambda}\boldsymbol{G}_{\lambda\lambda}^{-1}\boldsymbol{\Lambda}^{\mathrm{T}}\boldsymbol{T}_{\mathrm{A}}^{k}\boldsymbol{\Lambda}\left(\boldsymbol{\Lambda}^{\mathrm{T}}\boldsymbol{\Lambda}\right)^{-1/2}\boldsymbol{y} \\ \asymp \boldsymbol{y}^{\mathrm{T}}\boldsymbol{y}\,, \quad \forall \boldsymbol{y} \in \left(\operatorname{span}\mathbf{1}_{\Lambda}\right)^{\perp}.\end{aligned} \tag{8.94}$$

By using (8.71), we obtain

$$\begin{aligned}\boldsymbol{x}^{\mathrm{T}}\left(\boldsymbol{\Lambda}^{\mathrm{T}}\boldsymbol{\Lambda}\right)^{-1/2}\boldsymbol{\Lambda}^{\mathrm{T}}\boldsymbol{T}_{\mathrm{A}}^{0}\boldsymbol{\Lambda}\left(h^{-2}\right)\boldsymbol{\Lambda}^{\mathrm{T}}\boldsymbol{T}_{\mathrm{A}}^{0}\boldsymbol{\Lambda}\left(\boldsymbol{\Lambda}^{\mathrm{T}}\boldsymbol{\Lambda}\right)^{-1/2}\boldsymbol{x} \\ \asymp \boldsymbol{x}^{\mathrm{T}}\boldsymbol{x}\,, \quad \forall \boldsymbol{x} \in \left(\operatorname{span}\mathbf{1}_{\Lambda}\right)^{\perp}.\end{aligned} \tag{8.95}$$

We define $\check{\boldsymbol{\Lambda}} = \boldsymbol{\Lambda}/h$ noting that

$$\begin{aligned}\left(\boldsymbol{\Lambda}^{\mathrm{T}}\boldsymbol{\Lambda}\right)^{-1/2}\boldsymbol{\Lambda}^{\mathrm{T}}\boldsymbol{T}_{\mathrm{A}}^{0}\,\boldsymbol{\Lambda}\left(h^{-2}\right)\boldsymbol{\Lambda}^{\mathrm{T}}\boldsymbol{T}_{\mathrm{A}}^{0}\boldsymbol{\Lambda}\left(\boldsymbol{\Lambda}^{\mathrm{T}}\boldsymbol{\Lambda}\right)^{-1/2} \\ = \left(\check{\boldsymbol{\Lambda}}^{\mathrm{T}}\check{\boldsymbol{\Lambda}}\right)^{-1/2}\check{\boldsymbol{\Lambda}}^{\mathrm{T}}\left(\boldsymbol{T}_{\mathrm{A}}^{0}\right)^{\dagger}\check{\boldsymbol{\Lambda}}\check{\boldsymbol{\Lambda}}^{\mathrm{T}}\boldsymbol{T}_{\mathrm{A}}^{0}\check{\boldsymbol{\Lambda}}\left(\check{\boldsymbol{\Lambda}}^{\mathrm{T}}\check{\boldsymbol{\Lambda}}\right)^{-1/2}.\end{aligned} \tag{8.96}$$

Furthermore, we notice that the singular values of

$$\check{\boldsymbol{\Lambda}}^{\mathrm{T}}\boldsymbol{T}_{\mathrm{A}}^{0}\check{\boldsymbol{\Lambda}}\left(\check{\boldsymbol{\Lambda}}^{\mathrm{T}}\check{\boldsymbol{\Lambda}}\right)^{-1/2} \tag{8.97}$$

are by definition of the SVD the square roots of the singular values of

$$\left(\check{\boldsymbol{\Lambda}}^{\mathrm{T}}\check{\boldsymbol{\Lambda}}\right)^{-1/2}\check{\boldsymbol{\Lambda}}^{\mathrm{T}}\left(\boldsymbol{T}_{\mathrm{A}}^{0}\right)^{\dagger}\check{\boldsymbol{\Lambda}}\check{\boldsymbol{\Lambda}}^{\mathrm{T}}\boldsymbol{T}_{\mathrm{A}}^{0}\check{\boldsymbol{\Lambda}}\left(\check{\boldsymbol{\Lambda}}^{\mathrm{T}}\check{\boldsymbol{\Lambda}}\right)^{-1/2}, \tag{8.98}$$

which implies that the matrix in (8.97) is well-conditioned.

The absolute value of the largest eigenvalue can always be bounded from above by the largest singular value and the smallest eigenvalue can always be bounded from below by the smallest singular value. The second half of this statement is not entirely helpful since the smallest eigenvalue and singular value are both zero. However, since the left null space and the right null space of (8.97) are identical, we can show that the smallest non-zero absolute eigenvalue $\nu_{\min}$ can be bounded from below by the smallest non-zero singular value $s_{\min}$ .

To see this, let $\boldsymbol{v}$ be the unit eigenvector associated with $\nu_{\min}$ and we use the abbreviation $\boldsymbol{A} = \breve{\boldsymbol{\Lambda}}^{\mathrm{T}}\boldsymbol{T}_{\mathrm{A}}^{0}\breve{\boldsymbol{\Lambda}}(\breve{\boldsymbol{\Lambda}}^{\mathrm{T}}\breve{\boldsymbol{\Lambda}})^{-1/2}$. We have

$$|\nu_{\min}|^2 = \boldsymbol{v}^{\mathrm{T}}\boldsymbol{A}^{\mathrm{T}}\boldsymbol{A}\boldsymbol{v} \geq \min_{\|\boldsymbol{x}\|_2=1 \wedge \boldsymbol{x}\perp\boldsymbol{1}_{\Lambda}} \boldsymbol{x}^{\mathrm{T}}\boldsymbol{A}^{\mathrm{T}}\boldsymbol{A}\boldsymbol{x} = s_{\min}^2 \tag{8.99}$$

following the properties of the SVD noting that $\|\boldsymbol{v}\|_2 = 1$ and $\boldsymbol{v} \perp \boldsymbol{1}_{\Lambda}$.

Similar matrices have the same eigenvalues and thus $\boldsymbol{A}$ and $(\boldsymbol{\Lambda}^{\mathrm{T}}\boldsymbol{\Lambda})^{-1/4}\boldsymbol{A}(\boldsymbol{\Lambda}^{\mathrm{T}}\boldsymbol{\Lambda})^{1/4}$ have the same eigenvalues. Since

$$\left(\breve{\boldsymbol{\Lambda}}^{\mathrm{T}}\breve{\boldsymbol{\Lambda}}\right)^{-1/4}\boldsymbol{A}\left(\breve{\boldsymbol{\Lambda}}^{\mathrm{T}}\breve{\boldsymbol{\Lambda}}\right)^{1/4} = \left(\breve{\boldsymbol{\Lambda}}^{\mathrm{T}}\breve{\boldsymbol{\Lambda}}\right)^{-1/4}\breve{\boldsymbol{\Lambda}}^{\mathrm{T}}\boldsymbol{T}_{\mathrm{A}}^{0}\breve{\boldsymbol{\Lambda}}\left(\breve{\boldsymbol{\Lambda}}^{\mathrm{T}}\breve{\boldsymbol{\Lambda}}\right)^{-1/4} \tag{8.100}$$

is a symmetric, positive semidefinite matrix, the eigenvalues and singular values coincide and thus

$$\left(\breve{\boldsymbol{\Lambda}}^{\mathrm{T}}\breve{\boldsymbol{\Lambda}}\right)^{-1/4}\breve{\boldsymbol{\Lambda}}^{\mathrm{T}}\boldsymbol{T}_{\mathrm{A}}^{0}\breve{\boldsymbol{\Lambda}}\left(\breve{\boldsymbol{\Lambda}}^{\mathrm{T}}\breve{\boldsymbol{\Lambda}}\right)^{-1/4} \tag{8.101}$$

is well-conditioned up to its null space. □

Given Proposition 8.2, we can conclude that if the matrix $\breve{\boldsymbol{\Lambda}}(\breve{\boldsymbol{\Lambda}}^{\mathrm{T}}\breve{\boldsymbol{\Lambda}})^{-1/4}$ is used as solenoidal basis, we obtain a well-conditioned matrix with bounded norm. Thus if we were to pursue a classical *explicit* quasi-Helmholtz decomposition scheme, we could use the basis $\left[\breve{\boldsymbol{\Lambda}}(\breve{\boldsymbol{\Lambda}}^{\mathrm{T}}\breve{\boldsymbol{\Lambda}})^{-1/4} \quad \boldsymbol{H}\right]$ as preconditioner for $\boldsymbol{T}_{\mathrm{A}}$ on multiply connected geometries. Using (8.45), it follows that the matrix

$$\begin{bmatrix}\left(\breve{\boldsymbol{\Lambda}}^{\mathrm{T}}\breve{\boldsymbol{\Lambda}}\right)^{-1/4}\breve{\boldsymbol{\Lambda}}^{\mathrm{T}} \\ \boldsymbol{H}^{\mathrm{T}}\end{bmatrix}\boldsymbol{T}_{\mathrm{A}}^{0}\left[\breve{\boldsymbol{\Lambda}}\left(\breve{\boldsymbol{\Lambda}}^{\mathrm{T}}\breve{\boldsymbol{\Lambda}}\right)^{-1/4} \quad \boldsymbol{H}\right] \tag{8.102}$$

is well-conditioned in $h$ up to the null space of the loop functions since the basis transformation matrix has full rank (up to the null space of the loop functions) and since the blocks on the main diagonal are well-conditioned and all blocks are

bounded: the boundedness of $\boldsymbol{H}^{\mathrm{T}}\boldsymbol{T}_{\mathrm{A}}^{0}\check{\boldsymbol{\lambda}}(\check{\boldsymbol{\lambda}}^{\mathrm{T}}\check{\boldsymbol{\lambda}})^{-1/4}$ and of $(\check{\boldsymbol{\lambda}}^{\mathrm{T}}\check{\boldsymbol{\lambda}})^{-1/4}\check{\boldsymbol{\lambda}}^{\mathrm{T}}\boldsymbol{T}_{\mathrm{A}}^{0}\boldsymbol{H}$ follows from the boundedness of the blocks on the main diagonal.

Now, it remains to return from the explicit quasi-Helmholtz decomposition of (8.102) to the new formulation in (8.90).

**Proposition 8.3.** *We have the spectral equivalence*

$$\boldsymbol{x}^{\mathrm{T}}\boldsymbol{P}_{\Lambda\mathrm{H}}\left(\boldsymbol{T}_{\mathrm{A}}^{k}\right)^{\dagger}\left(\boldsymbol{\Lambda}\boldsymbol{G}_{\lambda\lambda}^{-1}\boldsymbol{\Lambda}^{\mathrm{T}}+\boldsymbol{P}_{\Lambda\mathrm{H}}\right)\boldsymbol{T}_{\mathrm{A}}^{k}\boldsymbol{P}_{\Lambda\mathrm{H}}\boldsymbol{x}\asymp\boldsymbol{x}^{\mathrm{T}}\boldsymbol{P}_{\Lambda\mathrm{H}}\boldsymbol{x}\,,\quad\forall\boldsymbol{x}\in\mathbb{R}^{N}\,. \tag{8.103}$$

*Proof.* We define

$$\boldsymbol{T}_{\check{\lambda}H}\;:=\begin{bmatrix}\check{\boldsymbol{\Lambda}}^{\mathrm{T}}\\ \boldsymbol{H}^{\mathrm{T}}\end{bmatrix}\boldsymbol{T}_{\mathrm{A}}^{0}\begin{bmatrix}\check{\boldsymbol{\Lambda}} & \boldsymbol{H}\end{bmatrix}, \tag{8.104}$$

$$\boldsymbol{Q}_{\check{\lambda}H}\;:=\begin{bmatrix}\left(\check{\boldsymbol{\Lambda}}^{\mathrm{T}}\check{\boldsymbol{\Lambda}}\right)^{-1/4} & \\ & \boldsymbol{I}\end{bmatrix}, \tag{8.105}$$

and observe

$$\begin{bmatrix}\left(\check{\boldsymbol{\Lambda}}^{\mathrm{T}}\check{\boldsymbol{\Lambda}}\right)^{-1/4}\check{\boldsymbol{\Lambda}}^{\mathrm{T}}\\ \boldsymbol{H}^{\mathrm{T}}\end{bmatrix}\boldsymbol{T}_{\mathrm{A}}^{0}\begin{bmatrix}\check{\boldsymbol{\Lambda}}\left(\check{\boldsymbol{\Lambda}}^{\mathrm{T}}\check{\boldsymbol{\Lambda}}\right)^{-1/4} & \boldsymbol{H}\end{bmatrix}=\boldsymbol{Q}_{\check{\lambda}H}\boldsymbol{T}_{\check{\lambda}H}\boldsymbol{Q}_{\check{\lambda}H}\,. \tag{8.106}$$

In other words, we can interpret $\boldsymbol{Q}_{\check{\lambda}H}$ as a preconditioner for the standard loop/-global loop discretized $\boldsymbol{T}_{\check{\lambda}H}$.

We note that $\boldsymbol{T}_{\check{\lambda}H}$ and $\boldsymbol{Q}_{\check{\lambda}H}$ are symmetric matrices and that they have the same null space (i.e., the null space due to the linear dependency of the loop functions). Summarizing, we have the Rayleigh quotient

$$\boldsymbol{x}^{\mathrm{T}}\boldsymbol{Q}_{\check{\lambda}H}\boldsymbol{T}_{\check{\lambda}H}\boldsymbol{Q}_{\check{\lambda}H}\boldsymbol{x}\asymp\boldsymbol{x}^{\mathrm{T}}\boldsymbol{x}\,,\quad\forall\boldsymbol{x}\in\left(\operatorname{null}\boldsymbol{Q}_{\check{\lambda}H}\right)^{\perp}. \tag{8.107}$$

By using the substitution $\boldsymbol{y}=\boldsymbol{Q}_{\check{\lambda}H}\boldsymbol{x}$, we obtain

$$\boldsymbol{y}^{\mathrm{T}}\boldsymbol{T}_{\check{\lambda}H}\boldsymbol{y}\asymp\boldsymbol{y}^{\mathrm{T}}\boldsymbol{Q}_{\check{\lambda}H}^{-2}\boldsymbol{y}\,,\quad\forall\boldsymbol{y}\in\left(\operatorname{null}\boldsymbol{Q}_{\check{\lambda}H}\right)^{\perp} \tag{8.108}$$

from which immediately

$$\boldsymbol{y}^{\mathrm{T}}\boldsymbol{T}_{\check{\lambda}H}^{2}\boldsymbol{y}\asymp\boldsymbol{y}^{\mathrm{T}}\boldsymbol{Q}_{\check{\lambda}H}^{-4}\boldsymbol{y}\,,\quad\forall\boldsymbol{y}\in\left(\operatorname{null}\boldsymbol{Q}_{\check{\lambda}H}\right)^{\perp} \tag{8.109}$$

and thus

$$\boldsymbol{x}^{\mathrm{T}}\boldsymbol{Q}_{\breve{\boldsymbol{\Lambda}}\boldsymbol{H}}^{2}\boldsymbol{T}_{\breve{\boldsymbol{\Lambda}}\boldsymbol{H}}^{2}\boldsymbol{Q}_{\breve{\boldsymbol{\Lambda}}\boldsymbol{H}}^{2}\boldsymbol{x} \asymp \boldsymbol{x}^{\mathrm{T}}\boldsymbol{x}\,, \quad \forall \boldsymbol{x} \in \left(\operatorname{null}\boldsymbol{Q}_{\breve{\boldsymbol{\Lambda}}\boldsymbol{H}}\right)^{\perp} \tag{8.110}$$

follows.

Moreover, we notice that

$$\begin{aligned}\boldsymbol{T}_{\breve{\boldsymbol{\Lambda}}\boldsymbol{H}}^{2} &= \begin{bmatrix}\breve{\boldsymbol{\Lambda}}^{\mathrm{T}}\\ \boldsymbol{H}^{\mathrm{T}}\end{bmatrix}\boldsymbol{T}_{\mathrm{A}}^{0}\begin{bmatrix}\breve{\boldsymbol{\Lambda}} & \boldsymbol{H}\end{bmatrix}\begin{bmatrix}\breve{\boldsymbol{\Lambda}}^{\mathrm{T}}\\ \boldsymbol{H}^{\mathrm{T}}\end{bmatrix}\boldsymbol{T}_{\mathrm{A}}^{0}\begin{bmatrix}\breve{\boldsymbol{\Lambda}} & \boldsymbol{H}\end{bmatrix}\\ &= \begin{bmatrix}\breve{\boldsymbol{\Lambda}}^{\mathrm{T}}\\ \boldsymbol{H}^{\mathrm{T}}\end{bmatrix}\boldsymbol{T}_{\mathrm{A}}^{0}\left(\breve{\boldsymbol{\Lambda}}\breve{\boldsymbol{\Lambda}}^{\mathrm{T}} + \boldsymbol{H}\boldsymbol{H}^{\mathrm{T}}\right)\boldsymbol{T}_{\mathrm{A}}^{0}\begin{bmatrix}\breve{\boldsymbol{\Lambda}} & \boldsymbol{H}\end{bmatrix}\end{aligned} \tag{8.111}$$

using that $\boldsymbol{H}^{\mathrm{T}}\breve{\boldsymbol{\Lambda}} = \boldsymbol{0}$.

The global loop transformation matrix is not uniquely defined, but a possible transformation matrix can always be constructed from $\boldsymbol{P}_{\mathrm{H}} := \boldsymbol{I} - \boldsymbol{P}_{\Lambda} - \boldsymbol{P}_{\Sigma}$ by using its SVD so that $\boldsymbol{H}$ is the column space of it. Hence, we can always obtain

$$\boldsymbol{P}_{\mathrm{H}} = \boldsymbol{H}\boldsymbol{H}^{\mathrm{T}}\,. \tag{8.112}$$

By using (8.111) and (8.112), we have

$$\begin{aligned}&\boldsymbol{Q}_{\breve{\boldsymbol{\Lambda}}\boldsymbol{H}}^{2}\boldsymbol{T}_{\breve{\boldsymbol{\Lambda}}\boldsymbol{H}}^{2}\boldsymbol{Q}_{\breve{\boldsymbol{\Lambda}}\boldsymbol{H}}^{2}\\ &\qquad= \begin{bmatrix}\left(\breve{\boldsymbol{\Lambda}}^{\mathrm{T}}\breve{\boldsymbol{\Lambda}}\right)^{-1/2}\breve{\boldsymbol{\Lambda}}^{\mathrm{T}}\\ \boldsymbol{H}^{\mathrm{T}}\end{bmatrix}\boldsymbol{T}_{\mathrm{A}}^{0}\left(\breve{\boldsymbol{\Lambda}}\breve{\boldsymbol{\Lambda}}^{\mathrm{T}} + \boldsymbol{P}_{\mathrm{H}}\right)\boldsymbol{T}_{\mathrm{A}}^{0}\begin{bmatrix}\breve{\boldsymbol{\Lambda}}\left(\breve{\boldsymbol{\Lambda}}^{\mathrm{T}}\breve{\boldsymbol{\Lambda}}\right)^{-1/2} & \boldsymbol{H}\end{bmatrix}.\end{aligned} \tag{8.113}$$

We also note that the transformation $\begin{bmatrix}\breve{\boldsymbol{\Lambda}}(\breve{\boldsymbol{\Lambda}}^{\mathrm{T}}\breve{\boldsymbol{\Lambda}})^{-1/2} & \boldsymbol{H}\end{bmatrix}$ is well-conditioned, in fact,

$$\begin{bmatrix}\breve{\boldsymbol{\Lambda}}\left(\breve{\boldsymbol{\Lambda}}^{\mathrm{T}}\breve{\boldsymbol{\Lambda}}\right)^{-1/2} & \boldsymbol{H}\end{bmatrix}\begin{bmatrix}\left(\breve{\boldsymbol{\Lambda}}^{\mathrm{T}}\breve{\boldsymbol{\Lambda}}\right)^{-1/2}\breve{\boldsymbol{\Lambda}}^{\mathrm{T}}\\ \boldsymbol{H}^{\mathrm{T}}\end{bmatrix} = \boldsymbol{P}_{\Lambda\mathrm{H}}\,. \tag{8.114}$$

Thus we have

$$\begin{aligned}&\boldsymbol{x}^{\mathrm{T}}\begin{bmatrix}\breve{\boldsymbol{\Lambda}}\left(\breve{\boldsymbol{\Lambda}}^{\mathrm{T}}\breve{\boldsymbol{\Lambda}}\right)^{-1/2} & \boldsymbol{H}\end{bmatrix}\boldsymbol{Q}_{\breve{\boldsymbol{\Lambda}}\boldsymbol{H}}^{2}\boldsymbol{T}_{\breve{\boldsymbol{\Lambda}}\boldsymbol{H}}^{2}\boldsymbol{Q}_{\breve{\boldsymbol{\Lambda}}\boldsymbol{H}}^{2}\begin{bmatrix}\left(\breve{\boldsymbol{\Lambda}}^{\mathrm{T}}\breve{\boldsymbol{\Lambda}}\right)^{-1/2}\breve{\boldsymbol{\Lambda}}^{\mathrm{T}}\\ \boldsymbol{H}^{\mathrm{T}}\end{bmatrix}\boldsymbol{x}^{\mathrm{T}}\\ &\qquad\qquad\asymp \boldsymbol{x}^{\mathrm{T}}\boldsymbol{P}_{\Lambda\mathrm{H}}\boldsymbol{x}\,, \quad \forall \boldsymbol{x} \in \mathbb{R}^{N}\,,\end{aligned} \tag{8.115}$$

where we note that the preconditioned system matrix can be expressed as

$$\left[\check{\boldsymbol{\lambda}}\left(\check{\boldsymbol{\lambda}}^{\mathrm{T}}\check{\boldsymbol{\lambda}}\right)^{-1/2} \quad \boldsymbol{H}\right]\boldsymbol{Q}_{\check{\lambda}\boldsymbol{H}}^{2}\boldsymbol{T}_{\check{\lambda}\boldsymbol{H}}^{2}\boldsymbol{Q}_{\check{\lambda}\boldsymbol{H}}^{2}\begin{bmatrix}\left(\check{\boldsymbol{\lambda}}^{\mathrm{T}}\check{\boldsymbol{\lambda}}\right)^{-1/2}\check{\boldsymbol{\lambda}}^{\mathrm{T}}\\ \boldsymbol{H}^{\mathrm{T}}\end{bmatrix}\boldsymbol{x}^{\mathrm{T}} = \boldsymbol{P}_{\Lambda\mathrm{H}}\boldsymbol{T}_{\mathrm{A}}^{0}\left(\check{\boldsymbol{\lambda}}\check{\boldsymbol{\lambda}}^{\mathrm{T}}+\boldsymbol{P}_{\mathrm{H}}\right)\boldsymbol{T}_{\mathrm{A}}^{0}\boldsymbol{P}_{\Lambda\mathrm{H}}\,. \tag{8.116}$$

We can replace $\boldsymbol{P}_{\mathrm{H}}$ by $\boldsymbol{P}_{\Lambda\mathrm{H}}$ since the matrix $\boldsymbol{P}_{\Lambda\mathrm{H}}\boldsymbol{T}_{\mathrm{A}}^{0}\boldsymbol{P}_{\Lambda}\boldsymbol{T}_{\mathrm{A}}^{0}\boldsymbol{P}_{\Lambda\mathrm{H}}$ is symmetric, positive definite and

$$\left\|\boldsymbol{P}_{\Lambda\mathrm{H}}\boldsymbol{T}_{\mathrm{A}}^{0}\boldsymbol{P}_{\Lambda}\boldsymbol{T}_{\mathrm{A}}^{0}\boldsymbol{P}_{\Lambda\mathrm{H}}\right\|_{2} \lesssim \|\boldsymbol{P}_{\Lambda\mathrm{H}}\|_{2}\left\|\boldsymbol{T}_{\mathrm{A}}^{0}\right\|_{2}\|\boldsymbol{P}_{\Lambda}\|_{2}\left\|\boldsymbol{T}_{\mathrm{A}}^{0}\right\|_{2}\|\boldsymbol{P}_{\Lambda\mathrm{H}}\|_{2} \lesssim 1 \tag{8.117}$$

is bounded, where $\left\|\boldsymbol{T}_{\mathrm{A}}^{0}\right\|_{2} \lesssim 1$ follows from the compactness of $\mathcal{T}_{\mathrm{A}}$. Likewise, the dynamic kernel is a compact perturbation and by substituting back from $\check{\boldsymbol{\lambda}}$ to $\boldsymbol{\Lambda}$ and $\boldsymbol{G}_{\lambda\lambda}^{-1}$, we obtain that the matrix

$$\boldsymbol{P}_{\Lambda\mathrm{H}}\left(\boldsymbol{T}_{\mathrm{A}}^{k}\right)^{\dagger}\left(\boldsymbol{\Lambda}\boldsymbol{G}_{\lambda\lambda}^{-1}\boldsymbol{\Lambda}^{\mathrm{T}}+\boldsymbol{P}_{\Lambda\mathrm{H}}\right)\boldsymbol{T}_{\mathrm{A}}^{k}\boldsymbol{P}_{\Lambda\mathrm{H}}\boldsymbol{x} \asymp \boldsymbol{x}^{\mathrm{T}}\boldsymbol{P}_{\Lambda\mathrm{H}}\boldsymbol{x}\,,\ \boldsymbol{x}\in\mathbb{R}^{N} \tag{8.118}$$

is well-conditioned (up to its null space). □

## $\beta$) Scalar Potential Operator

In this section, we are going to establish that the matrix

$$\boldsymbol{P}_{\mathrm{g}\Sigma}^{\mathrm{T}}\left(\boldsymbol{T}_{\Phi}^{k}\right)^{\dagger}\check{\boldsymbol{P}}_{\mathrm{m}\Sigma}\boldsymbol{T}_{\Phi}^{k}\boldsymbol{P}_{\mathrm{g}\Sigma} \tag{8.119}$$

is well-conditioned (up to its null space).

As for the vector potential operator, we need some lemmas and auxiliary matrices. We define the matrix

$$\mathring{\boldsymbol{V}} := \left(\boldsymbol{\Sigma}^{\mathrm{T}}\boldsymbol{\Sigma}\right)^{+}\boldsymbol{\Sigma}^{\mathrm{T}}\boldsymbol{\Sigma}\boldsymbol{V}\boldsymbol{\Sigma}^{\mathrm{T}}\boldsymbol{\Sigma}\left(\boldsymbol{\Sigma}^{\mathrm{T}}\boldsymbol{\Sigma}\right)^{+}. \tag{8.120}$$

This matrix is important since it is connected to the scalar potential by (see (5.20))

$$\mathring{\boldsymbol{V}} \equiv \left(\boldsymbol{\Sigma}^{\mathrm{T}}\boldsymbol{\Sigma}\right)^{+}\boldsymbol{\Sigma}^{\mathrm{T}}\boldsymbol{T}_{\Phi}^{0}\boldsymbol{\Sigma}\left(\boldsymbol{\Sigma}^{\mathrm{T}}\boldsymbol{\Sigma}\right)^{+}. \tag{8.121}$$

**Lemma 8.4.** *We have the spectral equivalence*

$$\boldsymbol{x}^{\mathrm{T}}\boldsymbol{V}\boldsymbol{G}_{pp}^{-1}\boldsymbol{V}\boldsymbol{x} \asymp \boldsymbol{x}^{\mathrm{T}}\mathring{\boldsymbol{V}}\boldsymbol{G}_{pp}^{-1}\mathring{\boldsymbol{V}}\boldsymbol{x}\,, \quad \forall \boldsymbol{x} \in \left(\operatorname{span}\mathbf{1}_{\Sigma}\right)^{\perp}. \tag{8.122}$$

*Proof.* If $\boldsymbol{x}$ is such that $\mathbf{1}_{\Sigma}^{\mathrm{T}}\boldsymbol{x} = 0$, then we have

$$\boldsymbol{\Sigma}^{\mathrm{T}}\boldsymbol{\Sigma}\left(\boldsymbol{\Sigma}^{\mathrm{T}}\boldsymbol{\Sigma}\right)^{+}\boldsymbol{x} = \boldsymbol{x} \tag{8.123}$$

and thus

$$\boldsymbol{x}^{\mathrm{T}}\boldsymbol{V}\boldsymbol{x} = \boldsymbol{x}^{\mathrm{T}}\mathring{\boldsymbol{V}}\boldsymbol{x}\,. \tag{8.124}$$

Clearly, we have for such $\boldsymbol{x}$ also

$$\boldsymbol{x}^{\mathrm{T}}\boldsymbol{V}\boldsymbol{V}\boldsymbol{x} = \boldsymbol{x}^{\mathrm{T}}\mathring{\boldsymbol{V}}\mathring{\boldsymbol{V}}\boldsymbol{x}\,, \tag{8.125}$$

and since $\boldsymbol{y}^{\mathrm{T}}\boldsymbol{G}_{pp}^{-1}\boldsymbol{y} \asymp \boldsymbol{y}^{\mathrm{T}}\boldsymbol{y}$ holds for all $\boldsymbol{y} \in \mathbb{R}^{N_{\mathrm{C}}}$, we have

$$\boldsymbol{x}^{\mathrm{T}}\boldsymbol{V}\boldsymbol{G}_{pp}^{-1}\boldsymbol{V}\boldsymbol{x} \asymp \boldsymbol{x}^{\mathrm{T}}\mathring{\boldsymbol{V}}\boldsymbol{G}_{pp}^{-1}\mathring{\boldsymbol{V}}\boldsymbol{x}\,. \tag{8.126}$$

□

**Corollary 8.1.** *We have the spectral equivalence*

$$\boldsymbol{x}^{\mathrm{T}}\breve{\boldsymbol{\Delta}}\boldsymbol{x} \asymp \boldsymbol{x}^{\mathrm{T}}\left(\boldsymbol{\Sigma}^{\mathrm{T}}\boldsymbol{\Sigma} + \mathbf{1}_{\Sigma}\mathbf{1}_{\Sigma}^{\mathrm{T}}h^{4}\right)\boldsymbol{x}\,, \quad \forall \boldsymbol{x} \in \mathbb{R}^{N_{\mathrm{C}}}\,. \tag{8.127}$$

*Proof.* Follows from Lemma 8.3. □

**Lemma 8.5.** *The vector $\mathbf{1}_{\Sigma}$ is a right eigenvector of $\boldsymbol{G}_{\tilde{\lambda}p}^{-\mathrm{T}}$, that is, $\mathbf{1}_{\Sigma} = \boldsymbol{G}_{\tilde{\lambda}p}^{-\mathrm{T}}\mathbf{1}_{\Sigma}$.*

*Proof.* If

$$\tilde{\lambda}_{\boldsymbol{y}} = p_{\boldsymbol{x}} = 1\,, \quad \forall \boldsymbol{r} \in \Gamma\,, \tag{8.128}$$

then $\boldsymbol{y} = \mathbf{1}_{\Sigma}$ and $\left[\boldsymbol{x}\right]_i = A_i$, where $\tilde{\lambda}_{\boldsymbol{y}} = \sum_{n=0}^{N_{\mathrm{V}}}\left[\boldsymbol{y}\right]_n\tilde{\lambda}_n$ and $p_{\boldsymbol{x}} = \sum_{n=1}^{N_{\mathrm{C}}}\left[\boldsymbol{x}\right]_n p_n$. Testing this equation with $p_i$ yields

$$\boldsymbol{G}_{p\tilde{\lambda}}\mathbf{1}_{\Sigma} = \boldsymbol{G}_{pp}\boldsymbol{x} = \mathbf{1}_{\Sigma}\,. \tag{8.129}$$

Since $\boldsymbol{G}_{p\tilde{\lambda}} = \boldsymbol{G}_{\tilde{\lambda}p}^{\mathrm{T}}$, we have $\mathbf{1}_{\Sigma} = \boldsymbol{G}_{\tilde{\lambda}p}^{-\mathrm{T}}\mathbf{1}_{\Sigma}$. □

**Corollary 8.2.** *For any mean value free vector $\boldsymbol{x}$, that is, $\mathbf{1}_{\Sigma}^{\mathrm{T}}\boldsymbol{x} = 0$, we have that the vector $\boldsymbol{G}_{\tilde{\lambda}p}^{-1}\boldsymbol{x}$ is mean value free as well.*

*Proof.* This follows from Lemma 8.5 since if we have $\mathbf{1}_{\Sigma}^{\mathrm{T}}\boldsymbol{x} = 0$, then

$$\mathbf{1}_{\Sigma}^{\mathrm{T}}\boldsymbol{G}_{\tilde{\lambda}p}^{-1}\boldsymbol{x} = \mathbf{1}_{\Sigma}^{\mathrm{T}}\boldsymbol{x} = 0\,. \tag{8.130}$$

□

**Proposition 8.4.** *We have the spectral equivalence*

$$\boldsymbol{x}^{\mathrm{T}}\boldsymbol{P}_{\mathrm{g}\Sigma}^{\mathrm{T}}\left(\boldsymbol{T}_{\Phi}^{k}\right)^{\dagger}\check{\boldsymbol{P}}_{\mathrm{m}\Sigma}\boldsymbol{T}_{\Phi}^{k}\boldsymbol{P}_{\mathrm{g}\Sigma}\boldsymbol{x} \asymp \boldsymbol{x}^{\mathrm{T}}\boldsymbol{P}_{\Sigma}\boldsymbol{x}\,, \quad \forall \boldsymbol{x} \in \mathbb{R}^{N}\,. \tag{8.131}$$

*Proof.* We start with (8.63)

$$\boldsymbol{x}^{\mathrm{T}}\hat{\widetilde{\boldsymbol{W}}}\boldsymbol{G}_{\tilde{\lambda}\tilde{\lambda}}^{-1}\hat{\widetilde{\boldsymbol{W}}}\boldsymbol{x} \asymp \boldsymbol{x}^{\mathrm{T}}\hat{\widetilde{\boldsymbol{\Delta}}}\boldsymbol{x}\,, \quad \forall \boldsymbol{x} \in \mathbb{R}^{N_{\mathrm{C}}} \tag{8.132}$$

and applying the substitution $\boldsymbol{x} = \boldsymbol{G}_{\tilde{\lambda}\tilde{\lambda}}^{-1/2}\boldsymbol{y}$ yields

$$\begin{aligned}\boldsymbol{y}^{\mathrm{T}}\boldsymbol{G}_{\tilde{\lambda}\tilde{\lambda}}^{-1/2}\hat{\widetilde{\boldsymbol{W}}}\boldsymbol{G}_{\tilde{\lambda}\tilde{\lambda}}^{-1}\hat{\widetilde{\boldsymbol{W}}}\boldsymbol{G}_{\tilde{\lambda}\tilde{\lambda}}^{-1/2}\boldsymbol{y} &= \boldsymbol{y}^{\mathrm{T}}\left(\boldsymbol{G}_{\tilde{\lambda}\tilde{\lambda}}^{-1/2}\hat{\widetilde{\boldsymbol{W}}}\boldsymbol{G}_{\tilde{\lambda}\tilde{\lambda}}^{-1/2}\right)^{2}\boldsymbol{y} \\ &\asymp \boldsymbol{y}^{\mathrm{T}}\boldsymbol{G}_{\tilde{\lambda}\tilde{\lambda}}^{-1/2}\hat{\widetilde{\boldsymbol{\Delta}}}\boldsymbol{G}_{\tilde{\lambda}\tilde{\lambda}}^{-1/2}\boldsymbol{y}\,, \quad \forall \boldsymbol{y} \in \mathbb{R}^{N_{\mathrm{C}}}\,,\end{aligned} \tag{8.133}$$

and hence

$$\boldsymbol{y}^{\mathrm{T}}\boldsymbol{G}_{\tilde{\lambda}\tilde{\lambda}}^{1/2}\hat{\widetilde{\boldsymbol{W}}}^{-1}\boldsymbol{G}_{\tilde{\lambda}\tilde{\lambda}}^{1/2}\boldsymbol{y} \asymp \boldsymbol{y}^{\mathrm{T}}\left(\boldsymbol{G}_{\tilde{\lambda}\tilde{\lambda}}^{1/2}\hat{\widetilde{\boldsymbol{\Delta}}}\boldsymbol{G}_{\tilde{\lambda}\tilde{\lambda}}^{1/2}\right)^{-1/2}\boldsymbol{y}\,, \quad \forall \boldsymbol{y} \in \mathbb{R}^{N_{\mathrm{C}}}\,. \tag{8.134}$$

From the Calderón identities and the theory outlined in [SW98; BC07; Hip06], we have

$$\boldsymbol{x}^{\mathrm{T}}\hat{\widetilde{\boldsymbol{W}}}\boldsymbol{x} \asymp \boldsymbol{x}^{\mathrm{T}}\boldsymbol{G}_{\tilde{\lambda}p}^{-\mathrm{T}}\boldsymbol{V}^{-1}\boldsymbol{G}_{\tilde{\lambda}p}^{-1}\boldsymbol{x}\,, \quad \forall \boldsymbol{x} \in \mathbb{R}^{N_{\mathrm{C}}}\,. \tag{8.135}$$

Inserting this in (8.134) and applying the back-substitution $\boldsymbol{y} = \boldsymbol{G}_{\tilde{\lambda}\tilde{\lambda}}^{1/2}\boldsymbol{x}$, we obtain

$$\boldsymbol{x}^{\mathrm{T}}\boldsymbol{G}_{\tilde{\lambda}p}^{-\mathrm{T}}\boldsymbol{V}\boldsymbol{G}_{\tilde{\lambda}p}^{-1}\boldsymbol{G}_{\tilde{\lambda}\tilde{\lambda}}\boldsymbol{G}_{\tilde{\lambda}p}^{-\mathrm{T}}\boldsymbol{V}\boldsymbol{G}_{\tilde{\lambda}p}^{-1}\boldsymbol{x} \asymp \boldsymbol{x}^{\mathrm{T}}\hat{\widetilde{\boldsymbol{\Delta}}}^{-1}\boldsymbol{x}\,, \quad \forall \boldsymbol{x} \in \mathbb{R}^{N_{\mathrm{C}}}\,. \tag{8.136}$$

The right-hand side can be simplified: it was shown in [And+13] that

$$\left(\boldsymbol{\Sigma}^{\mathrm{T}}\boldsymbol{\Sigma} + \mathbf{1}_{\Sigma}\mathbf{1}_{\Sigma}^{\mathrm{T}}/N_{\mathrm{C}}\right)^{-1} = \left(\boldsymbol{\Sigma}^{\mathrm{T}}\boldsymbol{\Sigma}\right)^{+} + \mathbf{1}_{\Sigma}\mathbf{1}_{\Sigma}^{\mathrm{T}}/N_{\mathrm{C}} \tag{8.137}$$

holds. In addition with $N_{\mathrm{C}} \asymp 1/h^2$ and Corollary 8.1, we can simplify the right-hand side of (8.136) yielding

$$\boldsymbol{x}^{\mathrm{T}}\boldsymbol{G}_{\tilde{\lambda}p}^{-\mathrm{T}}\boldsymbol{V}\boldsymbol{G}_{\tilde{\lambda}p}^{-1}\boldsymbol{G}_{\tilde{\lambda}\tilde{\lambda}}\boldsymbol{G}_{\tilde{\lambda}p}^{-\mathrm{T}}\boldsymbol{V}\boldsymbol{G}_{\tilde{\lambda}p}^{-1}\boldsymbol{x} \asymp \boldsymbol{x}^{\mathrm{T}}\left(\left(\boldsymbol{\Sigma}^{\mathrm{T}}\boldsymbol{\Sigma}\right)^{+} + \mathbf{1}_{\Sigma}\mathbf{1}_{\Sigma}^{\mathrm{T}}\right)\boldsymbol{x}\,, \quad \forall \boldsymbol{x} \in \mathbb{R}^{N_{\mathrm{C}}}\,. \tag{8.138}$$

From [SW98; BC07], we can obtain

$$\boldsymbol{x}^{\mathrm{T}}\boldsymbol{G}_{pp}^{-1}\boldsymbol{x} \asymp \boldsymbol{x}^{\mathrm{T}}\boldsymbol{G}_{\tilde{\lambda}p}^{-1}\boldsymbol{G}_{\tilde{\lambda}\tilde{\lambda}}\boldsymbol{G}_{\tilde{\lambda}p}^{-\mathrm{T}}\boldsymbol{x}\,, \quad \forall \boldsymbol{x} \in \mathbb{R}^{N_{\mathrm{C}}}\,. \tag{8.139}$$

Inserting this into (8.138) yields

$$\boldsymbol{x}^{\mathrm{T}}\boldsymbol{G}_{\tilde{\lambda}p}^{-\mathrm{T}}\boldsymbol{V}\boldsymbol{G}_{pp}^{-1}\boldsymbol{V}\boldsymbol{G}_{\tilde{\lambda}p}^{-1}\boldsymbol{x} \asymp \boldsymbol{x}^{\mathrm{T}}\left(\left(\boldsymbol{\Sigma}^{\mathrm{T}}\boldsymbol{\Sigma}\right)^{+} + \mathbf{1}_{\Sigma}\mathbf{1}_{\Sigma}^{\mathrm{T}}\right)\boldsymbol{x}\,, \quad \forall \boldsymbol{x} \in \mathbb{R}^{N_{\mathrm{C}}}\,. \tag{8.140}$$

Then we use the substitution $\boldsymbol{x} = \boldsymbol{\Sigma}^{\mathrm{T}}\boldsymbol{y}$ and obtain

$$\boldsymbol{y}^{\mathrm{T}}\boldsymbol{\Sigma}\boldsymbol{G}_{\tilde{\lambda}p}^{-\mathrm{T}}\boldsymbol{V}\boldsymbol{G}_{pp}^{-1}\boldsymbol{V}\boldsymbol{G}_{\tilde{\lambda}p}^{-1}\boldsymbol{\Sigma}^{\mathrm{T}}\boldsymbol{y} \asymp \boldsymbol{y}^{\mathrm{T}}\boldsymbol{P}_{\Sigma}\boldsymbol{y}\,, \quad \forall \boldsymbol{y} \in \mathbb{R}^{N}\,, \tag{8.141}$$

since $\boldsymbol{\Sigma}\mathbf{1}_{\Sigma} = \mathbf{0}$. Due to this relationship, it is clear that all vectors $\boldsymbol{\Sigma}^{\mathrm{T}}\boldsymbol{y}$ with $\boldsymbol{y} \in \mathbb{R}^{N}$ are mean value free, that is, we have $\mathbf{1}_{\Sigma}^{\mathrm{T}}\boldsymbol{\Sigma}^{\mathrm{T}}\boldsymbol{y} = 0$. Thus we can invoke Lemma 8.4 and obtain

$$\boldsymbol{y}^{\mathrm{T}}\boldsymbol{\Sigma}\boldsymbol{G}_{\tilde{\lambda}p}^{-\mathrm{T}}\mathring{\boldsymbol{V}}\boldsymbol{G}_{pp}^{-1}\mathring{\boldsymbol{V}}\boldsymbol{G}_{\tilde{\lambda}p}^{-1}\boldsymbol{\Sigma}^{\mathrm{T}}\boldsymbol{y} \asymp \boldsymbol{y}^{\mathrm{T}}\boldsymbol{P}_{\Sigma}\boldsymbol{y}\,, \quad \forall \boldsymbol{y} \in \mathbb{R}^{N}\,. \tag{8.142}$$

Inserting the right-hand side from (8.121), we obtain

$$\boldsymbol{y}^{\mathrm{T}}\boldsymbol{P}_{\mathrm{g}\Sigma}^{\mathrm{T}}\boldsymbol{T}_{\Phi}^{0}\check{\boldsymbol{P}}_{\mathrm{m}\Sigma}\boldsymbol{T}_{\Phi}^{0}\boldsymbol{P}_{\mathrm{g}\Sigma}\boldsymbol{y} \asymp \boldsymbol{y}^{\mathrm{T}}\boldsymbol{P}_{\Sigma}\boldsymbol{y} \asymp \boldsymbol{y}^{\mathrm{T}}\boldsymbol{P}_{\Sigma}\boldsymbol{y}\,, \quad \forall \boldsymbol{y} \in \mathbb{R}^{N}\,. \tag{8.143}$$

As in Proposition 8.1, we note that the dynamic kernel only introduces a compact perturbation, and that by using $(\boldsymbol{T}_{\Phi}^{k})^{\dagger}$ for the left scalar potential operator matrix in (8.131), we yield a symmetric, positive semi-definite system. □

### $\gamma$) Preconditioned Electric Field Integral Equation

**Proposition 8.5.** *The new formulation is well-conditioned in the static limit, that is, the matrix in* (8.48) *satisfies*

$$\lim_{k\longrightarrow 0} \boldsymbol{x}^{\mathrm{T}} \check{\boldsymbol{P}}_{\mathrm{o}}{}^{\dagger} \boldsymbol{T}^{\dagger} \check{\boldsymbol{P}}_{\mathrm{m}} \boldsymbol{T} \check{\boldsymbol{P}}_{\mathrm{o}} \boldsymbol{x} \asymp \boldsymbol{x}^{\mathrm{T}} \boldsymbol{x}\,, \quad \forall \boldsymbol{x} \in \mathbb{R}^N\,. \tag{8.144}$$

*Proof.* We have

$$\begin{aligned}
&\check{\boldsymbol{P}}_{\mathrm{o}}{}^{\dagger} \boldsymbol{T}^{\dagger} \check{\boldsymbol{P}}_{\mathrm{m}} \boldsymbol{T} \check{\boldsymbol{P}}_{\mathrm{o}} \\
&\qquad = \boldsymbol{P}^{\dagger}_{\Lambda\mathrm{H}} \left(\boldsymbol{T}^{k}_{\mathrm{A}}\right)^{\dagger} \check{\boldsymbol{P}}_{\mathrm{m}\Lambda} \boldsymbol{T}^{k}_{\mathrm{A}} \boldsymbol{P}_{\Lambda\mathrm{H}} + \boldsymbol{P}^{\dagger}_{\mathrm{g}\Sigma} \left(\boldsymbol{T}^{k}_{\Phi}\right)^{\dagger} \check{\boldsymbol{P}}_{\mathrm{m}\Sigma} \boldsymbol{T}^{k}_{\Phi} \boldsymbol{P}_{\mathrm{g}\Sigma} \\
&\qquad + k^2 \boldsymbol{P}^{\dagger}_{\mathrm{g}\Sigma} \left(\boldsymbol{T}^{k}_{\mathrm{A}}\right)^{\dagger} \check{\boldsymbol{P}}_{\mathrm{m}\Lambda} \boldsymbol{T}^{k}_{\mathrm{A}} \boldsymbol{P}_{\mathrm{g}\Sigma} + k^4 \boldsymbol{P}^{\dagger}_{\mathrm{g}\Sigma} \left(\boldsymbol{T}^{k}_{\mathrm{A}}\right)^{\dagger} \check{\boldsymbol{P}}_{\mathrm{m}\Sigma} \boldsymbol{T}^{k}_{\mathrm{A}} \boldsymbol{P}_{\mathrm{g}\Sigma} \\
&\qquad \mathrm{i}k \boldsymbol{P}^{\dagger}_{\Lambda\mathrm{H}} \left(\boldsymbol{T}^{k}_{\mathrm{A}}\right)^{\dagger} \check{\boldsymbol{P}}_{\mathrm{m}\Lambda} \boldsymbol{T}^{k}_{\mathrm{A}} \boldsymbol{P}_{\mathrm{g}\Sigma} - \mathrm{i}k \boldsymbol{P}^{\dagger}_{\mathrm{g}\Sigma} \left(\boldsymbol{T}^{k}_{\mathrm{A}}\right)^{\dagger} \check{\boldsymbol{P}}_{\mathrm{m}\Lambda} \boldsymbol{T}^{k}_{\mathrm{A}} \boldsymbol{P}_{\Lambda\mathrm{H}} \\
&\qquad \mathrm{i}k^3 \boldsymbol{P}^{\dagger}_{\Lambda\mathrm{H}} \left(\boldsymbol{T}^{k}_{\mathrm{A}}\right)^{\dagger} \check{\boldsymbol{P}}_{\mathrm{m}\Sigma} \boldsymbol{T}^{k}_{\mathrm{A}} \boldsymbol{P}_{\mathrm{g}\Sigma} - \mathrm{i}k^3 \boldsymbol{P}^{\dagger}_{\mathrm{g}\Sigma} \left(\boldsymbol{T}^{k}_{\mathrm{A}}\right)^{\dagger} \check{\boldsymbol{P}}_{\mathrm{m}\Sigma} \boldsymbol{T}^{k}_{\mathrm{A}} \boldsymbol{P}_{\Lambda\mathrm{H}} \\
&\qquad \mathrm{i}k \boldsymbol{P}^{\dagger}_{\Lambda\mathrm{H}} \left(\boldsymbol{T}^{k}_{\mathrm{A}}\right)^{\dagger} \check{\boldsymbol{P}}_{\mathrm{m}\Sigma} \boldsymbol{T}^{k}_{\Phi} \boldsymbol{P}_{\mathrm{g}\Sigma} - \mathrm{i}k \boldsymbol{P}^{\dagger}_{\mathrm{g}\Sigma} \left(\boldsymbol{T}^{k}_{\Phi}\right)^{\dagger} \check{\boldsymbol{P}}_{\mathrm{m}\Sigma} \boldsymbol{T}^{k}_{\mathrm{A}} \boldsymbol{P}_{\Lambda\mathrm{H}}\,.
\end{aligned} \tag{8.145}$$

Thus we find

$$\lim_{k\longrightarrow 0} \check{\boldsymbol{P}}_{\mathrm{o}}{}^{\dagger} \boldsymbol{T}^{\dagger} \check{\boldsymbol{P}}_{\mathrm{m}} \boldsymbol{T} \check{\boldsymbol{P}}_{\mathrm{o}} = \boldsymbol{P}^{\dagger}_{\Lambda\mathrm{H}} \left(\boldsymbol{T}^{0}_{\mathrm{A}}\right)^{\dagger} \check{\boldsymbol{P}}_{\mathrm{m}\Lambda} \boldsymbol{T}^{k}_{\mathrm{A}} \boldsymbol{P}_{\Lambda\mathrm{H}} + \boldsymbol{P}^{\dagger}_{\mathrm{g}\Sigma} \left(\boldsymbol{T}^{0}_{\Phi}\right)^{\dagger} \check{\boldsymbol{P}}_{\mathrm{m}\Sigma} \boldsymbol{T}^{k}_{\Phi} \boldsymbol{P}_{\mathrm{g}\Sigma}\,. \tag{8.146}$$

Clearly, the new formulation is low-frequency stable and the well-conditioning in $h$ follows from Proposition 8.3 and Proposition 8.4 so that we have

$$\begin{aligned}
&\boldsymbol{x}^{\mathrm{T}} \left( \boldsymbol{P}^{\dagger}_{\Lambda\mathrm{H}} \left(\boldsymbol{T}^{0}_{\mathrm{A}}\right)^{\dagger} \check{\boldsymbol{P}}_{\mathrm{m}\Lambda} \boldsymbol{T}^{0}_{\mathrm{A}} \boldsymbol{P}_{\Lambda\mathrm{H}} + \boldsymbol{P}^{\dagger}_{\mathrm{g}\Sigma} \left(\boldsymbol{T}^{0}_{\Phi}\right)^{\dagger} \check{\boldsymbol{P}}_{\mathrm{m}\Sigma} \boldsymbol{T}^{0}_{\Phi} \boldsymbol{P}_{\mathrm{g}\Sigma} \right) \boldsymbol{x} \\
&\qquad\qquad \asymp \boldsymbol{x}^{\mathrm{T}} \boldsymbol{x}\,, \quad \forall \boldsymbol{x} \in \mathbb{R}^N\,.
\end{aligned} \tag{8.147}$$

□

For the dynamic case, we note that the additional terms appearing in (8.145) have at least up to a certain frequency a smaller norm than then principal terms in

(8.147). Numerical evidence suggests that even for geometries spanning several wavelengths, the new preconditioner shows a beneficial behavior compared with an unpreconditioned system.

The derivation also holds for the case that the mesh is non-uniform, that is, the condition number is still bounded after subsequent structured mesh refinements. If, however, only a local refinement is performed then the condition number can still grow. If in such a process only the conditioning of $\boldsymbol{G}_{pp}$ and $\boldsymbol{G}_{\lambda\lambda}$ is increased but not of $\boldsymbol{G}_{ff}$ and $\boldsymbol{G}_{ff}$, then this can be prevented.

In fact, only the preconditioner for the scalar potential part is affected. The reason for this is that we have used that

$$\left(\hat{\widetilde{\boldsymbol{W}}}\boldsymbol{G}_{\tilde{\lambda}\tilde{\lambda}}^{-1}\hat{\widetilde{\boldsymbol{W}}}\right)^{-1} = \hat{\widetilde{\boldsymbol{W}}}^{+}\boldsymbol{G}_{\tilde{\lambda}\tilde{\lambda}}\hat{\widetilde{\boldsymbol{W}}}^{-1}. \tag{8.148}$$

For $\boldsymbol{W}$, the same statement (with pseudo-inverses) is not true:

$$\left(\widetilde{\boldsymbol{W}}\boldsymbol{G}_{\tilde{\lambda}\tilde{\lambda}}^{-1}\widetilde{\boldsymbol{W}}\right)^{+} \neq \widetilde{\boldsymbol{W}}^{+}\boldsymbol{G}_{\tilde{\lambda}\tilde{\lambda}}\widetilde{\boldsymbol{W}}^{+}, \tag{8.149}$$

where we note that in our analysis $\widetilde{\boldsymbol{W}}^{+}$ does not appear since we have already moved to $\boldsymbol{V}$ and later on to $\mathring{\boldsymbol{V}}$ in the proof of Proposition 8.4.

What we have implicitly obtained in the proof is a spectral equivalence between $(\widetilde{\boldsymbol{W}}\boldsymbol{G}_{\tilde{\lambda}\tilde{\lambda}}^{-1}\widetilde{\boldsymbol{W}})^{+}$ and $\widetilde{\boldsymbol{W}}^{+}\boldsymbol{G}_{\tilde{\lambda}\tilde{\lambda}}\widetilde{\boldsymbol{W}}^{+}$, where however the bounding constants tend to deteriorate with an increasing ill-conditioning of $\boldsymbol{G}_{\tilde{\lambda}\tilde{\lambda}}$. If $\boldsymbol{G}_{\tilde{\lambda}\tilde{\lambda}}$ is modified such that it has a null space spanned by $\mathbf{1}_{\Sigma}$ resulting in the matrix $\mathring{\boldsymbol{G}}_{\tilde{\lambda}\tilde{\lambda}}$, then we would have

$$\left(\widetilde{\boldsymbol{W}}\mathring{\boldsymbol{G}}_{\tilde{\lambda}\tilde{\lambda}}^{+}\widetilde{\boldsymbol{W}}\right)^{+} = \widetilde{\boldsymbol{W}}^{+}\mathring{\boldsymbol{G}}_{\tilde{\lambda}\tilde{\lambda}}\widetilde{\boldsymbol{W}}^{+}, \tag{8.150}$$

and thus no deterioration would occur. Since in the end we are not interested in $\widetilde{\boldsymbol{W}}$ but in preconditioning $\mathring{\boldsymbol{V}}$, we replace $\boldsymbol{G}_{pp}^{-1}$ by $\boldsymbol{G}_{pp}^{\ddagger}$, which has a null space spanned by $\mathbf{1}_{\Sigma}$. Section 6.d confirms the effectiveness of this approach.

We have now assumed that $\boldsymbol{G}_{ff}$ and $\boldsymbol{G}_{\tilde{f}\tilde{f}}$ are reasonably conditioned. A study for the case that the condition number assumes extreme values is not within the scope of this work. For the non-canonical numerical examples, the condition number of $\boldsymbol{G}_{ff}$ or $\boldsymbol{G}_{\tilde{f}\tilde{f}}$ is up to around $1 \cdot 10^{3}$.

## d) Numerical Results

First, we considered a sphere, radius 1 m, to confirm the low-frequency stability by computing the condition number obtained by the new formulation and compared it with a loop-tree preconditioned system. Figure 8.1 shows that the new formulation is frequency stable and Figure 8.2 that the bistatic radar cross section can be accurately computed down to $1 \cdot 10^{-30}$ Hz. The saturation of the condition number in the case "no preconditioner" stems from numerical cancellation: the null space of $\boldsymbol{T}_\Phi$ exists only up to numerical precision and when $k$ becomes too small, the (numerical) norm of the null space of $\boldsymbol{T}_\Phi$ is larger than the norm of $\boldsymbol{T}_\mathrm{A}$ so that $\boldsymbol{T}_\mathrm{A}$ completely vanishes in numerical noise. To verify the dense-discretization stability, we computed the condition number for the new formulation and the loop-tree preconditioned system for an increasing spectral index $1/h$. We can see from Figure 8.3 that the new formulation is dense-discretization stable, whereas the loop-tree preconditioner is not.

In addition, we considered a plate as an example for an open structure. Similar to Calderón preconditioners, the condition number shows a slight growth in $1/h$ as displayed in Figure 8.4; however, it remains small compared with a loop-tree preconditioner. In order to confirm the low-frequency stability in the case for multiply connected geometries, we considered a closed structure with two global loops shown in Figure 8.5. Evidently, the new formulation remains stable.

Next, we considered more realistic structures. To compress the system matrix, we used an ACA with tolerance $1 \cdot 10^{-4}$. As iterative solver, we used the CG method for the new formulation and the CGS method for the other formulations since the CG method is only applicable if the matrix is HPD. We note that a single iteration step of CGS requires two matrix-vector products. We employed the AGMG library [Not; NN12] for the fast inversion of the graph Laplacians with solver tolerance $1 \cdot 10^{-14}$ to demonstrate that even for extreme small tolerances our preconditioner remains efficient.

As first realistic example, we considered as open and multiply connected structure the model of a MiG-15 displayed in Figure 8.6, which has one global loop. As excitation we used a plane wave and its electric size is $2 \cdot 10^{-2}\lambda$, where $\lambda$ is the wavelength. Several unstructured refinements where conducted ranging from 1518 to 306 036 unknowns. Figure 8.7 and Figure 8.8 show the number of iterations and total time, respectively, as a function of $1/h$. Clearly, the reduction in the number of iterations reflects in a saving of computational time.

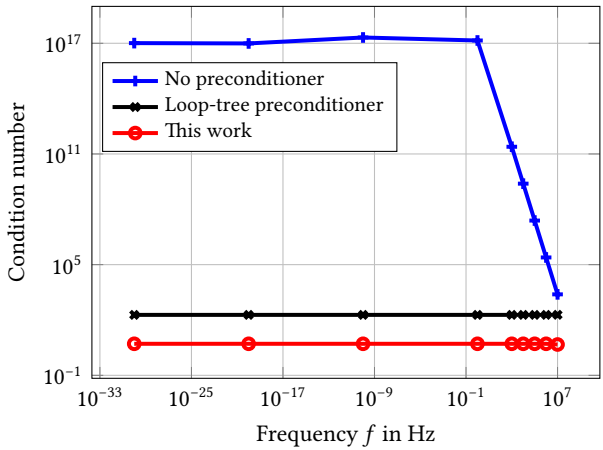


*Fig. 8.1.:* Sphere: the condition number as a function of the frequency.

Since the MiG-15 is an open structure, we were also interested to see how the new formulation behaves for high frequencies, that is, when the electric size of the model spans several wave lengths $\lambda$. To this end, we used as discretization of the MiG-15 with 306 036 unknowns, where the maximum edge length is 0.07 m and the average edge length $h$ is 0.025 m (standard deviation is 0.0023 m). We varied the frequency from 0.48 GHz, where $h = \lambda/25$, to 0.8 GHz, where $h = \lambda/15$. This frequency range corresponds to an electric size $\ell$ varying from 13 to 24. We considered a voltage gap and a plane wave excitation and compared the new formulation with an unpreconditioned EFIE. Table 8.1 summarizes or findings. We see that the new formulation behaves favorably even for higher frequencies, though it seems that its advantage is waning the higher the frequency becomes.

As an example of a simply connected and closed structure, we considered the model of a Rafale fighter shown in Figure 8.9a, which is discretized with a non-uniform mesh (see Figure 8.9b). We employed a coarse initial discretization with 18 171 unknowns and performed two structured refinement steps ending up with 290 736 unknowns (by using a structured refinement the geometry is not changed). We note that cond $\boldsymbol{G}_{pp} \approx 1.8 \cdot 10^5$ remains constant for all refinements, but $\boldsymbol{G}_{ff}$ varies from 276 of the initial discretization to 769 of the finest discretiza-

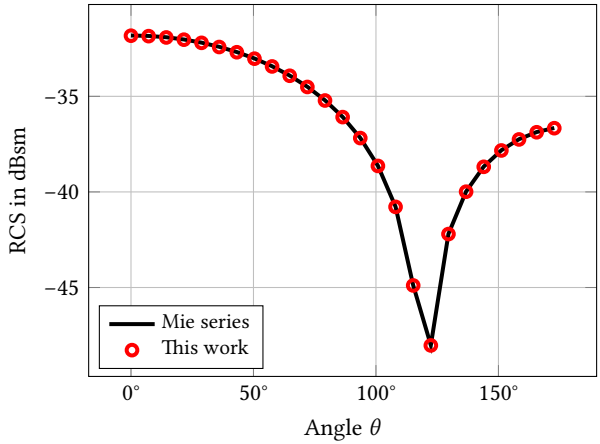


*(a)* Frequency: 1 MHz.

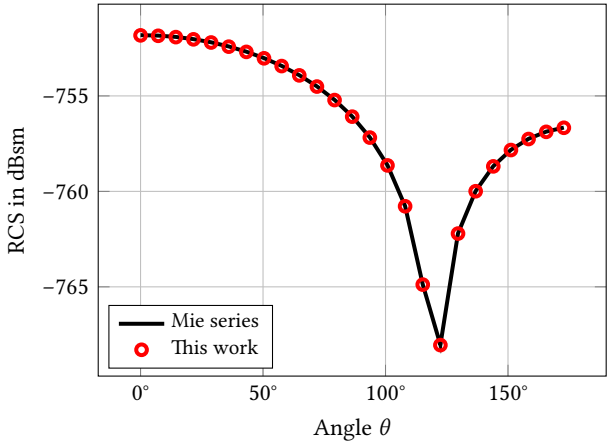


*(b)* Frequency: $1 \cdot 10^{-30}$ Hz.

*Fig. 8.2.:* Sphere: bistatic radar cross section.

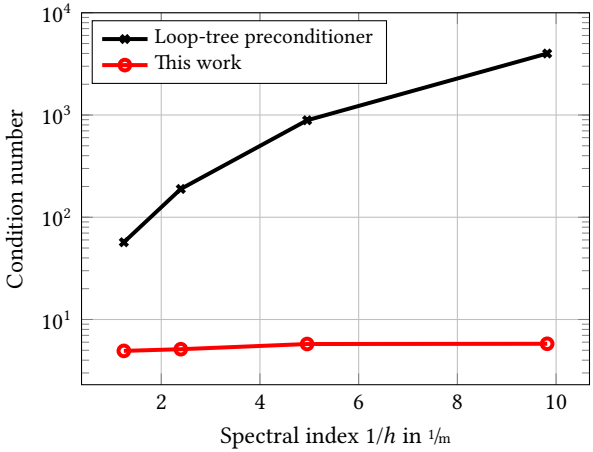


*Fig. 8.3.:* Sphere: the condition number as a function of the spectral index.

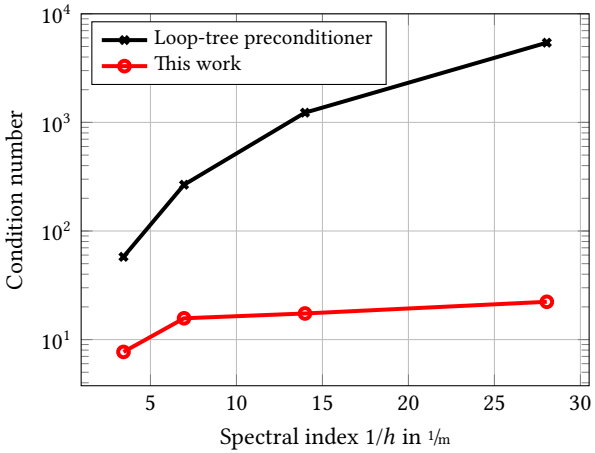


*Fig. 8.4.:* Plate: the condition number as a function of the spectral index.

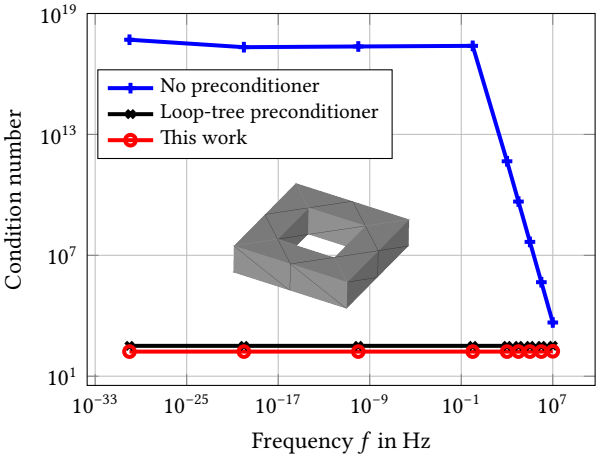


*Fig. 8.5.:* Toroidal structure: the condition number as a function of the frequency.

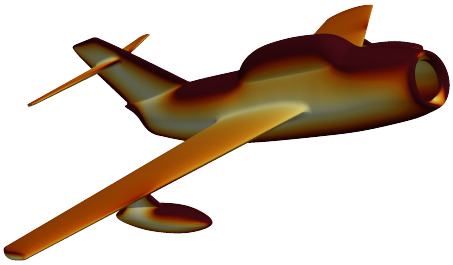

*Fig. 8.6.:* MiG-15: real part of $\boldsymbol{j}$ excited by an incident plane wave.

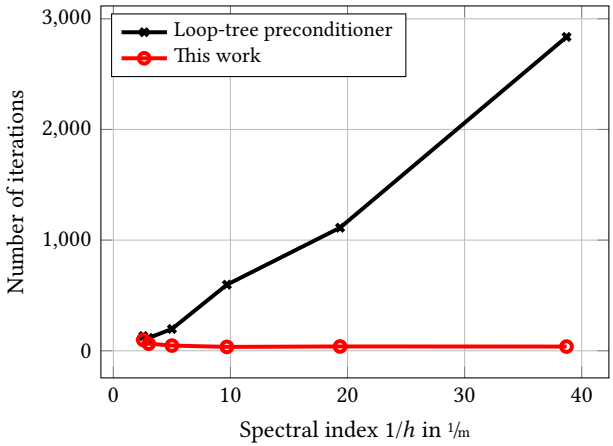


*Fig. 8.7.:* MiG-15: the number of iterations as a function of the spectral index.

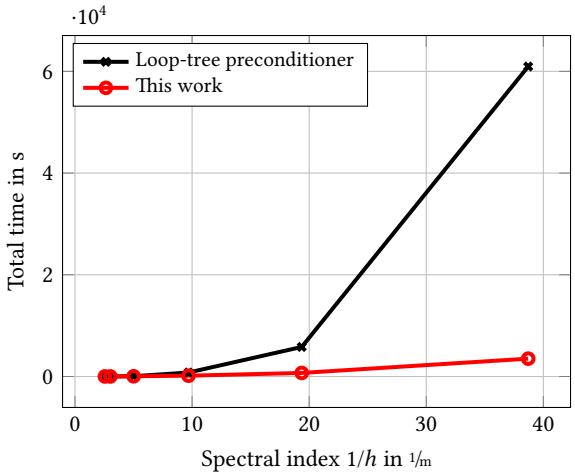


*Fig. 8.8.:* MiG-15: the total time as a function of the spectral index.

| $f$ | $\lambda/h$ | $\ell$ | Preconditioner | | | |
|---|---|---|---|---|---|---|
| | | | None | | This work | |
| | | | Iterations | Time* (h:m:s) | Iterations | Time* (h:m:s) |
| *Voltage gap excitation* | | | | | | |
| 0.48 | 25 | 13 | 13 189 | 89:03:11 | 705 | 12:10:09 |
| 0.6 | 20 | 16 | 17 546 | 180:17:37 | 1055 | 29:18:19 |
| 0.8 | 15 | 24 | 15 793 | 159:54:04 | 1943 | 59:18:11 |
| *Plane wave excitation* | | | | | | |
| 0.48 | 25 | 13 | 10 842 | 73:25:57 | 1413 | 24:08:18 |
| 0.6 | 20 | 16 | 16 654 | 171:08:41 | 1544 | 42:14:42 |
| 0.8 | 15 | 24 | 14 151 | 136:22:36 | 3223 | 79:53:03 |

* This is the total time including the setup costs for the preconditioners.

*Tab. 8.1.:* MiG-15: the number of iterations and the time used by the solver to obtain a residual error below $1 \cdot 10^{-4}$.

tion. Table 8.2 shows the number of iterations and total time. We can see that in this case the number of iterations grows also for the new formulation. This is not unexpected since the condition number of $\boldsymbol{G}_{ff}$ has grown for the first refinements. Further refinements would lead to a converging condition number of $\boldsymbol{G}_{ff}$ and hence, we can expect that the new formulation would converge likewise.

Lastly, as an example of a multiply connected and closed structure, we have chosen an model of the Fokker Dr.I depicted in Figure 8.10, which has 390 global loops. As excitation we considered both a plane wave and a voltage gap excitation. The model is discretized with 294 420 unknowns resulting in a non-uniform mesh with $\operatorname{cond} \boldsymbol{G}_{ff} \approx 3 \cdot 10^3$ and $\operatorname{cond} \boldsymbol{G}_{pp} \approx 7 \cdot 10^4$. Its electric length is $1 \cdot 10^{-3}\lambda$. From Table 8.3, we can see that there is not only a significant saving in the number of iterations, but also in time.

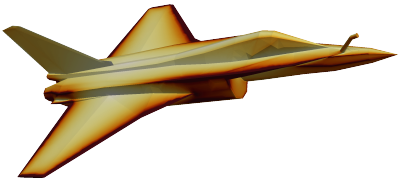

*(a)* Real part of $\boldsymbol{j}$ excited by an incident plane wave.

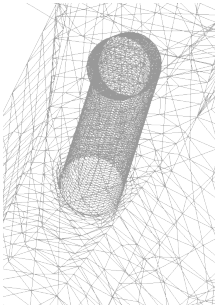

*(b)* Non-uniform mesh due to hose.

*Fig. 8.9.:* Rafale.

*Fig. 8.10.:* Fokker Dr.I: real part of $\boldsymbol{j}$ excited by an incident plane wave.

| $N$ | Preconditioner | | | |
|---|---|---|---|---|
| | Loop-tree | | This work | |
| | Iterations | Time* (h:m:s) | Iterations | Time* (h:m:s) |
| *Plane wave excitation* | | | | |
| 18 171 | 671 | 00:18:17 | 98 | 00:08:01 |
| 72 684 | 2054 | 04:14:05 | 129 | 00:43:41 |
| 290 736 | 5707 | 58:50:14 | 173 | 04:10:59 |
| *Voltage gap excitation* | | | | |
| 18 171 | 246 | 00:07:25 | 36 | 00:03:57 |
| 72 684 | 181 | 00:22:33 | 48 | 00:20:03 |
| 290 736 | 333 | 03:16:11 | 38 | 01:19:17 |

* This is the total time including the setup costs for the preconditioners.

*Tab. 8.2.:* Rafale: the number of iterations and the time used by the solver to obtain a residual error below $1 \cdot 10^{-4}$.

## e) Conclusion

We presented a preconditioner for the EFIE that yields a Hermitian, positive definite, and well-conditioned system matrix without requiring the use of a barycentrically refined mesh. While it outperforms a standard technique such as the loop-tree preconditioner in the low- and mid-frequency range, further investigations are necessary for electrically large problems.

| Preconditioner | Iterations | Time* | $l^2$-relative error† | |
|---|---|---|---|---|
| | | (h:m:s) | Current (%) | RCS (%) |
| *Plane wave excitation* | | | | |
| Loop-tree | 4846 | 31:46:57 | | |
| This work | 169 | 03:01:40 | 1.3086 | 0.0015 |
| *Voltage gap excitation* | | | | |
| Loop-tree | 2309 | 15:35:07 | | |
| This work | 26 | 00:44:11 | 0.0236 | 1.5917 |

* This is the total time including the setup costs for the preconditioners.

† The relative error is with respect to the solution obtained by using the loop-tree preconditioner.

*Tab. 8.3.:* Fokker Dr.I: the number of iterations and the time used by the solver to obtain a residual error below $1 \cdot 10^{-4}$.

Chapter 9

# A Hermitian, Positive Definite, and Well-Conditioned CFIE

*This last technical chapter sketches some preliminary results on a new preconditioner for the CFIE that gives rise to a Hermitian, positive definite system of linear equations. Different from other Calderón strategies, this scheme necessitates a standard discretization of the EFIE with RWG basis functions (i.e., no dual EFIE matrix required), is free from spurious resonances, and is stable down to the static limit for both simply* and *multiply connected geometries. The fact that the new system matrix is Hermitian, positive definite, and well-conditioned makes it amenable for fast iterative solvers. Numerical results demonstrate the effectiveness of the proposed approach. This work is based on the conference article [AAE16a].*

For closed, electrically large problems, the CFIE can be used to avoid interior resonances. Classical Calderón preconditioners have been extended to the CFIE [Bag+09; And+12]. However, these schemes demand the use of the Yukawa potential (i.e., an EFIE where the wavenumber $k$ in the Green's function is replaced by $+\mathrm{i}k$), thereby requiring the discretization of another operator and, furthermore, they do not give rise to Hermitian formulations.

In the previous chapter, a scheme has been presented that allows to precondition the EFIE without the need of dual basis functions and a barycentric refinement of the mesh. Based on this formulation, we present in this chapter a well-conditioned CFIE that has three key properties: (i) At the best of our knowledge it is the first CFIE formulation giving rise to a Hermitian, positive definite system matrix *at every frequency*. To obtain this, we use the RF-CMP for preconditioning the EFIE part of the CFIE leveraging on the fact that the matrix $\boldsymbol{P}_0$ is, up to the frequency scaling, a well-conditioned matrix. Therefore,

we can apply it to the MFIE part without jeopardizing its well-conditioning. (ii) Different from other Calderón-like preconditioning schemes, we can prove the resonance-freeness of the discretized equation under the assumption that the unpreconditioned CFIE is resonance-free. (iii) When compared with standard Calderón techniques, the computational costs of the new formulation presented here are substantially reduced since, while dual basis functions are still necessary for the MFIE, the EFIE can be discretized solely with standard RWG functions (no dual EFIE matrix is required). This chapter will define the new equation and analyze its theoretical properties in detail. Finally, numerical results will corroborate the theory and show the practical impact of the new scheme on real case scenarios.

## a) New Formulation

We define the abbreviation

$$\breve{\boldsymbol{M}} = \boldsymbol{G}_{ff}\boldsymbol{G}^{-1}_{\hat{\boldsymbol{n}}\times\tilde{f},f}\widetilde{\boldsymbol{M}}\,. \tag{9.1}$$

For resonance frequencies, $\boldsymbol{T}$ and $\breve{\boldsymbol{M}}$ are rank deficient, while the linear combination $\boldsymbol{T} + \breve{\boldsymbol{M}}$ has full rank, but is not well-conditioned due to $\boldsymbol{T}$ (i.e., in the case of multiply connected geometries, it is also not well-conditioned due to $\breve{\boldsymbol{M}}$). We propose the following preconditioned CFIE:

$$\boldsymbol{P}_{\mathrm{o}}^{\dagger}\left(\boldsymbol{T}^{\dagger}\boldsymbol{P}_{\mathrm{m}}\boldsymbol{T}/\nu + \widetilde{\boldsymbol{M}}^{\dagger}\widetilde{\boldsymbol{M}}/\gamma\right)\boldsymbol{P}_{\mathrm{o}}\boldsymbol{i} = \boldsymbol{P}_{\mathrm{o}}^{\dagger}\left(-\boldsymbol{T}^{\dagger}\boldsymbol{P}_{\mathrm{m}}\boldsymbol{e}\nu + \widetilde{\boldsymbol{M}}^{\dagger}\boldsymbol{h}/\gamma\right), \tag{9.2}$$

where $\boldsymbol{P}_{\mathrm{o}}$ and $\boldsymbol{P}_{\mathrm{m}}$ are the same as defined in Chapter 8, that is, as defined in (8.11) and (8.12), and we used the normalization factors

$$\nu = \left\|\boldsymbol{P}_{\mathrm{o}}^{\dagger}\boldsymbol{T}^{\dagger}\boldsymbol{P}_{\mathrm{m}}\boldsymbol{T}\boldsymbol{P}_{\mathrm{o}}\right\|, \tag{9.3}$$

$$\gamma = \left\|\boldsymbol{P}_{\mathrm{o}}^{\dagger}\widetilde{\boldsymbol{M}}^{\dagger}\widetilde{\boldsymbol{M}}\boldsymbol{P}_{\mathrm{o}}\right\|. \tag{9.4}$$

Since $\widetilde{\boldsymbol{M}}$ is well-conditioned except when $\Omega$ is multiply connected: the part quasi-harmonic Helmholtz subspace associated with the toroidal loops becomes a null space in the static limit [Bog+11]. As shown in the previous chapter, the

matrix $\boldsymbol{P}_{\mathrm{o}}^{\dagger}\boldsymbol{T}^{\dagger}\boldsymbol{P}_{\mathrm{m}}\boldsymbol{T}\boldsymbol{P}_{\mathrm{o}}$ is well-conditioned (at least in the static limit) and thus compensates the ill-conditioning of the MFIE associated with the toroidal subspace. Thus we can conclude that $\boldsymbol{P}_{\mathrm{o}}^{\dagger}\Big(\boldsymbol{T}^{\dagger}\boldsymbol{P}_{\mathrm{m}}\boldsymbol{T}/\nu + \widetilde{\boldsymbol{M}}^{\dagger}\widetilde{\boldsymbol{M}}/\gamma\Big)\boldsymbol{P}_{\mathrm{o}}$ is well-conditioned. It remains to show that the matrix does not suffer from interior resonances.

**Proposition 9.1.** *The matrix $\boldsymbol{T}^{\dagger}\boldsymbol{P}_{\mathrm{m}}\boldsymbol{T}/\nu + \widetilde{\boldsymbol{M}}^{\dagger}\widetilde{\boldsymbol{M}}/\gamma$ has full rank.*

*Proof.* We note that $\operatorname{null}\breve{\boldsymbol{M}} = \operatorname{null}\widetilde{\boldsymbol{M}}$. For all $\boldsymbol{x} \in \mathbb{R}^N \setminus \big(\operatorname{null}\boldsymbol{T} \cup \operatorname{null}\widetilde{\boldsymbol{M}}\big)$, we have

$$\boldsymbol{x}^{\dagger}\Big(\boldsymbol{T}^{\dagger}\boldsymbol{P}_{\mathrm{m}}\boldsymbol{T}/\nu + \widetilde{\boldsymbol{M}}^{\dagger}\widetilde{\boldsymbol{M}}/\gamma\Big)\boldsymbol{x} = \boldsymbol{x}^{\dagger}\boldsymbol{T}^{\dagger}\boldsymbol{P}_{\mathrm{m}}\boldsymbol{T}\boldsymbol{x}/\nu + \boldsymbol{x}^{\dagger}\widetilde{\boldsymbol{M}}^{\dagger}\widetilde{\boldsymbol{M}}\boldsymbol{x}/\gamma > 0\,, \tag{9.5}$$

since $\boldsymbol{T}^{\dagger}\boldsymbol{P}_{\mathrm{m}}\boldsymbol{T}$ and $\widetilde{\boldsymbol{M}}^{\dagger}\widetilde{\boldsymbol{M}}$ are positive definite on $\mathbb{R}^N \setminus \big(\operatorname{null}\boldsymbol{T} \cup \operatorname{null}\widetilde{\boldsymbol{M}}\big)$, that is,

$$\boldsymbol{x}^{\dagger}\boldsymbol{T}^{\dagger}\boldsymbol{P}_{\mathrm{m}}\boldsymbol{T}\boldsymbol{x}/\nu > 0 \tag{9.6}$$

and

$$\boldsymbol{x}^{\dagger}\widetilde{\boldsymbol{M}}^{\dagger}\widetilde{\boldsymbol{M}}\boldsymbol{x}/\gamma > 0 \tag{9.7}$$

using that $\gamma > 0$. Clearly, when either $\boldsymbol{x} \in \operatorname{null}\boldsymbol{T}$ or $\boldsymbol{x} \in \operatorname{null}\widetilde{\boldsymbol{M}}$, we still have

$$\boldsymbol{x}^{\dagger}\Big(\boldsymbol{T}^{\dagger}\boldsymbol{P}_{\mathrm{m}}\boldsymbol{T}/\nu + \widetilde{\boldsymbol{M}}^{\dagger}\widetilde{\boldsymbol{M}}/\gamma\Big)\boldsymbol{x} > 0\,, \tag{9.8}$$

and hence, the matrix is positive definite and thus has full rank at resonance frequencies. □

## b) Numerical Results

To verify the presented theory, we first tested the frequency stability. We used a sphere and compared the new formulation with an EFIE, CFIE, and a loop-tree preconditioned CFIE. Figures 9.1a and 9.1b show that from the standard techniques only the loop-tree preconditioned is frequency stable (the CFIE deteriorates for low-frequencies, the EFIE for low and high-frequencies), however, with a relatively high condition number compared with the new formulation. We can see that the new formulation does not suffer from interior resonances, though we observe a growth of the condition number with increasing frequency, which stems from the compact perturbation of the dynamic kernel.

| Formulation | Iterations | |
|---|---|---|
| | $f = 1\,\mathrm{MHz}$ | $f = 10\,\mathrm{MHz}$ |
| CFIE | 214 | 85 |
| CFIE: LT | 649 | 1245 |
| This Work | 40 | 274 |

*Tab. 9.1.:* Space Shuttle: the number of iterations; solver tolerance $1 \cdot 10^{-4}$.

To better assess the impact of the dynamical kernel on the iterative solver, we considered a plane wave excitation and solved the system by using the generalized minimal residual (GMRES) and CG method with solver tolerance $1 \cdot 10^{-4}$. Figure 9.1c displays the results. We can see a correspondence between the condition number and the number of iterations, though we note that for the highest frequency the ratio of the condition numbers of the conformingly discretized CFIE and the new formulation is around 18, while for the number of iterations the ratio is around 1.45.

Next, we verified the dense-discretization stability. To this end, we refined the toroidal structure (i.e., a multiply connected geometry, which has a harmonic subspace) depicted in Figure 9.2a. Figure 9.2b shows that for such a geometry even the MFIE is ill-conditioned, whereas the new formulation is stable. Eventually, we used a more realistic structure, the model of a Space Shuttle discretized with 3780 unknowns, where we employed a plane wave excitation with frequency 1 MHz and 10 MHz, respectively. For the latter, the electric length is $4\lambda$. The results are summarized in Figure 7.2; they confirm the observation from Figure 9.1c: for high frequencies the dynamic kernel deteriorates the conditioning of (9.2). If, however, a finer mesh would be used for the discretization, then the conforming CFIE would have a growing condition number, while the condition number of the matrix in (9.2) can be bounded.

## c) Conclusion

It was shown that it is possible to extend the RF-CMP to a conformingly discretized CFIE: the low-frequency and the dense-discretization breakdown are

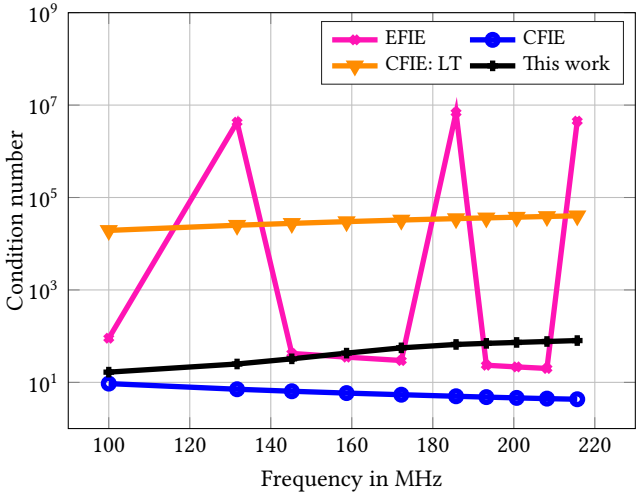


*(a)* The condition number as a function of the frequency. Average edge length $h = 0.2\,\text{m}$.

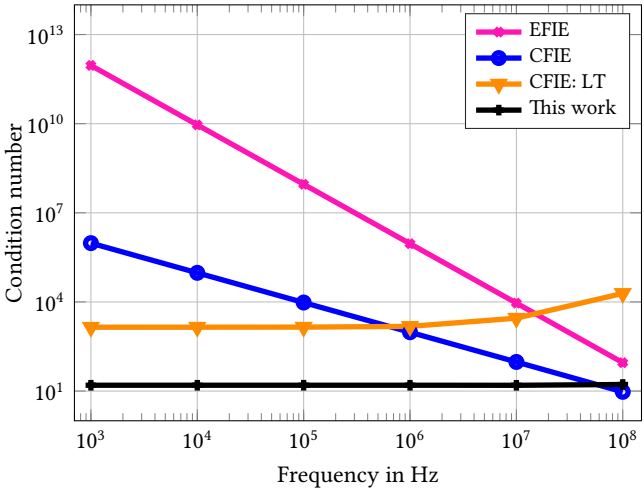


*(b)* The condition number as a function of the frequency. Average edge length $h = 0.2\,\text{m}$.

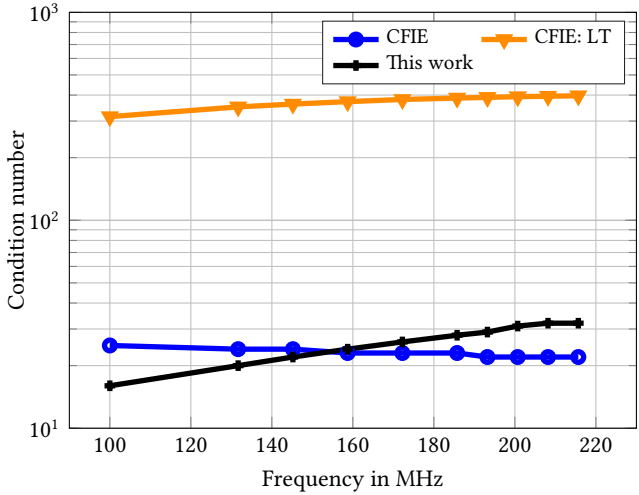


*(c)* The number of iterations as a function of the frequency. Average edge length $h = 0.2\,\mathrm{m}$. Plane wave excitation and GMRES method as solver for the unpreconditioned conforming CFIE and the loop-tree preconditioned conforming CFIE. Conjugate gradient method as solver for the new formulation.

*Fig. 9.1.:* Sphere: study of the impact of the frequency on the condition number and the number of iterations.

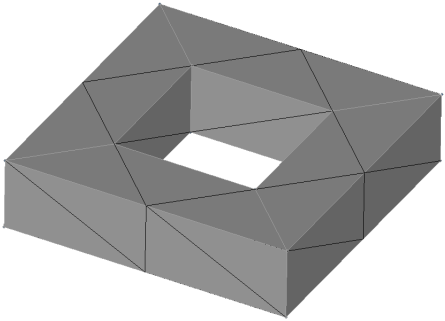

*(a)* The coarsest mesh, which was then dyadically refined. © IEEE 2016.

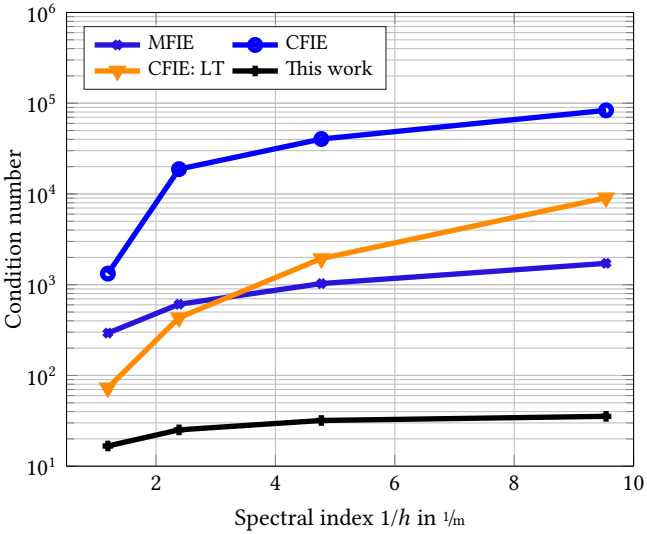


*(b)* The condition number as a function of the spectral index $1/h$. Frequency 1 MHz.

*Fig. 9.2.:* Toroidal structure

both cured. We observed, however, that the condition number starts to grow when the frequency is increased once a geometry dependent threshold is passed.

# Part IV.

# Finale

Chapter 10

# Concluding Scientific Postscript

> For small erections may be finished by their first architects; grand ones, true ones, ever leave the copestone to posterity.
>
> *Moby-Dick; or, The Whale*
> Herman Melville

Preconditioners for the EFIE and the CFIE based on hierarchical bases and on Calderón identities have been presented in this dissertation that sensibly advanced the state of the art: we have obtained preconditioned EFIEs and CFIEs where in the case of the hierarchical bases preconditioners the condition number is logarithmically bounded in the number of unknowns $N$ and where in the case of the RF-CMP preconditioner the condition number is bounded independently of $N$. Different from existing schemes, the results were obtained without the explicit use of dual basis functions. We did consider multiply connected geometries for both the hierarchical basis and the RF-CMP. The latter even yields an HPD system matrix, which allows to apply the CG method as solver, which, at least in theory, guarantees convergence.

A great German philosopher once said, "After the game, is before the game." While the presented preconditioners have already a certain degree of maturity, further work needs to be carried out to make them admissible for the usage in commercial software:

- In general, geometries are not necessarily Lipschitz polyhedral, for example, when they include T-junctions. The hierarchical basis needs extension to this scenario. The RF-CMP, is when it comes to the formulation, already applicable to structures with junctions since loop and star functions have

been defined on these structures before. It is, however, not clear how strong the preconditioning effect on a junction is. This needs careful evaluation and maybe further amendments.

- Often enough, we are also interested in solving scattering problems involving penetrable objects. The Poggio-Miller-Chang-Harrington-Wu-Tsai (PMCHWT) equation is due to the EFIE part of the operator ill-conditioned as well. Hierarchical basis preconditioners have been adapted to the PMCHWT [Guz+17]. In a next step, the RF-CMP should be extended to this equation.
- Many algebraic multigrid preconditioners have been presented in the past [Not; LB12; BOS15]. A study and comparison of the different methods would be desirable. Particular attention should be paid to the case of multi-body problems, where the null spaces are more complicated (as it was discussed in Section 4.d.$\alpha$). In addition, it would be desirable to have a (parallelized) algebraic multigrid solver at hand, developed under a liberal license both for commercial and academic use.

Further targets to tackle and questions to answer include:

- Throughout this thesis, it was assumed that the condition number of the RWG Gram matrix is reasonably large. What happens, however, if the RWG Gram matrix is highly ill-conditioned? To what degree can this problem be fixed?
- When the geometry is open, one observes for the Calderón preconditioner a growth of the condition number, which is of logarithmic nature. Even though this is not a critical issue, it would be interesting to obtain an optimal preconditioner for open problems.
- For non-linear problems, frequency domain methods cannot be used. Thus it would be desirable to extend the preconditioners to time-domain field integral equations.
- If the frequency is increased to the limit that $h \approx \lambda/10$, the number of iterations used by an iterative solver grows. Modified Calderón preconditioners have been presented to reduce this increase [BT14]. It should be possible to amend the RF-CMP in a similar way.

- It would be desirable to obtain a well-conditioned CFIE or CSIE that does not require dual basis functions.

Appendix A

# The Discretized Laplace-Beltrami and the Hypersingular Operator

In the following, we give a proof for the spectral equivalence of $\hat{\boldsymbol{W}}$ and $\hat{\boldsymbol{\Delta}}$ in the case that we have a nested sequence of piecewise linear function spaces.

**Proposition A.1.** *Let $X_{\lambda,j} \subset X_{\lambda,j+1}$, $j = 0, \dots, J-1$, denote a nested sequence of piecewise linear function spaces, $\lambda_i \in X_{\lambda,J}$, and $N_\mathrm{V} = \dim\left(X_{\lambda,J}\right)$ is the number of vertices of the mesh. Let $\hat{\boldsymbol{\Delta}}$ be the discretization of the modified Laplace-Beltrami operator $\hat{\Delta}_\Gamma$ with piecewise linear functions $\lambda_i \in X_{\lambda,J}$, that is,*

$$\left[\hat{\boldsymbol{\Delta}}\right]_{ij} = \left(\lambda_i, \hat{\Delta}_\Gamma \lambda_j\right)_{L^2(\Gamma)}. \tag{A.1}$$

*Then we have*

$$\boldsymbol{x}^\mathrm{T} \hat{\boldsymbol{\Delta}} \boldsymbol{x} \asymp \boldsymbol{x}^\mathrm{T} \hat{\boldsymbol{W}} \boldsymbol{G}_{\lambda\lambda}^{-1} \hat{\boldsymbol{W}} \boldsymbol{x}, \quad \forall \boldsymbol{x} \in \mathbb{R}^{N_\mathrm{V}}. \tag{A.2}$$

*Proof.* To prove this proposition, we leverage the stability results that Stevenson obtained for his three-point hierarchical wavelets [Ste98] (see also Chapter 7, where we have discussed the preconditioning effect of this basis). Let $\widehat{\boldsymbol{\lambda}}_\mathrm{T} \in \mathbb{R}^{N_\mathrm{V} \times N_\mathrm{V}}$ be the transformation matrix that maps from the three point hierarchical wavelets $\widehat{\lambda}_{\mathrm{T}i}$ to the piecewise linear basis $\lambda_i$. Then the following equivalences follow from [Ste98]:

$$\boldsymbol{x}^\mathrm{T} \widehat{\boldsymbol{\lambda}}_\mathrm{T}^\mathrm{T} \hat{\boldsymbol{\Delta}} \widehat{\boldsymbol{\lambda}}_\mathrm{T} \boldsymbol{x} \asymp \boldsymbol{x}^\mathrm{T} \hat{\boldsymbol{D}}^{+2} \widehat{\boldsymbol{\lambda}}_\mathrm{T}^\mathrm{T} \boldsymbol{G}_{\lambda\lambda} \widehat{\boldsymbol{\lambda}}_\mathrm{T} \hat{\boldsymbol{D}}^{+2} \boldsymbol{x}, \quad \forall \boldsymbol{x} \in \mathbb{R}^{N_\mathrm{V}}, \tag{A.3}$$

and

$$\boldsymbol{x}^\mathrm{T} \widehat{\boldsymbol{\lambda}}_\mathrm{T}^\mathrm{T} \hat{\boldsymbol{W}} \widehat{\boldsymbol{\lambda}}_\mathrm{T} \boldsymbol{x} \asymp \boldsymbol{x}^\mathrm{T} \hat{\boldsymbol{D}}^{+1} \widehat{\boldsymbol{\lambda}}_\mathrm{T}^\mathrm{T} \boldsymbol{G}_{\lambda\lambda} \widehat{\boldsymbol{\lambda}}_\mathrm{T} \hat{\boldsymbol{D}}^{+1} \boldsymbol{x}, \quad \forall \boldsymbol{x} \in \mathbb{R}^{N_\mathrm{V}}, \tag{A.4}$$

where

$$\left[\hat{\boldsymbol{D}}\right]_{ii} = 2^{\hat{l}_\Lambda(i)/2}, \quad i = 1, \dots, N_\mathrm{V} \tag{A.5}$$

and the function $\hat{l}_\Lambda(i)$ returns the level on which the function $\hat{\lambda}_{\mathrm{T}i}$ was defined. Equations (A.3) and (A.4) can be further simplified by considering that $\lambda_i$ are $L^2$-stable satisfying (8.71), and the $L^2$-stability of $\hat{\lambda}_{\mathrm{T}i}$ (properly rescaled by $\hat{\boldsymbol{D}}^{+2}$) can be expressed as

$$\boldsymbol{x}^{\mathrm{T}}\boldsymbol{x} \asymp \boldsymbol{x}^{\mathrm{T}}\hat{\boldsymbol{D}}^{+2}\widehat{\boldsymbol{\lambda}}_{\mathrm{T}}^{\mathrm{T}}\boldsymbol{G}_{\lambda\lambda}\widehat{\boldsymbol{\lambda}}_{\mathrm{T}}\hat{\boldsymbol{D}}^{+2}\boldsymbol{x} \asymp \boldsymbol{x}^{\mathrm{T}}\hat{\boldsymbol{D}}^{+2}\widehat{\boldsymbol{\lambda}}_{\mathrm{T}}^{\mathrm{T}}\widehat{\boldsymbol{\lambda}}_{\mathrm{T}}\hat{\boldsymbol{D}}^{+2}\boldsymbol{x}h^2\,, \quad \forall \boldsymbol{x} \in \mathbb{R}^{N_{\mathrm{V}}}, \tag{A.6}$$

where we assumed without loss of generality that $\left\|\widehat{\boldsymbol{\lambda}}_{\mathrm{T}}^{\mathrm{T}}\widehat{\boldsymbol{\lambda}}_{\mathrm{T}}\right\| \asymp 1$ (due to the definition we have used here, the functions $\hat{\lambda}_{\mathrm{T}i}$ are, if not rescaled at all, $H^1$-stable). Thus we find by substitution

$$\boldsymbol{x}^{\mathrm{T}}\widehat{\boldsymbol{\lambda}}_{\mathrm{T}}^{\mathrm{T}}\widehat{\boldsymbol{\lambda}}_{\mathrm{T}}\boldsymbol{x}h^2 \asymp \boldsymbol{x}^{\mathrm{T}}\hat{\boldsymbol{D}}^{-4}\boldsymbol{x}, \quad \forall \boldsymbol{x} \in \mathbb{R}^{N_{\mathrm{V}}}. \tag{A.7}$$

Since the matrices are invertible, we also have

$$\boldsymbol{x}^{\mathrm{T}}\widehat{\boldsymbol{\lambda}}_{\mathrm{T}}^{-1}\widehat{\boldsymbol{\lambda}}_{\mathrm{T}}^{-\mathrm{T}}\boldsymbol{x} \asymp \boldsymbol{x}^{\mathrm{T}}\hat{\boldsymbol{D}}^{4}\boldsymbol{x}h^2\,, \quad \forall \boldsymbol{x} \in \mathbb{R}^{N_{\mathrm{V}}}. \tag{A.8}$$

Using (A.6) in (A.3) and (A.4), we find

$$\boldsymbol{x}^{\mathrm{T}}\widehat{\boldsymbol{\lambda}}_{\mathrm{T}}^{\mathrm{T}}\hat{\boldsymbol{\Delta}}\widehat{\boldsymbol{\lambda}}_{\mathrm{T}}\boldsymbol{x} \asymp \boldsymbol{x}^{\mathrm{T}}\boldsymbol{x}\,, \quad \forall \boldsymbol{x} \in \mathbb{R}^{N_{\mathrm{V}}}\,, \tag{A.9}$$

and

$$\boldsymbol{x}^{\mathrm{T}}\widehat{\boldsymbol{\lambda}}_{\mathrm{T}}^{\mathrm{T}}\hat{\boldsymbol{W}}\widehat{\boldsymbol{\lambda}}_{\mathrm{T}}\boldsymbol{x} \asymp \boldsymbol{x}^{\mathrm{T}}\hat{\boldsymbol{D}}^{-2}\boldsymbol{x}\,, \quad \forall \boldsymbol{x} \in \mathbb{R}^{N_{\mathrm{V}}}\,. \tag{A.10}$$

By using the substitution $\boldsymbol{y} = \widehat{\boldsymbol{\lambda}}_{\mathrm{T}}\boldsymbol{x}$ in (A.9) and (A.10), we obtain

$$\boldsymbol{x}^{\mathrm{T}}\hat{\boldsymbol{\Delta}}\boldsymbol{x} \asymp \boldsymbol{x}^{\mathrm{T}}\widehat{\boldsymbol{\lambda}}_{\mathrm{T}}^{-\mathrm{T}}\widehat{\boldsymbol{\lambda}}_{\mathrm{T}}^{-1}\boldsymbol{x}\,, \quad \forall \boldsymbol{x} \in \mathbb{R}^{N_{\mathrm{V}}}\,, \tag{A.11}$$

and

$$\boldsymbol{x}^{\mathrm{T}}\hat{\boldsymbol{W}}\boldsymbol{x} \asymp \boldsymbol{x}^{\mathrm{T}}\widehat{\boldsymbol{\lambda}}_{\mathrm{T}}^{-\mathrm{T}}\hat{\boldsymbol{D}}^{-2}\widehat{\boldsymbol{\lambda}}_{\mathrm{T}}^{-1}\boldsymbol{x}\,, \quad \forall \boldsymbol{x} \in \mathbb{R}^{N_{\mathrm{V}}}\,. \tag{A.12}$$

Summarizing, we obtain the spectral equivalence

$$\begin{aligned}
\boldsymbol{x}^{\mathrm{T}}\hat{\boldsymbol{W}}\boldsymbol{G}_{\lambda\lambda}^{-1}\hat{\boldsymbol{W}}\boldsymbol{x} &\overset{(8.71)}{\asymp} \boldsymbol{x}^{\mathrm{T}}\hat{\boldsymbol{W}}^2\boldsymbol{x}/h^2 \\
&\overset{(A.12)}{\asymp} \boldsymbol{x}^{\mathrm{T}}\left(\widehat{\boldsymbol{\lambda}}_{\mathrm{T}}^{-\mathrm{T}}\hat{\boldsymbol{D}}^{-2}\widehat{\boldsymbol{\lambda}}_{\mathrm{T}}^{-1}h^2\right)^2\boldsymbol{x}/h^2 \\
&\asymp \boldsymbol{x}^{\mathrm{T}}\widehat{\boldsymbol{\lambda}}_{\mathrm{T}}^{-\mathrm{T}}\hat{\boldsymbol{D}}^{-2}\widehat{\boldsymbol{\lambda}}_{\mathrm{T}}^{-1}\widehat{\boldsymbol{\lambda}}_{\mathrm{T}}^{-\mathrm{T}}\hat{\boldsymbol{D}}^{4}h^2\hat{\boldsymbol{D}}^{-2}\widehat{\boldsymbol{\lambda}}_{\mathrm{T}}^{-1}\boldsymbol{x}/h^2 \\
&\overset{(A.8)}{\asymp} \boldsymbol{x}^{\mathrm{T}}\widehat{\boldsymbol{\lambda}}_{\mathrm{T}}^{-\mathrm{T}}\widehat{\boldsymbol{\lambda}}_{\mathrm{T}}^{-1}\boldsymbol{x} \asymp \boldsymbol{x}^{\mathrm{T}}\hat{\boldsymbol{\Delta}}\boldsymbol{x}\,, \quad \forall \boldsymbol{x} \in \mathbb{R}^{N_{\mathrm{V}}}\,.
\end{aligned} \tag{A.13}$$

□

# Nomenclature

## List of Variables and Other Mathematical Symbols

The following list summarizes frequently used variables and mathematical symbols.

| Symbol | Description |
|---|---|
| *Accents and Operations* | |
| $\widehat{\phantom{x}}$ | The wide hat symbols denotes the involvement of a hierarchical basis |
| $\hat{\phantom{x}}$ | The standard hat denotes a unit vector, or that a null space of an operator has been deflected |
| $\widetilde{\phantom{x}}$ | The wide tilde denotes the involvement of dual basis functions |
| $\boldsymbol{A}^{-1}$ | Inverse of the matrix $\boldsymbol{A}$ (if it exists) |
| $\boldsymbol{A}^{+}$ | Moore-Penrose pseudo-inverse of the matrix $\boldsymbol{A}$ |
| $\boldsymbol{A}^{\mathrm{T}}$ | Transpose of the matrix $\boldsymbol{A}$ |
| $\overline{\boldsymbol{A}}$, $\overline{u(\boldsymbol{r})}$ | Conjugate of the matrix $\boldsymbol{A}$ or the function $u$, respectively |
| $\boldsymbol{A}^{\dagger}$ | $\left(\overline{\boldsymbol{A}}\right)^{\mathrm{T}}$ |
| $\boldsymbol{A}^{-\mathrm{T}}$ | $\left(\boldsymbol{A}^{-1}\right)^{\mathrm{T}}$ |
| $\boldsymbol{I}$ | Unit matrix |
| *Physical Quantities* | |
| $\boldsymbol{r}$, $\boldsymbol{r}'$ | Position vectors, defined in (2.2) |
| $\hat{\boldsymbol{n}}$ | Surface normal unit vector directed to the exterior |
| $\varepsilon$ | Permittivity |
| $\mu$ | Permeability |
| $\varepsilon_0$ | Permittivity of vacuum |
| $\mu_0$ | Permeability of vacuum |
| $\varepsilon_{\mathrm{r}}$ | Relative permittivity |

| | |
|---|---|
| $\mu_\mathrm{r}$ | Relative permeability |
| $k$ | Wavenumber |
| $f$ | Frequency |
| $\eta$ | Wave impedance |
| $\omega$ | Angulary frequency |
| $\boldsymbol{j}$ | Electric current density |
| $\boldsymbol{m}$ | Magnetic current density |
| $\rho_\mathrm{e}$ | Electric charge density |
| $\rho_\mathrm{m}$ | Magnetic charge density |
| $\boldsymbol{E}$ | Electric field |
| $\boldsymbol{H}$ | Magnetic field |
| $\boldsymbol{D}$ | Electric flux density |
| $\boldsymbol{B}$ | Magnetic flux density |
| $G^k(\boldsymbol{r}, \boldsymbol{r'})$ | Green's function, see (3.51) |

*Vector Spaces and Sets*

| | |
|---|---|
| $\mathbb{B}_r^d(\boldsymbol{r})$ | Ball with radius $r$ centered at $\boldsymbol{r}$, see Definition 2.3 |
| $\Omega$ | Denotes a domain in $\mathbb{R}^3$ |
| $\Gamma$ | Boundary of $\Omega$ |
| $\overline{\Omega}$ | Closure of $\Omega$ |
| $\Omega^\mathrm{c}$ | Complement of $\Omega$ |
| supp $u$ | Support of the function $u$, defined in (2.48) |
| $C^k(\Omega)$ | Space of functions with $k$ continuous derivatives, norm defined in (2.4) |
| $L^p(\Omega)$ | Space of Lebesgue integral functions, see (2.50) |
| $L^2(\Omega)$ | Space of square integral functions, see (2.51) |
| $L^1_\mathrm{loc}(\Omega)$ | Locally integrable functions, defined in (2.52) |
| $\mathcal{D}(\Omega)$ | Space of test functions, defined in (2.49) |
| $\mathcal{S}(\Omega)$ | Schwartʒ space, defined in Definition 2.16 |
| $V'$ | Dual space of $V$, see Definition 2.13 |
| $H^s(\mathbb{R}^d)$ | Sobolev space, see Definition 2.17 |
| $H^s(\Omega)$ | Sobolev space, defined in (2.69) |
| $X_f$ | Finite element space spanned by the functions $f_n$ |
| $L^2(\Gamma)$ | Space of square integrable functions on a surface, see also (2.80) |
| $H^s(\Gamma)$ | Sobolev space on a surface, see also (2.81) |

| | |
|---|---|
| $\boldsymbol{H}^s(\Gamma)$ | Sobolev space of vector functions on a surface, defined in Equation (2.82) |
| $\boldsymbol{L}^2(\Gamma)$ | See (2.84) |
| $\boldsymbol{H}^s(\mathrm{div}_\Gamma, \Gamma)$ | See (2.90) |
| $\boldsymbol{H}^s(\mathrm{curl}_\Gamma, \Gamma)$ | See (2.91) |

*Operators*

| | |
|---|---|
| $\mathrm{D}^{\boldsymbol{\alpha}}$ | Derivative operator, see (2.1) |
| $\mathrm{grad}_\Gamma$ | Surface gradient, see Definition 2.5 |
| $\mathrm{curl}_\Gamma$ | Surface curl, defined in Definition 2.6 |
| $\Delta_\Gamma$ | Laplace-Beltrami operator, see Definition 2.7 |
| $\mathrm{div}_\Gamma$ | Surface divergence, see Definition 2.9 |
| $\mathbf{curl}_\Gamma$ | Surfacic curl, see Definition 2.10 |
| $\boldsymbol{\mathcal{T}}$ | EFIE operator, defined in (3.61) |
| $\boldsymbol{\mathcal{T}}_{\mathrm{A}}$ | Vector potential operator, defined in (3.62) |
| $\boldsymbol{\mathcal{T}}_{\Phi}$ | Scalar potential operator, defined in (3.64) |
| $\boldsymbol{\mathcal{M}}$ | MFIE operator, defined in (3.74) |
| $\boldsymbol{\mathcal{C}}$ | CFIE operator, defined in (3.78) |
| $\boldsymbol{\mathcal{K}}$ | Defined in (3.60) |
| $\boldsymbol{\mathcal{I}}, \mathcal{I}$ | Identity operators (vector and scalar functions) |
| $\mathcal{V}$ | Single layer operator, defined in (3.84) |
| $\mathcal{W}$ | Hypersingular operator (3.87) |

*Matrices*

| | |
|---|---|
| $\boldsymbol{G}_{fg}$ | Gram matrix of $f_n$ and $g_n$ functions |
| $\boldsymbol{T}^k$ | $\boldsymbol{\mathcal{T}}$ operator discretized with RWG functions, see (4.20) |
| $\boldsymbol{T}_{\mathrm{A}}^k$ | $\boldsymbol{\mathcal{T}}_{\mathrm{A}}$ discretized with RWG functions, defined (4.22) |
| $\boldsymbol{T}_{\Phi}^k$ | $\boldsymbol{\mathcal{T}}_{\Phi}$ discretized with RWG functions, defined in (4.24) |
| $\boldsymbol{e}$ | $\hat{\boldsymbol{n}} \times \boldsymbol{E}^{\mathrm{i}}$ discretized, defined in (4.25) |
| $\boldsymbol{j}$ | Unknown vector, see (4.19) |
| $\boldsymbol{M}$ | Discretized $\boldsymbol{\mathcal{M}}$ operator, defined in (4.28) |
| $\boldsymbol{h}$ | $\hat{\boldsymbol{n}} \times \boldsymbol{H}^{\mathrm{i}}$ discretized, defined in (4.32) |
| $\widetilde{\boldsymbol{M}}$ | Discretized $\boldsymbol{\mathcal{M}}$ operator, tested with rotated dual functions, defined in (4.34) |
| $\tilde{\boldsymbol{h}}$ | $\hat{\boldsymbol{n}} \times \boldsymbol{H}^{\mathrm{i}}$ discretized, defined in (4.38) |
| $\boldsymbol{C}$ | Standard CFIE system matrix, defined in (4.40) |

| | |
|---|---|
| $\widetilde{\boldsymbol{C}}$ | Conforming CFIE system matrix, defined in (4.42) |
| $\boldsymbol{V}$ | Discretized $\mathcal{V}$ operator, defined in (4.43) |
| $\boldsymbol{W}$ | Discretized $\mathcal{W}$ operator, defined in (4.44) |
| $\boldsymbol{\Delta}$ | Discretized $\Delta_\Gamma$ operator, defined in (8.4) |
| $\widetilde{\boldsymbol{\Delta}}$ | Discretized $\Delta_\Gamma$ operator with dual basis functions, defined in (8.5) |
| $\mathbf{1}_\Lambda$ | All-one vector, defined in (4.74) |
| $\mathbf{1}_\Sigma$ | All-one vector, defined in (4.75) |
| $\boldsymbol{\Lambda}$ | Loop transformation matrix, defined in (4.66) |
| $\boldsymbol{\Sigma}$ | Star transformation matrix, defined in (4.67) |
| $\boldsymbol{H}$ | Globel loop transformation matrix |
| $\boldsymbol{P}_\Lambda$ | Projector to solenoidal Helmholtz subspace, defined in (4.76) |
| $\boldsymbol{P}_\Sigma$ | Projector to non-solenoidal Helmholtz subspace, defined in (4.77) |
| $\boldsymbol{P}_\mathrm{H}$ | Projector to quasi-harmonic Helmholtz subspace, defined in (4.78) |
| $\boldsymbol{Q}$ | Loop-star transformation matrix, defined in (4.68) |
| $\boldsymbol{P}$ | Helmholtz projector based preconditioner, see (4.85) |
| $\widehat{\boldsymbol{\Lambda}}$ | Transformation matrix of a solenoidal hierarchical basis. Definition varies from chapter to chapter. |
| $\widehat{\boldsymbol{\Sigma}}$ | Transformation matrix of a non-solenoidal hierarchical basis. Definition varies from chapter to chapter. |

*Basis functions*

| | |
|---|---|
| $p_n$ | Piecewise constant functions, defined in (4.14) |
| $\lambda_n$ | Piecewise linear functions, defined in (4.15) |
| $\boldsymbol{f}_n$ | Rao-Wilton-Glisson (RWG) functions, defined in (4.16) |
| $\tilde{\boldsymbol{f}}_n$ | Functions dual to the RWG functions, such as the BC functions |
| $\hat{p}_n$ | Dual piecewise constant functions, defined in (5.1) |
| $\hat{\lambda}_n$ | Buffa-Christiansen piecewise linear functions |

*Variables*

| | |
|---|---|
| $N$ | Number of unknowns |
| $N_\mathrm{C}$ | Number of cells of the mesh |
| $N_\mathrm{V}$ | Number of (inner) vertices of the mesh |
| $N_\Lambda$ | Number of linearly independent solenoidal functions, which can be formed with RWG functions |
| $N_\Sigma$ | Number of linearly independent non-solenoidal functions, which can be formed with RWG functions |

| | |
|---|---|
| $A_n$ | Area of the $n$th cell |
| $A_\Gamma$ | Area of the surface $\Gamma$ |
| $h$ | Average edge length of the mesh |
| $\alpha_C$ | CFIE parameter |

# Abbreviations

| | |
|---|---|
| ACA | adaptive cross approximation |
| BC | Buffa-Christiansen |
| CFIE | combined field integral equation |
| CG | conjugate gradient |
| CGS | conjugate gradient squared |
| CMP | Calderón multiplicative preconditioner |
| CSIE | combined source integral equation |
| CW | Chen-Wilton |
| EFIE | electric field integral equation |
| FDTD | finite difference time domain |
| FEM | finite element method |
| FIT | finite integration technique |
| GMRES | generalized minimal residual |
| HB-S | hierarchical basis for structured meshes |
| HB-U | hierarchical basis for unstructured meshes |
| HPD | Hermitian, positive definite |
| LBB | Ladyzhenskaya-Babuska-Brezzi |
| MFIE | magnetic field integral equation |
| MLFMM | multilevel fast multipole method |
| MLMDA | multilevel matrix decomposition algorithm |
| PEC | perfectly electrically conducting |
| PMCHWT | Poggio-Miller-Chang-Harrington-Wu-Tsai |
| RF-CMP | refinement-free Calderón multiplicative preconditioner |
| RWG | Rao-Wilton-Glisson |
| SAI | sparse approximate inverse |
| SPD | symmetric, positive definite |
| SVD | singular value decomposition |
| TLM | transmission line matrix method |

# Bibliography


[AAE14a] S. B. Adrian, F. P. Andriulli, and T. F. Eibert. "A Calderón Preconditioner for the EFIE Operator Without Barycentric Refinement of the Mesh". In: *IEEE International Symposium on Antennas and Propagation*. Memphis, USA: IEEE, July 2014, pp. 2180–2181 (cit. on p. 127).

[AAE14b] S. B. Adrian, F. P. Andriulli, and T. F. Eibert. "Hierarchical Bases Preconditioners for the Electric Field Integral Equation on Multiply Connected Geometries". In: *IEEE Transactions on Antennas and Propagation* 62.11 (Nov. 2014), pp. 5856–5861. © 2014 IEEE (cit. on pp. 93, 128).

[AAE15] S. B. Adrian, F. P. Andriulli, and T. F. Eibert. "A Hermitian and Well-Conditioned EFIE for Fast Iterative and Direct Solvers". In: *IEEE Antennas and Propagation International Symposium*. Vancouver, Canada, July 2015, pp. 742–743 (cit. on p. 127).

[AAE16a] S. B. Adrian, F. P. Andriulli, and T. F. Eibert. "A Well-Conditioned, Hermitian, Positive Definite, Combined Field Integral Equation for Simply and Multiply Connected Geometries". In: *URSI International Symposium on Electromagnetic Theory (EMTS)*. Espoo, Finland: IEEE, Aug. 2016, pp. 561–564. © 2016 IEEE (cit. on p. 163).

[AAE16b] S. B. Adrian, F. P. Andriulli, and T. F. Eibert. "On the Hierarchical Preconditioning of the Combined Field Integral Equation". In: *IEEE Antennas and Wireless Propagation Letters* 15 (2016), pp. 1897–1900. © 2016 IEEE (cit. on p. 111).

[AAE17] S. B. Adrian, F. P. Andriulli, and T. F. Eibert. "A Hierarchical Preconditioner for the Electric Field Integral Equation on Unstructured Meshes Based on Primal and Dual Haar Bases". In: *Journal of Com-*

*putational Physics* 330 (Feb. 2017), pp. 365–379 (cit. on pp. 65, 93, 95, 112).

[AC04] R. Adams and N. Champagne. "A Numerical Implementation of a Modified Form of the Electric Field Integral Equation". In: *IEEE Transactions on Antennas and Propagation* 52.9 (Sept. 2004), pp. 2262–2266 (cit. on p. 10).

[Ada04] R. Adams. "Physical and Analytical Properties of a Stabilized Electric Field Integral Equation". In: *IEEE Transactions on Antennas and Propagation* 52.2 (Feb. 2004), pp. 362–372 (cit. on pp. 10, 127).

[AEA13] S. B. Adrian, T. F. Eibert, and F. P. Andriulli. "Hierarchical Bases Regularizations of the EFIE Without the Search for Global Loops". In: *IEEE International Symposium on Antennas and Propagation*. Orlando, USA, July 2013 (cit. on p. 96).

[AK01] O. Axelsson and I. Kaporin. "Error Norm Estimation and Stopping Criteria in Preconditioned Conjugate Gradient Iterations". In: *Numerical Linear Algebra with Applications* 8.4 (2001), pp. 265–286 (cit. on pp. 7, 55).

[Ala+03] G. Ala, M. Di Silvestre, E. Francomano, and A. Tortorici. "An Advanced Numerical Model in Solving Thin-Wire Integral Equations by Using Semi-Orthogonal Compactly Supported Spline Wavelets". In: *IEEE Transactions on Electromagnetic Compatibility* 45.2 (May 2003), pp. 218–228 (cit. on p. 11).

[Alp+93] B. Alpert, G. Beylkin, R. Coifman, and V. Rokhlin. "Wavelet-like Bases for the Fast Solution of Second-Kind Integral Equations". In: *SIAM Journal on Scientific Computing* 14.1 (1993), pp. 159–184 (cit. on p. 11).

[And+05] F. Andriulli, G. Vecchi, F. Vipiana, P. Pirinoli, and A. Tabacco. "Optimal a Priori Clipping Estimation for Wavelet-Based Method of Moments Matrices". In: *IEEE Transactions on Antennas and Propagation* 53.11 (Nov. 2005), pp. 3726–3734 (cit. on p. 11).

[And+08] F. P. Andriulli, K. Cools, H. Bagci, F. Olyslager, A. Buffa, S. Christiansen, and E. Michielssen. "A Multiplicative Calderon Preconditioner for the Electric Field Integral Equation". In: *IEEE Transactions on Antennas and Propagation* 56.8 (Aug. 2008), pp. 2398–2412 (cit. on pp. 11, 127, 128).

[And+12] F. P. Andriulli, K. Cools, I. Bogaert, H. Bagci, P. Yla-Ojiala, and E. Michielssen. "Analysis and Discretization of the Yukawa-Calderon Preconditioned CFIE". In: *28th Annual Review of Progress in Applied Computational Electromagnetics*. Curran Associates, Inc., 2012, pp. 454–463 (cit. on p. 163).

[And+13] F. P. Andriulli, K. Cools, I. Bogaert, and E. Michielssen. "On a Well-Conditioned Electric Field Integral Operator for Multiply Connected Geometries". In: *IEEE Transactions on Antennas and Propagation* 61.4 (Apr. 2013), pp. 2077–2087 (cit. on pp. 9, 60–62, 96, 99, 118, 128, 129, 131, 132, 150).

[And12a] F. Andriulli. "Loop-Star and Loop-Tree Decompositions: Analysis and Efficient Algorithms". In: *IEEE Transactions on Antennas and Propagation* 60.5 (May 2012), pp. 2347–2356 (cit. on pp. 9, 13, 60, 67, 94, 96, 113–115, 128, 130, 134, 139, 141).

[And12b] F. P. Andriulli. "Hierarchical EM Preconditioners with Spectral Domain Partitioning". In: *6th European Conference on Antennas and Propagation (EUCAP)*. Mar. 2012, pp. 296–298 (cit. on pp. 66, 102).

[Art13] J. W. Arthur. "The Evolution of Maxwell's Equations from 1862 to the Present Day". In: *IEEE Antennas and Propagation Magazine* 55.3 (2013), pp. 61–81 (cit. on p. 3).

[ATV07] F. P. Andriulli, A. Tabacco, and G. Vecchi. "A Multiresolution Approach to the Electric Field Integral Equation in Antenna Problems". In: *SIAM Journal on Scientific Computing* 29.1 (Jan. 2007), pp. 1–21 (cit. on pp. 12, 66, 93, 95).

[ATV10] F. P. Andriulli, A. Tabacco, and G. Vecchi. "Solving the EFIE at Low Frequencies with a Conditioning That Grows Only Logarithmically with the Number of Unknowns". In: *IEEE Transactions on Antennas and Propagation* 58.5 (May 2010), pp. 1614–1624 (cit. on pp. 12, 13, 56, 59, 66, 83–86, 93, 95, 102, 111–114).

[AVV08] F. P. Andriulli, F. Vipiana, and G. Vecchi. "Hierarchical Bases for Nonhierarchic 3-D Triangular Meshes". In: *IEEE Transactions on Antennas and Propagation* 56.8 (Aug. 2008), pp. 2288–2297 (cit. on pp. 12, 13, 66, 67, 93, 95, 112).

[Bab71] I. Babuška. "Error-Bounds for Finite Element Method". In: *Numerische Mathematik* 16.4 (Jan. 1971), pp. 322–333 (cit. on pp. 46, 47).

[Bag+09] H. Bagci, F. Andriulli, K. Cools, F. Olyslager, and E. Michielssen. "A Calderón Multiplicative Preconditioner for the Combined Field Integral Equation". In: *IEEE Transactions on Antennas and Propagation* 57.10 (Oct. 2009), pp. 3387–3392 (cit. on p. 163).

[BC01a] A. Buffa and P. Ciarlet. "On Traces for Functional Spaces Related to Maxwell's Equations Part I: An Integration by Parts Formula in Lipschitz Polyhedra". In: *Mathematical Methods in the Applied Sciences* 24.1 (Jan. 2001), pp. 9–30 (cit. on pp. 18, 40).

[BC01b] A. Buffa and P. Ciarlet. "On Traces for Functional Spaces Related to Maxwell's Equations Part II: Hodge Decompositions on the Boundary of Lipschitz Polyhedra and Applications". In: *Mathematical Methods in the Applied Sciences* 24.1 (Jan. 2001), pp. 31–48 (cit. on pp. 18, 40).

[BC07] A. Buffa and S. H. Christiansen. "A Dual Finite Element Complex on the Barycentric Refinement". In: *Mathematics of Computation* 76.260 (Oct. 2007), pp. 1743–1770 (cit. on pp. 11, 49, 127, 129, 131, 149, 150).

[BCP13] M. M. Bibby, C. M. Coldwell, and A. F. Peterson. "A High Order Numerical Investigation of Electromagnetic Scattering From a Torus and a Circular Loop". In: *IEEE Transactions on Antennas and Propagation* 61.7 (July 2013), pp. 3656–3661 (cit. on p. 3).

[BCS02a] A. Buffa, M. Costabel, and C. Schwab. "Boundary Element Methods for Maxwell's Equations on Non-Smooth Domains". In: *Numerische Mathematik* 92.4 (Oct. 2002), pp. 679–710 (cit. on p. 40).

[BCS02b] A. Buffa, M. Costabel, and D. Sheen. "On Traces for $H(\mathrm{curl}, \Omega)$ in Lipschitz Domains". In: *Journal of Mathematical Analysis and Applications* 276.2 (Dec. 2002), pp. 845–867 (cit. on pp. 18, 40).

[Beb00] M. Bebendorf. "Approximation of Boundary Element Matrices". In: *Numerische Mathematik* 86.4 (2000), pp. 565–589 (cit. on p. 5).

[Beg+13] Y. Beghein, K. Cools, H. Bagci, and D. De Zutter. "A Space-Time Mixed Galerkin Marching-on-in-Time Scheme for the Time-Domain Combined Field Integral Equation". In: *IEEE Transactions on Antennas and Propagation* 61.3 (Mar. 2013), pp. 1228–1238 (cit. on p. 53).

[Ben02] M. Benzi. "Preconditioning Techniques for Large Linear Systems: A Survey". In: *Journal of Computational Physics* 182.2 (Nov. 2002), pp. 418–477 (cit. on p. 9).

[Ber94] J.-P. Berenger. "A Perfectly Matched Layer for the Absorption of Electromagnetic Waves". In: *Journal of Computational Physics* 114.2 (Oct. 1994), pp. 185–200 (cit. on p. 4).

[BH03] A. Buffa and R. Hiptmair. "Galerkin Boundary Element Methods for Electromagnetic Scattering". In: *Topics in Computational Wave Propagation.* Ed. by T. J. Barth et al. Vol. 31. Berlin, Heidelberg: Springer Berlin Heidelberg, 2003, pp. 83–124 (cit. on pp. 40, 41, 51).

[BH04] A. Buffa and R. Hiptmair. "A Coercive Combined Field Integral Equation for Electromagnetic Scattering". In: *SIAM Journal on Numerical Analysis* 42.2 (Jan. 2004), pp. 621–640 (cit. on p. 41).

[BK95] M. Burton and S. Kashyap. "A Study of a Recent, Moment-Method Algorithm That Is Accurate to Very Low Frequencies". In: *Applied Computational Electromagnetics Society Journal* 10.3 (1995), pp. 58–68 (cit. on pp. 9, 57, 65, 96).

[BLA05] S. Borel, D. Levadoux, and F. Alouges. "A New Well-Conditioned Integral Formulation for Maxwell Equations in Three Dimensions". In: *IEEE Transactions on Antennas and Propagation* 53.9 (Sept. 2005), pp. 2995–3004 (cit. on p. 11).

[BLB14] Y. Brick, V. Lomakin, and A. Boag. "Fast Direct Solver for Essentially Convex Scatterers Using Multilevel Non-Uniform Grids". In: *IEEE Transactions on Antennas and Propagation* 62.8 (Aug. 2014), pp. 4314–4324 (cit. on p. 7).

[Bog+11] I. Bogaert, K. Cools, F. Andriulli, J. Peeters, and D. De Zutter. "Low Frequency Stability of the Mixed Discretization of the MFIE". In: *Proceedings of the 5th European Conference on Antennas and Propagation (EUCAP)*. Apr. 2011, pp. 2463–2465 (cit. on pp. 14, 56, 115, 120, 164).

[BOS15] W. N. Bell, L. N. Olson, and J. B. Schroder. "PyAMG: Algebraic Multigrid Solvers in Python v3.0". In: (2015) (cit. on p. 174).

[BR03] M. Bebendorf and S. Rjasanow. "Adaptive Low-Rank Approximation of Collocation Matrices". In: *Computing* 70.1 (Feb. 2003), pp. 1–24 (cit. on p. 5).

[Bra+00] H. Braunisch, Y. Zhang, C. Ao, S.-E. Shih, Y. Yang, K.-H. Ding, J. Kong, and L. Tsang. "Tapered Wave with Dominant Polarization State for All Angles of Incidence". In: *IEEE Transactions on Antennas and Propagation* 48.7 (July 2000), pp. 1086–1096 (cit. on p. 8).

[Bre74] F. Brezzi. "On the Existence, Uniqueness and Approximation of Saddle-Point Problems Arising from Lagrangian Multipliers". In: *Revue française d'automatique, informatique, recherche opérationnelle. Analyse numérique* 8.R2 (1974), pp. 129–151 (cit. on pp. 46, 47).

[Bro+08] I. N. Bronštejn, K. A. Semendjaev, G. Musiol, H. Mühlig, and I. N. Bronstein, eds. *Taschenbuch der Mathematik*. 7., vollst. überarb. und erg. Aufl. Frankfurt am Main: Deutsch, 2008 (cit. on pp. 20, 36).

[Bru+09] O. Bruno, T. Elling, R. Paffenroth, and C. Turc. "Electromagnetic Integral Equations Requiring Small Numbers of Krylov-Subspace Iterations". In: *Journal of Computational Physics* 228.17 (Sept. 2009), pp. 6169–6183 (cit. on p. 11).

[BS97] I. M. Babuška and S. A. Sauter. "Is the Pollution Effect of the FEM Avoidable for the Helmholtz Equation Considering High Wave Numbers?" In: *SIAM Journal on Numerical Analysis* 34.6 (Dec. 1997), pp. 2392–2423 (cit. on p. 4).

[BSJ05] W. Bandlow, G. Schneider, and A. Jacob. "Vector-Valued Wavelets with Triangular Support for Method of Moments Applications". In: *IEEE Transactions on Antennas and Propagation* 53.10 (Oct. 2005), pp. 3340–3346 (cit. on p. 12).

[BT14] Y. Boubendir and C. Turc. "Well-Conditioned Boundary Integral Equation Formulations for the Solution of High-Frequency Electromagnetic Scattering Problems". In: *Computers & Mathematics with Applications* 67.10 (June 2014), pp. 1772–1805 (cit. on p. 174).

[BT80] A. Bayliss and E. Turkel. "Radiation Boundary Conditions for Wave-like Equations". In: *Communications on Pure and Applied Mathematics* 33.6 (Nov. 1980), pp. 707–725 (cit. on p. 4).

[Buf01] A. Buffa. "Hodge Decompositions on the Boundary of Nonsmooth Domains: The Multi-Connected Case". In: *Mathematical Models and Methods in Applied Sciences* 11.09 (Dec. 2001), pp. 1491–1503 (cit. on p. 40).

[Buf03] A. Buffa. "Trace Theorems on Non-Smooth Boundaries for Functional Spaces Related to Maxwell Equations: An Overview". In: *Computational Electromagnetics*. Springer, 2003, pp. 23–34 (cit. on pp. 18, 40).

[BW65] H. Brakhage and P. Werner. "Über das dirichletsche Außenraumproblem für die Helmholtzsche Schwingungsgleichung". In: *Archiv der Mathematik* 16.1 (1965), pp. 325–329 (cit. on pp. 6, 41).

[Car+05] B. Carpentieri, I. S. Duff, L. Giraud, and G. Sylvand. "Combining Fast Multipole Techniques and an Approximate Inverse Preconditioner for Large Electromagnetism Calculations". In: *SIAM Journal on Scientific Computing* 27.3 (Jan. 2005), pp. 774–792 (cit. on p. 10).

[Car09] B. Carpentieri. "Algebraic Preconditioners for the Fast Multipole Method in Electromagnetic Scattering Analysis from Large Structures: Trends and Problems". In: *Electronic Journal of Boundary Elements* 7.1 (Mar. 2009) (cit. on p. 9).

[CB12] B. Carpentieri and M. Bollhöfer. "Symmetric Inverse-Based Multilevel ILU Preconditioning for Solving Dense Complex Non-Hermitian Systems in Electromagnetics". In: *Progress In Electromagnetics Research* 128 (2012), pp. 55–74 (cit. on p. 10).

[CDG00] B. Carpentieri, I. Duff, and L. Giraud. "Experiments with Sparse Preconditioning of Dense Problems from Electromagnetic Applications". In: *CERFACS, Toulouse, France, Tech. Rep. TR/PA/00/04* (2000) (cit. on p. 9).

[Ces96] M. Cessenat. *Mathematical Methods in Electromagnetism: Linear Theory and Applications*. Series on advances in mathematics for applied sciences v. 41. Singapore ; River Edge, NJ: World Scientific, 1996 (cit. on p. 94).

[Che+01] S. Y. Chen, W. C. Chew, J. M. Song, and J.-S. Zhao. "Analysis of Low Frequency Scattering from Penetrable Scatterers". In: *IEEE Transactions on Geoscience and Remote Sensing* 39.4 (2001), pp. 726–735 (cit. on p. 10).

[Che+09] R.-S. Chen, J. Ding, D. Ding, Z. Fan, and D. Wang. "A Multiresolution Curvilinear Rao-Wilton-Glisson Basis Function for Fast Analysis of Electromagnetic Scattering". In: *IEEE Transactions on Antennas and Propagation* 57.10 (2009), pp. 3179–3188 (cit. on pp. 66, 93, 95).

[CN02] S. H. Christiansen and J.-C. Nédélec. "A Preconditioner for the Electric Field Integral Equation Based on Calderon Formulas". In: *SIAM Journal on Numerical Analysis* 40.3 (Jan. 2002), pp. 1100–1135 (cit. on pp. 10, 127, 129).

[Con+02] H. Contopanagos, B. Dembart, M. Epton, J. Ottusch, V. Rokhlin, J. Visher, and S. Wandzura. "Well-Conditioned Boundary Integral Equations for Three-Dimensional Electromagnetic Scattering". In: *IEEE Transactions on Antennas and Propagation* 50.12 (Dec. 2002), pp. 1824–1830 (cit. on pp. 10, 127).

[Coo+09] K. Cools, F. Andriulli, F. Olyslager, and E. Michielssen. "Nullspaces of MFIE and Calderón Preconditioned EFIE Operators Applied to Toroidal Surfaces". In: *IEEE Transactions on Antennas and Propagation* 57.10 (Oct. 2009), pp. 3205–3215 (cit. on pp. 57, 129).

[Coo+11] K. Cools, F. P. Andriulli, D. De Zutter, and E. Michielssen. "Accurate and Conforming Mixed Discretization of the MFIE". In: *IEEE Antennas and Wireless Propagation Letters* 10 (2011), pp. 528–531 (cit. on p. 51).

[Cos88] M. Costabel. "Boundary Integral Operators on Lipschitz Domains: Elementary Results". In: *SIAM Journal on Mathematical Analysis* 19.3 (May 1988), pp. 613–626 (cit. on pp. 18, 40).

[CRW93] R. Coifman, V. Rokhlin, and S. Wandzura. "The Fast Multipole Method for the Wave Equation: A Pedestrian Prescription". In: *IEEE Antennas and Propagation Magazine* 35.3 (June 1993), pp. 7–12 (cit. on p. 94).

[CW90] Q. Chen and D. Wilton. "Electromagnetic Scattering by Three-Dimensional Arbitrary Complex Material/Conducting Bodies". In: *IEEE Antennas and Propagation Society International Symposium*. Dallas, USA, 1990, pp. 590–593 (cit. on pp. 11, 49).

[Dah97] W. Dahmen. "Wavelet and Multiscale Methods for Operator Equations". In: *Acta Numerica* 6 (1997), pp. 55–228 (cit. on p. 11).

[Dar00] E. Darve. "The Fast Multipole Method: Numerical Implementation". In: *Journal of Computational Physics* 160.1 (May 2000), pp. 195–240 (cit. on p. 5).

[DFW13] T. K. Dey, F. Fan, and Y. Wang. "An Efficient Computation of Handle and Tunnel Loops via Reeb Graphs". In: *ACM Transactions on Graphics* 32.4 (July 2013), p. 1 (cit. on p. 94).

[DJC11] J. Ding, Z. Jiang, and R.-S. Chen. "Multiresolution Preconditioner Combined with Matrix Decomposition – Singular Value Decomposition Algorithm for Fast Analysis of Electromagnetic Scatterers with Dense Discretisations". In: *IET Microwaves, Antennas & Propagation* 5.11 (Aug. 2011), pp. 1351–1358 (cit. on p. 67).

[DS99] W. Dahmen and R. Stevenson. "Element-by-Element Construction of Wavelets Satisfying Stability and Moment Conditions". In: *SIAM Journal on Numerical Analysis* 37.1 (Jan. 1999), pp. 319–352 (cit. on p. 112).

[Dun85] D. A. Dunavant. "High Degree Efficient Symmetrical Gaussian Quadrature Rules for the Triangle". In: *International Journal for Numerical Methods in Engineering* 21.6 (June 1985), pp. 1129–1148 (cit. on p. 51).

[EH04] J. Erickson and S. Har-Peled. "Optimally Cutting a Surface into a Disk". In: *Discrete & Computational Geometry* 31.1 (2004), pp. 37–59 (cit. on p. 94).

[Eib03] T. Eibert. “Iterative Near-Zone Preconditioning of Iterative Method of Moments Electric Field Integral Equation Solutions”. In: *IEEE Antennas and Wireless Propagation Letters* 2.1 (2003), pp. 101–102 (cit. on p. 10).

[Eib04] T. Eibert. “Iterative-Solver Convergence for Loop-Star and Loop-Tree Decompositions in Method-of-Moments Solutions of the Electric-Field Integral Equation”. In: *IEEE Antennas and Propagation Magazine* 46.3 (June 2004), pp. 80–85 (cit. on p. 9).

[ES07] S. Engleder and O. Steinbach. “Modified Boundary Integral Formulations for the Helmholtz Equation”. In: *Journal of Mathematical Analysis and Applications* 331.1 (July 2007), pp. 396–407 (cit. on p. 41).

[FA07] A. Föppl and M. Abraham. *Einführung in die Maxwellsche Theorie der Elektrizität: mit einem einleitenden Abschnitte über das Rechnen mit Vektorgrössen in der Physik*. Vol. 1. Leipzig: B. G. Teubner, 1907 (cit. on p. 3).

[Fra+14] M. A. Francavilla, M. Righero, F. Vipiana, and G. Vecchi. “Applications of a Hierarchical Multiresolution Preconditioner to the CFIE”. In: *8th European Conference on Antennas and Propagation (EuCAP)*. The Hague, Netherlands, Apr. 2014 (cit. on pp. 111, 112).

[Gau14] C. F. Gauss. “Methodus nova integralium valores per approximationem inveniendi”. In: *Commentationes Societatis Regiae Scientiarum Gottingensis Recentiores* 3 (1814), pp. 39–76 (cit. on p. 51).

[GCC95] J. Goswami, A. Chan, and C. Chui. “On Solving First-Kind Integral Equations Using Wavelets on a Bounded Interval”. In: *IEEE Transactions on Antennas and Propagation* 43.6 (June 1995), pp. 614–622 (cit. on p. 11).

[Ger+06] A. Geranmayeh, R. Moini, S. Sadeghi, and A. Deihimi. “A Fast Wavelet-Based Moment Method for Solving Thin-Wire EFIE”. In: *IEEE Transactions on Magnetics* 42.4 (Apr. 2006), pp. 575–578 (cit. on p. 11).

[GHM13] H. Guo, J. Hu, and E. Michielssen. “On MLMDA/Butterfly Compressibility of Inverse Integral Operators”. In: *IEEE Antennas and Wireless Propagation Letters* 12 (2013), pp. 31–34 (cit. on p. 7).

[Gib14] W. C. Gibson. *The Method of Moments in Electromagnetics*. Second edition. Boca Raton: CRC Press/Taylor & Francis, 2014 (cit. on p. 39).

[GJM14] H. Guo, H. Jun, and E. Michielssen. "Investigation on the Butterfly Reconstruction Methods for MLMDA-Based Direct Integral Equation Solver". In: *IEEE International Symposium on Antennas and Propagation*. IEEE, July 2014, pp. 283–283 (cit. on p. 7).

[Gol13] G. H. Golub. *Matrix Computations*. 4th ed. Johns Hopkins Studies in the Mathematical Sciences. Baltimore: The Johns Hopkins University Press, 2013 (cit. on p. 82).

[GR87] L. Greengard and V. Rokhlin. "A Fast Algorithm for Particle Simulations". In: *Journal of Computational Physics* 73.2 (Dec. 1987), pp. 325–348 (cit. on p. 5).

[Gra93] R. Graglia. "On the Numerical Integration of the Linear Shape Functions Times the 3-D Green's Function or Its Gradient on a Plane Triangle". In: *IEEE Transactions on Antennas and Propagation* 41.10 (October 1993), pp. 1448–1455 (cit. on p. 51).

[Guo+16] H. Guo, Y. Liu, J. Hu, and E. Michielssen. "A Butterfly-Based Direct Integral Equation Solver Using Hierarchical LU Factorization for Analyzing Scattering from Electrically Large Conducting Objects". In: *arXiv preprint arXiv:1610.00042* (2016) (cit. on p. 7).

[Guz+17] J. E. O. Guzman, S. B. Adrian, R. Mitharwal, Y. Beghein, T. F. Eibert, K. Cools, and F. P. Andriulli. "On the Hierarchical Preconditioning of the PMCHWT Integral Equation on Simply and Multiply Connected Geometries". In: *IEEE Antennas and Wireless Propagation Letters* 16 (2017), pp. 1044–1047 (cit. on p. 174).

[Haa10] A. Haar. "Zur Theorie der orthogonalen Funktionensysteme: Erste Mitteilung". In: *Mathematische Annalen* 69.3 (Sept. 1910), pp. 331–371 (cit. on p. 11).

[Har01] R. F. Harrington. *Time-Harmonic Electromagnetic Fields*. IEEE Press Series on Electromagnetic Wave Theory. New York: IEEE Press : Wiley-Interscience, 2001 (cit. on pp. 5, 31, 33–36).

[Hea] O. Heaviside. *Electrical Papers*. London: Maximillan (cit. on p. 3).

[Hea93] O. Heaviside. *Electromagnetic Theory*. London: Electrician Publishers, 1893 (cit. on p. 3).

[Her84] H. Hertz. "Ueber die Beziehungen zwischen den Maxwell'schen electrodynamischen Grundgleichungen und den Grundgleichungen der gegnerischen Electrodynamik". In: *Annalen der Physik* 259.9 (1884), pp. 84–103 (cit. on p. 3).

[Her90] H. Hertz. "Ueber die Grundgleichungen der Electrodynamik für ruhende Körper". In: *Annalen der Physik* 276.8 (1890), pp. 577–624 (cit. on p. 3).

[HHT08] N. Hale, N. J. Higham, and L. N. Trefethen. "Computing $A^\alpha$, $\log(A)$, and Related Matrix Functions by Contour Integrals". In: *SIAM Journal on Numerical Analysis* 46.5 (Jan. 2008), pp. 2505–2523 (cit. on p. 118).

[Hip06] R. Hiptmair. "Operator Preconditioning". In: *Computers & Mathematics with Applications* 52.5 (Sept. 2006), pp. 699–706 (cit. on pp. 55, 78, 149).

[HK97] G. C. Hsiao and R. E. Kleinman. "Mathematical Foundations for Error Estimation in Numerical Solutions of Integral Equations in Electromagnetics". In: *IEEE Transactions on Antennas and Propagation* 45.3 (Mar. 1997), pp. 316–328 (cit. on p. 23).

[HKS05] H. Harbrecht, U. Kähler, and R. Schneider. "Wavelet Galerkin BEM on Unstructured Meshes". In: *Computing and Visualization in Science* 8.3-4 (2005), pp. 189–199 (cit. on pp. 68, 74).

[HM12] R. Hiptmair and S. Mao. "Stable Multilevel Splittings of Boundary Edge Element Spaces". In: *BIT Numerical Mathematics* 52.3 (Sept. 2012), pp. 661–685 (cit. on pp. 12, 66, 93).

[HN89] W. Hackbusch and Z. P. Nowak. "On the Fast Matrix Multiplication in the Boundary Element Method by Panel Clustering". In: *Numerische Mathematik* 54.4 (July 1989), pp. 463–491 (cit. on p. 5).

[Hoe85] W. Hoefer. "The Transmission-Line Matrix Method–Theory and Applications". In: *IEEE Transactions on Microwave Theory and Techniques* 33.10 (Oct. 1985), pp. 882–893 (cit. on p. 4).

[HS52] M. R. Hestenes and E. Stiefel. *Methods of Conjugate Gradients for Solving Linear Systems*. Vol. 49. Journal of Conjugate Gradients for Solving Linear Systems 6. NBS, 1952 (cit. on p. 7).

[JB71] P. Johns and R. Beurle. "Numerical Solution of 2-Dimensional Scattering Problems Using a Transmission-Line Matrix". In: *Proceedings of the Institution of Electrical Engineers* 118.9 (1971), p. 1203 (cit. on p. 4).

[Jin14] J.-M. Jin. *The Finite Element Method in Electromagnetics*. Third edition. Hoboken. New Jersey: John Wiley & Sons Inc, 2014 (cit. on p. 4).

[Jin15] J.-M. Jin. *Theory and Computation of Electromagnetic Fields*. Second edition. Hoboken, New Jersey: John Wiley & Sons, Inc, 2015 (cit. on p. 4).

[Kel62] J. B. Keller. "Geometrical Theory of Diffraction". In: *Journal of the Optical Society of America* 52.2 (Feb. 1962), p. 116 (cit. on p. 4).

[Kir10] R. C. Kirby. "From Functional Analysis to Iterative Methods". In: *SIAM Review* 52.2 (Jan. 2010), pp. 269–293 (cit. on p. 56).

[KK98] G. Karypis and V. Kumar. "A Fast and High Quality Multilevel Scheme for Partitioning Irregular Graphs". In: *SIAM Journal on Scientific Computing* 20.1 (1998), pp. 359–392 (cit. on p. 70).

[KP74] R. Kouyoumjian and P. Pathak. "A Uniform Geometrical Theory of Diffraction for an Edge in a Perfectly Conducting Surface". In: *Proceedings of the IEEE* 62.11 (1974), pp. 1448–1461 (cit. on p. 4).

[Lau67] P. Laurin. "Scattering by a Torus". PhD thesis. University of Michigan, 1967 (cit. on p. 3).

[Laz+01] F. Lazarus, M. Pocchiola, G. Vegter, and A. Verroust. "Computing a Canonical Polygonal Schema of an Orientable Triangulated Surface". In: *Proceedings of the Seventeenth Annual Symposium on Computational Geometry*. 2001, pp. 80–89 (cit. on p. 94).

[LB12] O. E. Livne and A. Brandt. "Lean Algebraic Multigrid (LAMG): Fast Graph Laplacian Linear Solver". In: *SIAM Journal on Scientific Computing* 34.4 (Jan. 2012), pp. 499–522 (cit. on pp. 61, 174).

[LLB03] J.-F. Lee, R. Lee, and R. Burkholder. “Loop Star Basis Functions and a Robust Preconditioner for EFIE Scattering Problems”. In: *IEEE Transactions on Antennas and Propagation* 51.8 (Aug. 2003), pp. 1855–1863 (cit. on p. 9).

[LO98] R. Lorentz and P. Oswald. “Multilevel Finite Element Riesz Bases in Sobolev Spaces”. In: *DD9 Proceedings, Domain Decomposition Press, Bergen* (1998), pp. 178–187 (cit. on pp. 111, 113, 115).

[LZL04] J. Lee, J. Zhang, and C.-C. Lu. “Sparse Inverse Preconditioning of Multilevel Fast Multipole Algorithm for Hybrid Integral Equations in Electromagnetics”. In: *IEEE Transactions on Antennas and Propagation* 52.9 (Sept. 2004), pp. 2277–2287 (cit. on p. 10).

[MA14] R. Mitharwal and F. P. Andriulli. “On the Multiplicative Regularization of Graph Laplacians on Closed and Open Structures With Applications to Spectral Partitioning”. In: *IEEE Access* 2 (2014), pp. 788–796 (cit. on p. 70).

[Mar09] P.-G. Martinsson. “A Fast Direct Solver for a Class of Elliptic Partial Differential Equations”. In: *Journal of Scientific Computing* 38.3 (Mar. 2009), pp. 316–330 (cit. on p. 7).

[Mau49] A. W. Maue. “Zur Formulierung eines allgemeinen Beugungsproblems durch eine Integralgleichung”. In: *Zeitschrift für Physik* 126.7-9 (1949), pp. 601–618 (cit. on p. 6).

[Max65] J. C. Maxwell. “A Dynamical Theory of the Electromagnetic Field”. In: *Philosophical Transactions of the Royal Society of London* 155.0 (Jan. 1865), pp. 459–512 (cit. on p. 3).

[MB96] E. Michielssen and A. Boag. “A Multilevel Matrix Decomposition Algorithm for Analyzing Scattering from Large Structures”. In: *IEEE Transactions on Antennas and Propagation* 44.8 (August 1996), pp. 1086–1093 (cit. on p. 5).

[McL00] W. C. H. McLean. *Strongly Elliptic Systems and Boundary Integral Equations*. 1st ed. Cambridge University Press, 2000 (cit. on p. 40).

[MG07] T. Malas and L. Gürel. "Incomplete LU Preconditioning with the Multilevel Fast Multipole Algorithm for Electromagnetic Scattering". In: *SIAM Journal on Scientific Computing* 29.4 (Jan. 2007), pp. 1476–1494 (cit. on pp. 9, 10).

[MH78] J. R. Mautz and R. F. Harrington. "H-Field, E-Field, and Combined-Field Solutions for Conducting Bodies of Revolution". In: *Archiv für Elektronik und Übertragungstechnik* 32 (1978), pp. 157–163 (cit. on pp. 6, 41, 111).

[MH79] J. Mautz and R. Harrington. "A Combined-Source Solution for Radiation and Scattering from a Perfectly Conducting Body". In: *IEEE Transactions on Antennas and Propagation* 27.4 (July 1979), pp. 445–454 (cit. on p. 6).

[Mie08] G. Mie. "Beiträge zur Optik trüber Medien, speziell kolloidaler Metallösungen". In: *Annalen der Physik* 330.3 (1908), pp. 377–445 (cit. on p. 3).

[MLV07] L. Matekovits, V. A. Laza, and G. Vecchi. "Analysis of Large Complex Structures With the Synthetic-Functions Approach". In: *IEEE Transactions on Antennas and Propagation* 55.9 (Sept. 2007), pp. 2509–2521 (cit. on p. 8).

[Mül48] C. Müller. "Die Grundzüge einer mathematischen Theorie elektromagnetischer Schwingungen". In: *Archiv der Mathematik* 1.4 (July 1948), pp. 296–302 (cit. on p. 39).

[Mv77] J. A. Meijerink and H. A. van der Vorst. "An Iterative Solution Method for Linear Systems of Which the Coefficient Matrix Is a Symmetric $M$-Matrix". In: *Mathematics of Computation* 31.137 (Jan. 1977), pp. 148–148 (cit. on p. 9).

[Néd01] J.-C. Nédélec. *Acoustic and Electromagnetic Equations: Integral Representations for Harmonic Problems.* Applied Mathematical Sciences 144. New York: Springer, 2001 (cit. on pp. 17, 18, 23, 30, 38, 40, 43, 59, 113, 133, 135, 137).

[NN12] A. Napov and Y. Notay. "An Algebraic Multigrid Method with Guaranteed Convergence Rate". In: *SIAM Journal on Scientific Computing* 34.2 (Jan. 2012), pp. 1079–1109 (cit. on pp. 61, 87, 153).

[Not] Y. Notay. *AGMG Software and Documentation* (cit. on pp. 61, 87, 153, 174).

[OCE15] A. E. Ofluoglu, T. Ciftci, and O. Ergul. "Magnetic-Field Integral Equation [EM Programmer's Notebook]". In: *IEEE Antennas and Propagation Magazine* 57.4 (Aug. 2015), pp. 134–142 (cit. on p. 120).

[Osw94] P. Oswald. *Multilevel Finite Element Approximation*. Teubner, 1994 (cit. on p. 74).

[Osw98] P. Oswald. "Multilevel Norms for $H^{-1/2}$". In: *Computing* 61.3 (Sept. 1998), pp. 235–255 (cit. on pp. 74, 117).

[Pen+16] Z. Peng, R. Hiptmair, Y. Shao, and B. MacKie-Mason. "Domain Decomposition Preconditioning for Surface Integral Equations in Solving Challenging Electromagnetic Scattering Problems". In: *IEEE Transactions on Antennas and Propagation* 64.1 (Jan. 2016), pp. 210–223 (cit. on p. 8).

[Pet+98] A. F. Peterson, S. L. Ray, R. Mittra, and IEEE Antennas and Propagation Society. *Computational Methods for Electromagnetics*. New York; Oxford: IEEE Press ; Oxford University Press, 1998 (cit. on p. 5).

[PM03] V. V. S. Prakash and R. Mittra. "Characteristic Basis Function Method: A New Technique for Efficient Solution of Method of Moments Matrix Equations". In: *Microwave and Optical Technology Letters* 36.2 (2003), pp. 95–100 (cit. on p. 8).

[PS14] X.-M. Pan and X.-Q. Sheng. "Sparse Approximate Inverse Preconditioner for Multiscale Dynamic Electromagnetic Problems". In: *Radio Science* 49.11 (Nov. 2014), pp. 1041–1051 (cit. on p. 10).

[PWL11] Z. Peng, X.-C. Wang, and J.-F. Lee. "Integral Equation Based Domain Decomposition Method for Solving Electromagnetic Wave Scattering From Non-Penetrable Objects". In: *IEEE Transactions on Antennas and Propagation* 59.9 (Sept. 2011), pp. 3328–3338 (cit. on p. 8).

[QC08] Z. G. Qian and W. C. Chew. "An Augmented Electric Field Integral Equation for High-Speed Interconnect Analysis". In: *Microwave and Optical Technology Letters* 50.10 (Oct. 2008), pp. 2658–2662 (cit. on pp. 8, 9).

[Rig+16] M. Righero, I. M. Bulai, M. A. Francavilla, F. Vipiana, M. Bercigli, A. Mori, M. Bandinelli, and G. Vecchi. "Hierarchical Bases Preconditioner to Enhance Convergence of CFIE With Multiscale Meshes". In: *IEEE Antennas and Wireless Propagation Letters* 15 (2016), pp. 1901–1904 (cit. on p. 112).

[RL10] V. Rawat and J.-F. Lee. "Nonoverlapping Domain Decomposition with Second Order Transmission Condition for the Time-Harmonic Maxwell's Equations". In: *SIAM Journal on Scientific Computing* 32.6 (Jan. 2010), pp. 3584–3603 (cit. on p. 8).

[RT77] P.-A. Raviart and J.-M. Thomas. "A Mixed Finite Element Method for 2-Nd Order Elliptic Problems". In: *Mathematical Aspects of Finite Element Methods*. Springer, 1977, pp. 292–315 (cit. on p. 48).

[Rud91] W. Rudin. *Functional Analysis*. 2nd ed. International series in pure and applied mathematics. New York: McGraw-Hill, 1991 (cit. on pp. 15, 24, 43).

[Rum54] V. H. Rumsey. "Reaction Concept in Electromagnetic Theory". In: *Physical Review* 94.6 (June 1954), pp. 1483–1491 (cit. on pp. 6, 50).

[RWG82] S. Rao, D. Wilton, and A. Glisson. "Electromagnetic Scattering by Surfaces of Arbitrary Shape". In: *IEEE Transactions on Antennas and Propagation* 30.3 (May 1982), pp. 409–418 (cit. on pp. 48, 75).

[Saa03] Y. Saad. *Iterative Methods for Sparse Linear Systems*. 2nd ed. Philadelphia: SIAM, 2003 (cit. on p. 9).

[Sar83] T. K. Sarkar. "A Study of the Various Methods for Computing Electromagnetic Field Utilizing Thin Wire Integral Equations". In: *Radio Science* 18.01 (1983), pp. 29–38 (cit. on p. 5).

[Sar97] C. Sarkar. "A Multiscale Moment Method for Solving Fredholm Integral Equation of the First Kind". In: *Progress in Electromagnetics Research* 17 (1997), pp. 237–264 (cit. on p. 11).

[SC39] J. A. Stratton and L. J. Chu. "Diffraction Theory of Electromagnetic Waves". In: *Physical Review* 56.1 (July 1939), pp. 99–107 (cit. on p. 5).

[She94] J. R. Shewchuk. "An Introduction to the Conjugate Gradient Method Without the Agonizing Pain". In: (1994) (cit. on p. 7).

[Sil84] S. Silver, ed. *Microwave Antenna Theory and Design*. IEE electromagnetic waves series 19. London, UK: P. Peregrinus on behalf of the Institution of Electrical Engineers, 1984 (cit. on p. 39).

[SL93] B. Steinberg and Y. Leviatan. "On the Use of Wavelet Expansions in the Method of Moments (EM Scattering)". In: *IEEE Transactions on Antennas and Propagation* 41.5 (May 1993), pp. 610–619 (cit. on p. 11).

[SLC97] J. Song, C.-C. Lu, and W. C. Chew. "Multilevel Fast Multipole Algorithm for Electromagnetic Scattering by Large Complex Objects". In: *IEEE Transactions on Antennas and Propagation* 45.10 (October 1997), pp. 1488–1493 (cit. on p. 5).

[SM00] E. Suter and J. R. Mosig. "A Subdomain Multilevel Approach for the Efficient Mom Analysis of Large Planar Antennas". In: *Microwave and Optical Technology Letters* 26.4 (Aug. 2000), pp. 270–277 (cit. on p. 8).

[SS02] C. Su and T. Sarkar. "Adaptive Multiscale Moment Method (AMMM) for Analysis of Scattering from Three-Dimensional Perfectly Conducting Structures". In: *IEEE Transactions on Antennas and Propagation* 50.4 (Apr. 2002), pp. 444–450 (cit. on p. 11).

[SS03] D. Sengupta and T. Sarkar. "Maxwell, Hertz, the Maxwellians, and the Early History of Electromagnetic Waves". In: *IEEE Antennas and Propagation Magazine* 45.2 (Apr. 2003), pp. 13–19 (cit. on p. 3).

[SS11] S. A. Sauter and C. Schwab. *Boundary Element Methods*. Heidelberg; New York: Springer, 2011 (cit. on pp. 42, 133).

[Ste10] O. Steinbach. *Numerical Approximation Methods for Elliptic Boundary Value Problems: Finite and Boundary Elements*. New York: Springer Science + Business Media, 2010 (cit. on pp. 23, 25, 26, 43, 45, 53, 77, 137).

[Ste98] R. Stevenson. “Stable Three-Point Wavelet Bases on General Meshes”. In: *Numerische Mathematik* 80.1 (July 1998), pp. 131–158 (cit. on pp. 112, 115, 177).

[Sun+95] D. Sun, J. Manges, X. Yuan, and Z. Cendes. “Spurious Modes in Finite-Element Methods”. In: *IEEE Antennas and Propagation Magazine* 37.5 (Oct. 1995), pp. 12–24 (cit. on p. 97).

[SV00] K. Sertel and J. L. Volakis. “Incomplete LU Preconditioner for FMM Implementation”. In: *Microwave and Optical Technology Letters* 26.4 (Aug. 2000), pp. 265–267 (cit. on p. 9).

[Sv97] C. Schwab and T. von Petersdorff. “Fully Discrete Multiscale Galerkin BEM”. In: *Wavelet Analysis and Its Applications*. Vol. 6. Elsevier, 1997, pp. 287–346 (cit. on p. 11).

[SW98] O. Steinbach and W. L. Wendland. “The Construction of Some Efficient Preconditioners in the Boundary Element Method”. In: *Advances in Computational Mathematics* 9.1-2 (1998), pp. 191–216 (cit. on pp. 10, 55, 78, 133, 149, 150).

[Ufi07] P. Y. Ufimtsev. *Fundamentals of the Physical Theory of Diffraction*. John Wiley & Sons, 2007 (cit. on p. 4).

[Var59] R. S. Varga. *Factorization and Normalized Iterative Methods*. Tech. rep. Westinghouse Electric Corp. Bettis Plant, Pittsburgh, 1959 (cit. on p. 9).

[Vec99] G. Vecchi. “Loop-Star Decomposition of Basis Functions in the Discretization of the EFIE”. In: *IEEE Transactions on Antennas and Propagation* 47.2 (Feb. 1999), pp. 339–346 (cit. on pp. 9, 57, 59, 75, 94, 128).

[Ven06] G. Venkov. “Low-Frequency Electromagnetic Scattering by a Perfectly Conducting Torus. The Rayleigh Approximations.” In: *International Journal of Applied Electromagnetics and Mechanics* 24.1/2 (2006), p. 91 (cit. on p. 3).

[Vic+16] F. Vico, M. Ferrando, L. Greengard, and Z. Gimbutas. “The Decoupled Potential Integral Equation for Time-Harmonic Electromagnetic Scattering”. In: *Communications on Pure and Applied Mathematics* 69.4 (2016), pp. 771–812 (cit. on pp. 8, 11).

[VPV05] F. Vipiana, P. Pirinoli, and G. Vecchi. "A Multiresolution Method of Moments for Triangular Meshes". In: *IEEE Transactions on Antennas and Propagation* 53.7 (July 2005), pp. 2247–2258 (cit. on pp. 12, 66, 93, 95, 111, 112).

[VVP07] F. Vipiana, G. Vecchi, and P. Pirinoli. "A Multiresolution System of Rao-Wilton-Glisson Functions". In: *IEEE Transactions on Antennas and Propagation* 55.3 (Mar. 2007), pp. 924–930 (cit. on p. 12).

[VY90] G. Vegter and C. K. Yap. "Computational Complexity of Combinatorial Surfaces". In: *Proceedings of the Sixth Annual Symposium on Computational Geometry*. 1990, pp. 102–111 (cit. on p. 94).

[WC95] R. L. Wagner and W. C. Chew. "A Study of Wavelets for the Solution of Electromagnetic Integral Equations". In: *IEEE Transactions on Antennas and Propagation* 43.8 (August 1995), pp. 802–810 (cit. on p. 11).

[WE13] O. Wiedenmann and T. F. Eibert. "The Effect of Near-Zone Preconditioning on Electromagnetic Integral Equations of First and Second Kind". In: *Advances in Radio Science* 11 (July 2013), pp. 61–65 (cit. on p. 10).

[Wei77] T. Weiland. "A Discretization Model for the Solution of Maxwell's Equations for Six-Component Fields". In: *Archiv Elektronik und Übertragungstechnik* 31 (1977), pp. 116–120 (cit. on p. 4).

[WG81] D. R. Wilton and A. W. Glisson. "On Improving the Stability of the Electric Field Integral Equation at Low Frequencies". In: *USNC/URSI Spring Meeting Digest*. 1981, p. 24 (cit. on pp. 9, 57).

[WGK95] W.-L. Wu, A. W. Glisson, and D. Kajfez. "A Study of Two Numerical Solution Procedures for the Electric Field Integral Equation". In: *Applied Computational Electromagnetics Society Journal* 10.3 (1995), pp. 69–80 (cit. on pp. 9, 57, 65, 87, 96).

[Wil83] D. Wilton. "Topological Consideration in Surface Patch and Volume Cell Modeling of Electromagnetic Scatterers". In: *Proc. URSI Int. Symp. Electromagn. Theory*. 1983, pp. 65–68 (cit. on p. 96).

[XZ03] J. Xu and L. Zikatanov. “Some Observations on Babuška and Brezzi Theories”. In: *Numerische Mathematik* 94.1 (Mar. 2003), pp. 195–202 (cit. on pp. 46, 47).

[Yee66] K. Yee. “Numerical Solution of Initial Boundary Value Problems Involving Maxwell’s Equations in Isotropic Media”. In: *IEEE Transactions on Antennas and Propagation* 14.3 (May 1966), pp. 302–307 (cit. on p. 4).

[Yla+13] P. Yla-Oijala, S. P. Kiminki, J. Markkanen, and S. Jarvenpaa. “Error-Controllable and Well-Conditioned MoM Solutions in Computational Electromagnetics: Ultimate Surface Integral-Equation Formulation”. In: *IEEE Antennas and Propagation Magazine* 55.6 (Dec. 2013), pp. 310–331 (cit. on p. 7).

[Yse86] H. Yserentant. “On the Multi-Level Splitting of Finite Element Spaces”. In: *Numerische Mathematik* 49.4 (July 1986), pp. 379–412 (cit. on pp. 11, 12, 112, 115).

[ZC00] J.-S. Zhao and W. C. Chew. “Integral Equation Solution of Maxwell’s Equations from Zero Frequency to Microwave Frequencies”. In: *IEEE Transactions on Antennas and Propagation* 48.10 (Oct. 2000), pp. 1635–1645 (cit. on p. 9).

[Zha+03] Y. Zhang, T. J. Cui, W. C. Chew, and J.-S. Zhao. “Magnetic Field Integral Equation at Very Low Frequencies”. In: *IEEE Transactions on Antennas and Propagation* 51.8 (Aug. 2003), pp. 1864–1871 (cit. on p. 127).

[ZVL05] K. Zhao, M. Vouvakis, and J.-F. Lee. “The Adaptive Cross Approximation Algorithm for Accelerated Method of Moments Computations of EMC Problems”. In: *IEEE Transactions on Electromagnetic Compatibility* 47.4 (Nov. 2005), pp. 763–773 (cit. on pp. 5, 94, 103).

# Publications

## Journal Articles


[AAE14c] S. B. Adrian, F. P. Andriulli, and T. F. Eibert. "Hierarchical Bases Preconditioners for the Electric Field Integral Equation on Multiply Connected Geometries". In: *IEEE Transactions on Antennas and Propagation* 62.11 (Nov. 2014), pp. 5856–5861. © 2014 IEEE.

[AAE16c] S. B. Adrian, F. P. Andriulli, and T. F. Eibert. "On the Hierarchical Preconditioning of the Combined Field Integral Equation". In: *IEEE Antennas and Wireless Propagation Letters* 15 (2016), pp. 1897–1900. © 2016 IEEE.

[AAE17a] S. B. Adrian, F. P. Andriulli, and T. F. Eibert. "A Hierarchical Preconditioner for the Electric Field Integral Equation on Unstructured Meshes Based on Primal and Dual Haar Bases". In: *Journal of Computational Physics* 330 (Feb. 2017), pp. 365–379.

[AAE18a] S. B. Adrian, F. P. Andriulli, and T. F. Eibert. "On a Refinement-Free Calderòn Multiplicative Preconditioner for the Electric Field Integral Equation". In: *ArXiv e-prints* (Mar. 2018).

[Guz+17] J. E. O. Guzman, S. B. Adrian, R. Mitharwal, Y. Beghein, T. F. Eibert, K. Cools, and F. P. Andriulli. "On the Hierarchical Preconditioning of the PMCHWT Integral Equation on Simply and Multiply Connected Geometries". In: *IEEE Antennas and Wireless Propagation Letters* 16 (2017), pp. 1044–1047.

[Rah+18] L. Rahmouni, S. B. Adrian, K. Cools, and F. P. Andriulli. "Conforming Discretizations of Boundary Element Solutions to the Electroencephalography Forward Problem". In: *Comptes Rendus Physique* 19.1-2 (Jan. 2018), pp. 7–25.

[SAE12] U. Siart, S. B. Adrian, and T. F. Eibert. “Properties of Axial Surface Waves Along Dielectrically Coated Conducting Cylinders”. In: *Advances in Radio Science* 10 (Sept. 2012), pp. 79–84.

## Conference Proceedings

[AA12] S. B. Adrian and F. P. Andriulli. “Helmholtz Subspaces Preserving Fast Solvers Based on Multigrid Inversions of Loop-Star Decompositions”. In: *IEEE International Symposium on Antennas and Propagation*. Chicago, USA, July 2012.

[AAE14a] S. B. Adrian, F. P. Andriulli, and T. F. Eibert. “A Calderón Preconditioner for the EFIE Operator Without Barycentric Refinement of the Mesh”. In: *IEEE International Symposium on Antennas and Propagation*. Memphis, USA: IEEE, July 2014, pp. 2180–2181.

[AAE14b] S. B. Adrian, F. P. Andriulli, and T. F. Eibert. “Hierarchical Bases on the Standard and Dual Graph for Stable Solutions of the EFIE Operator”. In: *31st URSI General Assembly and Scientific Symposium*. Beijing, China, Aug. 2014.

[AAE14d] S. B. Adrian, F. P. Andriulli, and T. F. Eibert. “Laplacian Based Hierarchical Regularization of the Electric Field Integral Equation”. In: *Kleinheubacher Tagung*. Miltenberg, Germany, Sept. 2014.

[AAE15a] S. B. Adrian, F. P. Andriulli, and T. F. Eibert. “A Hermitian and Well-Conditioned EFIE for Fast Iterative and Direct Solvers”. In: *IEEE Antennas and Propagation International Symposium*. Vancouver, Canada, July 2015, pp. 742–743.

[AAE15b] S. B. Adrian, F. P. Andriulli, and T. F. Eibert. “Hierarchical Bases Preconditioners for a Conformingly Discretized Combined Field Integral Equation Operator”. In: *9th European Conference on Antennas and Propagation (EuCAP)*. Lisbon, Portugal, Apr. 2015.

[AAE15c] S. B. Adrian, F. P. Andriulli, and T. F. Eibert. “Laplace-Matrizenbasierte Vorkonditionierung der Elektrischen Feldintegralgleichung”. In: *Kleinheubacher Tagung*. Miltenberg, Germany, Sept. 2015.

[AAE16a] S. B. Adrian, F. P. Andriulli, and T. F. Eibert. "A Hermitian, Positive Definite, and Well-Conditioned Combined Field Integral Equation". In: *IEEE Antennas and Propagation International Symposium*. Fajardo, Puerto Rico, July 2016.

[AAE16b] S. B. Adrian, F. P. Andriulli, and T. F. Eibert. "A Well-Conditioned, Hermitian, Positive Definite, Combined Field Integral Equation for Simply and Multiply Connected Geometries". In: *URSI International Symposium on Electromagnetic Theory (EMTS)*. Espoo, Finland: IEEE, Aug. 2016, pp. 561–564. © 2016 IEEE.

[AAE17b] S. B. Adrian, F. P. Andriulli, and T. F. Eibert. "On the Preconditioning of the Hypersingular Operator via a Dual Haar Basis in the Stabilization of the Electric Field Integral Equation". In: *13th International Conference on Mathematical and Numerical Aspects of Wave Propagation (WAVES 2017)*. Minneapolis, USA, May 2017, pp. 3–4.

[AAE17c] S. B. Adrian, F. P. Andriulli, and T. F. Eibert. "Primal and Dual Wavelets for Fast Electric Field Integral Equation Solutions on Unstructured Meshes". In: *IEEE International Symposium on Antennas and Propagation*. San Diego, USA: IEEE, July 2017, pp. 2180–2181.

[AEA13b] S. B. Adrian, T. F. Eibert, and F. P. Andriulli. "Hierarchical Bases Regularizations of the EFIE Without the Search for Global Loops". In: *IEEE International Symposium on Antennas and Propagation*. Orlando, USA, July 2013.

[AEA13c] S. B. Adrian, T. F. Eibert, and F. P. Andriulli. "Primal and Dual Graph Haar Bases for the Hierarchical Regularization of the EFIE on Unstructured Meshes". In: *International Conference on Electromagnetics in Advanced Applications (ICEAA)*. Turin, Italy, Sept. 2013, pp. 942–944.

[GAE13] M. E. Gruber, S. B. Adrian, and T. F. Eibert. "A Finite Element Boundary Integral Formulation Using Cavity Green's Function and Spectral Domain Factorization for Simulation of Reverberation Chambers". In: *International Conference on Electromagnetics in Advanced Applications (ICEAA)*. Turin, Italy, Sept. 2013, pp. 460–463.

[Ort+16a] J. E. Ortiz Guzman, S. B. Adrian, R. Mitharwal, Y. Beghein, T. F. Eibert, K. Cools, and F. P. Andriulli. "Hierarchical Basis Preconditioners and Their Application to the PMWCHT Integral Equation". In: *10th European Conference on Antennas and Propagation (EuCAP)*. Davos, Swiss, Apr. 2016.

[Ort+16b] J. E. Ortiz Guzman, S. B. Adrian, R. Mitharwal, Y. Beghein, T. Eibert, K. Cools, and F. P. Andriulli. "Hierarchical Preconditioners for the PMCHWT Integral Equation". In: *IEEE Antennas and Propagation International Symposium*. Fajardo, Puerto Rico: IEEE, July 2016.

[Rah+17] L. Rahmouni, S. B. Adrian, K. Cools, and F. P. Andriulli. "A Mixed Discretized Adjoint Double Layer Formulation for the Electroencephalography Forward Problem with High Brain-Skull Contrast Ratios". In: *International Conference on Electromagnetics in Advanced Applications (ICEAA)*. Turin, Italy: IEEE, Sept. 2017, pp. 1817–1820.

## Workshops

[AEA13a] S. B. Adrian, T. F. Eibert, and F. P. Andriulli. "Advanced Preconditioning Techniques for the Electric Field Integral Equation". In: *URSI - B Workshop Felder Und Wellen*. Insel Poel, Germany, Mar. 2013.

[AEA17] S. B. Adrian, T. F. Eibert, and F. P. Andriulli. "Vorkonditionierung der elektrischen Feldintegralgleichung mittels einer dualen Haar-Basis". In: *URSI - B Workshop Felder und Wellen*. Groß Behnitz, Germany, June 2017.

# List of Supervised Student Projects

[Alt14] R. Altmiks. *Implementierung und Evaluierung eines Lösers der elektrischen Feldintegralgleichung unter Verwendung der Bibliothek BEM++*. Bachelor's Thesis. Munich, Germany: Technical University of Munich, July 2014.

[Bra13] M. Brandmeier. *Benchmark of Linear Algebra Back-ends*. Ingenieurpraxis für Mathematiker. Munich, Germany: Technical University of Munich, Aug. 2013.

[Dem17] S. Demmel. *On the Low-Frequency Electromagnetic Scattering by a Perfectly Conducting Torus*. Master's Thesis. Munich, Germany: Technical University of Munich, Sept. 2017.

[Gei16] D. Geisinger. *Investigation of the Thin Wire Electric Field Integral Equation Implemented in Julia*. Bachelor's Thesis. Munich, Germany: Technical University of Munich, June 2016.

[Gri14] F. Grimm. *Implementation of an Electromagnetic Solver with BETL*. Ingenieurspraxis. Munich, Germany: Technical University of Munich, June 2014.

[Han16] N. Han. *Investigation of Haar Basis Preconditioners for Computational Electrostatic Problems*. Bachelor's Thesis. Beijing, China: Beihang University, July 2016.

[Moo15] M. Moosbühler. *Implementation and Evaluation of an Algorithm That Solves Symmetric Diagonally Dominant Systems in Nearly Linear Time*. Bachelor's Thesis. Munich, Germany: Technical University of Munich, Sept. 2015.

[Sch17] M. Schewa. *Investigation of Gaussian Quadrature Rules on Triangles*. Bachelor's Thesis. Munich, Germany: Technical University of Munich, Aug. 2017.

[Wei18] J. Weindl. *Implementation of a Finite Element Multiscale Wavelet Method for Partial Differential Equations*. Master's Thesis. Munich, Germany: Technical University of Munich, Mar. 2018.

# Index